A NONLINEAR CONTROL STRATEGY FOR GRID-CONNECTED AND STAND-ALONE WIND ENERGY CONVERSION SYSTEM

STRATÉGIE DE COMMANDE NON LINÉAIRE POUR UN SYSTÈME DE CONVERSION D'ÉNERGIE ÉOLIENNE CONNECTÉ AU RÉSEAU ET AUTONOME

A Thesis Submitted to the Division of Graduate Studies
of the Royal Military College of Canada
by

Boubacar Housseini

In Partial Fulfillment of the Requirements for the Degree of
Doctor of Philosophy in Electrical Engineering

May, 2019

Abstract

Contrary to conventional electric power generators, such as diesel generators and hydroelectric power generators, existing wind energy conversion systems (WECS) are designed to operate in either grid-connected or stand-alone mode only. Different controllers are therefore designed for each mode of operation. The trend is that WECS should be able to work in both modes. Very few studies have been done to address this issue. The available control methods use the conventional linear PID-based control method. These methods are not always effective for high order multivariable nonlinear systems such as WECS. This thesis presents the development of a robust nonlinear controller for a hybrid wind energy battery-storage system that can operate in both grid-connected and stand-alone modes using a single unified controller. A new approach is proposed to improve the efficiency and increase the reliability of the hybrid wind turbine system. The proposed control strategy includes a power estimation module obtained based on the Thévenin equivalent model of the grid side subsystem. While ensuring a seamless transition between the two modes, the controller efficiently manages the power distribution between the load, the battery, and the grid. Next, an adaptive control algorithm is proposed to overcome parameter change which could occur due to extreme weather conditions such as Canadian winter conditions. This algorithm is based on the Lyapunov stability theory, which guarantees that the parameters are bounded and the state variables converge asymptotically to steady-state values. Mathematical analysis and results are presented to validate the performance of the proposed techniques. This was successfully applied for both wind-based three-phase power generation systems and single-phase residential applications.

Résumé

Contrairement aux générateurs d'énergie électrique conventionels, tels que les générateurs diesel et les générateurs hydroélectriques, les systèmes de conversion d'énergie éolienne existants (SCEE) sont conçus uniquement pour fonctionner en mode connecté au réseau ou en mode autonome. Différents contrôleurs sont donc conçus pour chaque mode de fonctionnement. La tendance est que les SCEE devraient être capable de fonctionner dans les deux modes. Très peu d'études ont été réalisées pour résoudre ce problème. Les méthodes de contrôle disponibles utilisent les méthodes de contrôle classique basée sur le proportionnel-intégral-dérivé (PID) linéaire. Ces méthodes ne sont pas toujours efficaces pour les systèmes non linéaires multivariés d'ordre élevé tels que les SCEE. Cette thèse présente le développement d'un contrôleur non linéaire robuste pour un système hybride d'énergie éolienne avec batterie de stockage pouvant fonctionner à la fois en mode connecté au réseau qu'en mode autonome en utilisant un seul contrôleur unifié. Une nouvelle approche est proposée pour améliorer l'efficacité et la fiabilité du système éolienne hybride. La stratégie de contrôle proposée comprend un module d'estimation de la puissance obtenu sur la base du modèle équivalent Thévenin du sous-système côté réseau. Tout en assurant une transition souple entre les deux modes, le contrôleur gère efficacement la répartition de la puissance entre la charge, la batterie et le réseau. Ensuite, un algorithme de contrôle adaptatif est proposé pour surmonter le problème de changement des paramètres qui pourrait survenir en raison de conditions météorologiques extrêmes telles que les conditions hivernales canadiennes. Cet algorithme est basé sur la théorie de la stabilité de Lyapunov, qui garantit que les paramètres sont bornés et que les variables d'état convergent de manière asymptotique vers des valeurs à l'état d'équilibre. L'analyse mathématique et les

résultats sont présentés afin de valider les performances des techniques proposées. Ceci a été appliqué avec succès à la fois pour les systèmes triphasés de production d'énergie éolienne et les applications résidentielles monophasées.

For:

My dear mother, Hadiza

&

My dear father, Housseini

Acknowledgements

Bismillah-hir Rahman-nir Rahim.
Alhamdulillahi Rabbil 'alamin. Wassalatu wassalamu ala Rasulillah.

All Praise is due to Allah, the Lord of the worlds, the Most Compassionate, the Most Merciful. I thank Him for His mercy, help and guidance.

I would like to express my deepest gratitude to my supervisors, Prof. Aimé Francis Okou and Dr. Rachid Beguenane for their guidance and support. This work would not have been possible without their belief in my abilities. Their mentorship and personalities have been an extraordinary source of support throughout my research.

I am especially thankful to Prof. Mohammed Tarbouchi and Prof. Derrick Bouchard for their help and valuable advice with this research. Discussions with them have been insightful.

My sincere thanks goes to Dr. Kiari Goni Boulama who has always been helpful with ideas and provided me lots of encouragement. I thank him for his friendship and for making my time at RMC a wonderful experience.

I must also gratefully acknowledge the help of Dr. Mahamadou Abdou Tankari on this project. I thank him for the long hour discussions, suggestions and support, since at the very begin of this project.

I would like also to thank Dr. Hussein Ibrahim, former research manager of TechnoCentre éolien of Quebec, for allowing me to visit their research facility and sharing with me his valuable field expertise. This experience has allowed me to

see all parts of wind power generation chain and its interaction to the grid, which has helped me to shape my research.

My special thanks are extended to Jocelyne Beaulieu and the staff of ECE Department at the Royal Military College of Canada for their help in offering me the resources in conducting this research.

I'm grateful to Vanner inc. for their support and for allowing me to stay after work writing my dissertation.

I am also grateful to all my extended family, teachers, friends, neighbors, fellow grad students, labmates, colleagues and all who supported me in any way on this journey. I thank them for sharing their passions, experiences, and encouragements with me.

To my dear wife, Najma, I cannot find words to express my gratitude to her for her patience and taking care of the kids while I stay late at the university. Thank you for being supportive of me through all these years, more than a decade now. All I can say is jazakillahu khair! I am also in debt to my kids, Hadiza, Abdallah and Maryam who have never known their dad as anything but a student. Thank you for your patience. You have always been a source of joy for me.

Last, and most importantly, I would like to thank my dear parents for raising me, giving me the values that I have and supporting me throughout my life. I owe them everything.

Glossary

List of Acronyms

$B2B$	Back-to-Back
BSU	Battery Storage Unit
CAD	Canadian Dollar
$DFIG$	Doubly-Fed Induction Generator
EKF	Extended KalmanFilter
EMI	Electromagnetic Interference
FL	Feedback Linearization
GC	grid-connected
GW	Gigawatt
$MIMO$	Multiple-Input Multiple-Output
$MPPT$	Maximum Power Point Tracking
PID	Proportional Integral Derivative
PLL	Phase-Locked Loop
$PMSG$	Permanent Magnet Synchronous Generators
PV	Photovoltaic Generator
SA	stand-alone
$SCIG$	Squirrel Cage Induction Generator
THD	Total Harmonic Distortion
$TSLA$	Taylorseries Expansion Linear Approximation
TW	Terawatt
UG	utility grid
UPS	Uninterruptible PowerSupply

$WECS$	Wind Energy Conversion System
WT	Wind Turbine
ZDC	Zero d-Axis Current

System Dynamics

i_{ds}	Generator stator d-axis current (A)
i_{qs}	Generator stator q-axis current (A)
u_{ds}	Generator stator d-axis voltage (V)
u_{qs}	Generator stator q-axis voltage (V)
ω_r	Rotor electrical angular speed
i_{di}	Grid-side converter output d-axis current (A)
i_{qi}	Grid-side converter output q-axis current (A)
u_{di}	Grid-side converter output d-axis voltage (V)
u_{qi}	Grid-side converter output q-axis voltage (V)
i_{lb}	Current through the buck-boost converter inductor (A)
E_{dc}	Electric energy of the dc-link capacitor (J)
P_m	Rated Mechanical Power (MW)
λ_r	Rated Rotor Flux Linkage (Wb)
u_g	Grid Voltage Line-to-Line Module (V)
u_{dc}	dc-link Voltage (V)
u_{bat}	Battery Rated Voltage (V)
P_{bat}	Battery Power (MW)
P_l	Load Active Power (MW)
Q_l	Load Reactive Power (MW)
E_{th}	Thévenin-Equivalent Voltage (J)
Z_{th}	Thévenin-Equivalent Impedance (J)

System Parameters

P	Number of Pole Pairs
J	Moment Inertia of the Generator ($kg.m^2$)
R_s	Stator Winding Resistance ($m\Omega$)
L_{ds}	d-axis Synchronous Inductance (mH)
L_{qs}	q-axis Synchronous Inductance (mH)
V_w	Rated Wind speed (m/s)
R	Blade Radius (m)
ρ	Air Density (kg/m^3)
λ_{opt}	Optimal Tip Speed Ratio)
C_{dc}	dc-link Capacitor (μF)
L_f	Grid-side Filter (mH)
L_g	Grid Inductance (mH)

Contents

List of Tables

List of Figures

Co-Authorship

1. B. Housseini, A. F. Okou, R. Beguenane, and M. A. Tankari, "Online Parameter Estimation and Nonlinear Adaptive Control for Stand-Alone and Grid-Connected Hybrid Wind Energy System," *IEEE Transactions on Reliability Journal*. (under revision).

2. B. Housseini, A. F. Okou, R. Beguenane, and M. A. Tankari, "Single-Phase Stand-Alone and Grid-Connected DQ Nonlinear Controller Design for Enhancing the Resilience of Hybrid Wind-Battery Microgrid," *Electric Power Components and Systems Journal*. (under revision).

3. B. Housseini, A. F. Okou, R. Beguenane, and M. A. Tankari, "Comprehensive Literature Review of On-Grid/Off-Grid Wind Energy Conversion Con-

trol System," *IEEE Transactions on Industrial Informatics Journal.* (under revision).

4. B. Housseini, A. F. Okou, and R. Beguenane, "Robust nonlinear con-troller design for on-grid/off-grid wind energy battery-storage system," IEEE Transactions on Smart Grid, vol. 9, no. 6, pp. 5588–5598, 2018.

5. B. Housseini, A. F. Okou, R. Beguenane, and M. A. Tankari, "Dq synchronous frame nonlinear controller design for a single-phase stand-alone and grid-connected hybrid wind/battery system," *IECON 2018-44th Annual Conference of the IEEE Industrial Electronics Society.* IEEE, 2018, pp. 145-152.

6. B. Housseini, A. F. Okou, and R. Beguenane, "Nonlinear adaptive control of on-grid/off-grid wind energy battery-storage system," *2017 Twelfth International Conference on Ecological Vehicles and Renewable Energies (EVER).* IEEE, 2017, pp. 18.

7. B. Housseini, A. F. Okou, and R. Beguenane, "Performance comparison of variable speed pmsg-based wind energy conversion system control algorithms," *2017 Twelfth International Conference on Ecological Vehicles and Renewable Energies (EVER).* IEEE, 2017, pp. 110.

8. B. Housseini, A. F. Okou, and R. Beguenane, "Energy management strategy of on-grid/off-grid wind energy batterystorage system," *2016 IEEE Canadian Conference on Electrical and Computer Engineering (CCECE).* IEEE, 2016, pp. 1-6.

9. B. Housseini, A. F. Okou, and R. Beguenane, "A unified nonlinear controller design for on-grid/off-grid wind energy battery-storage system," *IECON 2015-41st Annual Conference of the IEEE Industrial Electronics Society.* IEEE, 2015, pp. 005 273-005 278.

Chapter 1

Introduction

1.1 Introduction

Presently, renewable generation systems such as wind turbines (WT) and photovoltaic (PV) generators, because of their intermittent nature, are not designed to operate in both stand-alone (or off-grid) and grid-connected (or on-grid) mode. Therefore, once a power outage occurs, they have to be automatically disconnected from the main utility grid (UG), which causes huge financial losses to electricity suppliers. The trend is that they should be maintained under operation in both situations, whether the utility grid is available or not, to feed local loads. Thus, one of the new challenges facing today's wind energy-based electricity supply industry is how to adapt a single wind turbine model to both stand-alone (SA) and grid-connected (GC) modes.

Successful utilization of wind energy conversion system (WECS) for both uses will have a wide impact in the electricity supply industry by increasing the wind energy penetration, in particular in remote areas and in developing countries where utility grid outages are widespread. However, this requires adequate power electronics and an effective controller.

The overall objective of this research project is to help overcome these issues, i.e. to develop, perform fundamental analyses and design an effective hybrid control system, for making it viable to utilize a single wind turbine adjustable in both

on-grid and off-grid modes. To ensure a seamless transition between the two modes effectively with the minimum impact on the critical loads and the utility grid, a robust control algorithm is required. Most of the currently used approaches to control WECS employ classical control strategies that don't take into account the dynamic aspects of all the different components of the system. The suggestion, in this research, is to adopt a modern control theory approach, feedback linearization based nonlinear controller design for large size of WECS. This method is shown to be intrinsically more effective than PI controllers. Hence, a new control method was proposed to improve the dynamic response and the efficiency of the on-grid/off-grid WECS. Besides, a battery storage unit (BSU) was added to the system to make it more autonomous.

1.2 Justification and Motivation

1.2.1 Global Context of the Study

Energy is a key factor in human development. It is used in every aspect of daily life: agriculture, transportation, heating, cooling, waste collection, information technology, and communications. Its demand continues to increase worldwide. By 2040, energy is expected to increase by more than 50%. It is clear that the largest share of the world electricity generation is still provided by the conventional coal energy, although its share declines over the projection period as shown in Fig. 1.1 [1].

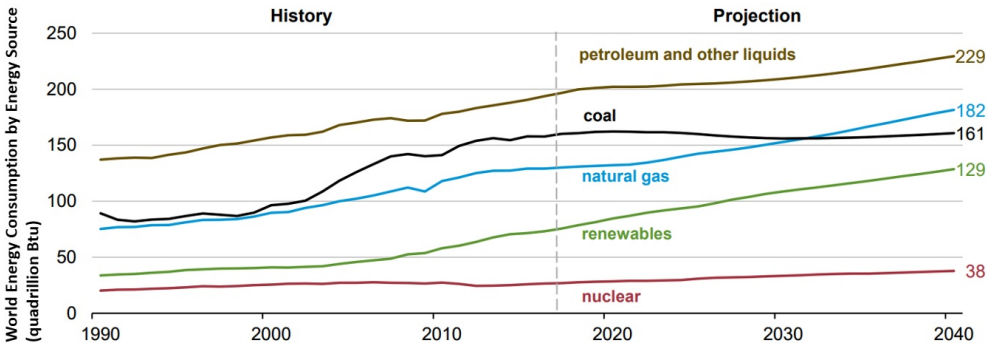

Figure 1.1: World Energy Consumption by Energy Source, 2017 [1].

Using electrical energy with conventional technologies has already brought with it several serious problems. Some of them, such as climate change, present potentially serious risks to the world. Therefore, it is urgent for the world to develop alternative sustainable energy sources that are non-polluting (not carbon-based) to respond to the needed expected amount of energy. Significant progress has been made in the last twenty years. Renewable energy continued to grow strongly and supplied an estimated 20.4% of global final energy consumption in 2016 as shown in Fig. 1.2. In 2017, about 70% of net new electricity capacity installed worldwide was renewable-based. Fig. 1.3 presents renewable power capacities in the world, EU-28, BRICS, and the top six countries in 2017 [2].

Among renewable energy technologies, wind energy is one of the fastest-growing [2]. At the end of 2018, as shown in Fig. 1.3, its global power capacity was 539 Gigawatts (GW). Also, its operation and maintenance cost is continuing to drop, boosting the competitiveness of the sector significantly. To maintain the strong growth that the wind energy industry has experienced in recent years, we need a fair policy supports from governments worldwide and fast development in innovative technologies dealing with new challenges.

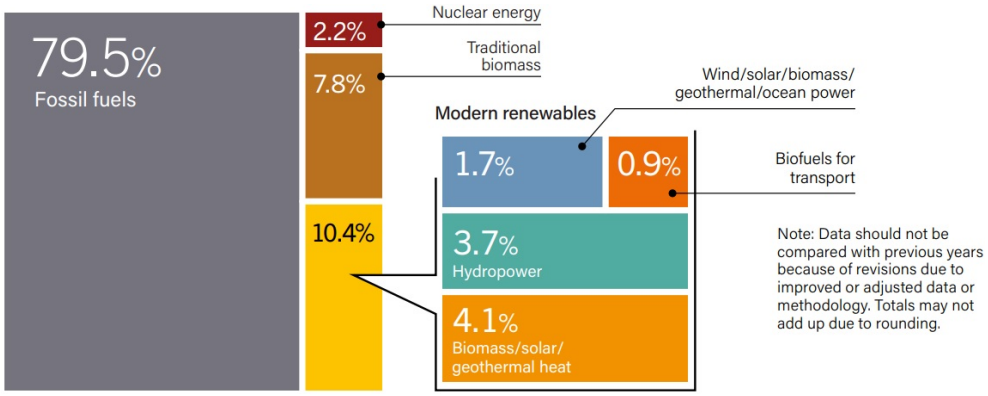

Figure 1.2: Estimated Renewable Energy Share of Global Final Energy Consumption, 2016.

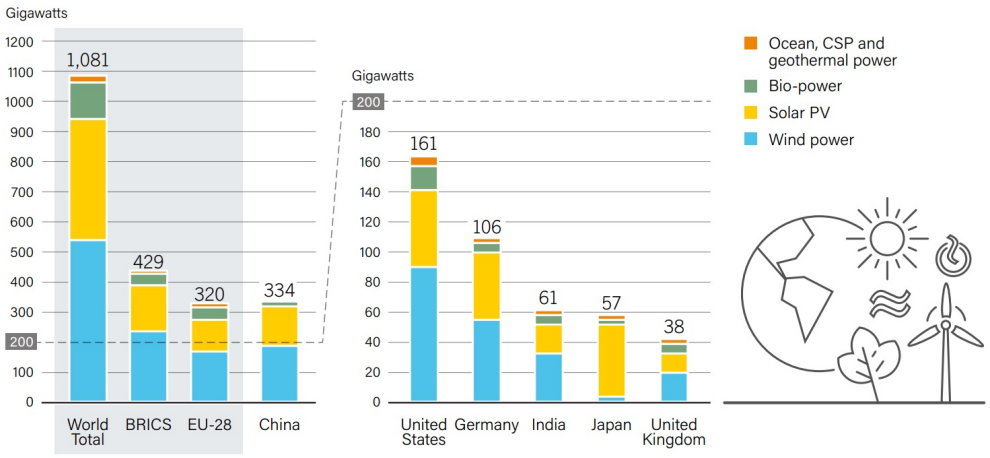

Figure 1.3: Renewable Power Capacities in World, $EU-27$, BRICS, and Top Six Countries, 2017 [2].

1.2.2 Canada Context of the Study

Canada has the 6th largest electrical network in the world producing and distributing 648.4 terawatt-hours (TWh) of power in 2016 [3]. About 66% of its electricity comes from renewable sources, predominantly hydro [4]. In 2014, total electricity exports to the United States were 72 TWh valued at more than $3.8 billion [5]. However, Canada has much to be done in renewable energy to preserve its electricity benefits and ease the environmental burden. When it comes to wind energy, Canada has trailed most of the developed world, although it is growing dynamically. In 2018, the total wind-based installed capacity was $12,816$ MW, driving over CAD 1 billion in investment and creating $64,500$ person-years of employment [6]. There is potential for further expansion on land and offshore.

Despite the progress of Canada on renewable energy, diesel-generated electricity remains the most commonly used power source to produce heat or electricity in rural areas. Approximately 200,000 people live in more than 300 remote communities (Yukon, Northwest Territories, Nunavut, islands). Diesel-generated electricity is more expensive than large electric production plants (gas, hydro, nuclear, wind), because of the transport and associated environmental cost. Moreover, it is responsible for the emission of 1.2 million tons of greenhouse gases annually [7, 8].

Unfortunately, most of the existing wind turbines in Canada are grid-connected only. So they have to stop operating in case of a power outage as they are not equipped with smart technology that allows them to switch in stand-alone mode and continue operating. Therefore, adaptable grid-connected/stand-alone WECS is a good solution to keep wind turbines under operation and avoid financial loss. Also, this technology could provide a sustainable and cost-effective alternative to the diesel generators or other unsustainable energy sources, such as kerosene lamps and traditional biomass, that would be otherwise deployed in rural areas.

1.2.3 Developing Countries Context of the Study

Electricity plays an essential role in economic and social development, yet there are still over 1.3 billion people in remote areas who don't have access to it. More than 99% of them live in developing regions, and 4/5 of them are in rural South Asia and sub-Saharan Africa [9]. These countries have the particularity of having a growing population coupled with very low investment to increase capacity in the electricity sector. This situation has led to increased power demand, in addition to inadequate transmission lines. As a result, rolling blackouts have become a common or perhaps a normal daily event in many developing countries. Having wind turbines that can flexibly connect to the grid and switch to the stand-alone mode in case of a power outage, could significantly reduce the harmful consequences of long-duration grid failures in developing countries.

1.3 Problem Statement

The majority of wind turbines operating in the industry are on-grid systems (Fig. 1.4.a). One of the main problems of this category of wind turbines is that they can only produce and send energy to the utility grid. Therefore, they cannot operate in case of a power outage (Fig. 1.4.c), which can lead to considerable financial losses.

It is reported in [10] that electrical power outages cause the Canadian economy annual damage of over 12 billion CAD. On the other hand, off-grid WECS (Fig.

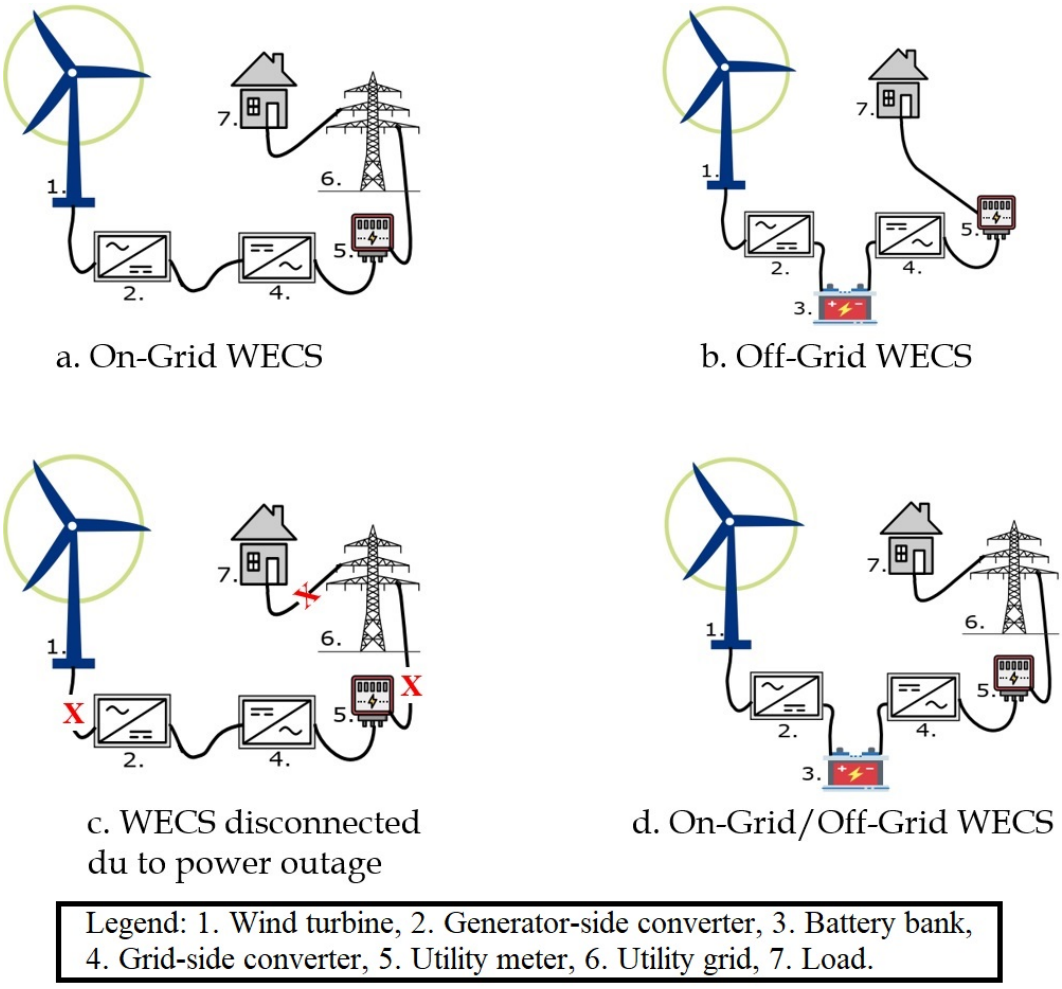

Figure 1.4: On-Grid/Off-Grid WECS.

1.4.b) are limited in terms of power availability as wind speeds fluctuate. Hence, the need to have multiple power sources to increase the resilience of the system. On-grid/off-grid WECS (Fig. 1.4.d) gives that flexibility. It allows a single WECS to operate both in grid-connected mode when the grid is available and in stand-alone mode in case of power interruption. However, such a system requires adequate power electronics and effective control strategies.

On-grid/off-grid WECS control began with UPS (uninterruptible power supply) applications (Fig. 1.5.d) where the primary energy source connected to the dc-bus is considered stable. This is not the case for WECS which is subject to

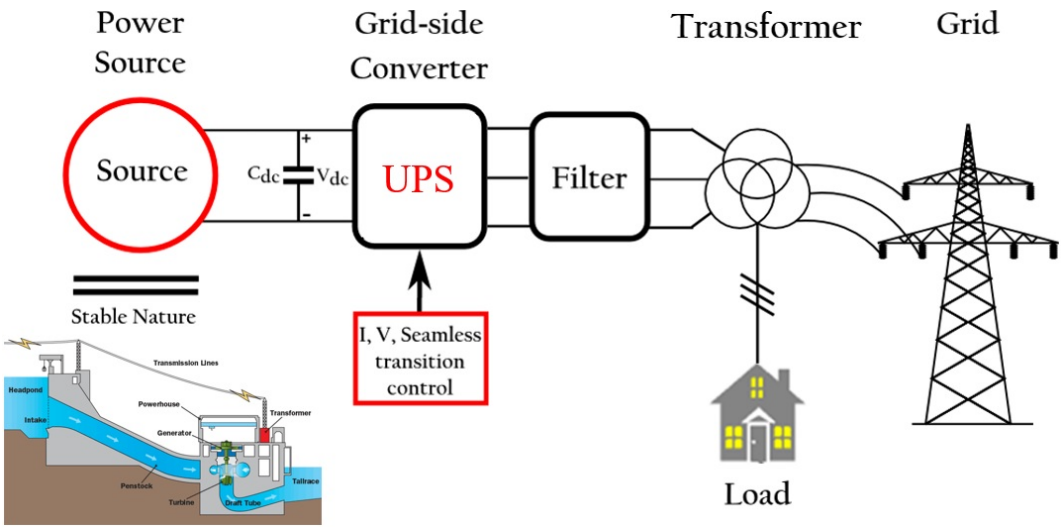

Figure 1.5: On-Grid/Off-Grid for UPS Applications.

the stochastic behavior of the wind velocity. In recent years, many researchers have started investigating the On-grid/off-grid control solution for WECS applications. An extensive literature review is given in Chapter 2 in this regard. Therein, we presented the state-of-the-art as well as the theoretical and methodological contributions to this topic. Most of the proposed control methods found in the literature employed two different controllers depending on whether the system is operating in grid-connected or in stand-alone mode. Some authors suggested the use of a unified controller for both modes. However, these controllers are mainly proportional-integral-derivative (PID) control based. PID-based controllers appear to be less effective for high-order nonlinear systems such as WECS [11, 12]. In addition, they may fail to limit the converter current rise below the permitted limit during the islanding to the grid detection transition period.

In this research project, the design of a unified multi-input-multi-output (MIMO) nonlinear controller for a WECS was investigated. The challenge was that the system should operate in both grid-connected and standalone modes using a single controller. In addition, the controller should guaranty a seamless transition between the two modes and efficient power distribution between the load, the battery, and the grid.

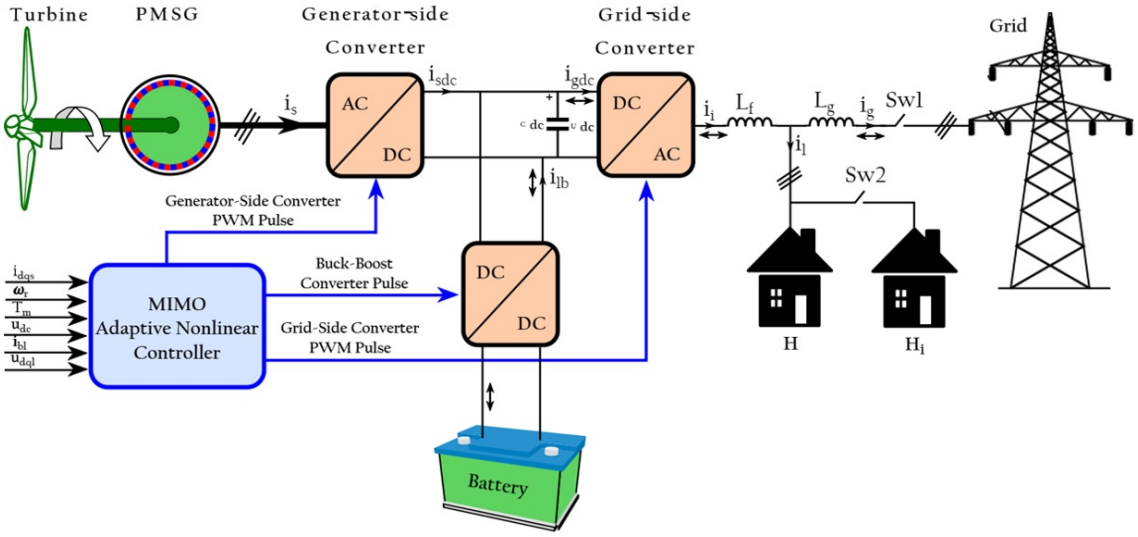

Figure 1.6: On-Grid/Off-Grid Wind Energy COnversion System.

Although good wind sites are important for the wind turbine power density, they are often located in remote harsh environment locations. The weather conditions such as low temperatures can have an impact on the physical properties of materials used in the fabrication of the wind turbines. Hence, changing the parameters of the WECS. Conventional controllers cannot guarantee the stability and performance of such systems due to their time-varying nature. To address this issue, we proposed an adaptive controller where the controller does not require a priori knowledge of the system parameters. The control algorithm continuously adapted its parameters with time to maintain the performance of the control system.

Lastly, in order to apply the proposed techniques originally designed for three-phase systems to single-phase residential wind turbine systems, a DQ-synchronous/single phase transformation module was proposed.

The block diagram of the system considered in this work is depicted in Fig. 1.6. It consists of a PMSG driven by a wind turbine, a generator-side AC/DC converter and a grid-side DC/AC converter that connects the load and the grid to the system. Furthermore, it includes a storage capacity to cover the energy demands of low wind time intervals when the wind turbine is not generating electricity or

period, during which planned the power is not available for numerous unforeseeable contingencies. A power management strategy was proposed for this purpose. A bi-directional buck-boost DC/DC converter is used to connect the storage unit to the DC-link. In the stand-alone mode, the switch *Sw1* is opened and the system supplies critical local loads only. The switch *Sw1* is closed in the grid-connected mode. The switch *Sw2* is used to add more load to the system. The role of the wind turbine is to convert part of the kinetic energy of the wind into mechanical energy. This energy is converted into electrical energy via the generator. Since the generator output frequency is variable (depends on the wind conditions), the back-to-back converter synchronizes its output with the grid frequency. The buck/boost converter adjusts the dc-link voltage to the required battery voltage.

The tests in this study were carried out using the SimPowerSystems toolbox [13] in Matlab/Simulink software.

1.4 Objectives

The main objective of the present work was to study the design of a robust nonlinear controller for a hybrid wind energy conversion system that is capable of flexibly operate in both grid-connected and stand-alone mode using a single controller. The second objective was to address the problem of parameter change of WECS in harsh environment operation conditions by developing an adaptive nonlinear controller for the grid-connected/stand-alone system where the knowledge of the parameters of the system is not necessary. The third objective was to investigate the transferability of the on-grid/off-grid control concept, initially designed for three-phase WECS, to single-phase residential on-grid/off-grid WECS.

In order to achieve the first objective, the MIMO feedback linearization control design methodology was adopted to find the controller equations. A variable-speed wind turbine based permanent magnet synchronous generator (PMSG) was used. A back-to-back (AC/DC and DC/AC) power converter was used to connect the WECS to the grid, the battery bank, and the load. Also, a bi-directional buck-boost DC/DC converter was used to regulate directly the dc-link voltage and the

load power based on the system stability and the energy balance between the components of the hybrid system. In addition, the controller of the system should achieve the following system's performance:

1. Maximum power point tracking (MPPT) control, i.e., keeping the wind turbine operating at its optimum rotor speed allowing extracting the maximum power from the wind turbine.

2. Zero d-axis current (ZDC) control: this control scheme is employed to achieve a linear relationship between the generator stator current and its electromagnetic torque for effective control performance.

3. The converter DC bus voltage should always be kept constant to ensure power transfer from the generator-side subsystem to the load/grid-side subsystem through the back-to-back (B2B) power converter.

4. The grid-side converter output voltage needs to be controlled in terms of amplitude and frequency when the grid is not available in order to match the load requirements.

5. Managing the power distribution between the load, the battery bank, and the grid. The algorithm took into account several scenarios, based on the produced power, the grid availability and the load demand, to determine the amount of energy that should be taken from the battery or stored into the battery. Therefore, a load power estimation module that dynamically calculates the load active power and reactive power requirements, was developed.

6. The system controller should be flexible and fast enough to guarantee a seamless transition between the stand-alone and the grid-connected operation modes and vice-versa.

7. All the sub-objectives above should be achieved by using a single controller with no need to switch between two controllers.

The first objective was achieved based on the assumption that all the parameters of the system were well known. This is not always the case, especially, in

a harsh environment such as Canadian cold weather conditions where certain parameters are subjected to change. Hence, the need to go beyond the first objective. Therefore, as a second objective, an adaptive nonlinear control algorithm, which estimates the parameters of the system, was developed. All the parameters of the system (15 in total) were considered unknown. Based on the Lyapunov stability theory, an adaptive law that ensures the parameters are bounded and the state variables converge asymptotically to steady-state values was proposed.

In order to broaden the scope of the proposed unified on-grid/off-grid control approach to domestic dwelling applications, a novel single-phase DQ transformation module was proposed. This module converts the grid-side converter three-phase output signals in a single-phase DQ synchronous frame. The single-phase WECS control was performed without changing the dynamic equations of the controller. This constitutes the third objective of the thesis.

1.5 Research Contributions

This research project has four main contributions:

1. A novel unified robust nonlinear controller was proposed for WECS, which guarantees the operation of the system in both grid-connected and stand-alone modes with smooth transition between modes. A single controller was used to accomplish this task contrary to conventional methods found in the literature.

2. An energy management strategy between the wind-turbine, the load, the storage unit, and the grid was proposed. This was done in such a way that the grid contribution is significantly reduced and the storage unit can provide backup energy or store the surplus wind energy efficiently to preserve system reliability. It can also support the grid by selling power back to the grid during high wind conditions.

3. An online parameter estimation algorithm for on-grid/off-grid WECS was proposed, which suppresses the need for accurate knowledge of system pa-

rameters for it to operate.

4. A DQ-synchronous frame transformation module for single-phase full-bridge converter was proposed, which allows the control to be used for single-phase residential applications.

1.6 Thesis Organization

This thesis is presented in an article-based format and is divided into six chapters. Chapter 2 reviews different control algorithms and approaches proposed in the literature for on-grid/off-grid WECS. It is under revision in the IEEE Transactions on Industrial Informatics journal. Chapter 3 investigates the motivation for selecting the feedback linearization design approach for the controller in this work. Hence, performance comparative analysis of three different control algorithms for WECS is presented therein as illustrated in Fig. 1.7. They are namely, the conventional PID-based control, the Taylor series expansion linear approximation based (TSLA-based) control and the feedback linearization based (FL-based) nonlinear control. From that comparative study, the FL-based nonlinear control method appears to show the better system performance. Therefore, the next three controllers
were designed based on that design methodology. Chapter 3 is presented in the form of manuscript format and is published in the International Conference on Ecological Vehicles and Renewable Energies (EVER). Chapter 4 presents the description of the on-grid/off-grid WECS, including its mathematical model and the design methodology of the proposed unified on-grid/off-grid nonlinear controller. Chapter 4 is published in the IEEE Transactions on Smart Grid journal. Chapter 5 discusses the online parameter estimation of the hybrid wind energy system. It is also presented in the form of a research article and is under revision in the IEEE Transactions on Reliability journal. Chapter 6 presents the DQ single-phase synchronous frame transformation module that allows the nonlinear controller initially designed for three-phase on-grid/off-grid WECS to work for single-phase residential systems. This chapter is under revision in the Electric Power Components

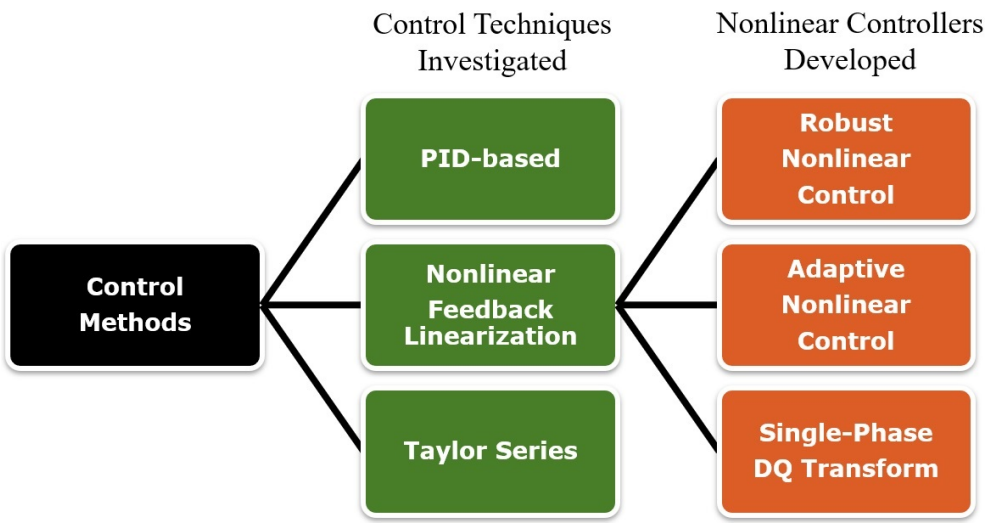

Figure 1.7: Control Techniques Investigated.

and Systems journal. Finally, an overall summary, conclusion and recommended future work are presented in Chapter 7.

Chapter 2

Comprehensive Literature Review of On-Grid/Off-Grid Wind Energy Conversion Control System

Abstract

Current wind turbine systems are not designed to operate in both stand-alone (or off-grid) and grid-connected (or on-grid) modes. Therefore, when a power outage occurs, they are automatically disconnected from the main utility grid. The trend is that they should be able to work in both modes, whether they are connected to local loads or to the utility grid. This has been the subject of several recent research investigations. In this contribution, a comprehensive review on on-grid/off-grid wind energy conversion system control strategies is presented. From the conventional control methods which use two separate controllers to the single unified control approach are investigated. Their main advantages and drawbacks that can be found in the literature are studied. A description of their control structure is given. In addition, their main characteristics and some of the works that analyze and compare them are presented.

Index terms— Wind turbine, control, PID control, PMSG, linear control, nonlinear control, grid-connected, stand-alone.

2.1 Introduction

Nowadays, renewable energy has become the focal point of any green economy and sustainable development strategy. More and more governments around the world acknowledge its environmental, social and economic benefits, and long-term positive impact. In developed countries, the influence of environmental organizations, civil society and pressure groups, on the nation wide policy making processes is increasingly evident. In addition, consumers have come to expect a secure, reliable, carbon free and high-quality electricity supply. These explain the peak increase of wind and solar based energy sources integration to the grid in the last twenty years. Electricity supply industry has gone through many decentralization, privatization and deregulation programs worldwide. This new situation has created many new business opportunities in the electrical energy sector but also some of the greatest operational challenges in the history of electricity supply. One of these issues is the effective integration of wind energy into utility grid. The fact that presently, wind turbines can only operate either in stand-alone mode (or off-grid) or grid-connected (or on-grid) mode makes the integration more difficult. They are not designed to operate in both modes. Therefore, when a power outage occurs, they are automatically disconnected from the main utility grid (UG). This may causes significant financial losses to electricity suppliers [14, 15]. Therefore, one of the new challenges the wind energy based electricity supply industry will have to address is the adaptation of a single wind turbine so that it can operate in both modes [16]. The trend is to use the grid-side converter to disengage the wind turbine system from the grid to allow a continuous supply to critical loads during a power outage. Moreover, transitions between the two modes should be fast and seamless to minimize any abrupt voltage or current changes [17]. Several studies have been conducted to deal with issues related to the on-grid/off-grid mode of operation. This is investigated in this paper.

The trend toward on-grid/off-grid systems also occurs within a context where the nature of grid users is drastically changing, electricity generation is becoming less controllable and the electricity consumption is becoming increasingly varied; the architecture and technology used for the transmission and distribution

grids and their system interaction will need to change. Legal frameworks must be adapted to go along with this evolution of the electricity system and grids. Hence, an evolution to so-called smart grids is inevitable. As the European Telecommunications Standards Institute (ETSI) defines it, the smart grid is an electricity network that can intelligently integrate the actions of all users connected to it – generators, consumers and those that do both – in order to efficiently deliver sustainable, economic and secure electricity supplies [18]. Having a WT (wind turbine) system which will be able to operate in both modes of operation is necessary to cover the energy demands of low wind time intervals when WT are not generating electricity, winter days in cold climate regions when not enough heat is generated by wind power or heat pumps and during intervals (days or weeks) when planned power is not available for unforeseen contingencies. Additionally, future grids will also require massive amounts of storage, relying on technologies such as bulk storage and hydro energy in the mountain regions, and distributed storage relying on other technologies, e.g. electrochemical [19].

For a large country where access to electricity in rural or remote areas is a concern, on-grid/off-grid technology can play an important role. It can provide a sustainable and cost-effective alternative to the diesel generators or other unsustainable energy sources, such as kerosene lamps and traditional biomass, that would be otherwise deployed in remote areas. Therefore, successful utilization of wind energy conversion system (WECS) that is capable to operate in both modes will have a significant impact in electricity supply industry by increasing the wind energy penetration, in particular in remote areas and in developing countries. However, this requires adequate power electronics and effective control strategies.

This paper presents a comprehensive review of on-grid/off-grid control strategies that can be found in the literature. A comparative study highlighting the advantages and drawbacks of the different control methods is given. Moreover, their control structures is discussed. Two main approaches can be distinguished for on-grid/off-grid WECS. The first one is by using two separate controllers, one for on-grid mode et the other for off-grid mode with the ability to smoothly transition between the two modes. The other approach is the unified on-grid/off-grid

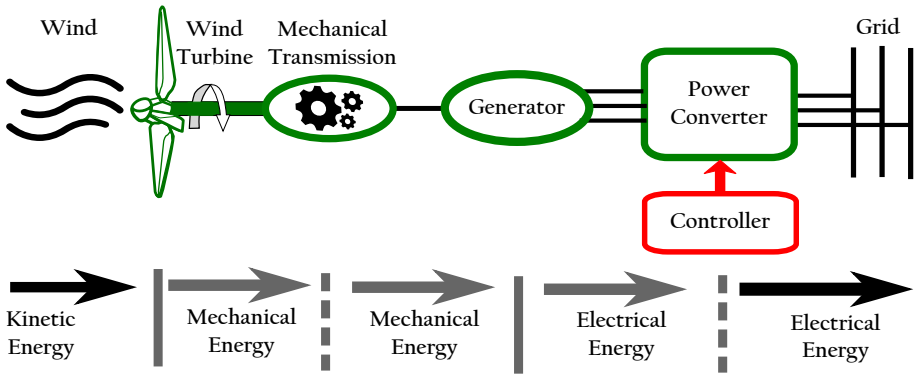

Figure 2.1: Wind Energy Conversion System (WECS).

control strategy which uses a single controller for both mode of operation.

The paper is organized as follows. First, in section 2.2, the background of WECS is explained. A literature review of on-grid/off-grid control strategies WECS is presented in section 2.3. Section 2.4 presents a case study. Finally a discussion on the advantages and disadvantages of the different control strategies is given in 2.5.

2.2 Wind Energy Conversion System (WECS)

2.2.1 Wind Turbine

Wind turbines are mechanical devices specifically designed to convert part of the kinetic energy of the wind into useful mechanical energy [20]. Several designs have been devised throughout the times. Most of them comprise a rotor that turns round propelled by lift or drag forces, which result from its interaction with the wind. Depending on the position of the rotor axis, wind turbines are classified into vertical-axis and horizontal-axis ones [21]. A schematic diagram of a basic WECS system is depicted in Fig. 2.1. The main components are the wind-turbine, the gear box, the generator, the power converter, the controller and the grid. A battery-storage unit is often used in the case of stand-alone WT system.

Fig. 2.2 shows turbine mechanical power as a function of rotor speed at various wind speeds. The power for a certain wind speed is maximum at a certain value of

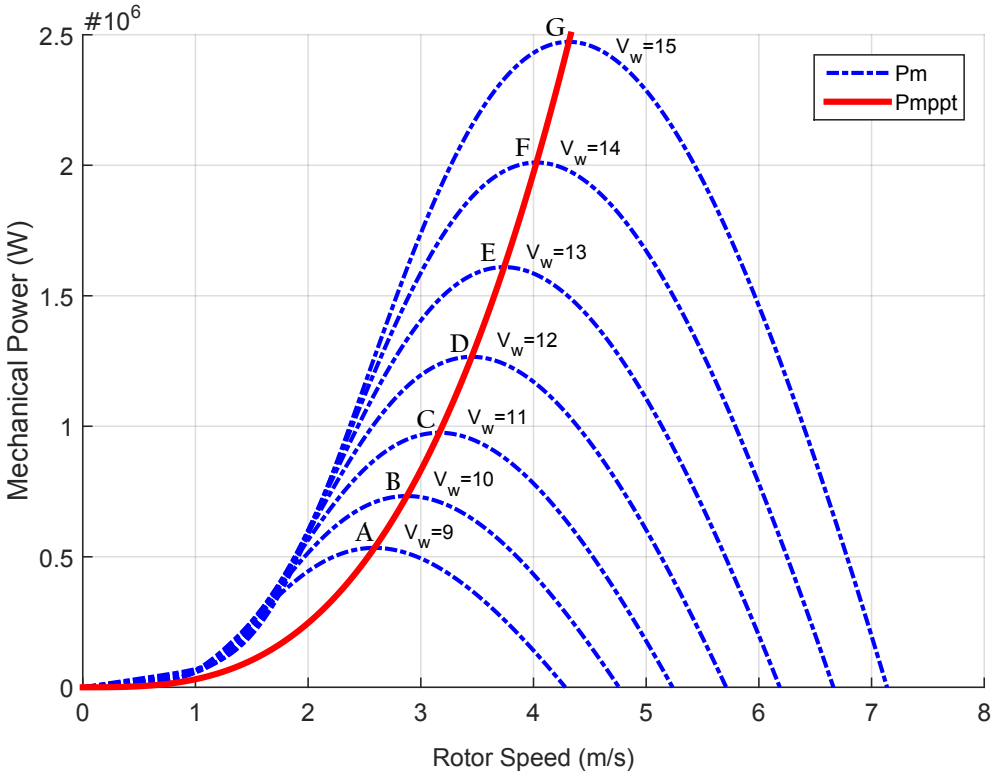

Figure 2.2: P_m as a function of rotor speed for various wind speeds.

rotor speed called optimum rotor speed ω_{mopt}. This is the speed which corresponds to optimum tip speed ratio λ_{opt}. In order to have maximum possible power, the turbine should always operate at λ_{opt}. This is possible by controlling the rotational speed of the turbine so that it always rotates at the optimum speed of rotation. A maximum power point tracking (MPPT) control methods survey has been provided in [22, 23, 24]

2.2.2 Generator

The type of machine used is important in WECS. Many industrial motors make effective and affordable wind generators. Three groups of generators are usually used for variable speed wind turbine systems: permanent magnet synchronous generator (PMSG), squirrel cage induction generator (SCIG) and doubly-fed induction generator (DFIG). The first group, PMSG, has the advantage of having

higher efficiency and smaller size, but more expensive. The SCIG are inexpensive, robust and can operate in any environmental condition. They are maintenance free generator due to the absence of brushes, commutators and slip rings. However, they require external reactive power support from the grid to operate. DFIG is three-phase variable speed generator. Its main advantage is its low power converter rating, which is lower than the generator rating. Hence, reduces the inverter and output filter cost. With DFIG, active and reactive power can be decoupled and

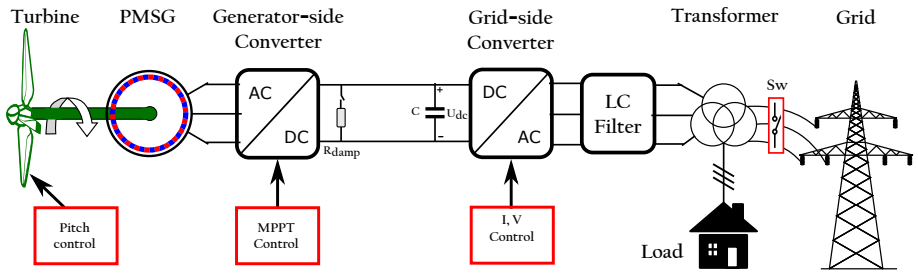

Figure 2.3: WECS based Permanent Magnet Synchronous Generator.

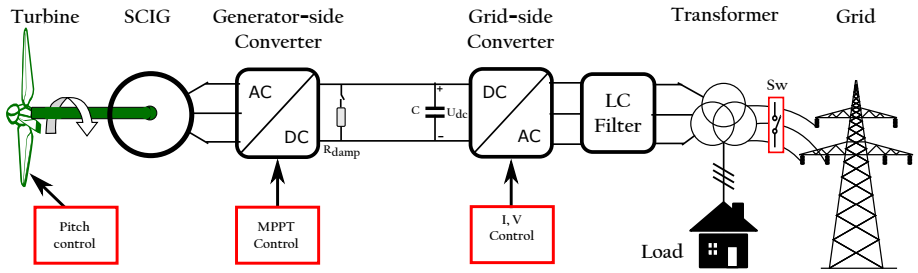

Figure 2.4: WECS based Squirrel Cage Induction Generator.

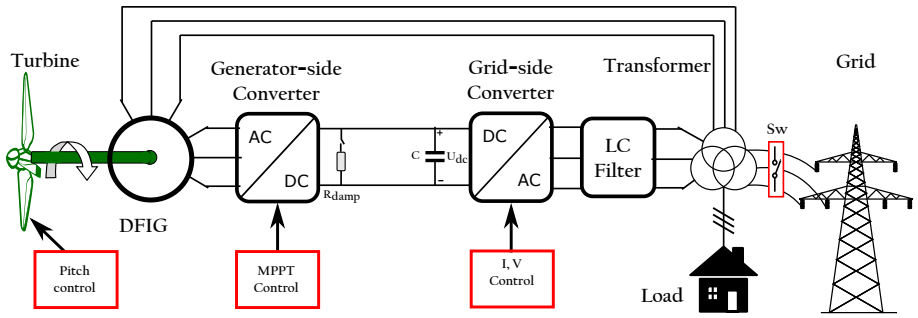

Figure 2.5: WECS based Double Fed Induction Generator.

controlled independently. However, this machine is very sensitive to grid faults. Depending on the type of generator and the power electronics converter configuration used in the WECS, a suitable controller is developed for its control. A detailed description and models of these generators can be found in [21].

2.2.3 Power Converters in WECS

Power converters have been widely used in industry for many different applications. According to the system power ratings and type of wind turbines, a variety of power converter configurations are available in the literature for the optimal control of wind energy systems. A review of the state of the art of power electronics for wind turbines can be found in [25, 26].

In on-grid/off-grid WECS applications, the back-to-back converter is mainly used. It is composed of two identical voltage source converters (VSC) connected by a capacitor. Fig. 2.6 depicts the back-to-back converter layout. As it can be seen, the power flow can be bidirectional. Therefore the VSC can operate as a rectifier or as an inverter. First, the AC is converted to DC through the generator side converter and then the DC is converted to AC through the grid-side converter. Therefore, the generator-side converter works as a rectifier and the grid-side converter works as an inverter. The DC-link voltage must be higher than the peak main voltage and it is regulated by controlling the power flow to the AC grid. In fact, one important property of the back-to-back converter is the possibility of fast control of the power flow [27].

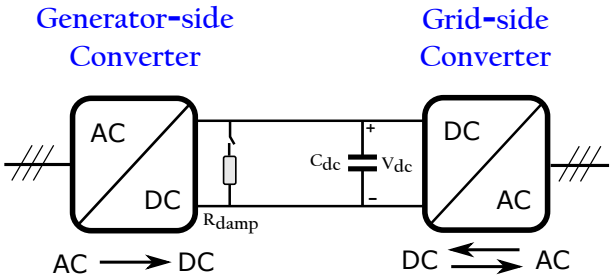

Figure 2.6: Back-to-back converter.

2.2.3.1 Generator-Side Converter

The generator-side converter (rectifier) is illustrated in Fig. 2.7. It transforms variable generator AC output voltage to an adjustable DC voltage. It also controls the speed/torque of the generator where the speed reference is chosen to be equal with the optimal speed in order to extract the maximum power from the wind turbine at a certain wind speed.

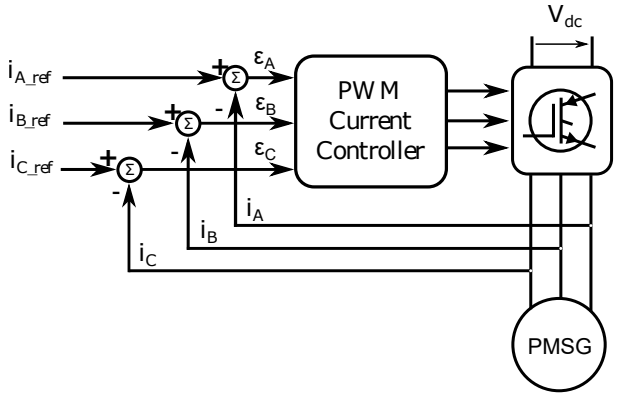

Figure 2.7: Basic block diagram of Current Controller PWM converter.

2.2.3.2 Grid-Side Converter

The grid-side converter is electrically similar to the generator-side converter, except for the presence of a line inductance L_f, which represents the leakage inductance of the transformer/filter. This converter controls the AC real current and AC reactive current feed into the AC grid in grid-connected mode. In case of grid unavailability, the controller makes sure that the terminal output voltage always matches the reference voltage of the load.

In off-grid mode, a battery storage unit is often used to store energy when there is more power generation than the load demand, as well as supply energy to the load on the other hand. This is described in the next section.

2.2.4 Bi-Directional Buck-Boost Converter Model

This converter operates as a boost converter during the discharging mode and as a buck during the charging mode. It is a bi-directional buck-boost converter. The dc-link voltage can be controlled through this converter rather than the grid-side converter like in the conventional method [28]. In general, its dynamic equation is derived from the power balance equation of the back-to-back converter.

There are two main operation modes of WECS: grid-connected and stand-alone. In recent years, more and more researchers have been studied the possibility of having an on-grid/off-grid WECS operation mode which is the focus of this paper. In the following, we give more details of these operation modes.

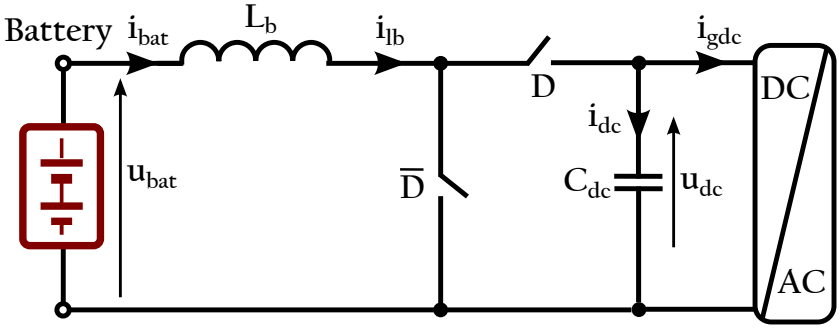

Figure 2.8: Bi-Directional Buck-Boost Converter.

2.2.5 Operating Modes of a WECS

2.2.5.1 On-Grid Mode

The majority of wind turbines operating in the industry are on-grid (or grid-connected) systems. Fig. 2.9 describes the on-grid WECS. It is mainly consist of a wind turbine, generator, power converter, utility meter and the grid. In this mode, the power generated is directly sent to the grid [21]. In addition, electric utilities, in many countries, allow net metering. It is an arrangement where the excess electricity generated by grid-connected WECS is fed back into the grid. And the costumer will be paid for every excess kilowatt hour.

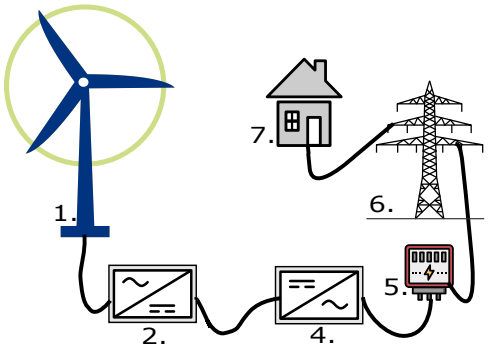

Figure 2.9: On-Grid WECS.

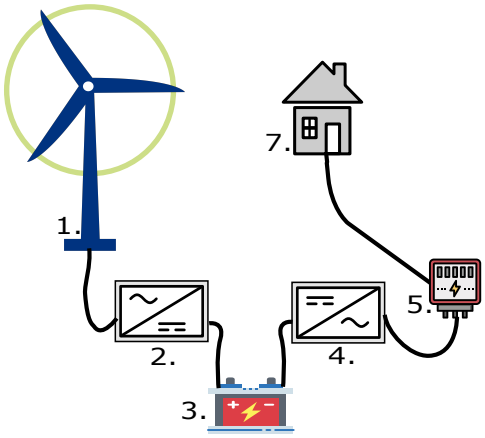

Figure 2.10: Off-Grid WECS.

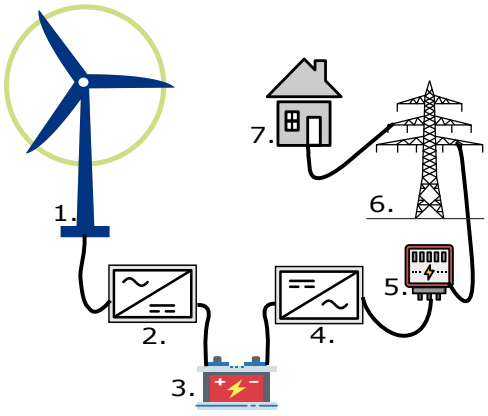

Figure 2.11: On-Grid/Off-Grid WECS.

The legend for Fig. 2.9, 2.10 and 2.11 is as follows: 1. Wind turbine, 2. Generator-side converter, 3. Battery bank, 4. Grid-side converter, 5. Utility meter, 6. Utility grid, 7. Load.

2.2.5.2 Off-Grid Mode

The wind turbine can operate as off-grid (or stand-alone) units. Fig. 2.10 describes the off-grid WECS. It is mainly consist of a wind turbine, generator, power converter, battery bank, utility meter, grid and load. They are usually small power capacity WECS to provide power to villages, farms, and islands where access to the utility grid is remote or costly [21]. But this system is also used by people who live near the grid and wish to obtain independence from the power provider or demonstrate a commitment to non-polluting energy sources.

Since the power generated from the wind is not constant, other energy sources are normally required in stand-alone systems. It is common that a stand-alone wind energy system operates with diesel generators, photovoltaic energy systems, or energy storage systems to form a more reliable distributed generation system [29].

2.2.5.3 On-grid/Off-grid Mode

On-grid/Off-grid WECS is a relatively new concept. As described in Fig. 2.11, it combines the two previous modes within one system. To better illustrate the concept, a more detailed on-grid/Off-grid WECS is shown in Fig. 2.12, where a back-to-back (B2B) power converter is employed with battery storage unit connected to the B2B converter DC-link trough a DC/DC converter. In the grid-connected mode, the switch Sw is closed and all of the produced power is sent to the grid. Whereas, in the stand-alone mode, the switch Sw is opened and the system supplies the critical local load only.

The basic concepts and WECS fundamentals and operation modes given in this section provide a technical background for the more advanced discussion in the other sections of this work.

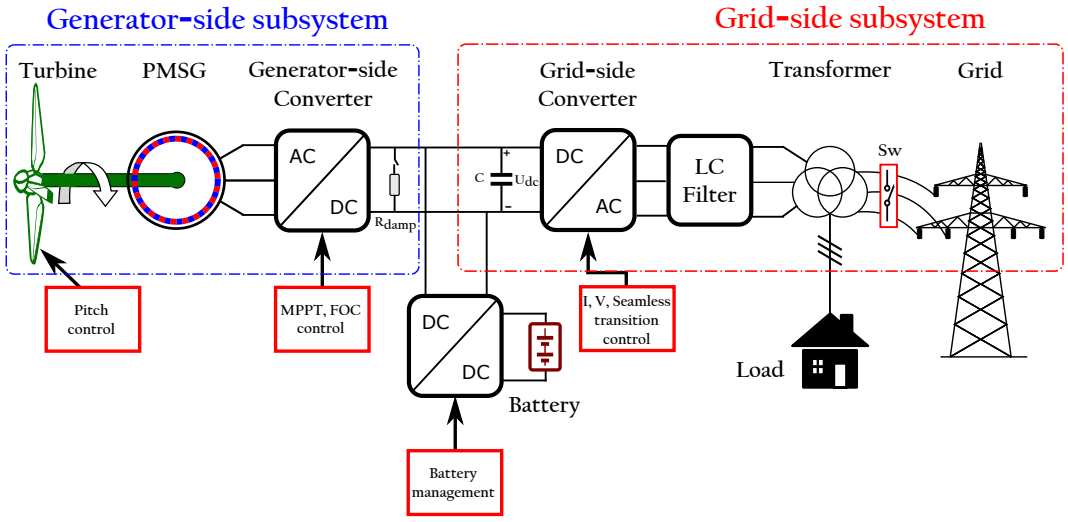

Figure 2.12: On-gri/Off-grid WECS based permanent magnet synchronous generator.

2.3 On-grid and Off-grid Control Strategies-Review

Their earliest usage of on-grid/off-grid control can be traced back to 2004, when a PI-based current/voltage control with a back-to-back converter for small wind turbines is proposed [16]. Since then, various studies with different PI-based and nonlinear control methods have been developed. The principle is that the grid-connected converter should be able to disengage itself from the grid and provides sustainable and high quality wind energy based power to emergency or critical loads during power outage. Moreover, the transition between the two modes should be smooth to minimize any sudden voltage change across the emergency or any sudden current change provided into the grid; also fast and precise to minimize the interruption in the power supply [17]. The main challenge to fulfill these requirements is a proper control algorithm, allowing to disconnect/connect grid-connected converter to utility grid without large shock [30].

In the following, we present a comprehensive study of on-grid/off-grid control strategies that can be found in the literature. Two main approaches can be distinguished. The first one is by using two separate controllers, one for on-grid mode et

the other for off-grid mode with the ability to smoothly transition between the two modes. The other approach is the unified on-grid/off-grid control strategy which uses a single controller for both mode of operation.

2.3.1 On-Grid Control

The purpose of the grid-side converter is to keep the DC-link voltage constant, regardless of the magnitude and the sign of the generator power.

In grid-connected control mode, all the available power that can be extracted from the wind turbine is transferred to the grid. Various current algorithms have been proposed in this regards. In addition, the grid-side converter must keep the DC-link voltage constant, regardless of the magnitude and the sign of the generator power. Also, reactive power compensation can be considered if required [16].

2.3.1.1 Synchronous PI current controller

The synchronous PI based current control is the most widely used algorithm for grid-connected and stand-alone converter control. Fig. 2.13 illustrates its basic concept, where two PI compensators of current vector components, defined in synchronous coordinates d-q, are used. The role of these compensators is to reduce the error between the reference current signals and measured ones to zero.

References [31, 32] propose concepts and tests results on a flexible sensorless control strategy for a PMSG driven by a small wind turbine with back-to-back power converters capable to function in both stand alone and grid connection mode. In grid-connected mode, the grid-side converter is current PI based controller with direct axis aligned to grid voltage vector, enabling independent control of the active and reactive power. Furthermore the paper investigates the ride-through performance of the proposed system during asymmetric power grid-voltage sags. A PMSG microturbine-based distributed generation system is also used in [33].

In [33], a dynamic model of a PMSG system, suitable for grid connection/islanding operation has been presented. A B2B converter is used as power electronic interface allowing a bidirectional power flow between the grid and PMSG system. The

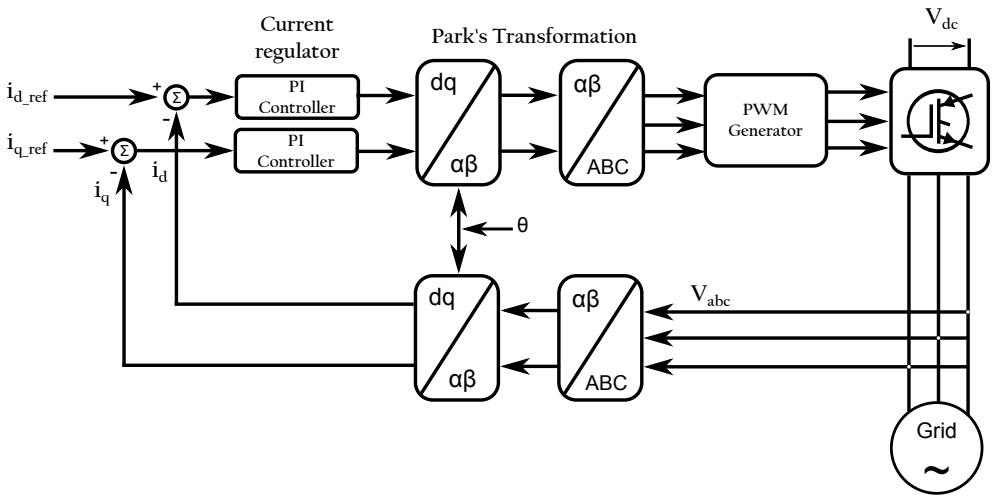

Figure 2.13: Synchronous PI controller in dq reference frame components.

machine-side converter controls the PMSG speed and displacement factor using synchronous PI current control PWM modulation technique. However, a gas turbine is used as a motor in this work instead of WT. Thus a stochastic behavior of WT was not at all a constraint in this case.

The authors in [16] use a SCIG as generator and standard PI-controllers for the grid currents control. The control method has one inner loop, to regulate the grid currents in the dq-synchronous frame, and one outer loop for the dc-voltage.

A modified SVPWM-based switching pattern for stand-alone and grid-connected three-phase single-stage boost inverters has been proposed in [34], using the topology of current-source inverters. The six main switching states, and two zeros, with three switches conducting at any given instant in conventional SVPWM techniques are modified into three-charging states and six discharging states with only two switches conducting at any given instant. But, this proposed method is particularly for small PV and fuel cell applications (output voltage 35V) with low switching frequency (3 kHz).

Several others PI-based grid-connected and stand-alone operations control, for DC/AC grid connected converter, have been recently reported [17, 35, 36, 37]. However, these techniques are purely oriented on power electronics (only grid-side converter control) and do not take into account the source of the DC voltage. The

main disadvantage of synchronous PI current control is that it does not guarantee optimal control of the system.

2.3.1.2 Droop Controller

The concept of current and frequency droop control is to use the active and reactive power exchange between a WE generator and the grid to control the grid current magnitude and frequency.

Several techniques of droop control have been proposed in the literature for active and reactive power control [38, 39, 40, 41]. In [39] an adaptive droop control with grid parameters estimation provided by an identification algorithm has been developed. Hence, the grid-side converter is able to injected independently active and reactive power to the grid. But this algorithm does not consider the dynamic of the primary energy source which leads to a fall-short in achieving seamless transfer between grid-connected and isolated microgrid modes. Fig. 2.14 depicts the control model where P and Q are first transformed into novel variables Pc and Qc respectively which are independent from the magnitude and phase of the grid impedance. Some techniques for detecting the grid parameters can be found in [42, 43, 44, 45, 46].

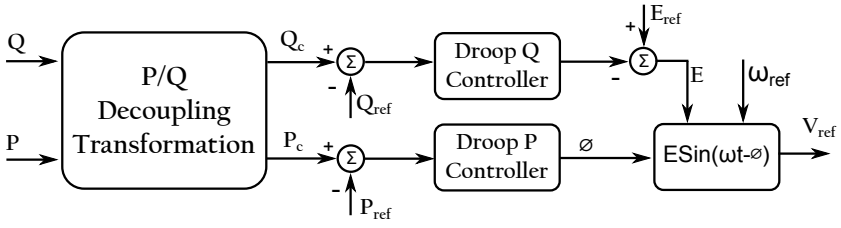

Figure 2.14: Block diagram of droop controller.

2.3.1.3 Hierarchical Controller

The hierarchical control structure is widely accepted in on-grid/off-grid WECS applications. In [47] a hierarchical control system of distributed generation converters for microgrid operation and seamless transfer between grid-connected and isolated modes has been reported. The proposed control scheme is given in Fig. 2.15. Other hierarchical controls are reported in [48, 49, 50, 51, 52, 53, 54]. However this control technique suffers from weak disturbance rejection performance [55].

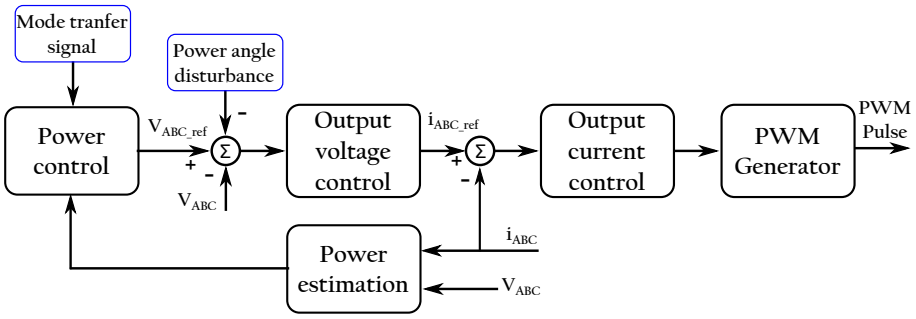

Figure 2.15: Block diagram of hierarchical controller.

2.3.1.4 Hysteresis Controller

Various hysteresis control methods are reported in the literature to control the current of the grid-side converter in grid-connected mode [56, 57, 58, 59, 60]. The hysteresis control has advantages of automatic peak-current limitation, simple implementation, load parameter independence and good stability [61, 62]. In grid-connected mode, the hysteresis controller is used to control the active and reactive power as described in Fig. 2.16.

2.3.1.5 Feedback Linearization Controller

Feedback linearization is an approach of nonlinear control design which has attracted increasing attention over the last two decades. The controller structure

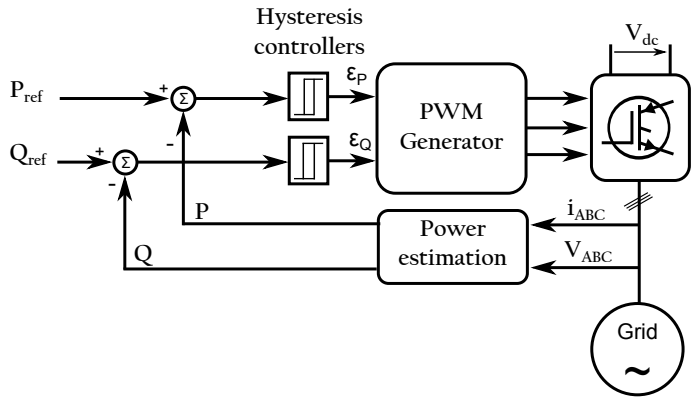

Figure 2.16: Block diagram of hysteresis controller.

is illustrated in Fig. 2.17. The main idea of this approach is to algebraically transform a nonlinear system dynamics into a fully or partly linear system, so that linear control techniques can be applied [63]. Feedback linearization approach has been successfully applied to a number of practical control problems including WECS [64, 65].

Author [64] studied a low-voltage ride-through control scheme for a PMSG wind power system using a combined PI-based and input-output feedback linearization control method. In the proposed method, the DC-bus voltage is controlled by the generator-side converter instead of the grid-side converter. However, the feedback linearization theory based controller is employed only to control the dc-link voltage. The other control signals such as the generator current, grid current and grid power are controlled by using a sequential PI controller. Thus, the nonlinear control

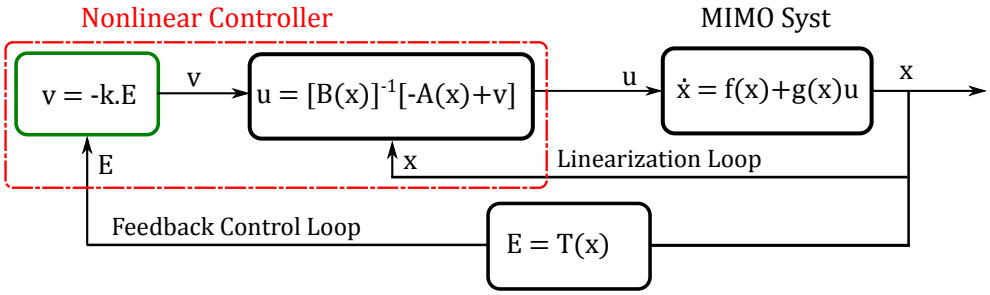

Figure 2.17: Proposed MIMO controller structure.

system is a SISO (single input, single output) model with the generator power as input and the DC-bus voltage as output.

Some proposed MIMO (multiple input multiple output) feedback linearization methods for UPS converter and hydraulic turbine applications can be found in [66, 67, 68] and [69] respectively. After the system is linearized, the tracking control law is obtained by using pole placement technique. The resulted control scheme gives high dynamic responses to load variation as well as a zero steady-state error. However, despite the advantages of the feedback linearization method, the fact that important intuition might be lost with the linearization can be seen as a disadvantage.

2.3.1.6 Sliding Mode Control

Sliding mode control is a variable structure control method which provides a systematic approach to the problem of maintaining stability in the presence of modeling imprecisions [63]. This nonlinear control method has been used for WECS in [70, 71, 72]. Reference [70] studied a power control strategy for a grid-connected variable-speed wind turbine, based on a doubly-fed induction generator (DFIG) with slip power recovery. The control design, based on the second-order sliding modes (SOSM) and Lyapunov with variable gains, is applied to nonlinear MIMO systems. In [71], a direct drive synchronous generator driving by a wind turbine with a back-to-back converter via a sliding mode control approach has been proposed. The objective is to avoid the increase of the grid current when network fault occurs. However, the drawback of using sliding mode control for high frequency power converter applications is the diversity of the switching frequency [73]. This can lead to a high THD (Total Harmonic Distortion) generation in the case of grid-connected/stand-alone control system.

2.3.1.7 Backstepping Control

The backstepping control method proposes a stepwise control design of a system based on a Lyapunov stability function. Author [74] came up with a robust adaptive nonlinear controller using backstepping approach for a Doubly-Fed Induction Generator (DFIG) wind turbine supplying a power grid. As grid parameters are assumed unknown, the controller is provided with an adaptation module that automatically readjusts the controller parameters when the grid condition changes. In [75], a backstepping power control design is proposed for the grid-side voltage source converter in a voltage source converter-based high-voltage DC wind power generation system. The method was compared with the traditional PI-based control strategy under a wide range of operating conditions and the possible occurrence of uncertainties. A sensorless control system of permanent magnet synchronous motor fed by current source inverter is presented in [76]. The adaptive backstepping control system and the backstepping speed observer are employed. The DC-link voltage and the output current vector pulsation are used as control variables. However, a disadvantage of this control method might be the exact knowledge of the nonlinear system model.

2.3.2 Off-Grid Control

In the off-grid (or stand-alone) mode, since the grid does not exist and the power generated from the wind is not constant, storage unit becomes necessary [77]. The role of the latter is to compensate or absorb the difference between the generated wind power and the required load power. This significantly reduces the grid contribution to the system. A system that contains multiple sources are known as hybrid power systems [78]. They require a suitable energy management strategy. In this mode, the load voltage is regulated (voltage control) in terms of amplitude and frequency by the grid-side converter with its phase dictated by the converter controller [17, 16, 79]. The transition between stand-alone and grid-connected operations, that will ensure continuous power delivery to the load, requires continuation in the phase of the system voltage [17]. Voltage control has been largely investigated and analyzed in literature. The basic block diagram is presented in Fig. 2.18.

2.3.2.1 PI-based Voltage Oriented Controller

The control scheme of the conventional voltage oriented control for stand-alone mode is given in Fig. 2.19. A standard PI controller operating in the synchronously rotating coordinate system, where Vq is kept to zero, is used. The PI controller maintains the dc voltage to the reference. The dc-link voltage controller is acting only when the dc-link is below the reference and it lowers the voltage reference of the main voltage controller in order to avoid inverter saturation. For fast response there is a direct forward connection to the voltage controller output [80].

In stand-alone mode, a PI-based voltage oriented control scheme with selective harmonic compensation has been reported in [31, 33, 32, 35, 38]. The PMSG motion-sensorless control system uses an active power controller and a PLL based observer to estimate the rotor position and speed without using the emf integration and initial rotor position. In [80], a PI-based grid-side converter output voltage control and dc-link voltage control have been presented with a minimal influence from the shape of the load currents or load transients. A PMSG is used as generator.

The reference [16] use a SCIG as generator and standard PI controller operating

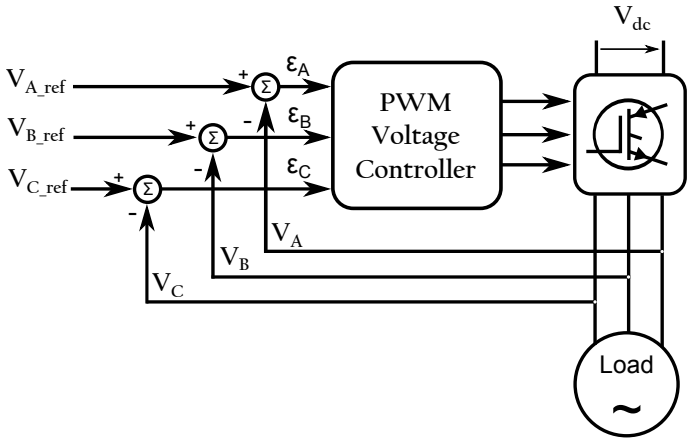

Figure 2.18: Stand-alone mode: grid-side converter voltage oriented control.

in the synchronously rotating coordinate system where Vq is kept to zero is used. The dc-voltage PI controller maintains the dc voltage to the reference. In addition, a damp resistor is employed to dissipate potential excess of power in the case of unbalance between the generated and the load-required power. As it has been said earlier, the disadvantage of synchronous PI voltage control is that it does not assure optimal control of a nonlinear system.

2.3.2.2 RMS Voltage Controller

RMS voltage control has been used in [17], for the SA converter operation. Fig. 2.20 shows the RMS voltage control method of the SA converter. The PI controller produces the right amount of inverter RMS voltage, and the result is multiplied with a sinusoidal variation based on the estimated utility phase. The PWM signals are generated from the reference sine-wave voltage for the inverter to produce the desired output voltage. This type of control method has the advantage of providing stable output voltage in the steady state, but transient performance may not be adequate for aggressive load transients [81] and [82] such as starting compressor-driven loads.

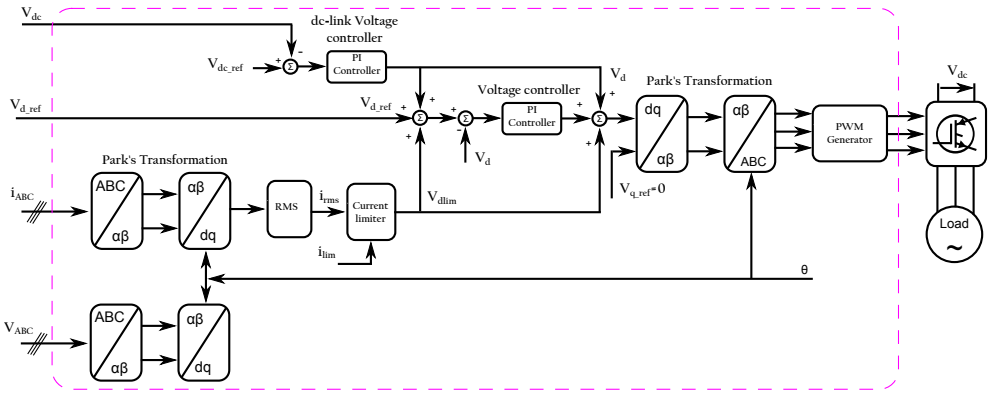

Figure 2.19: Grid-side converter voltage oriented control for stand-alone mode.

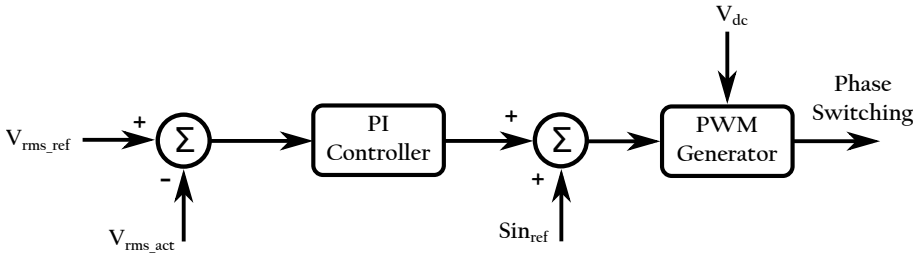

Figure 2.20: Basic block diagram of RMS voltage controller.

2.3.2.3 Instantaneous voltage controller

The block diagram for the instantaneous voltage control of the SA Converter is shown in Fig. 2.21. This regulation technique provides more aggressive control during transients [83]. However, the compensator is more difficult to design especially in the presence of noisy analog measurements [36]. In [84], an instantaneous voltage control has been used for DC/AC converter with three phase output using a PWM cycloconverter which converts a high frequency voltage into a three phase commercial frequency voltage in SA mode.

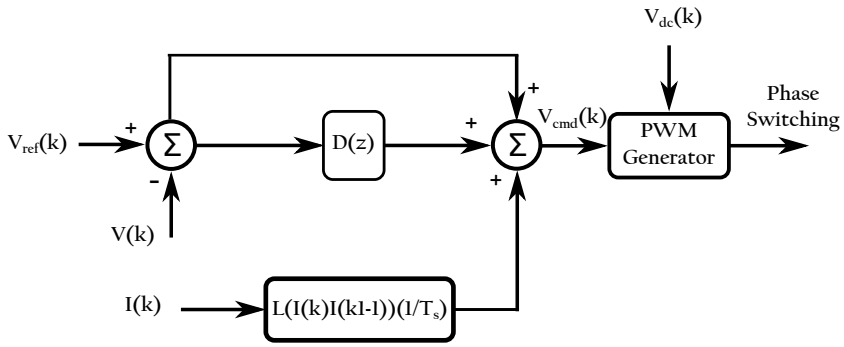

Figure 2.21: Instantaneous voltage controller for SA mode.

2.3.2.4 Multiloop Voltage Controller

References [85, 86, 87] investigate a multiloop voltage controller for SA mode with voltage differential feedback, and with output voltage decoupling and output current decoupling by using the output voltage feedback as shown in Fig. 2.22. The decoupling of output voltage and current makes the inner loop equivalent to a first-order system and thus improves to the system a better load disturbance rejection capability. However, this controller has high requirement for the accuracy and dynamic performance of the current sensor because filter capacitor current is small-scale. The pole placement technique has been used to design the inner loop and outer loop gain, with considering the effect of system control delay.

2.3.2.5 Time averaged approach voltage controller

A voltage source converter control is presented, based on time-averaging theory [88] in the synchronous reference frame [46]. In this method, the terminal voltage during the sampling interval from time $t = nT$ until $t = (n+1)T$ are approximated by

$$V_d(nT) \approx d_d(nT)kV_{dc} \text{ and } V_q(nT) \approx d_q(nT)kV_{ac} \tag{2.1}$$

Where k is the converter constant and $d_d(nT)$ and $d_q(nT)$ are the d- and q-axis duty cycles, subject to the constraint

$$d_d{}^2(nT) + d_q{}^2(nT) \leq 1 \tag{2.2}$$

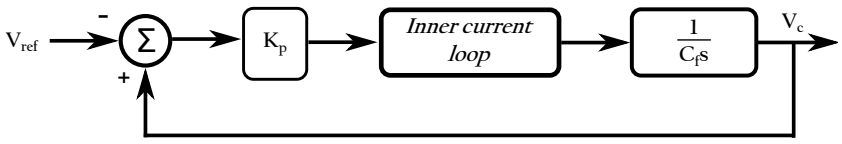

Figure 2.22: Multiloop voltage controller.

2.3.2.6 Predictive voltage controller

The predictive voltage controller offers a good reference tracking with less voltage harmonic distortion for balanced, unbalanced and nonlinear loading conditions [89, 90, 91, 92, 93, 94, 95]. A PI-based predictive voltage controller with a feed-forward voltage compensator is developed for a single phase Uninterruptible Power Supply (UPS) inverter of a stand-alone wind turbine system in [96, 97, 98]. In this scheme Dead-Time (DT) compensator is also used as volt-second compensation which is based on the well-known instantaneous average voltage method. The basic principle is to compensate for the average loss or gain of voltage per carrier period [99]. Fig. 2.23 shows the control diagram of this control technique. Within each control period, the system samples the inverter output voltage V0 and passes back to the predictor. This yields a predicted output voltage $V_0{}'$ for the next PWM period. Assuming the sampling period T is so tiny that the changes of the voltage could be regarded as linear. By using a simple linear extrapolation, we get:

$$V_0{}' \approx V_0[n+1] \approx (V_0[n] - V_0[n-1]) \tag{2.3}$$

$$V_0{}' \approx 2V_0[n] - V_0[n-1] \tag{2.4}$$

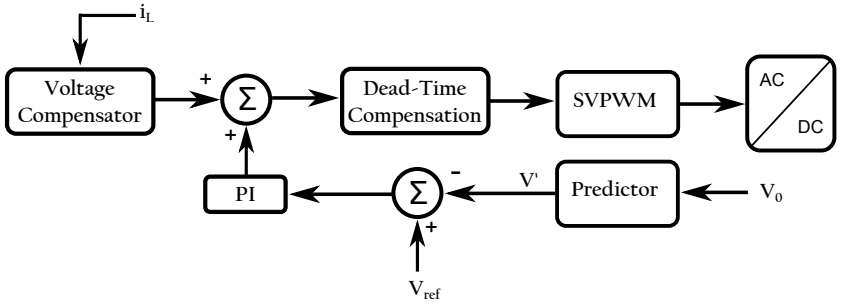

Figure 2.23: Predictive voltage controller.

2.3.3 Seamless transition control

In order to realize the seamless transfer between grid-connected and stand-alone modes, the load voltage must match the magnitude, frequency, and phase of the

grid voltage well before connecting to the utility. This is called the grid synchronization. The load voltage can match the grid voltage well through sampling the grid voltage as the reference voltage before connecting to the grid, especially in polluted grid voltage [33]. On the other hand, when the grid comes back, the system should be able to detect it automatically and then connect to it - anti-islanding detection - without any interruption. Thus, the grid synchronization and anti-islanding detection are the two main important parts of seamless transition period of time.

Reference [32] and [100] present a novel seamless (without load current interruption), PLL-method for automatic switching from the grid to the load, when the grid is disconnected and back to the grid when the latter is restored. The control strategy is applied on a PMSG driven by a small wind turbine with back-to-back power converters. In [34] a modified seamless transfer control method for single-phase grid-side converter, with no transfer between grid-connected and stand-alone modes controller, has been proposed.

2.3.3.1 Grid synchronization

In transition mode, the wind energy generator system is synchronized to grid thanks to the phase tracking module. Therefore, in the grid-connected mode, the grid frequency ($_g$) which is used in the dq-abc coordinate transformation is generated by the phase tracking module. However, in the stand-alone mode, $_g$ is generated internally by the controller. Several algorithms have been proposed [101, 102, 103, 104, 105, 106]. The easiest phase tracking algorithm is one which is based on zero crossing detection. However, the latter suffers from noise and higher order harmonics in the utility voltage; also, from speed, as it adapts to utility phasing only twice [107]. Furthermore, it can be only used when the input is a stable signal. [106].

The Phase-locked loop (PLL) techniques have better performance in tracking of the grid phase even in the presence of higher order harmonics in the grid volt-

age. But, PLL performance might decrease in the presence of unbalance in the grid voltage [81].

2.3.3.2 Anti-islanding Detection

Based on IEEE-1547 standards, all distribution generation systems must be disconnected from an islanded grid in a specified time [108, 109]. Thus, the anti-islanding detection algorithm should provide to the grid-connected converter, the ability to disconnect itself from the grid if the grid is interrupted for any reason. In the literature, a number of anti-islanding control methods have been suggested to the presence or interruption of the grid [108, 110, 111, 112, 113, 114, 115].

2.3.4 Unified On-Grid/Off-Grid Control

In all the aforementioned works, two distinct controllers are used for the system. One controller is used for the on-Grid mode and another one for the off-Grid mode. An islanding detection module is needed in these cases to take the decision to switch between the two controllers. More recently, researchers have been investigating the notion of the unified on-grid/off-grid control strategy. In this approach, a single controller is used for both modes of operation contrary to the other control methods. In [116], a unified control strategy of a three-phase inverter in uninterruptible power supply (UPS) applications was presented. The inverter operates as a current source in a grid-tied mode and as a voltage source in a stand-alone mode. PI controllers is used in the paper. A PI-based unified on-grid/off-grid energy management strategy for wind energy battery-storage system has been proposed in [117]. Authors in [28, 118, 119] propose a unified robust nonlinear control method for a wind energy battery-storage system that can operate in both grid-connected and stand-alone modes. The design method is based on the MIMO feedback linearization control technique. A back-to-back (B2B) power converter is used to connect the WECS to the grid and the load. In addition, a bi-directional buck-boost DC/DC converter is used to regulate directly the dc-link voltage and

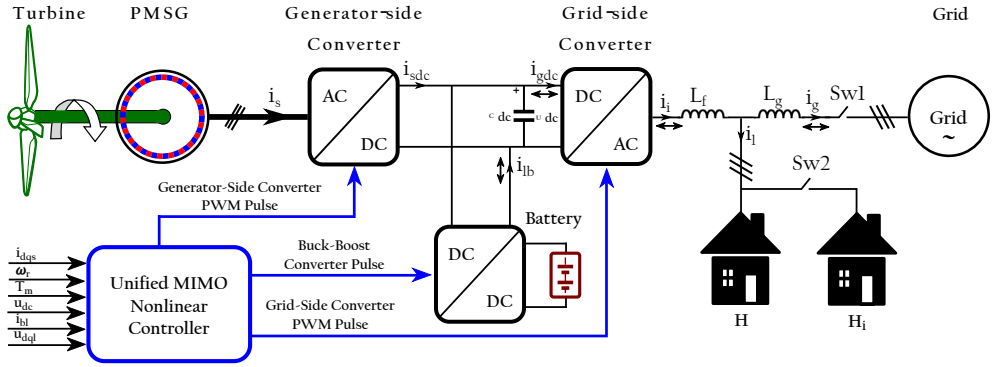

Figure 2.24: Proposed MIMO controller structure.

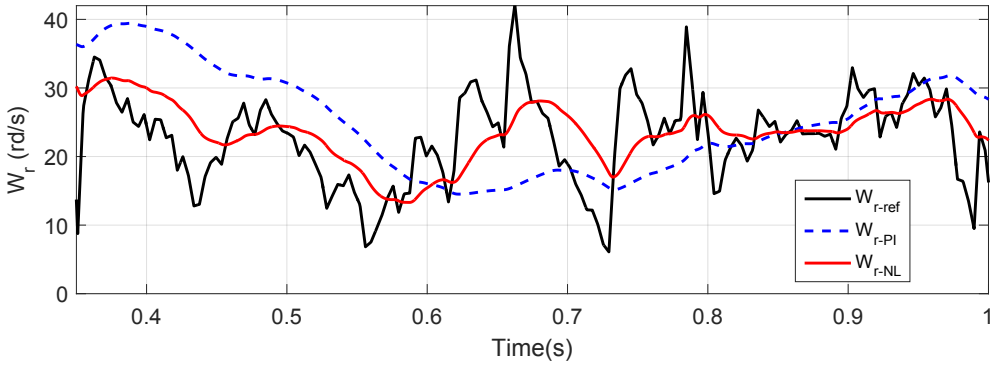

Figure 2.25: Unified Nonlinear Control based: Optimum Rotor Speed.

the load active power based on the energy balance and the system stability. The unified MIMO controller is able to calculate and generate the appropriate control signals for each converter. To validate and demonstrate the robustness the proposed control method, different types of loads are used, namely, 1) a balanced three-phase load, 2) an unbalanced three-phase load, 3) a single-phase nonlinear load, and 4) a dynamic load. Fig. 2.24 illustrates the structure of the proposed MIMO controller.

2.4 Case Study

A case study has been performed to compare a synchronous PI controller to a nonlinear feedback linearization-based controller using real wind speed data [120].

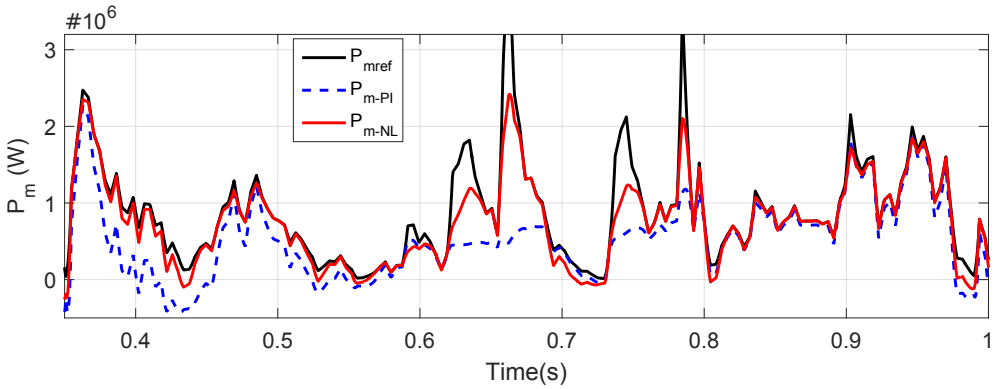

Figure 2.26: Unified Nonlinear Control based: Output Power.

The on-grid/off-grid WECS system consists of a 2.45 MW wind power generator supplying a $2MW$ nonlinear variable load. A variable speed nonsalient-pole PMSG is employed as generator. A back-to-back converter (AC/DC/AC) and a bi-directional buck-boost (DC/DC) are utilized to connect the generator and the grid to the load, and the battery-storage-unit to the dc-link voltage, respectively. The dynamic and steady-state performances of the system when it switches from one mode of operation to another is evaluated. The simulation starts with a stand-alone mode and switches in the grid-connected mode at time $t = 0.7$ sec. Fig. 2.25 and 2.26 show the generator rotor speed and output power, respectively. The black solid line, the dashed line and the red solid line stand for the reference signal, the signal for the PI controller and the signal for the nonlinear controller, respectively. It can be observed that the nonlinear controller has a fast and better dynamic behavior as well as a good tracking performance than the synchronous PI controller.

2.5 Discussion and Conclusion

We have seen through Section III that initially most of on-grid/off-grid converter control algorithms which have been developed are employed in UPS (Uninterruptible Power Supply) applications, where the primary energy source does not have stochastic nature as in the case of wind energy source. In recent years, more and

more studies have been undertaken to explore on-grid/off-grid control for wind turbine applications. Which has risen new challenges. Among them the controller has to be more faster and suitable in order to limit the converter current rise below the permitted limit during the islanding and the grid detection period. However, most of current control approaches for on-grid/off-grid WECS employ classical PI control methods as shown in Table 2.1 where a summary of the different control strategies discussed in this paper is given. The PI-based controllers have the advantage of being simple and easy to implement. On the other hand, they have some drawbacks that limit their effectiveness, in particular in high order MIMO nonlinear control systems such as WECS: (1) They are insensitive to systems having highly nonlinear components. Thus, in the presence of the high system nonlinearity, they may fail to provide sufficient control performance [11]. (2) They work best with SISO systems. In fact, with SISO systems, there is only one variable to control and only one actuation to apply. MIMO systems may be controlled with PID controllers by means of a sequential structure of a number of SISO PID controllers. However, this technique is not easily implemented. Because it implies the tuning of a number of coupled PID controllers. As the PID controllers are used sequentially, a wrong signal produced by one controller could lead the entire system to instability [12]. (3) They have very poor transient response and weak disturbance rejection because of the integral action. Thus, the integral action increases the oscillations in the output of the closed loop systems. Despite the fact that it helps to eliminate the steady state error. (4) They have difficulty to limit the converter current rise below the permitted limit during the islanding and the grid detection transition period [16]. (5) Another challenge for PID controllers is the tuning of the controller gains. Although Matlab provides an automatic tuning option. However, this does not usually result in an optimal overall system performance because stability is a concern. And tuning for better performance might lead to losing control over the system [12]. Several techniques have been proposed to improve PID behavior and system performance, such as increased loop rate and gain scheduling. However, one drawback with the latter is that PID gains tuning is required for the different operating points. The transition

between two operating points may lead to instabilities.

One of the ways to control the load voltage in islanding mode is by using predictive voltage control method. This strategy has a good reference tracking, but requires high computational resource to be implemented. It also requires a very well known model of the system.

Nonlinear control based methods such as feedback linearization control appear to be more suitable control strategy for on-grid/off-grid WECS. Feedback linearization control has the advantage of being able to both stabilize the nonlinearities of the system and also tracking many control reference signals (in MIMO control system configuration). Also, it allow the user to have a complete decoupled control system where each control variable can be controlled independently. In addition, in contrast to traditional PI-based method, is that it is possible to reduce the number of controlled variables with feedback linearization control method. In traditional schemes, at the generator-side, the generator active power and rotor speed are controlled through three variables (d-axis, q-axis of the generator stator current and the rotor synchronous speed) in cascade. Adding to that, three other variables (d-axis, q-axis of the grid-side converter current and the DC-voltage) are used to control the active/reactive power and DC-link voltage, at the grid-side. In contrast, in the feedback linearization method, only four variables are needed (instead of six) to perform the same task either it is in on-grid or off-grid operation mode. This helps for better control efficiency, providing fast response time and tracking capability. The two later are essential to insure a smooth transition between the two modes of operation.

The nonlinear unified on-grid/off-grid control approach appears to have the best performance compare to other approaches. It has the advantage off being nonlinear control method, hence being able to cancel all nonlinearities in the system. In addition, there is no need for switching between two different controllers, contrary to previous methods. Moreover, an islanding detection module is not necessary [121, 122] as the same controller can perform the MPPT, power management and load voltage control, regardless of the mode of operation. Therefore, problems related to the islanding detection, such as poor dynamic performance

[123, 38], poor load current waveform quality [124, 125] and inrush grid current [126] during the transition of operation mode, can be avoided.

Table 2.1: On-Grid/Off-Grid Control Methods Summary

Control Methods	**Advantages**	**Disadvantages**
Synchronous PI current	Simple implementation, suitable for SISO systems	Not optimal, use lookup table, multiple loops
Droop	Control independently active and reactive current	Mainly used for UPS applications, low seamless performance
Hierarchical	Simple implementation, Can limit peak-current	Multiple loops
Feedback linearization	Suitable for nonlinear systems, decoupled control system, stabilize MIMO systems, high dynamic responses to load variation, better efficiency	Might loss some dynamic performance with the linearization
Sliding mode	Suitable for imprecise systems	Low performance for high frequency converter applications, low THD reduction
Backstepping	Suitable for MIMO and nonlinear systems	Low load transients performance
PI-based voltage oriented	Simple	Not suitable for nonlinear systems
RMS voltage	Good steady state stability	Not adequate for aggressive load transients
Instantaneous voltage	Good aggressive load transient stability	Difficult to design for system of noisy analog measurements
Multiloop voltage	Good load disturbance rejection capability, require high accurate current sensor	Tuning of multiple gains
Predictive voltage	Good reference tracking, low voltage harmonic distortion for balanced, unbalanced and nonlinear loading conditions	Require high computational resource, low performance when the model of the system is not very well known
PLL grid synchronization	Simple to implement, good performance in tracking of grid phase	Not suitable for unbalance grid
Zero crossing detection	Simple to implement, good performance in tracking of grid phase	Suffer from noise and higher order harmonics in the grid voltage, required stable input signal

Chapter 3

Performance Comparison of Variable Speed PMSG-based Wind Energy Conversion System Control Algorithms

Abstract

This paper presents a comparative analysis of three control algorithms for a wind turbine generator using a variable speed permanent magnet synchronous generator (PMSG). The design methodologies of the conventional PI-based controller, the Taylor series expansion linear approximation based (TSLA-based) controller and the feedback linearization based (FL-based) nonlinear controller are provided. The objective is to keep the wind turbine operating at its optimum rotor speed (MPPT control), while insuring the power transfer from the turbine to the generator, regardless of the wind speed. The controller gains of the nonlinear controller are determined via Linear Quadratic Optimal Control (LQOC) approach. The results show a better control performance for the nonlinear controller. This performance is characterized by fast and smooth transient responses as well as a zero steady state error and reference tracking quality.

Index terms— Feedback linearization, multi-input muti-output controller, optimal control, permanent magnet synchronous generator, Taylor series expansion, wind turbine.

3.1 Introduction

Wind energy is one of the fastest growing renewable energy technologies. At the end of 2015 its global power capacity was around 433 Gigawatts (GW), representing cumulative market growth of more than 19%, an excellent industry growth rate given the economic climate [127].

Wind-turbine systems can work in two modes of operation: grid-connected and stand-alone. However, the majority of them operating in the field are grid-connected. In this mode, the power generated is directly uploaded to the grid [21]. When WT are not generating enough energy in low wind time intervals, electricity from the grid supplies costumer needs. WT in stand-alone mode are usually employed as small power capacity to power homes, farms, and isolated areas where access to the utility grid is remote or costly. Since the power generated from the wind is not always available, other energy sources are commonly required in stand-alone systems. It is common that a stand-alone wind energy system operates with diesel generators or energy storage systems to form a more reliable distributed generation (DG) system.

Due to their random nature, wind-turbine systems are characterized by an unpredictable output. Hence, a suitable control system is required to ensure a good system dynamic behavior and an efficient extraction of the power from a wind turbine. This has been the subject of several recent research investigations. Most of the proposed control methods for WECS in the literature employed the conventional PI-based control method with different techniques [128, 129, 130, 131].

Methods of nonlinear control that use input-output feedback linearization method for WECS have been reported in [119, 64, 65]. Feedback linearization control method has the advantage of being able to be used to both stabilize a nonlinear system, such as WECS, simultaneously tracking many control reference signals. Also, it allows the user to have a complete decoupled control system where each variable can be controlled independently.

The type of machine used is one of the most important part of the wind energy conversion system (WECS). Many industrial motors make effective and affordable

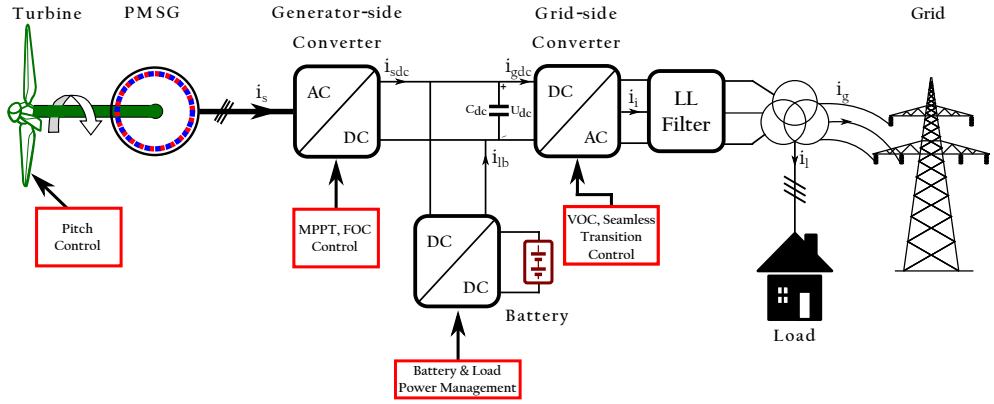

Figure 3.1: WECS based permanent magnet synchronous generator.

wind generators. Three groups of generators are usually used for variable speed wind turbine systems: permanent magnet synchronous generator, squirrel cage induction generator (SCIG) and doubly-fed induction generator (DFIG). Depending on the type of generator and the power electronics converter configuration used, a suitable controller is developed [21]. The most preferred option for variable speed wind turbine are the direct-drive PMSG and DFIG. PMSG has the advantage of having a very wide speed variation range (0-100% of the rated speed), high efficiency and high power density, due to its rare earth metal-based permanent magnets. This yields to a compact direct-drive small-scale wind turbine with capability to operate at very low-speed.

In this paper, feedback linearization is adopted as a design approach of the nonlinear MIMO controller. Moreover, optimal control technique is used to calculate the feedback gains. In contrast to pole placement technique, using optimal control allows us to assign one cost function to whole system. Hence a better control performance. The challenge is to control the generator's current and rotor speed at the same time through MIMO configuration instead of sequentially, while ensuring the operation of the system at its optimum rotor speed allowing the extracting of the maximum power from the wind turbine.

This paper is organized as follows. First, in Section 3.2, the WECS dynamic model depicted in Fig. 3.1 is described. Section 3.3 is dedicated to the design of the controllers. The simulation results are presented in Section 3.4. Finally, we

conclude with Section 3.5.

3.2 Wind Turbine System Dynamic Modeling

3.2.1 Wind Turbine

The wind turbine converts part of the kinetic energy of the wind into useful mechanical energy. Its generated mechanical power can be express as follows [119]:

$$P_m = \frac{1}{2}\pi\rho C_p(\lambda,\beta)R^2 v_w^3 \tag{3.1}$$

where ρ is the air density, C_p is the power coefficient, which is a function of λ, the tip speed ratio and β, the pitch angle. R is the radius of the turbine and v_w is the wind speed.

The tip speed ratio is defined as the ratio of the blade tip speed to the speed of the wind, given by [21]

$$\lambda = \frac{\omega_m R}{v_w},\ \omega_r = P\omega_m \tag{3.2}$$

where ω_m and and ω_r are the mechanical rotating speed of the blade and the electrical speed of the generator, respectively. Neglecting the friction forces, the dynamic equation of the wind turbine is given by [21]

$$\frac{\mathrm{d}\omega_m}{\mathrm{d}t} = \frac{P}{J}(T_m - T_e) \tag{3.3}$$

where P is the number of pole pairs, J is the moment of inertia of the generator, T_m is the torque developed by the turbine and T_e is the torque due to load which in this case is the generator electromagnetic torque.

3.2.2 PMSG Model

The dq reference frame model for the PMSG is given by [21]

$$\begin{cases} u_{ds} = R_s i_{ds} + L_d \dfrac{\mathrm{d}i_{ds}}{\mathrm{d}t} - \omega_r L_q i_{qs} & \text{(3.4a)} \\ u_{qs} = R_s i_{qs} + L_q \dfrac{\mathrm{d}i_{qs}}{\mathrm{d}t} + \omega_r L_d i_{ds} + \omega_r \lambda_r & \text{(3.4b)} \end{cases}$$

where, i_{ds} and i_{qs} are the stator dq-axis currents (A); R_s is the stator winding resistance (Ω); L_d and L_q are the stator dq-axis self-inductances (H); ω_r is the rotor electrical angular speed (rad/s); and λ_r is the rotor flux generated by the permanent magnets.

In this study, a round rotor PMSG is considered. The d- and q-axis magnetizing inductions are therefore equal ($L_d = L_q = L_s$). However, we keep L_d, L_q notations so that the derived equations can be applied to both salient and nonsalient (round) PMSG.

The electromagnetic torque is given by [21]

$$T_e = \frac{3P}{2} \left[\lambda_r i_{qs} - (L_d - L_q) i_{ds} i_{qs} \right] \tag{3.5}$$

3.2.3 PWM Voltage Source Converter Model

The PWM voltage source converter works as a rectifier. It converts the generator output voltage into a DC voltage. The generator active power and the rotor speed (MPPT control) are controlled through this converter. Two-level rectifier will be chosen and controlled using a space vector pulse width modulation (SVPWM) scheme. Compared to the traditional PWM, the SVPWM modulation technique offers a better THD and increases the DC-bus voltage utilization by about 15% [132].

The relationship between the modulation index, m_a, the DC-bus voltage, U_{dc}, and the rms value of the generator output voltage, u_{an}, in one of the rectifier legs is [21]

$$m_a = \sqrt{6} \frac{u_{an}}{U_{dc}} \tag{3.6}$$

The dq-axis synchronous reference frame representation of Eqn. (3.6) has the following form [21]

$$\begin{cases} u_{ds} = \dfrac{1}{\sqrt{6}} m_a U_{dc} \cos(\theta_r) & \text{(3.7a)} \\ u_{qs} = -\dfrac{1}{\sqrt{6}} m_a U_{dc} \sin(\theta_r) & \text{(3.7b)} \end{cases}$$

where θ_r is the generator rotor flux position angle and U_{dc}, the DC-link voltage.

3.3 Design of the Controllers

Three different types of control schemes are studied and designed herein. They are: 1) the traditional PI-based controller, 2) the state feedback controller based Taylor series expansion linear approximation (TSLA-based) and 3) the proposed nonlinear MIMO control feedback linearization based (FL-based). The performances and robustness of the three controllers are analyzed and compared in Section 3.4.

3.3.1 PI-based Controller Design

Fig. 3.2 illustrates the basic concept of the conventional PI-based control scheme. It consists of three PI compensators: two inner loops for the control of the dq-axis currents i_{ds} and i_{qs}, and one outer loop for the control of the generator rotor speed. The role of these compensators is to reduce the error between the reference signals and measured ones to zero.

The output of the decoupled PI current controllers can be written as

$$\begin{cases} u_{ds} = (k_{p_d} + \dfrac{k_{i_d}}{s})(i_{ds_{ref}} - i_{ds}) - \omega_r L_q i_{qs} + R_s i_{ds} & \text{(3.8a)} \\ u_{qs} = (k_{p_q} + \dfrac{k_{i_q}}{s})(i_{qs_{ref}} - i_{qs}) + \omega_r L_d i_{ds} + \omega_r \lambda_r + R_s i_{qs} & \text{(3.8b)} \end{cases}$$

where $[k_{p_d}, k_{i_d}]$ and $[k_{p_q}, k_{i_q}]$ are the gains of the d-axis current and q-axis current PI controllers respectively.

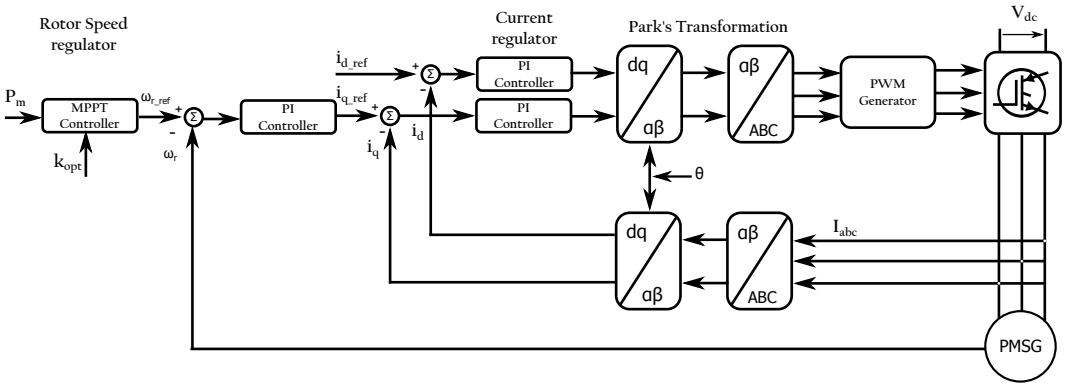

Figure 3.2: PI-based control scheme.

Substituting Eqn. (3.8) into Eqn. (3.4) yields

$$\begin{cases} \dfrac{\mathrm{d}i_{ds}}{\mathrm{d}t} = \dfrac{1}{L_d}(k_{p_d} + \dfrac{k_{i_d}}{s})(i_{ds_{ref}} - i_{ds}) & \text{(3.9a)} \\ \dfrac{\mathrm{d}i_{qs}}{\mathrm{d}t} = \dfrac{1}{L_q}(k_{p_q} + \dfrac{k_{i_q}}{s})(i_{qs_{ref}} - i_{qs}) & \text{(3.9b)} \end{cases}$$

The output of the generator rotor speed controller is

$$i_{qs_{ref}} = (k_{p_\omega} + \frac{k_{i_\omega}}{s})(\omega_{r_{ref}} - \omega_r) \tag{3.10}$$

where $[k_{p_w}, k_{i_w}]$ are the gains of the generator stator d-axis current and q-axis current controllers respectively.

3.3.2 TSLA-based Controller Design

The linearised model that approximates the system behaviour around the operating point using Taylor series expansion is expressed as follows:

$$\frac{\mathrm{d}}{\mathrm{d}t}\begin{bmatrix}\hat{i}_{ds}\\ \hat{i}_{qs}\\ \hat{\omega}_r\end{bmatrix} = \begin{bmatrix}-\frac{R_s}{L_d} & \frac{L_q}{L_d}\omega_{r0} & 0\\ -\frac{L_d}{L_q}\omega_{r0} & -\frac{R_s}{L_q} & -\frac{\lambda_r+L_d i_{ds0}}{L_q}\\ 0 & \frac{3P^2}{2J}\lambda_r & k_{wt}\frac{P^2}{J}\frac{v_{w0}^3}{\omega_{r0}^2}\end{bmatrix}\begin{bmatrix}\hat{i}_{ds}\\ \hat{i}_{qs}\\ \hat{\omega}_r\end{bmatrix} + \begin{bmatrix}\frac{1}{L_d} & 0\\ 0 & \frac{1}{L_q}\\ 0 & 0\end{bmatrix}\begin{bmatrix}\hat{u}_{ds}\\ \hat{u}_{qs}\end{bmatrix} + \begin{bmatrix}E_1(i_{ds0})\\ E_2(i_{ds0})\\ E_3(\omega_{r0})\end{bmatrix} \tag{3.11}$$

where $E_1(i_{ds0})$, $E_2(i_{ds0})$ and $E_3(\omega_{r0})$ are approximately equal to zero, and $(i_{ds0}, i_{ds0}, \omega_{r0}, v_{w0})$ is the operating point.

To stabilize the system at the operating point, a state feedback controller is used to design the TSLA-based Controller. The control input is as follows

$$\begin{bmatrix}u_{ds}\\ u_{qs}\end{bmatrix} = -k_{ts}\begin{bmatrix}i_{ds}-i_{ds0}\\ i_{qs}-i_{qs0}\\ \omega_r-\omega_{r0}\end{bmatrix} \tag{3.12}$$

where k_{ts}, given in Table 3.2, is the feedback gain matrix selected by pole placement.

3.3.3 Proposed MIMO Nonlinear Controller Design

For the design of the proposed MIMO nonlinear controller, two control objectives have been considered in order to: 1) keep the wind turbine operating at its maximum power by controlling ω_r; 2) achieve a linear relationship between the stator current and the electromagnetic torque by controlling the stator d-axis current, i_{ds}.

The input-output feedback linearization control is adopted as design method for the proposed nonlinear controller. Fig. 3.3 illustrates its structure.

One of the advantages of feedback linearization versus traditional PI-based method, is that it is possible to reduce the number of gains of controller with feedback linearization. In the traditional schemes, at the generator-side, the generator

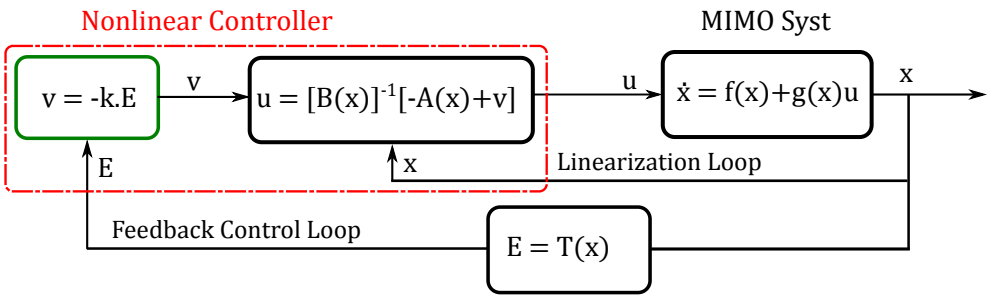

Figure 3.3: Proposed MIMO controller structure.

active power and rotor speed are controlled through three PI controllers in cascade with two gains each (k_p and k_i). In contrast, in the feedback linearization method proposed in this paper, only three gains are needed (instead of six in the case of PI) to perform the same task. This helps to better performance as it will be seen in the simulation results section. Thus, the chosen state space vector, control inputs and controlled outputs of the WECS are respectively

$$\begin{cases} x = [i_{ds}, i_{qs}, \omega_r]^T & \text{(3.13a)} \\ u = [u_{ds}, u_{qs}]^T & \text{(3.13b)} \\ y = [i_{ds}, \omega_r]^T & \text{(3.13c)} \end{cases}$$

By rewriting Eqs. (3.3) and (3.4), the dynamic model of the system can be expressed into the form as follows

$$\frac{\mathrm{d}}{\mathrm{d}t}\begin{bmatrix} i_{ds} \\ i_{qs} \\ \omega_r \end{bmatrix} = \begin{bmatrix} -\frac{R_s}{L_d} & \frac{L_q}{L_d}\omega_r & 0 \\ -\frac{L_d}{L_q}\omega_r & -\frac{R_s}{L_q} & -\frac{\lambda_r}{L_q} \\ 0 & \frac{3P^2}{2J}\lambda_r & k_{wt}\frac{P^2}{J}\frac{v_w^3}{\omega_r^2} \end{bmatrix}\begin{bmatrix} i_{ds} \\ i_{qs} \\ \omega_r \end{bmatrix} + \begin{bmatrix} \frac{1}{L_d} & 0 \\ 0 & \frac{1}{L_q} \\ 0 & 0 \end{bmatrix}\begin{bmatrix} u_{ds} \\ u_{qs} \end{bmatrix} \quad \text{(3.14)}$$

It can be observed from Eqn. (3.14) that the system is nonlinear. To make the system behave like a linear system, we design a nonlinear controller using the input-output linearization method.

As the controlled outputs are $y_1 = i_{ds}$ and $y_2 = \omega_r$, let differentiate each one until at least one input appears. For simplicity, not all steps are presented. Note that y_1 has been differentiated once, whereas, y_2 has been differentiated twice, before a control input emerges. Thus, we obtain

$$\underbrace{\begin{bmatrix} \dot{y}_1 \\ \ddot{y}_2 \end{bmatrix}}_{T(x)} = \underbrace{\begin{bmatrix} A_1(x) \\ A_2(x) \end{bmatrix}}_{A(x)} + \underbrace{\begin{bmatrix} \frac{1}{L_d} & 0 \\ 0 & \frac{3P^2}{2JL_q}\lambda_r \end{bmatrix}}_{B(x)} \underbrace{\begin{bmatrix} u_{ds} \\ u_{qs} \end{bmatrix}}_{u} \tag{3.15}$$

where

$$\begin{cases} A_1(x) = -\dfrac{R_s}{L_d} i_{ds} + \dfrac{L_q}{L_d}\omega_r i_{qs} & \text{(3.16a)} \\ A_2(x) = -\dfrac{3P^2 L_d \lambda_r}{2JL_q}\omega_r i_{ds} - \dfrac{3P^2 R_s \lambda_r}{2JL_q} i_{qs} \\ \qquad\quad - \dfrac{3P^2\lambda_r^2}{2JL_q}\omega_r + \dfrac{k_{wt}}{J(\frac{3\lambda_r}{2J} i_{qs} - \frac{k_{wt}}{J\omega_r} v_w^3)} v_w^3 & \text{(3.16b)} \end{cases}$$

Since the *relative degree* associated with y_1 and y_2 are 1 and 2 respectively. The total relative degree of the MIMO system is then $r = 1 + 2 = 3$.

Note that both the linearized input-output system (Eqn. (3.15)) and the original nonlinear system are of order three. Therefore, there is no internal dynamics. In other words, all the state variables can be seen from the input-output relationship.

By choosing a control input vector to be in the form

$$\begin{bmatrix} u_{ds} \\ u_{qs} \end{bmatrix} = \begin{bmatrix} \frac{1}{L_d} & 0 \\ 0 & \frac{3P^2}{2JL_q}\lambda_r \end{bmatrix}^{-1} \left[-\begin{bmatrix} A_1(x) \\ A_2(x) \end{bmatrix} + \begin{bmatrix} v_{gc_1} \\ v_{gc_2} \end{bmatrix} \right] \tag{3.17}$$

where v_i (with $i = 1, 2$) are the new inputs, the nonlinearity in Eqn. (3.14) is cancelled and a linear relationship between the outputs, $[\dot{y}_1, \ddot{y}_2]^T$, and new inputs, $[v_1, v_2]^T$, is obtained as follows:

$$\begin{bmatrix} \dot{y}_1 \\ \ddot{y}_2 \end{bmatrix} = \begin{bmatrix} v_1 \\ v_2 \end{bmatrix} \tag{3.18}$$

Now that the closed loop system is linear, it is simple to design a tracking controller, due to the availability of various linear control techniques. Therefore, we propose the feedback control law as follows:

$$\begin{bmatrix} v_1 \\ v_2 \end{bmatrix} = \underbrace{\begin{bmatrix} k_{11} & 0 & 0 \\ 0 & k_{21} & k_{22} \end{bmatrix}}_{k_{fl}} \underbrace{\begin{bmatrix} e_1 \\ e_2 \\ e_3 \end{bmatrix}}_{E_{fl}} \tag{3.19}$$

where K_{fl} is the feedback gain matrix and E_{fl} represents the errors between reference signals and the outputs of the linearized input-output system, defined as

$e_1 = i_{ds_{ref}} - i_{ds}$, $e_2 = \omega_{r_{ref}} - \omega_r$ and $e_3 = \dot{\omega}_{r_{ref}} - \dot{\omega}_r$.

Note that $i_{ds_{ref}}$ is constant and $\dot{\omega}_{r_{ref}}$ is assumed constant. Hence, $\dot{i}_{ds_{ref}} = 0$ and $\ddot{\omega}_{r_{ref}} = 0$.

Optimal control is a good alternative design strategy by which all the control design parameters can be determined even for MIMO systems. With this technique, the performance objectives of the control system can be directly formulated through a cost function, J, which need to be minimized. This can be written as

$$J(t) = \int_0^\infty \left[Y^T(t).Q.Y(t) + V^T(t).R.V(t) \right] dt \tag{3.20}$$

and the feedback gain matrix K_{fl} as

$$K_{fl} = R^{-1}B^T M \tag{3.21}$$

where B, C and D, given in Eqn. (3.23) are the input matrix, output matrix and feedforward matrix of the linearized system of Eqn. (3.18) respectively, whereas Q, R_{gc} and M are respectively the *state weighting matrix*, *control cost matrix* and the *optimal matrix that minimizes the objective function*, J. The latter is determined through the *Riccati equation* given in Eqn. (3.22) below. Full details on the linear optimal control can be found in [133].

$$A^T M + MA - MBR^{-1}B^T M + Q = 0 \tag{3.22}$$

where

$$A = \begin{bmatrix} 0 & 0 & 0 \\ 0 & 0 & 1 \\ 0 & 0 & 0 \end{bmatrix}, \quad B = \begin{bmatrix} 1 & 0 \\ 0 & 0 \\ 0 & 1 \end{bmatrix}, \quad C = \begin{bmatrix} 1 & 0 & 0 \\ 0 & 1 & 0 \\ 0 & 0 & 1 \end{bmatrix}, \quad D = \begin{bmatrix} 0 & 0 \\ 0 & 0 \\ 0 & 0 \end{bmatrix} \tag{3.23}$$

$$Y = \begin{bmatrix} e_1 \\ e_2 \\ e_3 \end{bmatrix}, \quad V = \begin{bmatrix} v_1 \\ v_2 \end{bmatrix}, \quad Q = \begin{bmatrix} 10 & 0 & 0 \\ 0 & 10^{11} & 0 \\ 0 & 0 & 1 \end{bmatrix}, \quad R = \begin{bmatrix} 1 & 0 \\ 0 & 1 \end{bmatrix}$$

The reference signals are chosen as follows:

$i_{ds_{ref}}$ is set to zero to realize the *zero d-Axis current (ZDC) control* scheme. This control scheme is employed to achieve a linear relationship between the stator current and the electromagnetic torque [21].

$i_{qs_{ref}}$ represents the torque-producing stator current, whereas $\omega_{r_{ref}}$ is generated from the MPPT controller. They are calculated, respectively, as

$$i_{qs_{ref}} = \frac{T_{e_{ref}}}{1.5P\lambda_r}, \; \omega_{m_{ref}} = \sqrt[3]{\frac{P_m}{k_{opt}}} \tag{3.24}$$

where

$$k_{opt} = \frac{0.5\pi\rho C_{pmax} R^5}{\lambda_{opt}^3} \tag{3.25}$$

P_m in Eqn. (3.10) is measured, whereas C_{pmax} and λ_{opt}, in Eqn. (3.25), are given in Table 3.1.

3.4 Results

In order to demonstrate the effectiveness of the proposed nonlinear MIMO control feedback linearization based scheme (FL-based), simulations have been carried out using Matlab/Simulink. The generator used in the study is a variable speed nonsalient-pole PMSG driven by a wind turbine whose electrical parameters are given Table 3.1 of Appendix Chapter 3. The performance and robustness of the

proposed controller have been compared to those of the two control techniques: (1) the traditional PI-based controller and (2) the feedback controller based Taylor series expansion linear approximation (TSLA-based). In the following pages, we present the simulation results of the three controllers tested for three different case studies: (1) constant wind speed, (2) variable wind speed and (3) variable wind speed with variable generator parameter.

Feedback controller gain matrices K_{ts} and K_{fl}, respectively, for Taylor series based linearized controller and feedback linearization based controller, are selected by optimal control. The gains are given in Table 3.2 of Appendix Chapter 3.

3.4.1 Nonlinear Controller

First, the power-versus-rotor speed characteristics of the system at different wind speeds are illustrated in Fig. 3.4. For each speed, the system operates at its

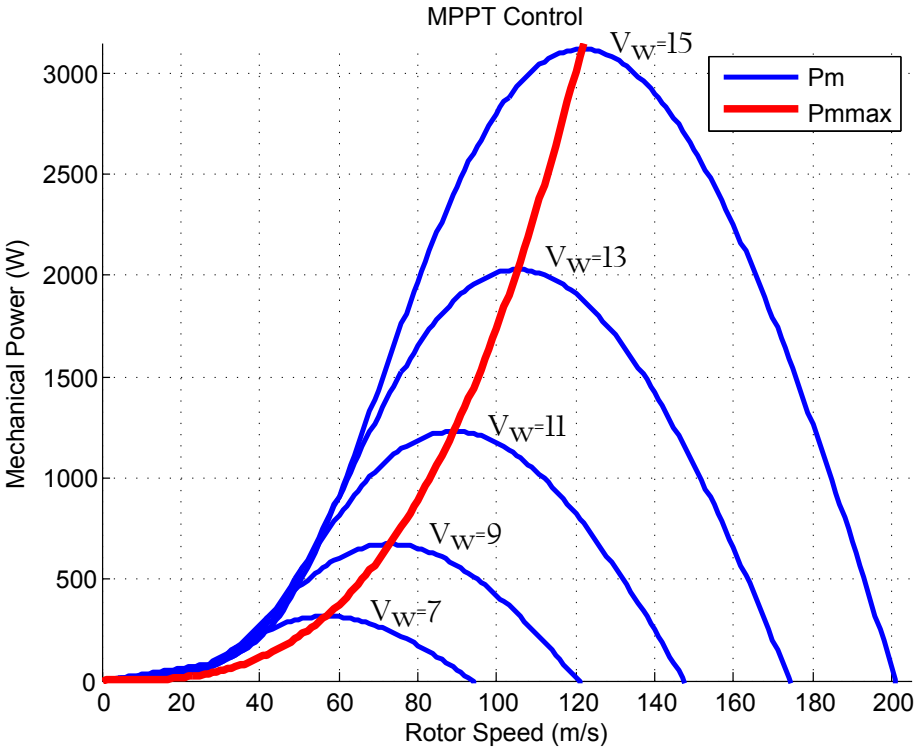

Figure 3.4: MPPT control: Mechanical power vs rotor speed.

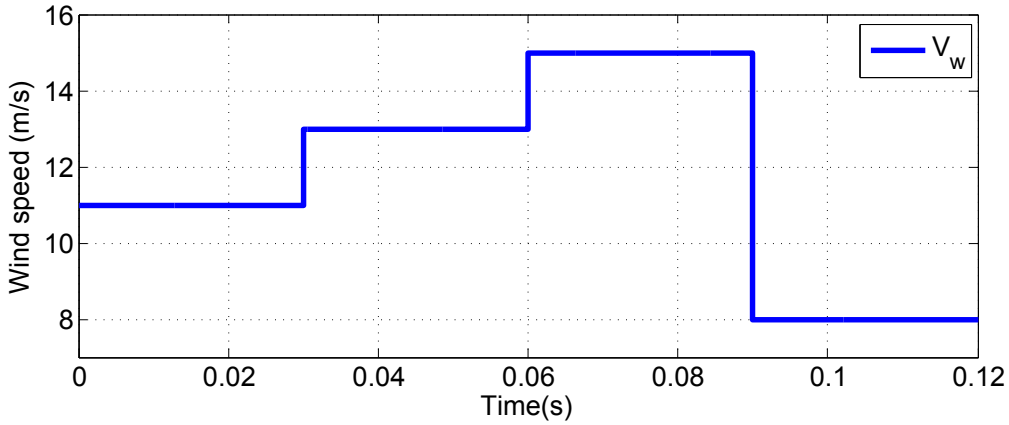

(a) Wind speed (m/s).

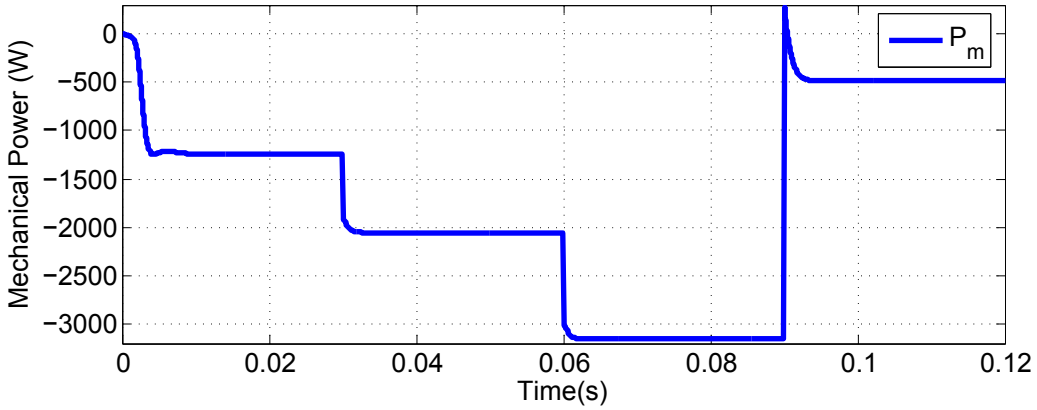

(b) Mechanical Power (W).

corresponding maximum power point as indicated by the red.

Next, the transients of a nonsalient-pole PMSG wind energy system caused by a step change in wind are investigated.

Fig. 3.5 illustrates the simulated waveforms for the feedback linearization based nonlinear control wind energy system when the wind speed changes from 11 m/s to 13 m/s, then to 15 m/s, and then decreases to 8 m/s. The waveforms include the wind speed, the rotor mechanical speed ω_m, generator electromagnetic torque T_e, three-phase stator current, i_s, and voltage v_s.

It can also be observed that the dq-axis stator currents, i_{ds} and i_{qs}, in the

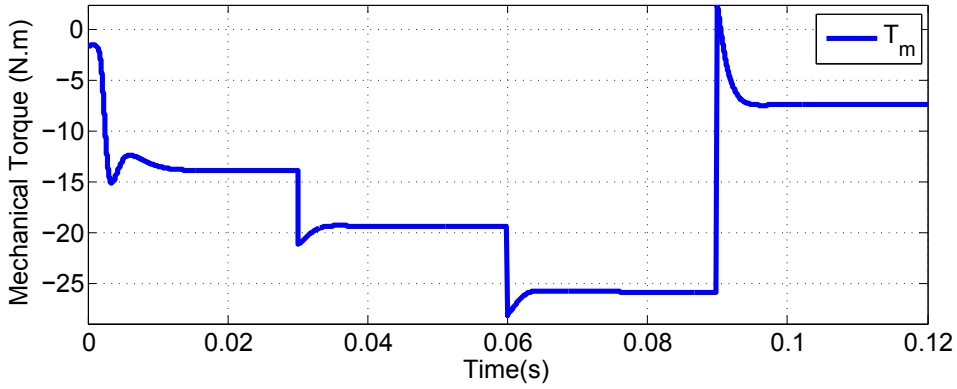

(c) Mechanical Torque (N.m).

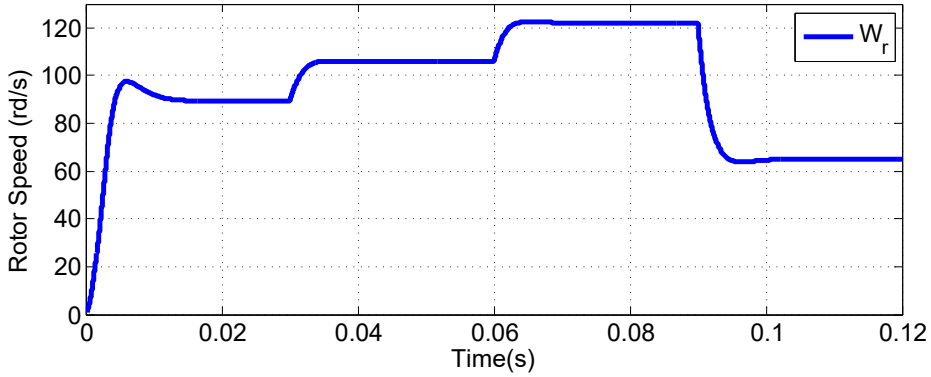

(d) Rotor Mechanical Speed (rd/s).

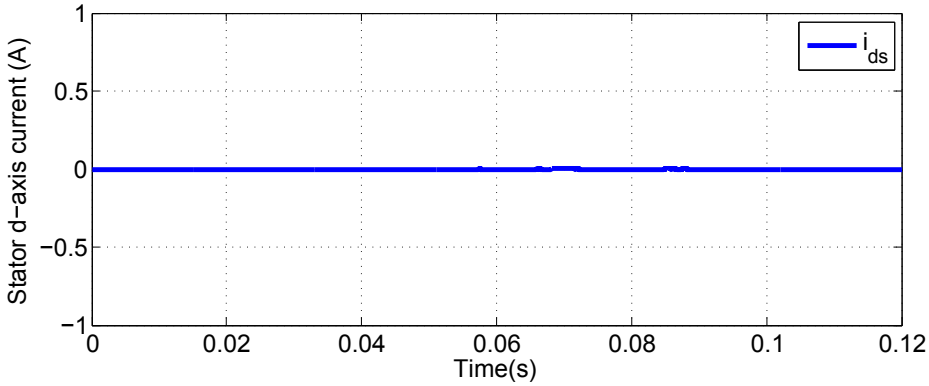

(e) Stator d-axis current (A).

synchronous frame are DC variables, whereas the *abc*-axis stator currents, i_{as}, i_{bs}, and i_{cs} in the stationary frame are sinusoids in steady state.

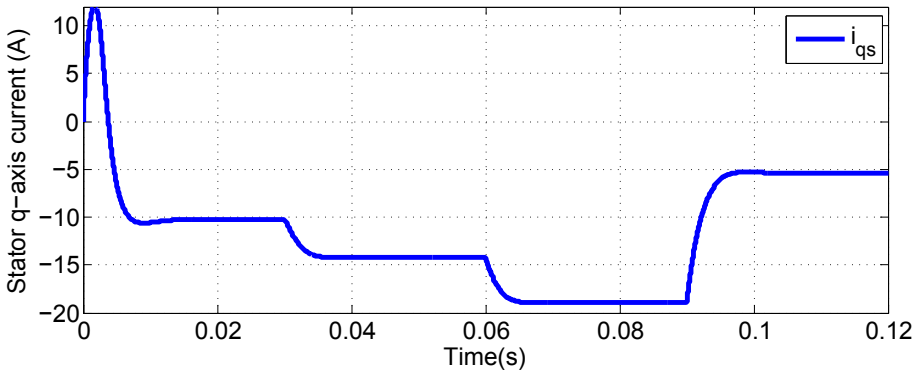

(f) Stator q-axis current (A).

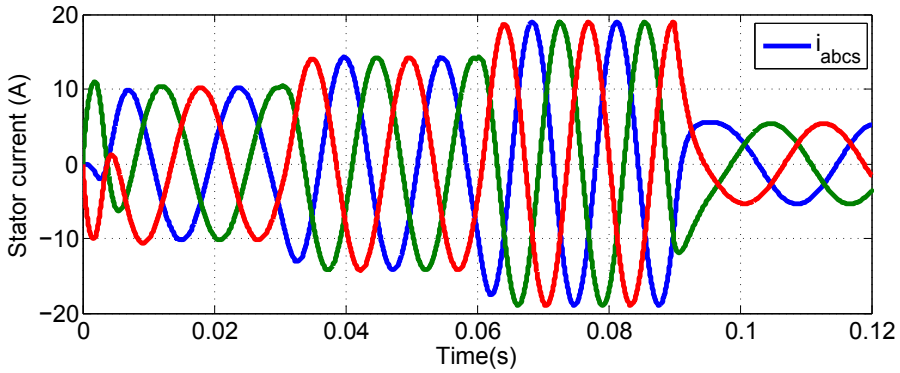

(g) Stator current (A).

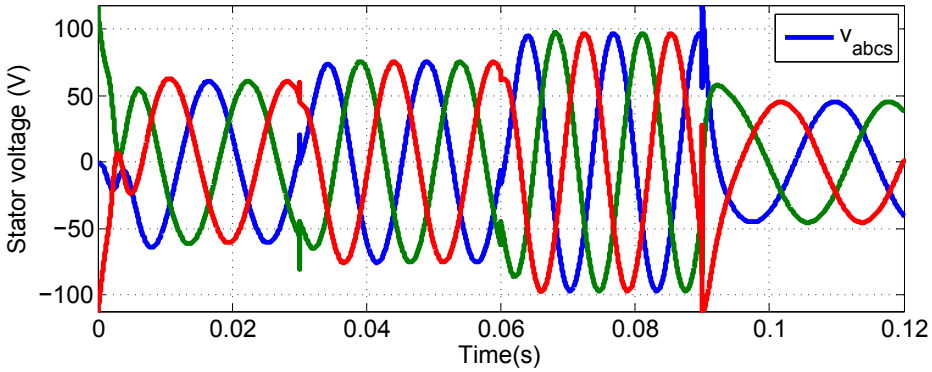

(h) Stator voltage (V).

Figure 3.5: Simulated waveforms for the FL nonlinear control WECS.

With the zero d-axis control scheme, the d-axis i_{ds} is kept at zero. The q-axis stator current i_{qs}, is proportional to the generator torque T_e. At $t = 0.005$ sec, the

wind speed starts to increase. It takes 0.01 sec for the system to reach 1230 W, the steady-state operating point with a negligible overshoot indicating that the nonlinear control WECS has a good dynamic performance.

3.4.2 Comparison to PI-based and Taylor Series Based Linear Controllers

To further study the proposed nonlinear control system performance, the waves-forms of the rotor mechanical speed ω_m and generator electromagnetic torque T_e of the proposed control scheme have been compared to the PI-based and TSLA-based control schemes, for the following three case studies.

Case 1: Constant wind speed

In this case, the wind turbine operates at its rated wind speed. As illustrated in Fig. 3.6 with ω_m and T_e wave-forms, the three controllers are very close in steady-state response. However, the transient response of the FL-based control

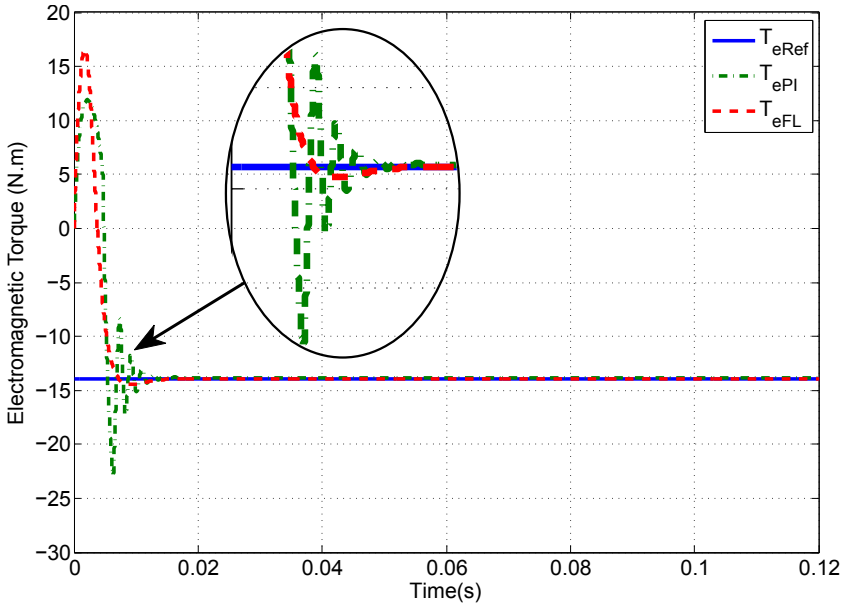

(a) FL vs PI controllers: Mechanical torque.

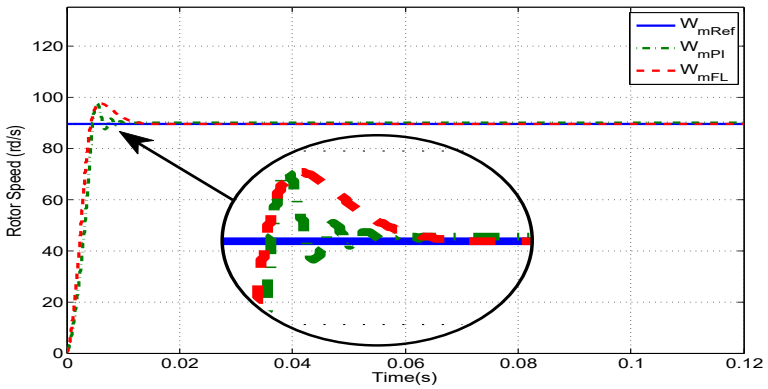

(b) FL vs PI controllers: Rotor speed.

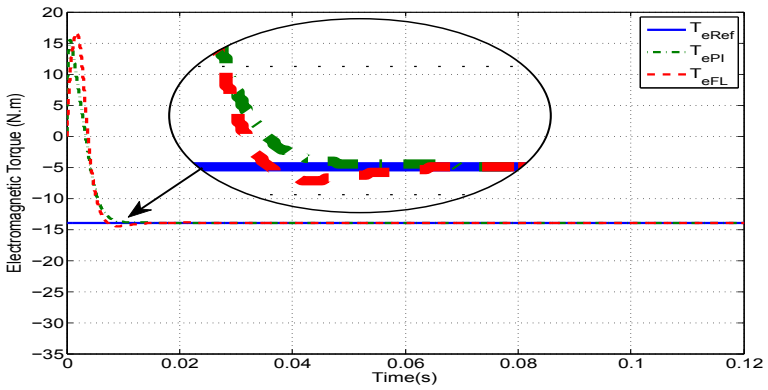

(c) FL vs TSLA controllers: Mechanical torque.

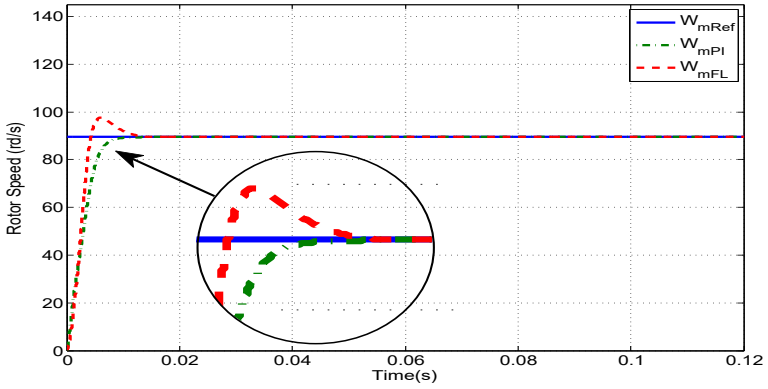

(d) FL vs TSLA controllers: Rotor speed.

Figure 3.6: Comparison of FL, PI and TSLA controllers for fix wind speed (rated speed, $V_w = 11$ m/s).

system is much smoother and faster compared to the other two. It can be noticed that, the TSLA-based control system has a close dynamic behavior to the FL-based one. This is due to the fact that the TSLA-system has been derived and approximated around the rated speed operating point which is 11 m/s.

Case 2: Variable wind speed with constant generator parameter

This case study investigates the transients and steady-state when the wind speed experiencese a series of suddenly increases and decreases. The simulated wavesforms of the rotor mechanical speed ω_m and generator electromagnetic torque T_e, depicted in Fig. 3.7, show that FL-based control system has the best transient and steady-state performance compared to the other two control systems.

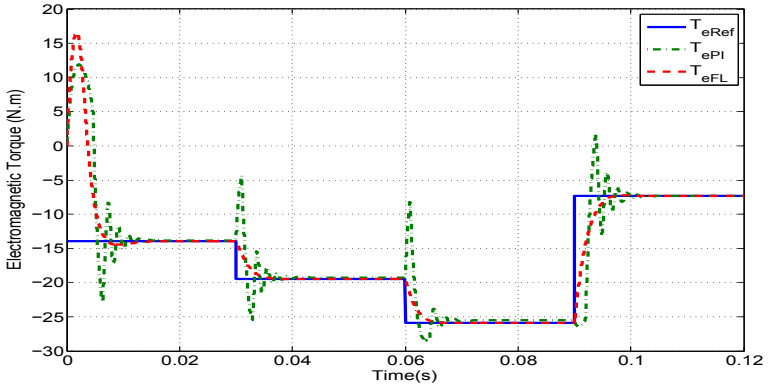

(a) FL vs PI controllers: Mechanical torque.

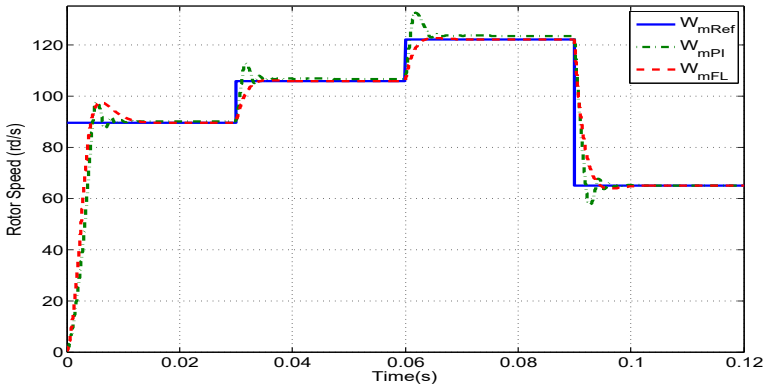

(b) FL vs PI controllers: Rotor speed.

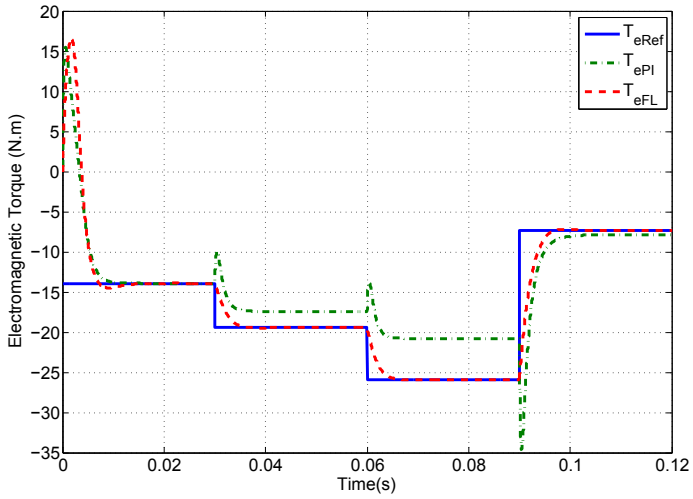

(c) FL vs TSLA controllers: Mechanical torque.

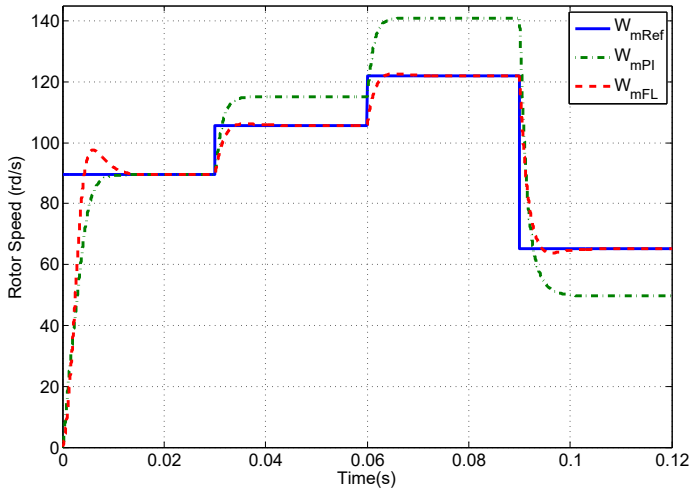

(d) FL vs TSLA controllers: Rotor speed.

Figure 3.7: Comparison of FL, PI and TSLA controllers for variable wind speed ($V_w = [11,\ 13,\ 15,\ 8]$ m/s).

Moreover, the FL-based control system has better tracking performance, whereas a high overshoot of the PI-based controller during each transient period can be observed. And the TSLA-based shows certain differences between the references and the actual torques and speeds at high wind speed.

Case 3: Variable wind speed with variable generator parameter

For this case, the robustness of the proposed nonlinear control system is tested by increasing the generator fixed magnetic flux, λ_r, by 30%. The torque and rotor speed successfully reaches their references signals with a good transition. However, the TSLA-based control method is sensitive to parameter variations. Fig. 3.8(d) shows the effects of it on the control performance. For TSLA-based control system,

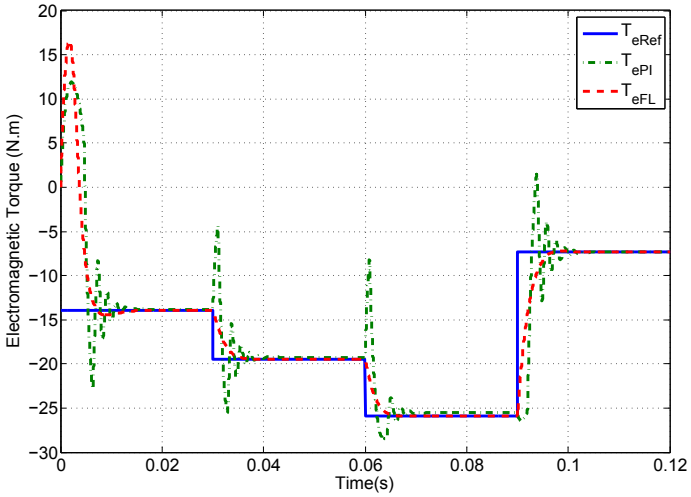

(a) FL vs PI controllers: Mechanical torque.

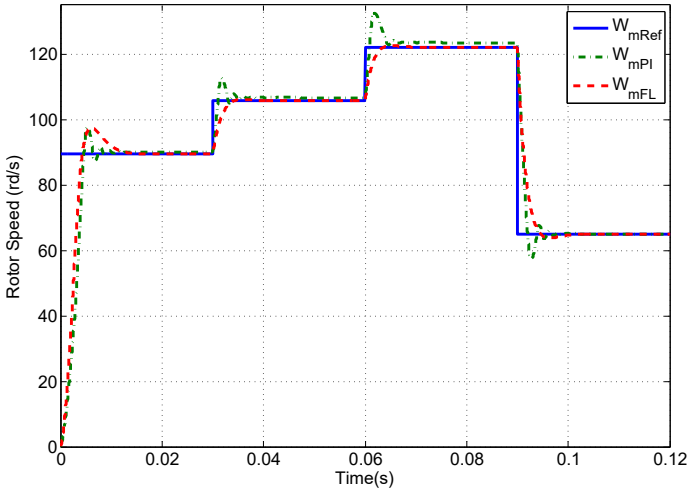

(b) FL vs PI controllers: Rotor speed.

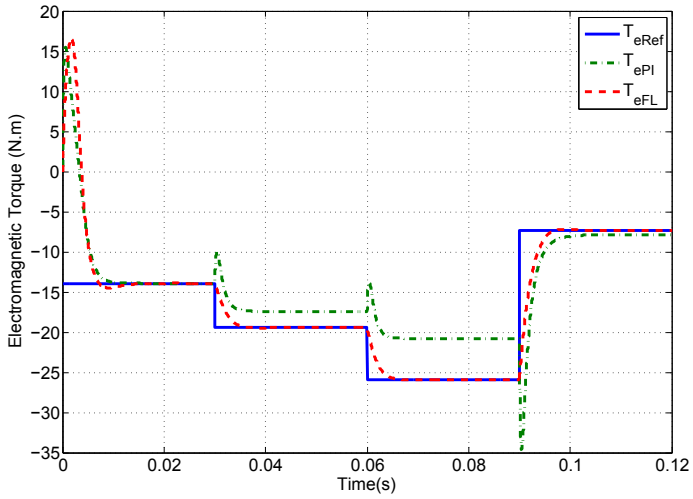

(c) FL vs TSLA controllers: Mechanical torque.

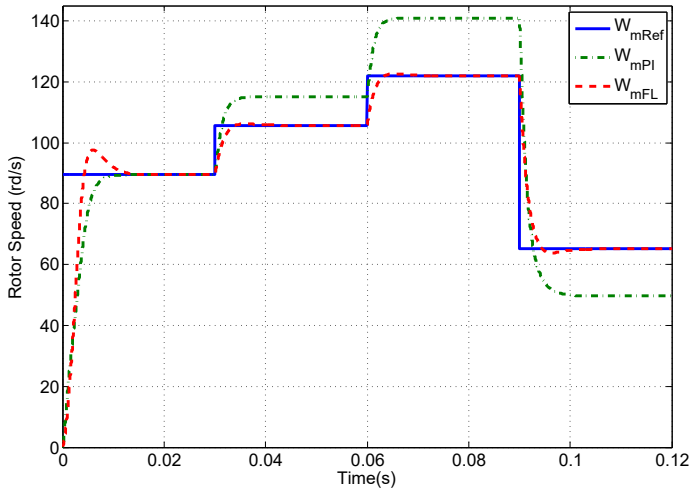

(d) FL vs TSLA controllers: Rotor speed.

Figure 3.8: Comparison of FL, PI and TSLA controllers for variable wind speed ($V_w = [11,\ 13,\ 15,\ 8]$ m/s) and variable parameter (by 30% of λ_r).

this variation of generator magnetic flux results in steady-state errors of 10 rd/s and 10 N.m in the rotor speed and electromagnetic torque, respectively. Fig. 3.8(d) shows also that the transient performance for the torque and the speed is superior for the nonlinear control system.

3.5 Conclusion

This paper has proposed a nonlinear MIMO controller based on feedback linearization theory to regulate the generator current and rotor speed of a WECS. The controller gains have been selected by using optimal control. The performance and robustness of the proposed controller have been compared to those of the traditional PI-based controller and the feedback controller based Taylor series expansion linear approximation (TSLA-based). For this purpose, full detailed PI-based and TSLA-based control schemes for WECS have also been given. The comparison has been done under three case of studies: 1) constant wind speed, 2) variable wind speed with constant generator parameters and 3) variable wind speed with variable generator parameters. The simulation results show that applying nonlinear feedback linearization based control strategy combined with optimal control, while keeping the wind turbine operating at its optimal maximum power and controlling the generator active power, provides a better control performance compare to the PI-based and TSLA-based control systems. This performance is characterized by fast and smooth transient response as well as good steady state stability and reference tracking quality, even with variable wind speed operation. However, this study focuses on the generator-side subsystem. A future work will be to include the utilities grid in the control system.

Appendix Chapter 3

Table 3.1: System Parameters

Parameter	Description	Value
P_m	Rated Mechanical Power (W)	3230
ω_m	Rated Rotor Speed (rd/s)	89
λ_r	Rated Rotor Flux Linkage (Wb)	0.2275
P	Number of Pole Pairs	4
J	Moment Inertia of the Generator $(kg.m^2)$	0.0008
R_s	Stator Winding Resistance (Ohm)	2.875
L_{ds}	d-axis Synchronous Inductance (H)	0.0085
L_{qs}	q-axis Synchronous Inductance (H)	0.0085
V_w	Rated Wind speed (m/s)	15
R	Blade Radius (m)	1
β	Pitch Angle $(degree)$	0
Rho	Air Density	1.25
λ_{opt}	Optimal Tip Speed Ratio	8.1

Table 3.2: Controller Gains

Controller Gains	Description	Value
PI_{il}	PI Inner Loop Gains	$K_p = 20, K_i = 40$
PI_{ol_d}	PI Outer Loop Gains for i_{ds}	$K_p = 2, K_i = 4$
PI_{ol_d}	PI Outer Loop Gains for i_{qs}	$K_p = 2, K_i = 4$
$K_{gc_{ts}}$	TSLA-based Gain Matrix	$\begin{bmatrix} 2.34 & -2.53 & -0.2 \\ -2.53 & 32.25 & 2.13 \end{bmatrix}$
$K_{gc_{fl}}$	FL-based Gain Matrix	$\begin{bmatrix} 1 & 0 & 0 \\ 0 & 316230 & 800 \end{bmatrix}$

Chapter 4

Robust Nonlinear Controller Design for On-grid/Off-grid Wind Energy Battery-Storage System

Abstract

This paper investigates the design of a unified robust nonlinear multi-input-multi-output (MIMO) controller for a wind energy battery-storage system. The system can be operated either in grid-connected mode or stand-alone mode. Feedback linearization control design method is used to find the controller equations. The main advantage of the proposed control strategy over the existing methods is that only a single controller is used to control the system regardless the mode of operation. With the new approach, the controller is designed so that the grid contribution is significantly reduced and the battery can provide a backup energy or store the surplus wind energy efficiently. In addition, the dc-link voltage and load power are regulated by adjusting the charging and discharging cycle of the battery through a bi-directional buck-boost DC/DC converter in contrast to existing methods where the dc-link is regulated by the grid-side converter. The robustness of the proposed controller is evaluated in simulation with various types of loads including unbalanced load and dynamic load. The results show that a good performance in closed loop is achieved.

Index terms— Battery storage, energy management, feedback linearization, grid-connected, nonlinear control, robust control, stand-alone, wind turbine conversion systems.

4.1 Introduction

Electric power generation sources are becoming broadly diversified with the advent of renewable energy sources such as wind turbines and photovoltaics (PV). In previous years, about half of new electric power generation sources in the world were renewable sources. Among them, wind power is one of the new electricity production means that has grown rapidly. The global installed wind power capacity was around 433 GW at the end 2015. This represents a market growth of more than 17% [127]. However, the energy generated by wind turbines is unpredictable due to their intermittent nature unlike conventional power plants. In addition, power systems management becomes more complex with this massive integration of wind energy sources. The architecture and technology used to control power grids will need to change. Control algorithms need to be adapted to go along with this evolution of power grids [134].

Current wind turbine systems are not designed to operate in both stand-alone (or off-grid) and grid-connected (or on-grid) modes. When a power outage occurs, they are automatically disconnected from the main utility grid (UG). This may causes significant financial losses to electricity suppliers [14, 15]. Therefore, one of the new challenges the wind energy based electricity supply industry will have to address is the adaptation of a single wind turbine so that it can operate in both modes [16]. The trend is to use the grid-side converter to disengage the wind turbine system from the grid to allow a continuous supply to critical loads during a power outage. Moreover, transitions between the two modes should be fast and seamless to minimize any abrupt voltage or current changes [17].

Several studies have been conducted to deal with issues related to this on-grid/off-grid mode of operation. References [135] and [32] propose concept and test results on a control strategy for a PMSG (Permanent Magnet Synchronous Gen-

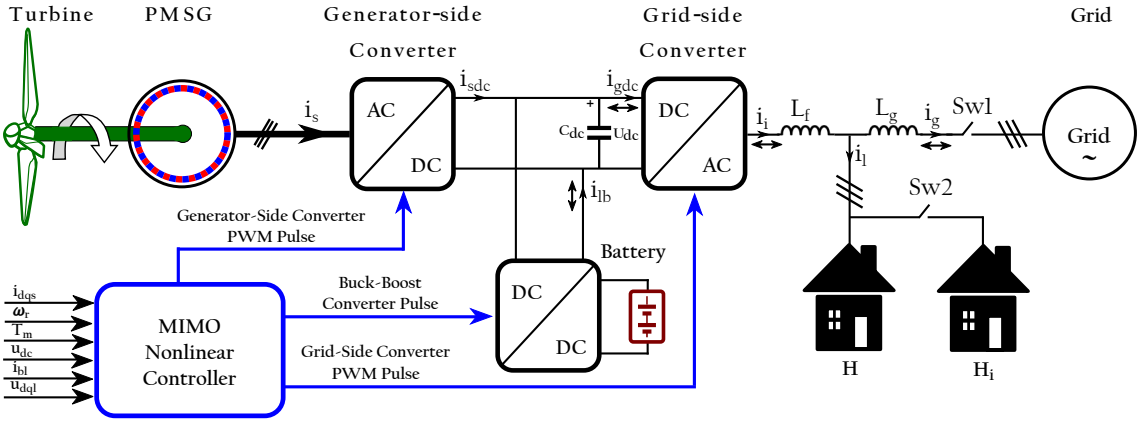

Figure 4.1: On-grid/Off-grid WECS based permanent magnet synchronous generator.

erator) driven by a small wind turbine capable to operate in both grid-connected and stand-alone modes. In the grid-connected mode, a PI current controller is used for the grid-side converter. The active and reactive power are controlled independently. The authors in [16] use a SCIM (Squirrel Cage Induction Machine) as a generator and PI current controllers. A modified space-vector pulse width modulation based (SVPWM) switching pattern for stand-alone and grid-connected three-phase single-stage boost inverters has been proposed in [34]. The proposed method is particularly for small PV and fuel cell applications (output voltage 35V) with low switching frequency (3 kHz).

In [80], a dynamic model of a PMSG system, suitable for a grid-connected/stand-alone operation has been presented. The machine-side converter controls the PMSG speed using a PI current control. A gas turbine is used instead of a wind-turbine to provide the mechanical power. Other grid-connected and stand-alone operations control for uninterruptible power supply (UPS) applications have been reported in [17, 47, 35, 39]. In these applications, the dynamics of the primary energy source is not taken into account. This may lead to a fall-short in achieving a seamless transfer between the grid-connected and stand-alone modes. Furthermore, the proposed control methods are PI-based. Although PI controllers have the advantage of being simple and easy to implement, they have several drawbacks. Indeed, they are sensitive to systems with highly nonlinear components

such as wind energy battery-storage systems [11]. They have a poor transient response and a weak disturbance rejection for non constant perturbations. They have difficulty to limit the converter current rise below the permitted limit during the off-grid and the grid detection transition period [16]. In all the aforementioned works, two distinct controllers are used for the system. One controller is used for the grid-connected mode and another one for the stand-alone mode. An islanding detection module is needed in this case to take the decision to switch between the two controllers.

Some nonlinear control methods have been proposed for Wind Energy Conversion Systems (WECS). This include backstepping [74] and feedback linearization controllers [64]. However they are mostly for grid-connected mode only. Moreover, no backup storage was used in these references. Since the grid does not exist in stand-alone mode and the power generated from the wind is not constant, storage unit becomes necessary [77]. The role of the latter is to compensate or absorb the difference between the generated wind power and the required load power. This significantly reduces the grid contribution to the system. A system that contains multiple sources are known as hybrid power systems [78]. They require a suitable energy management strategy. In [116], a unified control strategy of a three-phase inverter in uninterruptible power supply (UPS) applications was presented. The inverter operates as a current source in a grid-tied mode and as a voltage source in a stand-alone mode. PI controllers is used in the paper.

The main contribution of the paper is the utilization of a single robust nonlinear controller for a wind energy battery-storage system that can operate in both grid-connected and stand-alone modes. The challenge is that the system should operate in both modes with no need for switching between two different controllers, contrary to conventional methods found in the literature. In the proposed approach, there is no need for an islanding detection system [121, 122]. The same controller performs the MPPT, power management and load voltage control, regardless of the mode of operation. Thus, problems related to the islanding detection, such as poor dynamic performance [123, 38], poor load current waveform quality [124, 125] and inrush grid current [126] during the transition of operation mode, can be avoided.

The design method is based on the MIMO feedback linearization control technique. A back-to-back (B2B) power converter is used to connect the WECS to the grid and the load. In addition, a bi-directional buck-boost DC/DC converter is used to regulate directly the dc-link voltage and the load active power based on the energy balance and the system stability. Different types of loads are used to demonstrate the robustness of the proposed control method, namely, 1) a balanced three-phase load, 2) an unbalanced three-phase load, 3) a single-phase nonlinear load, and 4) a dynamic load.

The rest of this paper is organized as follows. Section 4.2 describes the system dynamic modeling. In Section 4.3, the design of the proposed controller is presented. Feedback linearization theory for MIMO systems is also presented therein. The robustness of the proposed control method is evaluated with various types of loads for both grid-connected and stand-alone modes of operation in Section 4.4. Finally, we conclude in Section 4.5.

4.2 System Dynamic Modeling

The schematic diagram of the system is depicted in Fig. 4.1. It consists of a PMSG driven by a wind turbine, a generator-side AC/DC converter, a grid-side DC/AC converter, a battery-storage unit connected to the DC-link trough a bi-directional buck-boost DC/DC converter. In the stand-alone mode, the switch *Sw1* is opened and the system supplies the critical local load only. The switch *Sw1* is closed in the grid-connected mode. The wind turbine converts part of the kinetic energy of the wind into mechanical energy. This energy is converted into electrical energy via the generator. Since the generator output frequency is variable (depends on the wind conditions), a back-to-back converter is used to synchronize its output with the grid frequency. The buck/boost converter is used to adjust the dc-link voltage to the required battery voltage. The mathematical model for each of the components will be presented in the following sections.

4.2.1 Wind Turbine

The wind turbine retrieves only a fraction of the wind's kinetic power. This power is determined by the area swept by the blades, S_w ($S_w = \pi R^2$), the wind speed, v_w, the air density, λ, and the power coefficient, C_p, which characterizes each turbine. Hence, the generated mechanical power, can be express as follows [21]:

$$P_m = \frac{1}{2}\pi\rho C_p(\lambda,\beta)R^2 v_w^3 \text{ and } \lambda = \frac{\omega_m R}{v_w} \tag{4.1}$$

where R is the radius of the turbine. C_p is a function of λ, the tip speed ratio and β, the pitch angle. ω_m is the turbine angular speed. Neglecting the friction forces, the dynamic equation of the wind turbine is given by

$$\frac{\mathrm{d}\omega_m}{\mathrm{d}t} = \frac{P}{J}(T_m - T_e) \tag{4.2}$$

where ω_m is the rotating speed of the blade, P, the number of pole pairs, J, the moment of inertia of the generator, T_m, the torque developed by the turbine and T_e, the torque due to load which in this case is the generator electromagnetic torque.

4.2.2 PMSG Model

The PMSG converts the mechanical energy obtained from the wind turbine to electrical energy. In order to simplify its analysis, the three-phase PMSG is modeled in the dq reference frame. It is given by [21]

$$\begin{cases} u_{ds} = R_s i_{ds} + L_d \dfrac{\mathrm{d}i_{ds}}{\mathrm{d}t} - \omega_r L_q i_{qs} & \text{(4.3a)} \\ u_{qs} = R_s i_{qs} + L_q \dfrac{\mathrm{d}i_{qs}}{\mathrm{d}t} + \omega_r L_d i_{ds} + \omega_r \lambda_r & \text{(4.3b)} \\ T_e = \dfrac{3P}{2}\left[\lambda_r i_{qs} - (L_d - L_q) i_{ds} i_{qs}\right] & \text{(4.3c)} \end{cases}$$

where u_{ds}, u_{qs} and i_{ds}, i_{qs} are the generator stator dq-axis voltages (V) and currents (A), respectively; R_s is the stator winding resistance (Ω); L_d and L_q are the stator dq-axis self-inductances (H); ω_r is the rotor electrical angular speed (rad/s); and

λ_r is the rotor flux (Wb) generated by the permanent magnets. Non-salient (or round) rotor PMSG is considered in this study, the d- and q-axis magnetizing inductions are therefore equal ($L_d = L_q$).

4.2.3 Back-to-back Converter Model

The back-to-back (B2B) converter consists of two identical voltage source converters (VSC) and a capacitor which is connected in between them. The generator-side VSC converts the three-phase generator AC output signal into DC voltage, whereas the grid-side VSC converts the DC voltage into the load input three-phase AC voltage. The power flow of the B2B converter can also be bidirectional, flowing from the grid to the battery. The load voltage will be controlled through the grid-side VSC. Its dq reference frame output voltage model is given by

$$\begin{cases} u_{di} = L_f \dfrac{\mathrm{d}i_{di}}{\mathrm{d}t} - \omega_g L_f i_{qi} + u_{dl} & \text{(4.4a)} \\ u_{qi} = L_f \dfrac{\mathrm{d}i_{qi}}{\mathrm{d}t} + \omega_g L_f i_{di} + u_{ql} & \text{(4.4b)} \end{cases}$$

where u_{di}, u_{qi} and i_{di}, i_{qi} are the grid-side converter output dq-axis voltages (V) and currents (A), respectively; u_{dl} and u_{ql} are the load dq-axis voltage (V); L_f and ω_g are the grid-side filter inductance (H) and the grid electrical angular speed (rad/s), respectively.

4.2.4 Bi-Directional Buck-Boost Converter Model

A bi-directional buck-boost converter will be used in this paper to interface the battery and the dc-bus. This converter, as illustrated in Fig. 4.2, operates as a boost converter during the discharging mode of the battery and as a buck during the charging mode. The dynamic equations of the current through the inductor, L_b, is given by

$$\begin{cases} \dfrac{\mathrm{d}i_{lb}}{\mathrm{d}t} = \dfrac{1}{L_b}(u_{bat} - D u_{dc}) & \text{(4.5a)} \\ \dfrac{\mathrm{d}E_{dc}}{\mathrm{d}t} = u_{dc} i_{sdc} - \dfrac{3}{2} u_{di} i_{di} + P_{bat} & \text{(4.5b)} \end{cases}$$

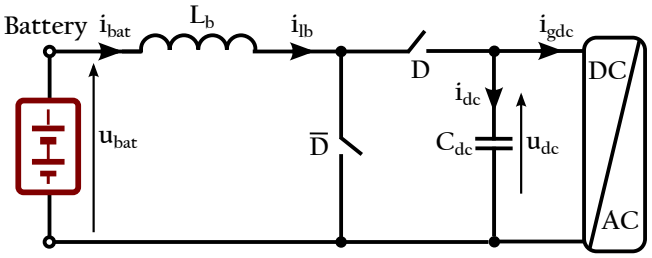

Figure 4.2: Bi-Directional Buck-Boost Converter.

where u_{bat}, i_{lb}, i_{sdc}, P_{bat} and D are the battery voltage, the current through the inductor L_b, the generator-side converter dc current, the battery power and the duty cycle respectively. D and $\bar{D}$, comprised between 0 and 1, determine the percentage of the PWM pulse period that the output is on. Also, note that the switches at D and $\bar{D}$ are logical complement of each other. The dc-link capacitor voltage, u_{dc}, will be regulated through E_{dc} where $E_{dc} = \frac{1}{2}C_{dc}u_{dc}^2$, using the bi-directional buck-boost converter rather than the grid-side converter. Eqn. (4.5b) is derived from the energy storage variation of the dc-link capacitor [119].

4.2.5 Battery Storage Unit Model

The battery-storage is connected to the dc-link through a bi-directional buck-boost converter. A *Nickel-Metal-Hydride* Model is used for the battery [136].

4.2.6 Grid-Side Circuit

The grid-side circuit is composed of a RL load, a filter, L_f, the line inductance, L_g, and the grid when the system operates in the grid-connected mode. For the sake of simplicity, the transformer leakage inductance is included in L_g. One of the advantages of the proposed control system is that the voltage of the load is constantly controlled in grid-connected mode and stand-alone mode. It is therefore not necessary to use a capacitor in the output filter of the converter. Characteristics and advantages of this strategy are discussed in Remark 6, Section 4.4.

For the design of a unique controller for this system which can operate in two different modes, it is proposed to represent the grid-side circuit by a model which

is valid in both modes of operation. The main idea behind this modeling approach is to represent the grid and the load by an equivalent Thévenin model. This model will be connected in series with L_f at A as illustrated in Fig. 4.3.

If $Z_l = R_l + j\omega_g L_l$ denotes the load impedance and $u_g = u_{dg} + ju_{qg}$ represents the grid voltage, then the Thévenin voltage and impedance in the grid-connected mode are given respectively by

$$\begin{cases} E_{th} = \dfrac{(R_l + j\omega_g L_l)(u_{dg} + ju_{qg})}{R_l + j\omega_g(L_l + L_g)} & \text{(4.6a)} \\ Z_{th} = \dfrac{j\omega_g L_g(R_l + j\omega_g L_l)}{R_l + j\omega_g(L_l + L_g)} & \text{(4.6b)} \end{cases}$$

Note that R_l and L_l are obtained from the active and reactive power supplied to the load as follows

$$R_l = \frac{\sqrt{3}u_{ll}^2 P_l}{P_l^2 + Q_l^2} \text{ and } L_l = \frac{\sqrt{3}u_{ll}^2 Q_l}{P_l^2 + Q_l^2} \tag{4.7}$$

where u_{ll} is the load line-to-line RMS voltage. P_l and Q_l are the load active and reactive power of the system, respectively. They can be obtained from the load current and voltage

$$P_l = \frac{3}{2}(u_{dl}i_{dl} + u_{ql}i_{ql}) \text{ and } Q_l = \frac{3}{2}(u_{ql}i_{dl} - u_{dl}i_{ql}) \tag{4.8}$$

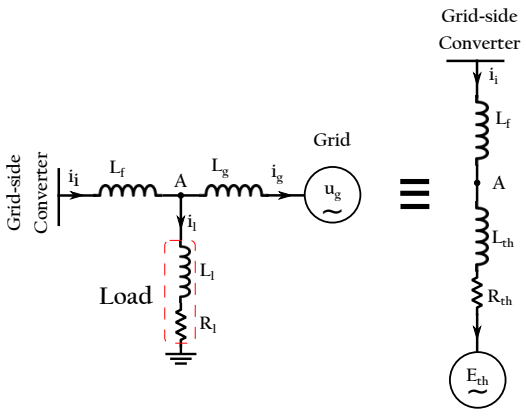

Figure 4.3: Grid-side circuit Thevenin equivalent.

When the grid is not available (in the stand-alone mode), the Thévenin voltage and impedance are respectively given by

$$E_{th} = u_l \text{ and } Z_{th} = Z_l \tag{4.9}$$

The grid-side circuit is assumed in a quasi-static mode, therefore, the following relationships are valid

$$\begin{cases} u_{dl} = R_{th} i_{di} - \omega_g L_{th} i_{qi} + E_{thd} & \text{(4.10a)} \\ u_{ql} = R_{th} i_{qi} + \omega_g L_{th} i_{di} + E_{thq} & \text{(4.10b)} \end{cases}$$

where R_{th} and $\omega_g L_{th}$ are real and imaginary parts of the Thévenin impedance, respectively ($Z_{th} = R_{th} + j\omega_g L_{th}$).

The next section presents the theory of feedback linearization for nonlinear multivariable systems.

4.3 Nonlinear Controller Design

Before applying the nonlinear multi-input-multi-output (MIMO) control to the wind energy conversion system (WECS), a background on the feedback linearization method for multivariable systems is described in the following section.

4.3.1 Feedback Linearization

Let consider the following MIMO system [63]

$$\begin{cases} \dot{\overline{x}} = f(\overline{x}) + g(\overline{x})\overline{u} & \text{(4.11a)} \\ \overline{y} = h(\overline{x}) & \text{(4.11b)} \end{cases}$$

where $\overline{x} \in \mathbb{R}^n$ is the state vector. $\overline{u} \in \mathbb{R}^m$ is the vector of m inputs u_i ($i = 1, ..., m$). $\overline{y} \in \mathbb{R}^m$ is the vector of m outputs y_j ($j = 1, ..., m$). f and g are smooth vector and matrix fields, respectively. h is the smooth vector function.

The input-output linearization method for MIMO systems consists of differentiating the outputs y_j until at least one input appears.

Consider $\mathcal{L}_f h$ and $\mathcal{L}_g h$ the Lie derivatives of h with respect to f and g, $\dot{y}_j$ can be written as

$$\dot{y}_j = \mathcal{L}_f h_j + \sum_{i=1}^{m} (\mathcal{L}_{g_i} h_j) u_i \tag{4.12}$$

If $\mathcal{L}_{g_i} h_j(x) = 0$ for all i, then no inputs appears and one has to differentiate again. Assumed that y_j needs to be differentiated r_j times before at least one input appears, then

$$y_j^{(r_j)} = \mathcal{L}_f^{r_j} h_j + \sum_{i=1}^{m} \mathcal{L}_{g_i} \mathcal{L}_f^{r_j - 1} h_j u_i, \ (j = 1, ..., m) \tag{4.13}$$

Eqn. (3) can be written into a matrix form as follows

$$\begin{bmatrix} y_1^{(r_1)} \\ \vdots \\ y_m^{(r_m)} \end{bmatrix} = \begin{bmatrix} \mathcal{L}_f^{r_1} h_1(x) \\ \vdots \\ \mathcal{L}_f^{r_m} h_m(x) \end{bmatrix} + B(x) \underbrace{\begin{bmatrix} u_1 \\ \vdots \\ u_m \end{bmatrix}}_{\overline{u}} \tag{4.14}$$

where the $m \times m$ matrix $B(x)$ is referred to as the decoupling matrix for the MIMO system. It has the following expression.

$$B(x) = \begin{bmatrix} \mathcal{L}_{g_1} \mathcal{L}_f^{r_1 - 1} h_1 & \cdots & \mathcal{L}_{g_m} \mathcal{L}_f^{r_1 - 1} h_1 \\ \vdots & \ddots & \vdots \\ \mathcal{L}_{g_1} \mathcal{L}_f^{r_m - 1} h_m & \cdots & \mathcal{L}_{g_m} \mathcal{L}_f^{r_m - 1} h_m \end{bmatrix} \tag{4.15}$$

Eqn. (4) is linearized by choosing the control input vector u as follows.

$$\overline{u} = -B^{-1} \begin{bmatrix} \mathcal{L}_f^{r_1} h_1(x) \\ \vdots \\ \mathcal{L}_f^{r_m} h_m(x) \end{bmatrix} + B^{-1} \underbrace{\begin{bmatrix} v_1 \\ \vdots \\ v_m \end{bmatrix}}_{\overline{v}} \tag{4.16}$$

where v is the new input yet to be determined.

The closed loop equation of the system is obtained by substituting Eqn. (6) into Eqn. (4) to get

$$\begin{bmatrix} y_1^{(r_1)} \\ \vdots \\ y_m^{(r_m)} \end{bmatrix} = \begin{bmatrix} v_1 \\ \vdots \\ v_m \end{bmatrix} \tag{4.17}$$

The input-output relationship given by Eqn. (7) is not only linear but also decoupled.

Remark 2: $(r_1, ..., r_m)$ is called the *relative degree* of the system (Eqn. 1) and the scalar $r = r_1 + ... + r_m$ is called the *total relative degree* of the system [63]. In the case where the total relative degree of the nonlinear system is smaller than the order of the system (n), the system (Eqn. 1) has some *internal dynamics* which cannot be seen from the output. There is no internal dynamics when the total relative degree is equal to n.

4.3.2 Proposed Nonlinear Controller Design

The design of a unified nonlinear MIMO control system for the wind energy storage-system, which is capable to operate in the grid connected and the stand-alone modes, is studied in this section. The MIMO controller will be able to calculate and generate the appropriate control signals for each converter. The controller is designed using the input-output feedback linearization method. Fig. 4.4 illustrates the structure of the proposed MIMO controller.

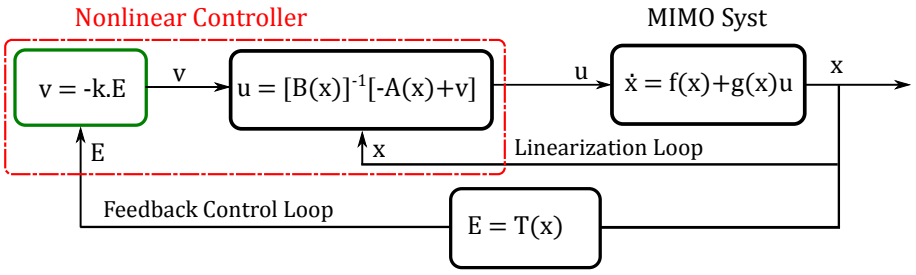

Figure 4.4: Proposed MIMO controller structure.

Five control objectives have been considered in order to: 1) keep the wind turbine operating at its maximum power by controlling ω_r; 2) achieve a linear relationship between the stator current and the electromagnetic torque by controlling the stator d-axis current, i_{ds}; 3) meet load voltage requirement by controlling both load d-axis and q-axis voltages, u_{dl} and u_{ql} respectively; 4) ensure the regulation of the dc-link voltage by controlling, u_{dc}, (through E_{dc}); 5) perform power management between the battery, load and grid subsystems by controlling the battery current, i_{lb}.

Regardless the mode of operation, the system to be controlled is represented by Eqs.(4.2), (4.3), (4.4) and (4.5). It is a seven-order nonlinear multivariable system that has six inputs and six outputs. The vector of state variables, $\overline{x} \in \mathbb{R}^n$, the vector of control inputs, $\overline{u} \in \mathbb{R}^m$, and the vector of controlled outputs, $\overline{y} \in \mathbb{R}^m$, are respectively

$$\begin{cases} \overline{x} = [i_{ds}, i_{qs}, \omega_r, i_{di}, i_{qi}, i_{bl}, E_{dc}]^T & \text{(4.18a)} \\ \overline{u} = [u_{ds}, u_{qs}, u_{di}, u_{qi}, P_{bat}, D]^T & \text{(4.18b)} \\ \overline{y} = [\tilde{i}_{ds}, \tilde{\omega}_r, \tilde{u}_{dl}, \tilde{u}_{ql}, \tilde{E}_{dc}, \tilde{i}_{lb}]^T & \text{(4.18c)} \end{cases}$$

where $\tilde{i}_{ds}, \tilde{\omega}_r, \tilde{u}_{dl}, \tilde{u}_{ql}, \tilde{E}_{dc}$ and $\tilde{i}_{lb}$ are defined as follows

$$\tilde{i}_{ds} = \int (i_{ds} - i^*_{ds}) d\delta, \qquad \tilde{\omega}_r = \int (\omega_r - \omega^*_r) d\delta \tag{4.19}$$

$$\tilde{u}_{dl} = \int (u_{dl} - u^*_{dl}) d\delta, \qquad \tilde{u}_{ql} = \int (u_{ql} - u^*_{ql}) d\delta \tag{4.20}$$

$$\tilde{E}_{dc} = \int (E_{dc} - E^*_{dc}) d\delta, \qquad \tilde{i}_{lb} = \int (i_{lb} - i^*_{lb}) d\delta \tag{4.21}$$

The output variables $\tilde{i}_{ds}, \tilde{\omega}_r, \tilde{u}_{dl}, \tilde{u}_{ql}, \tilde{E}_{dc}$ and $\tilde{i}_{lb}$ represent the integral of the errors between the variables $i_{ds}, \omega_r, u_{dl}, u_{ql}, E_{dc}$ and i_{lb} to be regulated, and their references $i^*_{ds}, \omega^*_r, u^*_{dl}, u^*_{ql}, E^*_{dc}$ and i^*_{bl}, respectively. Integral actions are added into the control-loop to ensure zero steady state errors and to increase the robustness of the controller when the system structure changes. This happens, for instance, when the system switches from the stand-alone mode to the grid-connected mode.

Note that integrators have increased the order of the system. The new system to be controlled is now represented by Eqs. (4.18)-(4.21) which is a 13-order nonlinear model.

The input-output feedback linearization control design method is used to linearize and decouple this nonlinear model. Each output is differentiated therefore until at least one input appears. For the sake of simplicity, not all of the design steps are presented. However, it can be noted that each controlled variable has been differentiated twice, before a control input emerges, except for $\tilde{\omega}_r$ which has been differentiated three times. One obtains

$$\underbrace{\begin{bmatrix} \ddot{\tilde{i}}_{ds} \\ \dddot{\tilde{\omega}}_r \\ \ddot{\tilde{u}}_{dl} \\ \ddot{\tilde{u}}_{ql} \\ \ddot{\tilde{E}}_{dc} \\ \ddot{\tilde{i}}_{lb} \end{bmatrix}}_{y_d(\overline{x})} = \underbrace{\begin{bmatrix} A_1 \\ A_2 \\ A_3 \\ A_4 \\ A_5 \\ A_6 \end{bmatrix}}_{A_{nl}(\overline{x})} + \underbrace{\begin{bmatrix} \frac{1}{L_d} & 0 & 0 & 0 & 0 & 0 \\ 0 & -\frac{3P^2\lambda_r}{2JL_q} & 0 & 0 & 0 & 0 \\ 0 & 0 & \frac{R_{th}}{L_f} & -\frac{\omega_g L_{th}}{L_f} & 0 & 0 \\ 0 & 0 & \frac{\omega_g L_{th}}{L_f} & \frac{R_{th}}{L_f} & 0 & 0 \\ 0 & 0 & 0 & 0 & 1 & 0 \\ 0 & 0 & 0 & 0 & 0 & -\frac{u_{dc}}{L_b} \end{bmatrix}}_{\overline{B}_{nl}} \underbrace{\begin{bmatrix} u_{ds} \\ u_{qs} \\ u_{di} \\ u_{qi} \\ P_{bat} \\ D \end{bmatrix}}_{\overline{u}_{nl}} \tag{4.22}$$

where

$$\begin{aligned}
A_1 &= -\frac{R_s}{L_d} i_{ds} + \frac{L_q}{L_d} \omega_r i_{qs} \\
A_2 &= -\frac{3P^2}{2JL_q} \lambda_r (-L_d \omega_r i_{ds} - R_s i_{qs} - \lambda_r \omega_r) - \frac{2K_{opt}\omega_r}{PJ^2} (\frac{3P^2\lambda_r}{2} i_{qs} - \frac{K_{opt}\omega_r^2}{P}) \\
A_3 &= R_{th}(\omega_g i_{qi} - \frac{u_{dl}}{L_f}) - \omega_g L_{th}(-\omega_g i_{di} - \frac{u_{ql}}{L_f}) + \dot{Eth}_d \\
A_4 &= R_{th}(-\omega_g i_{di} - \frac{u_{ql}}{L_f}) + \omega_g L_{th}(\omega_g i_{qi} - \frac{u_{dl}}{L_f}) + \dot{Eth}_q \\
A_5 &= u_{dc} i_{sdc} - \frac{3}{2} i_{di} u_{di} \text{ and} \\
A_6 &= \frac{u_{bat}}{L_b}
\end{aligned} \tag{4.23}$$

The control input has the following form

$$\overline{u}_{nl} = \left[\overline{B}_{nl}\right]^{-1} \left[-A_{nl}(\overline{x}) + \overline{v}_{nl}\right] \tag{4.24}$$

where $\overline{v}_{nl}$ is the new control inputs vector, yet to be determined. The suffix nl stands for nonlinear.

Eqn. (4.24) is valid since the determinant of the matrix $B_{nl}(\overline{x})$, given in Eqn. (4.25), is nonzero during the normal operation of the system. Indeed the dc-link voltage, u_{dc}, and the rated rotor flux linage, λ_r, are not equal to zero.

$$det(\overline{B}_{nl}) = \frac{-3P^2\lambda_r(R_{th}^2 + \omega_g^2 L_{th}^2)u_{dc}}{2JL_dL_qL_bL_f^2} \tag{4.25}$$

By choosing u_{nl} as in Eqn. (4.24), the nonlinearities in Eqn. (4.22) are canceled and the following linear relationship between the new outputs $y_d(\overline{x})$ and the new inputs, $\overline{v}_{nl}$, is obtained.

$$y_d(\overline{x}) = \overline{v}_{nl} \tag{4.26}$$

where $y_d(\overline{x}) = \left[\ddot{\tilde{i}}_{ds}, \dddot{\tilde{\omega}}_r, \ddot{\tilde{u}}_{dl}, \ddot{\tilde{u}}_{ql}, \ddot{\tilde{E}}_{dc}, \ddot{\tilde{i}}_{lb}\right]^T$ and $\overline{v}_{nl} = [v_1, v_2, v_3, v_4, v_5, v_6]^T$.

Note that the total relative degree ($r = 13$) is equal to the order of the system n ($n = 13$). Therefore the linearization is complete and there is no internal dynamics.

Remark 3: The closed loop system (Eqn. (4.26)) is consisted of six decoupled linear subsystems. There are five second-order subsystems ($\ddot{\tilde{i}}_{ds}, \ddot{\tilde{u}}_{dl}, \ddot{\tilde{u}}_{ql}, \ddot{\tilde{E}}_{dc}$ and $\ddot{\tilde{i}}_{lb}$), and only one third-order subsystems ($\dddot{\tilde{\omega}}_r$).

It becomes now simple to design a stabilizing controller for Eqn. (4.26). A state feedback controller is used. It has the following equation:

$$v_p = -k_{pq}e_p \tag{4.27}$$

where k_{pq} ($p \in \{1, 2, 3, 4, 5, 6\}$ and $q \in \{1, 2, 3\}$) is the feedback gain matrix and e_p represents the errors between the outputs variables ($\tilde{i}_{ds}, \tilde{\omega}_r, \tilde{u}_{dl}, \tilde{u}_{ql}, \tilde{E}_{dc}$ and $\tilde{i}_{lb}$)

and the reference signals. These references are equal to zero. Therefore, the v_p ($p \in \{1,2,3,4,5,6\}$) have the following expressions

$$\begin{aligned} v_1 &= -k_{11}\tilde{i}_{ds} - k_{12}\dot{\tilde{i}}_{ds}, & v_2 &= -k_{21}\tilde{\omega}_r - k_{22}\dot{\tilde{\omega}}_r - k_{23}\ddot{\tilde{\omega}}_r, \\ v_3 &= -k_{31}\tilde{u}_{dl} - k_{32}\dot{\tilde{u}}_{dl}, & v_4 &= -k_{41}\tilde{u}_{ql} - k_{42}\dot{\tilde{u}}_{ql}, \\ v_5 &= -k_{51}\tilde{E}_{dc} - k_{52}\dot{\tilde{E}}_{dc}, & v_6 &= -k_{61}\tilde{i}_{lb} - k_{62}\dot{\tilde{i}}_{lb} \end{aligned} \tag{4.28}$$

The feedback gain matrix, k_{ij}, is chosen so that the eigenvalues of the closed loop system are *Hurwitz*. They are calculated in such a way that the slowest dynamic, which is that of the mechanical speed, stabilizes in 0.3 seconds with a damping coefficient of 0.9. The desired poles are determined accordingly and given in the Table 4.1 below. The closed loop system is asymptotically stable. Consequently, errors between outputs and references will converge to zero.

Table 4.1: Performance Specifications

Dynamics	$\tilde{i}_{ds}$	$\tilde{\omega}_r$	$\tilde{u}_{dql}$	$\tilde{E}_{dc}$	$\tilde{i}_{lb}$
Desired Poles	$\begin{bmatrix} -50 \\ -10000 \end{bmatrix}$	$\begin{bmatrix} -15 \pm 6.5i \\ -1470 \end{bmatrix}$	$\begin{bmatrix} -2, -50 \\ -1, -10 \end{bmatrix}$	$\begin{bmatrix} -13 \\ -50 \end{bmatrix}$	$\begin{bmatrix} -6 \\ -700 \end{bmatrix}$

To choose the reference signals $i^*_{ds}, \omega^*_r, u^*_{dl}, u^*_{ql}, E^*_{dc}$ and i^*_{bl}, the following points are considered:

1. i^*_{ds} is set to zero to realize the *zero d-Axis current (ZDC) control* scheme. This control scheme is employed to achieve a linear relationship between the stator current and the electromagnetic torque.
2. ω^*_r is generated by the MPPT controller.
3. u^*_{dl} is aligned with the grid voltage vector to achieve voltage oriented control (VOC). Therefore, u^*_{dl} is equal to the gird voltage magnitude. Hence u^*_{ql} is equal to zero.
4. u_{dc^*} ($E^*_{dc} = \frac{1}{2}C_{dc}u^{*2}_{dc}$) is the reference of the *dc*-link voltage.

5. i_{bl}^{*} is generated from the *dc*-link voltage controller according to the load power requirement.

$\dot{\omega}_{r_{ref}}$ is assumed constant. Therefore, $\ddot{\omega}_{r_{ref}} = 0$

Remark 4: The synchronization to the grid is done by using a PLL (Phase-locked Loop) [104]. Therefore, in the grid-connected mode, the grid frequency (ω_g) which is used in the dq-abc coordinate transformation is generated by the PLL. However, in the stand-alone mode, ω_g is generated internally by the controller [135].

Performances of the proposed controller is evaluated in the next section. Simulations are performed to demonstrate the effectiveness and robustness of the MIMO nonlinear controller. Various case studies will be presented.

4.4 Results

Various tests are carried out using the SimPowerSystems toolbox [13] in Matlab/Simulink software to demonstrate the effectiveness and robustness of the proposed unified nonlinear control scheme in both grid-connected and stand-alone modes. As illustrated in Fig. 4.1, the system consisted of a 2.45 MW wind power generator supplying a nonlinear variable load (1-to-2 MW). A variable speed nonsalient-pole PMSG was employed as generator which parameters are given in Table 4.2 [21]. A back-to-back converter (AC/DC/AC) and a bi-directional buck-boost (DC/DC) were utilized to connect the generator and the grid to the load, and the battery-storage-unit to the dc-link voltage, respectively. The feedback gains k_{pq} of the nonlinear controller, is given in Table 4.3.

Three case studies have been conducted. In *Case 1*, the dynamic and steady-state performances of the system when it switches from one mode of operation to another is evaluated. The maximum power tracking capability under variable wind speed has been verified. The power management capability of the controller has been tested in *Case 2*. Finally, in *Case 3*, the robustness of the proposed controller is evaluated in the grid-connected and stand-alone modes under four different loads, namely, a balanced three-phase load, an unbalanced three-phase

load, a single-phase nonlinear load, and a dynamic load. An induction motor is used as the dynamic load.

4.4.1 Case 1: Dynamic Performance and Steady-State Analysis in On-grid/Off-grid Modes

To analyze the dynamic and steady-state performance of the system, simulations have been carried out under different wind speeds. The simulation starts with a

Table 4.2: System Parameters

Parameter	Rated Value	Parameter	Rated Value
P_m	2.45 MW	u_g	4000 V
ω_m	4.3 rd/s	u_{dc}	8000 V
λ_r	28 Wb	C_{dc}	1667 μF
P	8	L_f	16.884 mH
J	4000 $kg.m^2$	L_g	1.6884 mH
R_s	24.21 $m\Omega$	F_{gen}	740 Hz
L_{ds}, L_{ds}	9.81 mH	F_{grid}	2040 Hz
V_w	15 m/s	u_{ll}	4000 V
R	28.16 m	P_l	2 MW
Rho	1.25	u_{bat}	4000 V
λ_{opt}	8.1	P_{bat}	1.5 MW

Table 4.3: Controller Gains k_{pq}

Controller Gains Description	Value
$\tilde{i}_{ds}$ and $\dot{\tilde{i}}_{ds}$ Gains	$[K_{11}K_{12}] = [500, 1].10^3$
$\tilde{\omega}_r$, $\dot{\tilde{\omega}}_r$ and $\ddot{\tilde{\omega}}_r$ Gains	$[K_{21}K_{22}K_{23}] = [400, 45, 1.5].10^3$
$\tilde{u}_{dl}$ and $\dot{\tilde{u}}_{dl}$ Gains	$[K_{31}K_{32}] = [800, 600]$
$\tilde{u}_{ql}$ and $\dot{\tilde{u}}_{ql}$ Gains	$[K_{41}K_{42}] = [30, 300]$
$\tilde{E}_{dc}$ and $\dot{\tilde{E}}_{dc}$ Gains	$[K_{51}K_{52}] = [300, 0.3]$
$\tilde{i}_{lb}$ and $\dot{\tilde{i}}_{lb}$ Gains	$[K_{61}K_{62}] = [4000, 700]$

stand-alone mode and switches in the grid-connected mode at time $t = 1.2$ sec when the switch *Sw1*, in Fig. 4.1, closes. The wind speed is 12 m/s, from 0 to 0.8 sec, 14 m/s, from 0.8 to 1.6 sec, 16 m/s, from 1.6 to 2.1 and 13 m/s from 2.1 to 2.5 sec, respectively.

Fig. 4.5(a) shows the generator rotor reference speed (dashed line) and the actual speed (solid line), while Fig. 4.5(b) shows the generator output power. It can be observed that the waveforms reach their steady state fast and smoothly within approximately 0.5 sec. Fig. 4.6 shows the d-axis current, i_{ds} (solid line), and the q-axis current, i_{qs} (dashed line). It can be observed that the d-axis current is maintained to zero, while the q-axis and generated power profiles are similar. Fig. 4.7 shows the dq-components of the load voltage. One may notice that the d-axis load voltage, u_{dl} (solid line), and the q-axis load voltage, u_{ql} (dashed line) remain constant, despite the variation of the generated power. When the generator output power becomes higher than the load power, the extra energy is stored in

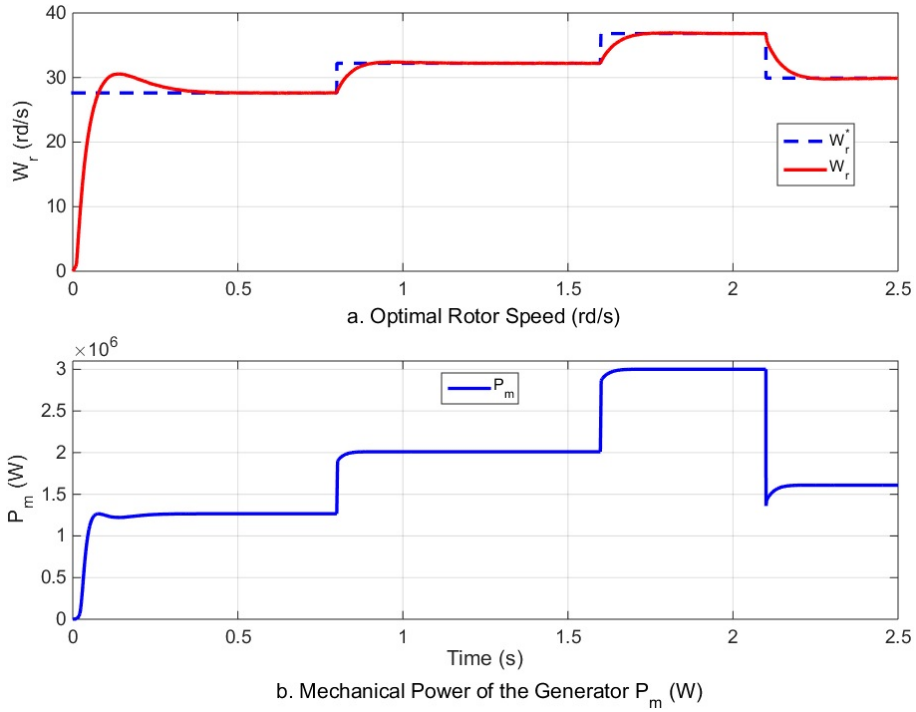

Figure 4.5: Optimum Rotor Speed and Output Power.

the battery. Throughout the simulation time, The dc-link voltage u_{dc} remains constant, allowing the power transfer between the two converters, as shown in Fig. 4.8.

Remark 5: Note that the transition between the stand-alone mode and the grid-connected mode is very smooth despite that no islanding detection mechanism was used. The generator stator current and all the variables ($\omega_r, i_{ds}, u_{dl}, u_{ql}, u_{dc}$) are stables before and after the switching time ($t = 1.2$ sec.), as it can be observed in Fig. 4.5(a), 4.6 and 4.7.

The robustness of the proposed controller has been compared to the conven-

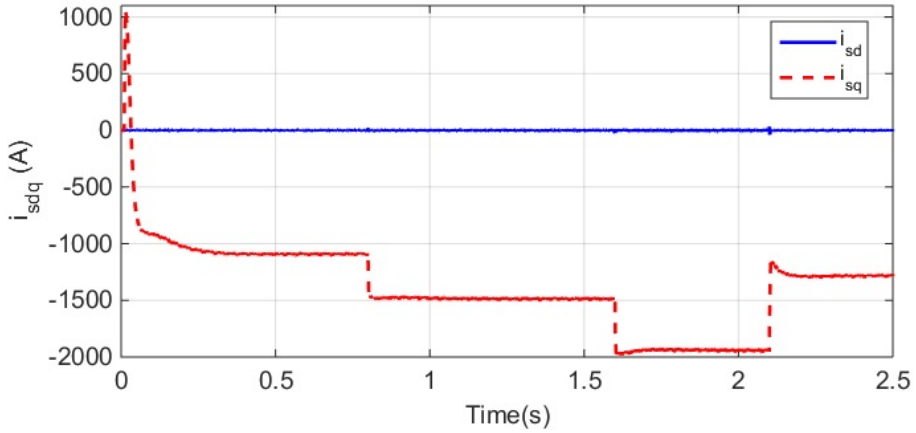

Figure 4.6: *dq*-components of the Generator Stator Current.

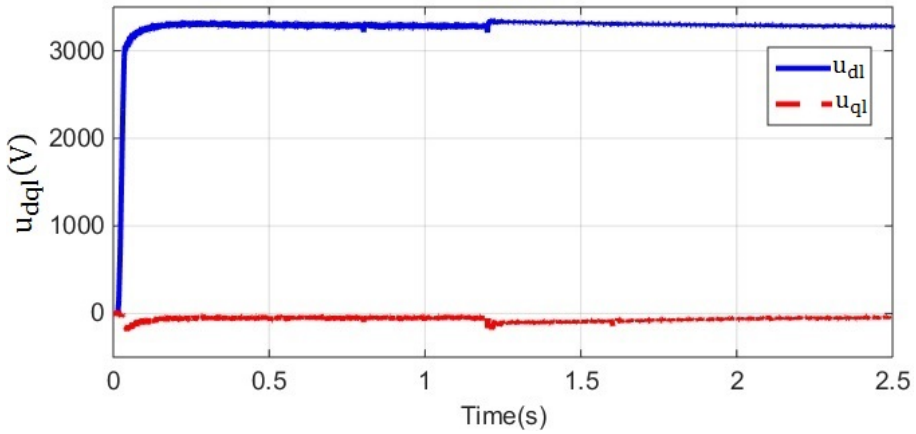

Figure 4.7: *dq*-components of the Load Voltage.

tional PI controller using real wind speed data [120]. Fig. 4.9 and 4.10 show the generator rotor speed and output power, respectively. The black solid line, the dashed line and the red solid line stand for the reference signal, the signal for the PI controller and the signal for the nonlinear controller, respectively. It can be

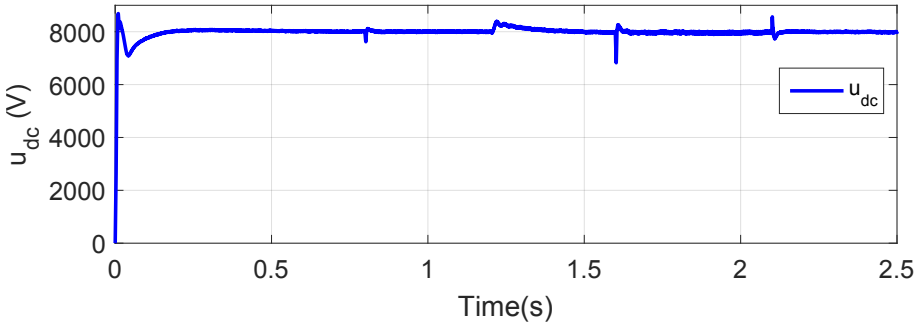

Figure 4.8: dc-link Voltage.

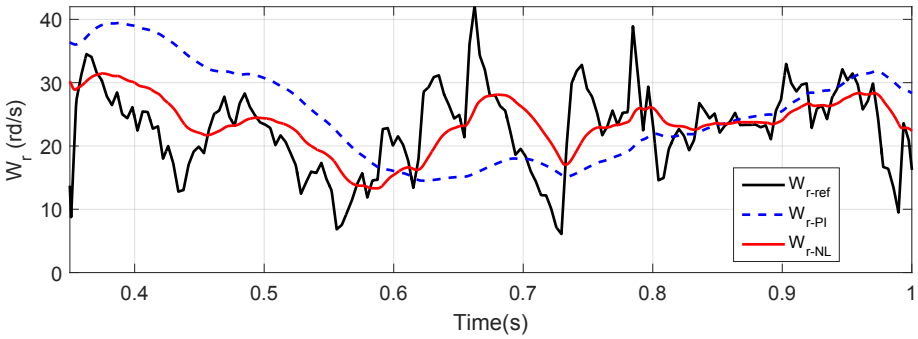

Figure 4.9: Optimum Rotor Speed.

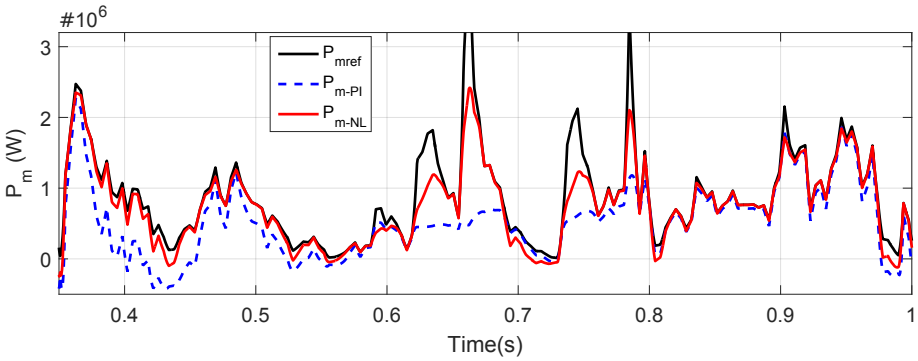

Figure 4.10: Output Power.

observed that the nonlinear controller has a fast and better dynamic behavior as well as a good tracking performance.

The controller capability to always operate the wind-turbine system at its maximum power (*MPPT*) has been tested during this case study. The generator rotor speed reference is generated by the MPPT module for the *MIMO* controller. The speed reference corresponds to the value at which the wind-turbine delivers its maximum power to the PMSG. Fig. 4.11 shows these maximum power operating points (MPP) for different wind speeds. For the tests, the wind was changed from 10 m/s to 11 m/s, 12 m/s, 13 m/s, 14 m/s, and 15 m/s. The corresponding generated active power were 0.5341 MW, 0.7327 MW, 0.9752 MW, 1.2660 MW, 2.0104 MW and 2.4727 MW respectively. One can see that these active power correspond to the operating points *B*, *C*, *D*, *E*, *F* and *G*, respectively. The MIMO controller is therefore able to operate the system at maximum power operating points. Transitions between operating points are fast and smooth as illustrated at Fig. 4.11.

4.4.2 Case 2: Power management between the wind-turbine, the load, the battery-storage and the grid

The power management capability of the system between the wind-turbine, the load, the battery-storage and the grid has been tested in this case study with two different wind speed profiles. In the first test (Fig. 4.12), a constant wind speed is used. It is kept at 13 m/s during the simulation time, which corresponds to a generated power of 1.61 MW. The system starts in the stand-alone mode and the battery is initially charged at 70%. Fig. 4.12 shows the wind-turbine output power (solid line), the load power (dashed line) and the battery power (dotted line) when a constant wind speed is applied. When $0 < t < 1$ sec, the generated power is higher than the load power. The surplus of energy is stored. This is indicated by the negative power for the battery in Fig. 4.12 (dotted line). At $t = 1$ sec, while the system is operating in stand-alone mode, the load power increases from 1 MW to 2 MW when the switch *Sw2* closes. The wind-turbine output power is therefore

not enough to supply the load. The battery provides the deficit of the required power. This is indicated by the positive power for the battery in Fig. 4.12 (dotted line). At $t = 2$ sec, the system switches in the grid-connected mode when the switch *Sw1* closes. The battery keeps on providing almost the same amount of

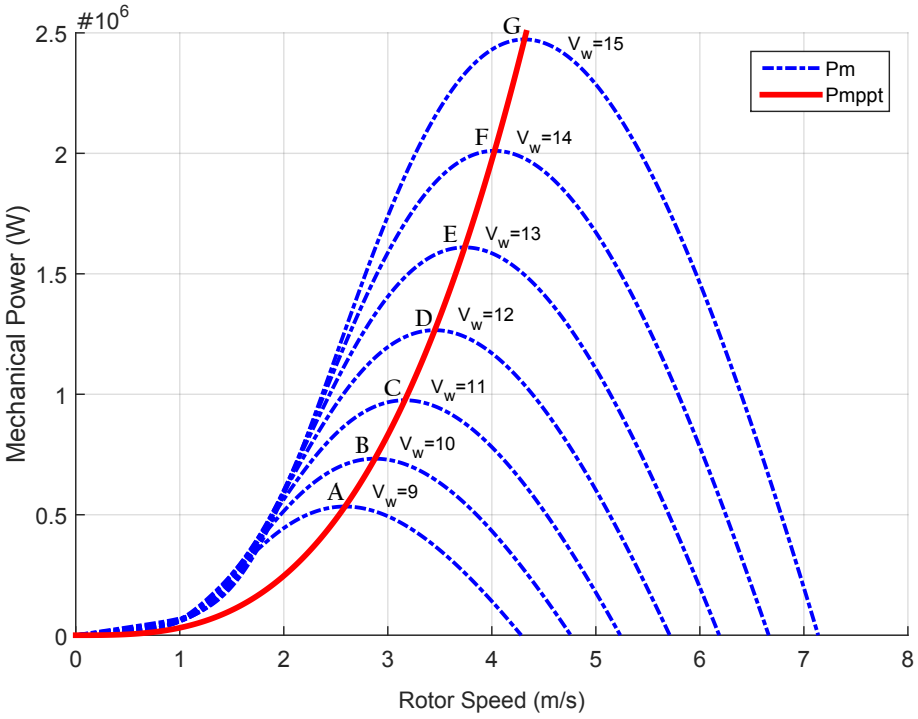

Figure 4.11: MPPT control: Output Power.

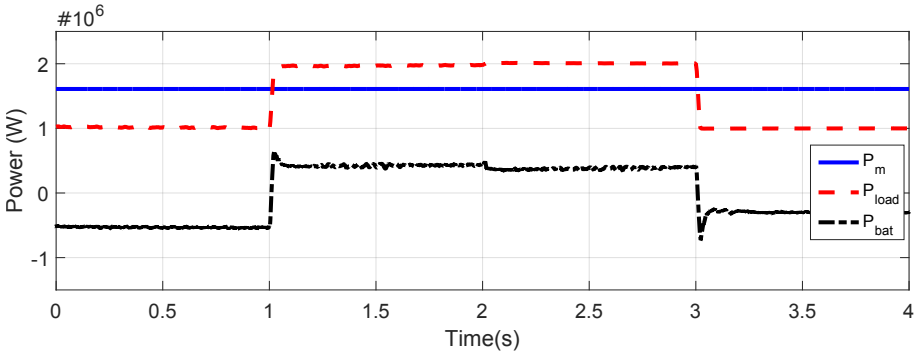

Figure 4.12: Powers of the Wind Turbine, the Load and the Battery with a Constant Wind Speed ($V_w = 13m/s$).

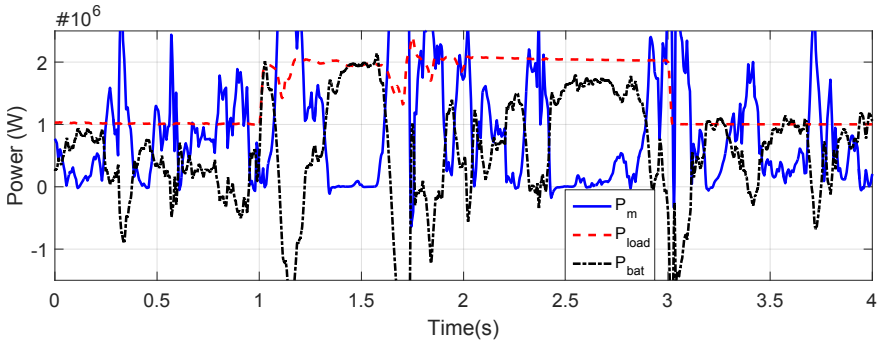

Figure 4.13: Powers of the Wind Turbine, the Load and the Battery with a Real Wind Speed Profile.

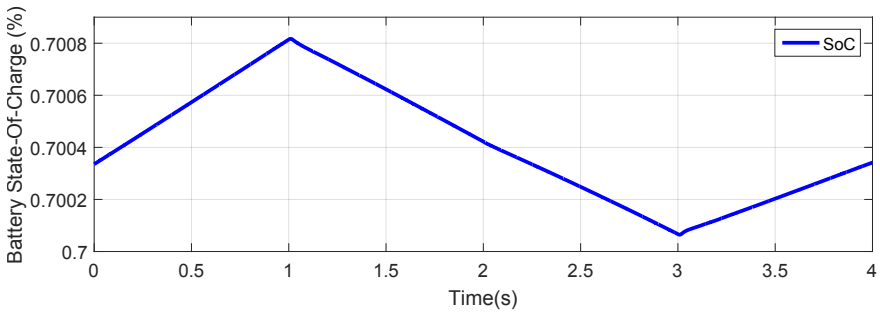

Figure 4.14: Battery's State-Of-Charge (0.70 corresponds to 70%).

power to the load. This reduces the grid contribution. When $2 < t < 4$ sec, while the system is operating in grid-connected mode, the load power decreases from 2 MW to 1 MW at $t = 3$ sec. At this moment, the load demand becomes lower than the generated power. The surplus of power is stored now in the battery as indicated in Fig. 4.12 (dotted line). In the second test, a real wind speed profile is used. The corresponding generated power is given at Fig. 4.13 (solid line). One can observe at Fig. 4.13 (dotted line) the battery-storage charging and discharging capability even under a real wind speed profile. When the generated power is high the battery stores more energy and it is low the battery compensates to supply the load requirements. A SOC (state of charge) control module is added to the system to prevent the battery from overcharging and undercharging when the SOC reaches 90% and 20%, respectively. Fig. 4.14 shows the battery's state-of-charge variation when it is charging and discharging.

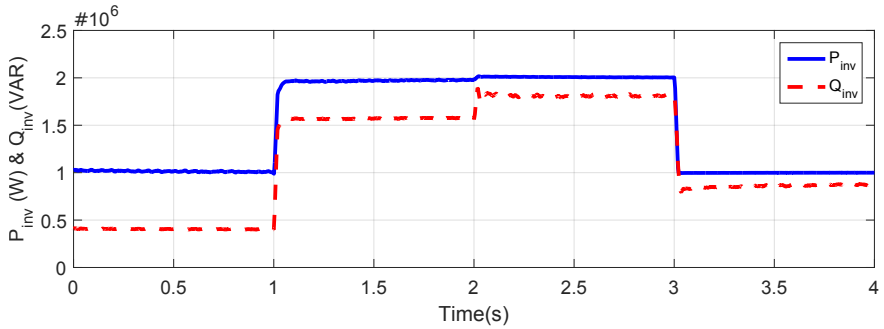

Figure 4.15: Grid-side Converter Output P & Q Power (Generator Sign Convention).

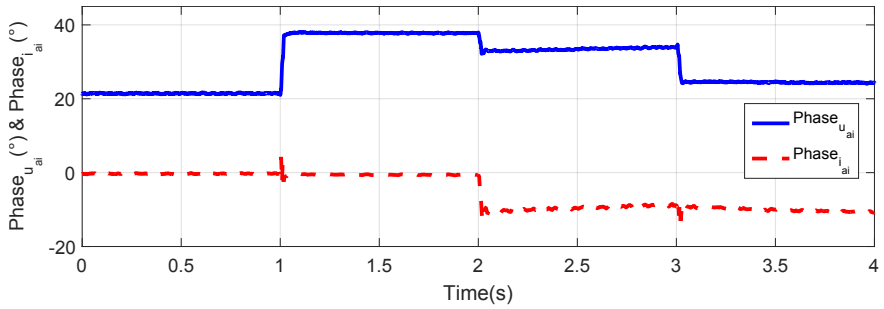

Figure 4.16: Grid-side Converter Output Voltage & Current Phases (Generator Sign Convention).

Remark 6: It is the control of load voltage that allows the use of an L filter even for high power applications [137]. The voltage drop across the bulky L filter is mitigated by the capacitive reactive power generated by the inverter. Fig. 4.15 clearly shows that the converter reactive power (dashed line) is quadrupled when the active power (solid line) doubled. The control system increases significantly the phase shift between the inverter voltage and its current while keeping the DC bus voltage constant. This is shown in Fig. 4.16 where the solid and the dashed lines represent the grid-side converter output voltage and current phases, respectively. The obvious advantages of this strategy are the reduction of the installation cost and the guarantee of stability for the load voltage. Indeed, the utilization of multi-level converters may not be required and the possible instability caused by LC filters could be avoided.

4.4.3 Case 3: Robustness test in both on-grid and Off-grid modes under 4 different loads

To study the robustness of the proposed nonlinear control system, the currents and powers when the system switches form one mode of operation to another have been analyzed for the loads given in Table 4.4 below.

A scenario similar to the previous case study (Section 4.4.2) is used. The simulation starts when the system is in the stand-alone mode and the generated power is 1.61 MW. The system is initially supplying a three-phase series RL load, indicated by H in Fig. 4.1. When $1 < t < 3$ sec, the second load (H_i, $i = 1$ to 4) is applied. The H_i are given in Table 4.4. At $t = 2$ sec, the system switches into the grid-connected mode.

4.4.4 Balanced three-phase load (H_1)

In Fig. 4.12 (red line), 4.17(a), the power and the current of the load are shown, respectively. Waveforms show that the current is sinusoidal. In addition, the tran-

Table 4.4: Loads

Loads	H_1	H_2	H_3	H_4
Type of Load	Balanced three-phase series RL	Unbalanced three-phase series RL	Nonlinear single-phase parallel RC	Induction motor
Value	R_1=16 Ω L_1=16 $m\Omega$	R_{21}=10 Ω L_{21}=11 $m\Omega$ R_{22}=20 Ω L_{22}=11 $m\Omega$ R_{23}=30 Ω L_{23}=11 $m\Omega$	R_3=50 Ω C_3=20 nF	S_3=149.2 kVA u_3=460 V Fr_3=60 Hz

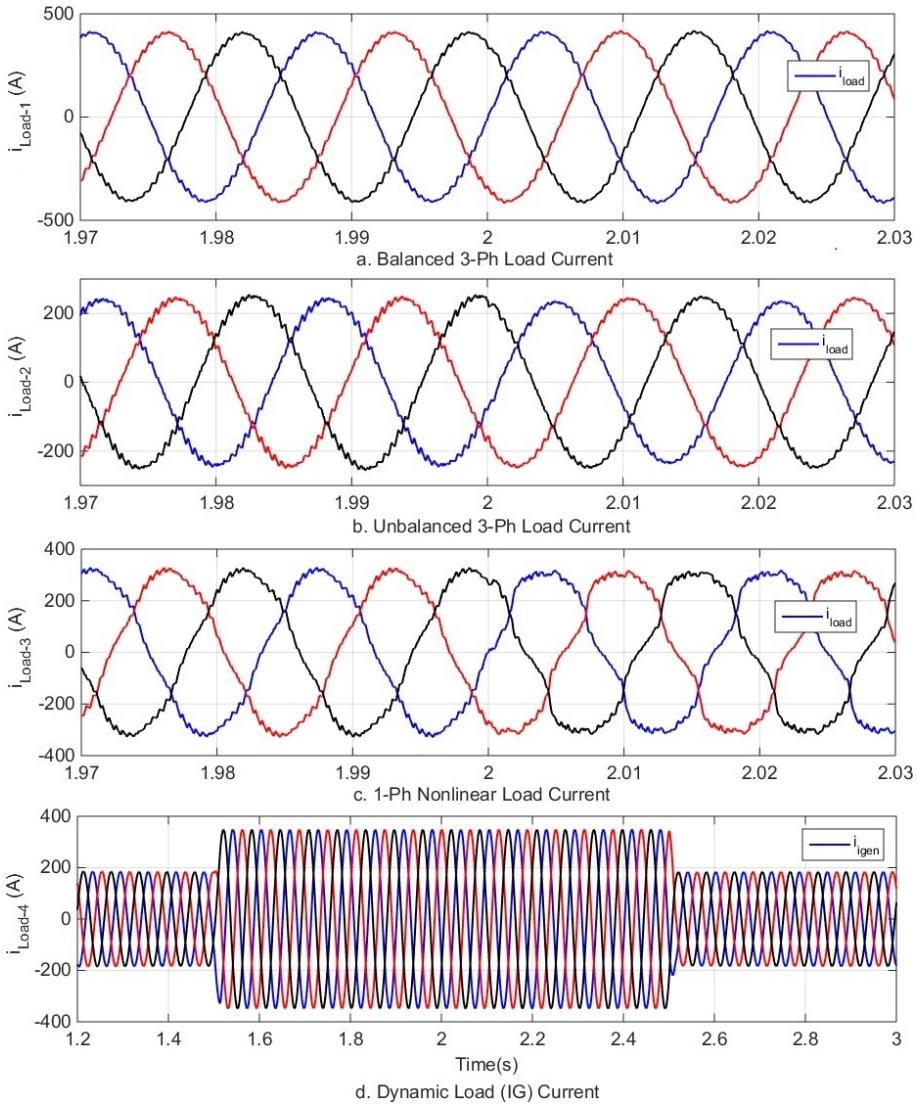

Figure 4.17: Current of Loads: a. Balanced 3-Ph Load, b. Unbalanced 3-Ph Load, c. 1-Ph Nonlineaer Load, d. Dynamic Load (IG).

sition between the stand-alone mode and the grid connected mode which occurred at $t = 2$ sec is smooth.

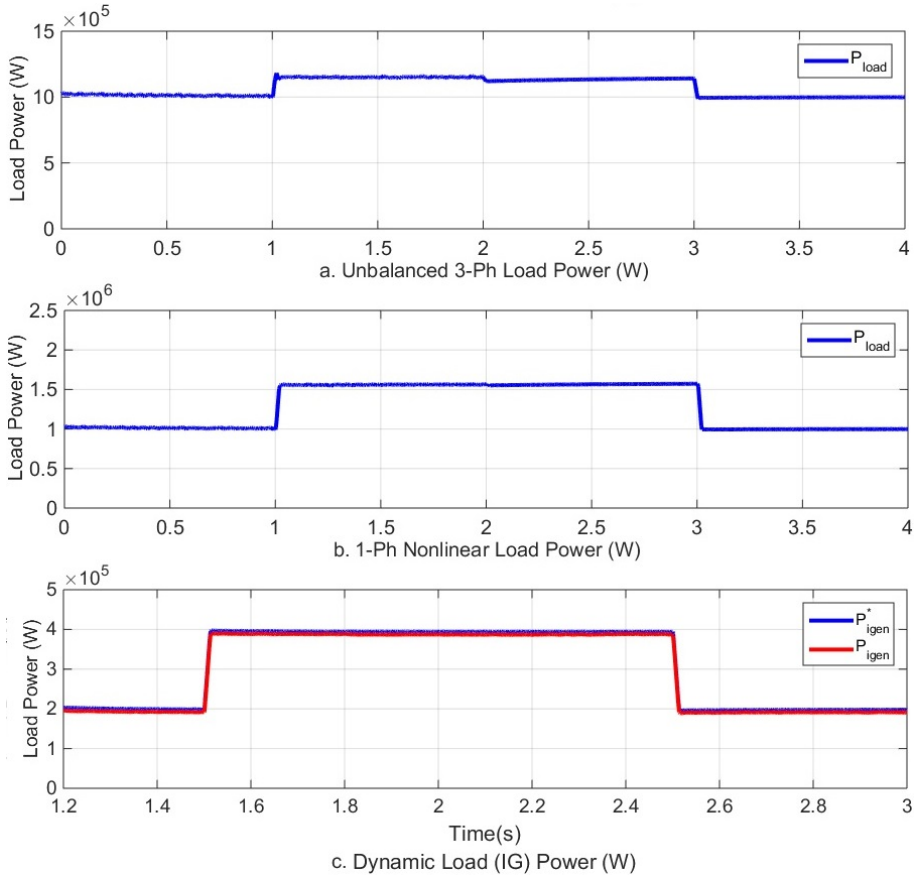

Figure 4.18: Powers of Loads: a. Unbalanced 3-Ph Load, b. 1-Ph Nonlineaer Load, c. Dynamic Load (IG).

4.4.5 Unbalanced three-phase load (H_2)

In Fig. 4.17(b), one can observe that the load three-phase current amplitudes are essentially different, whereas the voltages remain balanced. Therefore, the proposed controller can handle an unbalanced load. Fig. 4.18(a) shows the power waveform for H_2.

4.4.6 Nonlinear load (H_3)

This is a three-phase rectifier with parallel RC load. The nonlinear load, H_3, is simulated. Fig. 4.17(c) and 4.18(b) show its current and power, respectively.

Small ripples can be observed in the waveforms which are due to nonlinearities. However, waveforms are close to sinusoidal.

4.4.7 Dynamic load (H_4)

A 149.2 kVA, 460 V, 60 Hz, squirrel cage induction motor (SCIM) model from SimpowerSystem has been used as the dynamic load in this case study. The wind turbine supplies the SCIM through the step-down 4000V/460V transformer. The SCIM is equipped with two PI controllers, the speed controller and the field-oriented controller (FOC). The speed controller regulates the motor rotor speed, whereas the FOC regulates the load torque. As shown in Fig. 4.18(c), when H_4 is connected, a mechanical load power of 200 kW is applied to the SCIG, first. At $t = 1.5$, the mechanical load increases from 200 kW to the full nominal load, 396 kW. In Fig. 4.17(d), a zoom out plot of H_4 current is illustrated in order to observe the current flowing the change of the mechanical load power (from $t = 1.5$ to $t = 2.5$).

One can see from Fig. 4.12, 4.17 and 4.18 that the proposed nonlinear control system performs a seamless transition between the stand-alone and grid-connected mode, for the above different loads, even though their models were not taken into consideration when designing the controller. This demonstrates that the MIMO controller is robust with respect to unmodeled dynamics.

4.5 Conclusion

A robust unified nonlinear control strategy for a wind energy battery-storage system is proposed in this paper. The system has the capability to flexibly operate in grid-connected and standalone modes. Our approach is different from the conventional methods found in the literature, which use a different controller for each mode of operation. Instead, the proposed controller used only a single controller. Moreover, it does not need an islanding detection system. Consequently, problems related to the islanding and grid detection during the transition mode, such as poor system dynamic performance, poor load current quality and inrush grid cur-

rent, can be avoided. MIMO feedback linearization control technique is adopted as design method. Integrators are added into the control-loop to ensure zero steady state errors when the operating point changes. This considerably increases the robustness of the system. The MPPT, power management and load voltage control performance have been successfully evaluated for both grid-connected and standalone modes under four different loads: 1) balanced three-phase load, 2) unbalanced three-phase load, 3) single-phase nonlinear load, and 4) dynamic load. The simulation results show that the proposed control strategy provides a good control performance. This performance is characterized by fast and smooth transient responses and zero steady state error despite changes in the system model.

Chapter 5

Online Parameter Estimation and Nonlinear Adaptive Control for Stand-Alone and Grid-Connected Hybrid Wind Energy System

Abstract

Model-based design approach can be used to design a controller for a wind energy conversion system (WECS). However, this requires precise knowledge of the parameters of the system. Which is not always the case, in particular, in harsh environment where certain parameters are subject to change. The purpose of this paper is to study online parameter estimation of a hybrid wind energy system that is capable to flexibly operate in both grid-connected and stand-alone mode using a single controller. All the parameters (15 in total) of the system are assumed unknown. An adaptive law derived from Lyapunov stability theory ensures that the parameters are bounded and the state variables converge asymptotically to steady-state values. In addition, the hybrid system provides backup capability to preserve system reliability. The effectiveness of the proposed nonlinear adaptive control method has been evaluated in simulation using real wind speed profile under various type of loads including unbalanced and dynamic load. Moreover, the performance of the proposed adaptive controller has been compared to those of the traditional

PI-based controller and the nonadaptive controller. Results show that the adaptive control can both estimate and update the unknown parameters of the dynamic system online. Also, all the control objectives are achieved with rapid response, good stability and zero steady-state error performance.

Index terms— Adaptive nonlinear control, Battery storage, energy management, feedback linearization, grid-connected, Lyapunov stability, online parameter estimation, robust control, stand-alone, wind turbine.

5.1 Introduction

Although wind energy's contribution to Canada electricity continues to grow every year, their operation in the cold weather conditions arises new challenges which are not present in warmer areas. Among them are the reduction of production power or efficiency and the reduction of lifespan of equipment due to ice accretion. Based on a study conducted by Natural Resources Canada (NRCan) on the effect of cold climate on wind energy production in Canada, the average annual energy loss across the country were estimated to be around 959 GWh as of December 2015 [138]. Nowadays, wind turbine manufacturers are more and more acknowledging the impacts of cold weather operation and are developing turbines equipped with advanced control techniques to increase their performance and reliability in winter conditions. The generator parameters such as stator resistance (R_s) changes with temperature and operation frequency whereas stator self-inductance (L_s) changes with temperature and saturation of electromagnetic core [139, 140]. Any mismatch between the parameter values used in the controller and those in the generator can introduce parametric perturbations in the closed loop system and as a consequence influences the operation and stability of the control system [141].

Several researchers are still investigating the best control system that could support wind generators even with these new operating constraints. A comprehensive literature review on this topic is presented in [142]. Reference [143] presents a parameter estimation method with a grid synchronisation algorithm for wind turbine driven a doubly fed induction generators (DFIGs) by combining a sliding-

mode control (SMC) scheme with adaptive system observer. Extended Kalman Filter (EKF) is used as observer in [144]. Authors in [145] propose a particle swarm fuzzy algorithm based adaptive controller to achieve power maximization and minimization of the generator torque ramp rate. However, these methods are offline based estimation techniques. Also, the unknown parameters are considered to be the rotor position and speed, and not the actual system parameters. Therefore, the performance of such control systems becomes highly sensitive to the generator parameters as they are assumed known. Particularly in hostile environments [140] and [146]. Levenberg–Marquardt optimization method is used to estimate the drive system parameters of a WECS (wind energy conversion system) in [147]. However, a fixed wind speed induction machine is utilized as generator instead of variable speed and only the drive system parameters are estimated. Moreover, the dynamic induction machine is neglected in this application, consequently the system could only operate in the designed operation condition.

It is important, for large countries where access to electricity in rural or remote areas is a concern, to have wind turbine systems that can operate in both grid-connected mode and stand-alone mode. A such system is necessary to cope with power outages and enhance the resilience of the power grid. Unfortunately, the existing wind turbines are not designed to operate in both grid-connected and stand-alone modes, contrary to conventional electric power generators, such as diesel generators and hydroelectric power generators. This is due to their intermittent nature. There is nowadays a tendency in research on how to adapt a single wind turbine to operate in both modes, which constitutes a challenge. Many control algorithms have been proposed in the literature to deal with this issue. Authors in [135] and [32] suggest a control technique for a PMSG-based WECS which can operate in both stand-alone and grid-connected modes. A PI current controller has been used. A similar method is presented in [16] and [34] where an asynchronous generator is utilized as generator. In [148] and [149] a virtual generator control method is proposed where the WECS behaves like synchronous generators to support the grid. Although the system can operate in stand-alone and grid-connected modes, the WT (wind turbine) are modeled by

voltage sources with a magnitude and a phase, which is a system-level representation. Therefore, results may not be accurate when modeled at component level. In addition, different equations are used in stand-alone mode and grid-connected mode. This may require different controller for each mode of operation.

This paper investigates online parameter estimation of a hybrid wind/battery system. The main contribution is that, without prior knowledge of the parameters of the hybrid system different components (wind turbine, generator, converters, filter, grid, battery and load), it can flexibly operate in both grid-connected and stand-alone modes using a single controller. The controller includes an online Lyapunov-based adaptation module that continuously update its parameters when the system operation changes. In addition, the hybrid system provides backup capability to preserve system reliability. It can also support the grid by selling power back to the grid during high wind condition. Moreover, the system does not need an islanding detection module [121, 122] to seamlessly transit from one mode to another. Therefore, issues related to islanding detection, such as poor dynamic performance [123, 38], low quality load current waveform [124, 125] and inrush grid current [126] throughout the transition of operation mode, can be avoided. As opposed to the WT generator used in [28] where a nonsalient-pole one was used, a variable speed salient-pole permanent magnet synchronous machine is used here. A three-phase dual power converter is utilized to connect the wind turbine to the load and the grid. Additionally, the dc-link voltage and the power of the load are directly controlled through a bi-directional buck-boost DC/DC converter based on the power balance and also the system stability. Regardless of the mode of operation, the single controller performs the power point tracking, load voltage regulation and power management between the battery the load and the grid. The effectiveness of the proposed control scheme is demonstrated utilizing unbalanced three-phase load and single-phase nonlinear load under a real wind speed profile.

The paper is organized as follows. The description of the hybrid wind/battery system along with the dynamic equations of the system are presented in Section 5.2. The proposed nonlinear adaptive control strategy is discussed in Section 5.3. The results of the hybrid system simulated with different wind profiles and

load variations demonstrating the performance of the proposed control method are presented in Section 5.4. Section 5.5 concludes the paper.

5.2 Problem Formulation

The wind energy battery-storage system under study is illustrated in Fig. 5.1. It consists of a PMSG driven by a wind turbine, a generator-side AC/DC converter, a grid-side DC/AC converter, a battery-storage unit connected to the DC-link through a bi-directional buck-boost DC/DC converter. In the stand-alone mode, the switch *Sw1* is opened and the system supplies critical local load only. In the grid-connected mode, the switch *Sw1* is closed.

It has been shown in [150] that regardless the mode of operation, the mathematical model in the *dq* frame of the wind energy battery-storage system, can be represented by Eqn.(5.1).

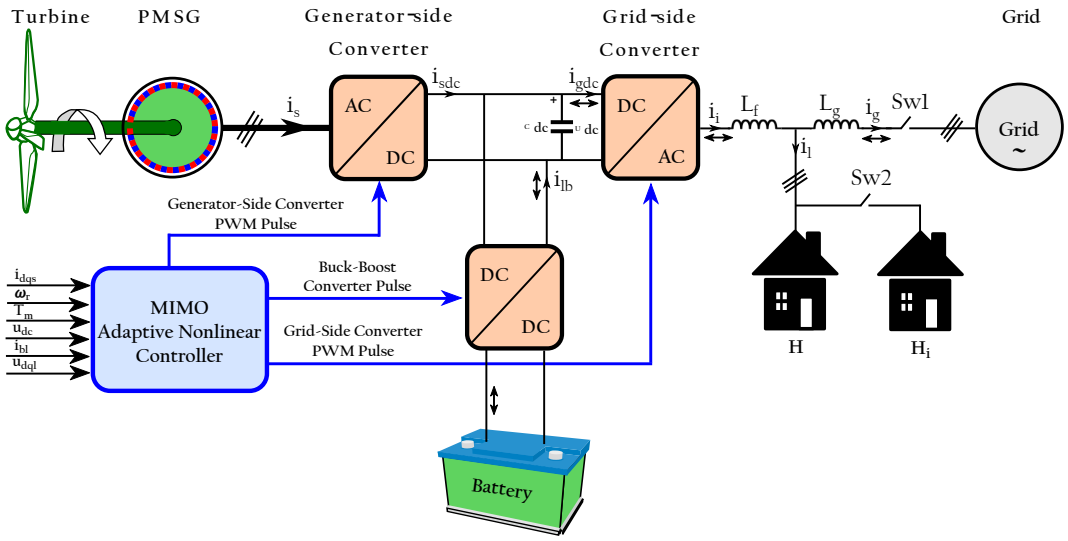

Figure 5.1: Grid-connected/Stand-alone WECS based permanent magnet synchronous generator.

$$\frac{\mathrm{d}}{\mathrm{d}t}\begin{bmatrix} i_{ds} \\ i_{qs} \\ \omega_r \\ i_{di} \\ i_{qi} \\ E_{dc} \\ i_{bl} \end{bmatrix} = \begin{bmatrix} -\frac{R_s}{L_d} & \frac{L_q}{L_d}\omega_r & 0 & 0 & 0 & 0 & 0 \\ -\frac{L_d}{L_q}\omega_r & -\frac{R_s}{L_q} & -\frac{\lambda_r}{L_q} & 0 & 0 & 0 & 0 \\ 0 & -\frac{3P^2\lambda_r}{2J} & \frac{k_{opt}}{JP}\omega_r & 0 & 0 & 0 & 0 \\ 0 & 0 & 0 & 0 & \omega_g & 0 & 0 \\ 0 & 0 & 0 & -\omega_g & 0 & 0 & 0 \\ 0 & 0 & 0 & -\frac{3}{2}u_{di} & 0 & 0 & 0 \\ 0 & 0 & 0 & 0 & 0 & 0 & 0 \end{bmatrix}\begin{bmatrix} i_{ds} \\ i_{qs} \\ \omega_r \\ i_{di} \\ i_{qi} \\ E_{dc} \\ i_{bl} \end{bmatrix}$$
$$+\begin{bmatrix} \frac{1}{L_d} & 0 & 0 & 0 & 0 & 0 \\ 0 & \frac{1}{L_q} & 0 & 0 & 0 & 0 \\ 0 & 0 & 0 & 0 & 0 & 0 \\ 0 & 0 & -\frac{1}{L_f} & 0 & 0 & 0 \\ 0 & 0 & 0 & -\frac{1}{L_f} & 0 & 0 \\ 0 & 0 & 0 & 0 & 1 & 0 \\ 0 & 0 & 0 & 0 & 0 & -\frac{u_{dc}}{L_b} \end{bmatrix}\begin{bmatrix} u_{ds} \\ u_{qs} \\ u_{di} \\ u_{qi} \\ P_{pat} \\ D \end{bmatrix} + \begin{bmatrix} 0 \\ 0 \\ 0 \\ \frac{1}{L_f}u_{dl} \\ \frac{1}{L_f}u_{ql} \\ i_{sdc}u_{dc} \\ \frac{1}{L_b}u_{bat} \end{bmatrix} \tag{5.1}$$

The description of the hybrid system variables is given in Table 5.1. One may observe that the system is a seven-order nonlinear multi-input-multi-output (MIMO) system. It has six inputs and six outputs. The vector of state variables, $\overline{x} \in \mathbb{R}^n$, the vector of control inputs, $\overline{u} \in \mathbb{R}^m$, and the vector of controlled outputs, $\overline{y} \in \mathbb{R}^m$, are respectively

$$\begin{cases} \overline{x} = [i_{ds}, i_{qs}, \omega_r, i_{di}, i_{qi}, E_{dc}, i_{bl}]^T & \text{(5.2a)} \\ \overline{u} = [u_{ds}, u_{qs}, u_{di}, u_{qi}, P_{bat}, D]^T & \text{(5.2b)} \\ \overline{y} = [i_{ds}, \omega_r, u_{dl}, u_{ql}, E_{dc}, i_{lb}]^T & \text{(5.2c)} \end{cases}$$

The study presented in [150] is done with the assumption that all the parameters of the system were well known. Let's see how that controller performs to large parameter changes before designing the adaptive controller. For the test, the inertia of the turbine generator was increased by 50%. The effect of this change on the performance of the system is shown in Fig. 5.2. The upper figure represents

Table 5.1: System Variables

Parameter	Description and Rated Value
i_{ds}, i_{qs}	Generator stator d- and q-axis currents (A)
u_{ds}, u_{qs}	Generator stator d- and q-axis voltages (V)
ω_r	Rotor electrical angular speed (4.3 rd/s)
i_{di}, i_{qi}	Grid-side converter output d- and q-axis currents (A)
u_{di}, u_{qi}	Grid-side converter output d- and q-axis voltage (V)
i_{lb}	Current through the dc/dc converter inductor (A)
E_{dc}	Electric energy of the dc-link capacitor (A)
P_m	Rated Mechanical Power (2.45 MW)
λ_r	Rated Rotor Flux Linkage (28 Wb)
P	Number of Pole Pairs (8)
J	Moment Inertia of the Generator (4000 $kg.m^2$)
R_s	Stator Winding Resistance (24.21 $m\Omega$)
L_{ds}	d-axis Synchronous Inductance (9.81 mH)
L_{qs}	q-axis Synchronous Inductance (16.7 mH)
V_w	Rated Wind speed (m/s)
R	Blade Radius (28.16 m)
β	Pitch Angle (0 $degree$)
Rho	Air Density (1.25 kg/m^3)
λ_{opt}	Optimal Tip Speed Ratio (8.1)
u_g	Grid Voltage Line-to-Line Module (4000 V)
u_{dc}	dc-link Voltage (8000 V)
C_{dc}	dc-link Capacitor (1667 μF)
L_f	Grid-side Filter (16.884 mH)
L_g	Grid Inductance (1.6884 mH)
u_{bat}	Battery Rated Voltage (4000 V)
P_{bat}	Battery Power (1.5 MW)

the generator rotor reference speed (dashed line) and the actual speed (solid line), ω_r, while the lower figure represents the generator output power, P_m, waveforms

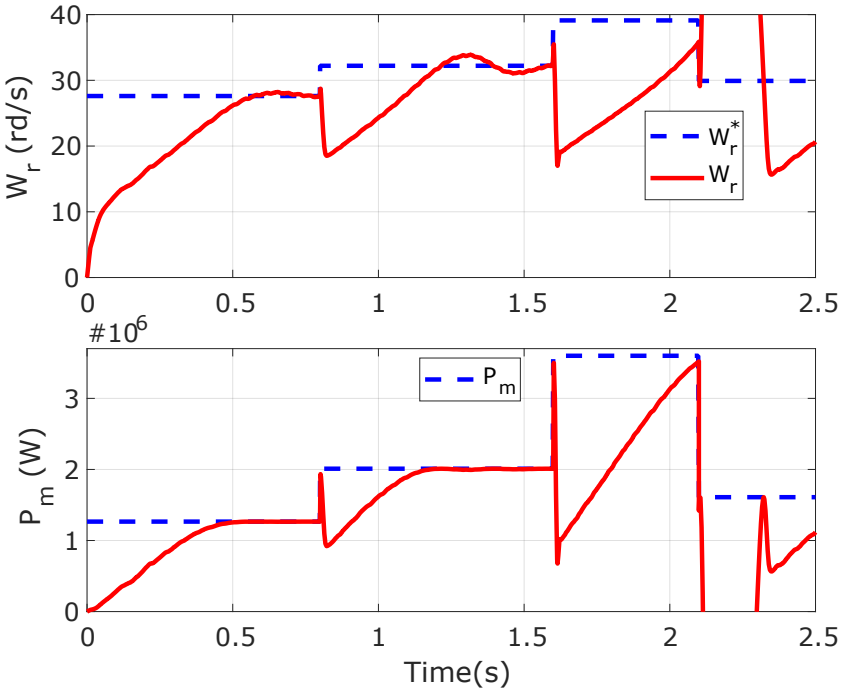

Figure 5.2: WT Rotor Speed and Output Power.

respectively.

One may observe that controller was sensitive to large parameter variation, which resulted to transient and steady-state errors as shown in Fig. 5.2. Hence, the importance of having a control scheme that is independent to the parameters of the system and that can allow the controller to handle large parameter changes, especially for operation in harsh environment. This is discussed in the next section.

5.3 Nonlinear Controller Design

This section presents the design of the proposed control scheme developed to stabilize the wind energy battery storage system and to meet the control objective, which are as follows: 1) keep the wind turbine operating at its maximum power by controlling ω_r; 2) achieve a linear relationship between the stator current and the electromagnetic torque by controlling the stator d-axis current, i_{ds}; 3) meet the load voltage requirement by controlling both load d-axis and q-axis voltages, u_{dl}

and u_{ql} respectively; 4) ensure the regulation of the dc-link voltage by controlling, u_{dc}; 5) perform power management between the battery, load and grid subsystems by controlling the battery current, i_{lb}; 6) estimate all the parameters of the system to be used in the controller as they are assumed unknown.

To find the controller equation and its structure, the input-output adaptive feedback linearization control is considered as design method. The controller structure is illustrated in Fig. 5.3. It includes an adaptation module to find the estimated parameters $\hat{\overline{\theta}}$, a change of variables $T(\overline{x}, \hat{\overline{\theta}})$, a nonlinear control, $\overline{u}(\overline{x})$, and the stabilizing linear control $\overline{v}_p$.

5.3.1 Feedback Linearization

If the generator parameters $(R_s, L_d, L_q, \lambda_r, P\ J)$, the grid and load parameters $(R_{th}, \omega_g L_{th}, E_{thd}, E_{thq})$, and the battery-buck-boost converter parameters (L_b, C_{dc}) were known, it has been shown in [28, 151] that the input-output feedback linearization design method could be used to design the controller. The corresponding change of variables, $\overline{z} = T(\overline{x})$, the nonlinear control, $\overline{u}(\overline{x})$, and the stabilizing linear control, $v_p(\overline{z})$, have the following expressions, respectively

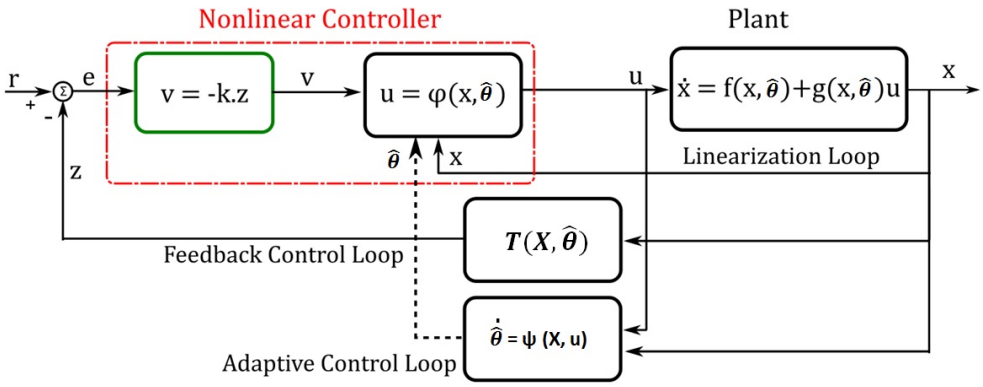

Figure 5.3: Proposed MIMO Adaptive controller structure.

$$
\begin{aligned}
z_1 &= \tilde{i}_{ds}, \qquad z_2 = i_{ds} - i^*_{ds}, \qquad z_3 = \tilde{i}_{qs}, \qquad z_4 = i_{qs} - i^*_{qs},\\
z_5 &= \tilde{\omega}_r,\ z_6 = \omega_r - \omega^*_r, \qquad z_7 = \frac{k_{opt}}{JP}\omega_r^2 - \frac{3P^2\lambda_r}{2J} i_{qs},\\
z_8 &= \tilde{u}_{dl},\ z_9 = u_{dl} - u^*_{dl}, \qquad z_{10} = \tilde{u}_{ql},\ z_{11} = u_{ql} - u^*_{ql},\\
z_{12} &= \tilde{E}_{dc},\ z_{13} = E_{dc} - E^*_{dc}, \qquad z_{14} = \tilde{i}_{lb},\ z_{15} = i_{lb} - i^*_{lb}
\end{aligned}
$$

$$
\overline{u} = [B(\overline{x})]^{-1}\left[-A(\overline{x}) + \overline{v}\right]
$$

$$
\begin{aligned}
v_1 &= -k_{11}\tilde{i}_{ds} - k_{12}\dot{\tilde{i}}_{ds}, \qquad v_2 = -k_{21}\tilde{\omega}_r - k_{22}\dot{\tilde{\omega}}_r - k_{23}\ddot{\tilde{\omega}}_r,\\
v_3 &= -k_{31}\tilde{u}_{dl} - k_{32}\dot{\tilde{u}}_{dl}, \qquad v_4 = -k_{41}\tilde{u}_{ql} - k_{42}\dot{\tilde{u}}_{ql},\\
v_5 &= -k_{51}\tilde{E}_{dc} - k_{52}\dot{\tilde{E}}_{dc}, \qquad v_6 = -k_{61}\tilde{i}_{lb} - k_{62}\dot{\tilde{i}}_{lb}
\end{aligned} \tag{5.3}
$$

the matrix A and B were provided in [119] and $\overline{v}_p$ is the new control inputs vector. The controller gains k_{pq} are determined such that the close loop system is asymptotically stable.

5.3.2 Adaptive Controller Design

All the parameters of the system are assumed unknown. Therefore, they need to be determined by the adaptive controller. The objective here is to find the new expression of the input $\overline{u} = [u_{ds}, u_{qs}, u_{di}, u_{qi}, P_{bat}, D]^T$ using the vector $\overline{z}$. First, let's define the following change of variables of the system parameters

$$
\begin{aligned}
&\theta_1 = \frac{R_s}{L_d}, \quad \theta_2 = \frac{L_q}{L_d}, \quad \theta_3 = \frac{1}{L_d}, \quad \theta_4 = \frac{L_d}{L_q}, \quad \theta_5 = \frac{R_s}{L_q},\\
&\theta_6 = \frac{\lambda_r}{L_q}, \quad \theta_7 = \frac{1}{L_q}, \quad \theta_8 = \frac{Pk_{opt}}{J} \text{ and } \quad \theta_9 = \frac{3P^2\lambda_r}{2J}, \quad \theta_{10} = R_{th}\\
&\theta_{11} = \omega_g L_{th}, \quad \theta_{12} = E_{thd}, \quad \theta_{13} = E_{thq}, \quad \theta_{14} = \frac{1}{L_b}, \quad \theta_{15} = \frac{1}{L_f}
\end{aligned} \tag{5.4}
$$

The corresponding change of variable signals of the system, $\overline{\Omega} = T(\overline{x}, \overline{\hat{\theta}})$ has the following expressions

$$\begin{cases} \Omega_1 = \tilde{i}_{ds} \\ \Omega_2 = i_{ds} - i_{ds}^* \\ \Omega_3 = \tilde{\omega}_r \\ \Omega_4 = \omega_r - \omega_r^* \\ \hat{\Omega}_5 = \theta_8 \omega_r^2 - \theta_9 i_{qs} \\ \Omega_6 = \tilde{u}_{dl} \\ \hat{\Omega}_7 = \theta_{10} i_{di} - \theta_{11} i_{qi} + \theta_{12} - u_{dl}^* \\ \Omega_8 = \tilde{u}_{ql} \\ \hat{\Omega}_9 = \theta_{10} i_{qi} + \theta_{11} i_{di} + \theta_{13} - u_{ql}^* \\ \Omega_{10} = \tilde{E}_{dc} \\ \Omega_{11} = E_{dc} - E_{dc}^* \\ \Omega_{12} = \tilde{i}_{lb} \\ \Omega_{13} = i_{lb} - i_{lb}^* \end{cases} \tag{5.5}$$

The vectors $\overline{\theta}$ and $\overline{\Omega}$ are defined respectively as

$$\overline{\theta} = [\theta_1, \theta_2, \theta_3, \theta_4, \theta_5, \theta_6, \theta_7, \theta_8, \theta_9, \theta_{10}, \theta_{11}, \theta_{12}, \theta_{13}, \theta_{14}, \theta_{15}]^T,$$

$$\overline{\Omega} = [\Omega_1, \Omega_2, \Omega_3, \Omega_4, \Omega_5, \Omega_6, \Omega_7, \Omega_8, \Omega_9, \Omega_{10}, \Omega_{11}, \Omega_{12}, \Omega_{13}]^T$$

$\hat{\Omega}_5, \hat{\Omega}_7$ and $\hat{\Omega}_9$ represent the estimated value of Ω_5, Ω_7 and Ω_9, respectively, as they contain θ in their equations (Eqn. 5.5).

The dynamic equation of the system can be written as in Eqn. (5.6).

$$
\begin{cases}
\dot{\Omega}_1 = i_{ds} - i_{ds}^* \\
\dot{\hat{\Omega}}_2 = -\theta_1 i_{ds} + \theta_2 \omega_r i_{qs} + \theta_3 u_{ds} \\
\dot{\Omega}_3 = \omega_r - \omega_r^* \\
\dot{\hat{\Omega}}_4 = \theta_8 \omega_r^2 - \theta_9 i_{qs} \\
\dot{\hat{\Omega}}_5 = 2\hat{\theta}_8 \omega_r (\theta_8 \omega_r^2 - \theta_9 i_{qs}) - \hat{\theta}_9 (-\theta_4 \omega_r i_{ds} - \theta_5 i_{qs} - \theta_6 \omega_r + \theta_7 u_{qs}) \\
\qquad + \dot{\hat{\theta}}_8 \omega_r^2 - \dot{\hat{\theta}}_9 i_{qs} \\
\dot{\hat{\Omega}}_6 = \theta_{10} i_{di} - \theta_{11} i_{qi} + \theta_{12} - u_{dl}^* \\
\dot{\hat{\Omega}}_7 = \hat{\theta}_{10} (\omega_g i_{qi} - \theta_{15} u_{dl} + \theta_{15} u_{di}) - \hat{\theta}_{11} (-\omega_g i_{di} - \theta_{15} u_{ql} + \theta_{15} u_{qi}) \\
\qquad + \dot{\hat{\theta}}_{10} i_{di} - \dot{\hat{\theta}}_{11} i_{qi} + \dot{\hat{\theta}}_{12} \\
\dot{\hat{\Omega}}_8 = \theta_{10} i_{qi} + \theta_{11} i_{di} + \theta_{13} - u_{ql}^* \\
\dot{\hat{\Omega}}_9 = \hat{\theta}_{10} (-\omega_g i_{di} - \theta_{15} u_{ql} + \theta_{15} u_{qi}) + \hat{\theta}_{11} (\omega_g i_{qi} - \theta_{15} u_{dl} + \theta_{15} u_{di}) \\
\qquad + \dot{\hat{\theta}}_{10} i_{qi} + \dot{\hat{\theta}}_{11} i_{di} + \dot{\hat{\theta}}_{13} \\
\dot{\Omega}_{10} = E_{dc} - E_{dc}^* \\
\dot{\Omega}_{11} = u_{dc} i_{sdc} - \dfrac{3}{2} i_{di} u_{di} + P_{pat} \\
\dot{\Omega}_{12} = i_{lb} - i_{lb}^* \\
\dot{\hat{\Omega}}_{13} = \theta_{14} u_{bat} - \theta_{14} D u_{dc}
\end{cases}
\tag{5.6}
$$

To compensate for the unknown actual parameters $\overline{\theta}$, let introduce $\overline{\hat{\theta}}$ as its estimated values, where $\overline{\theta} = \overline{\hat{\theta}} + \overline{\tilde{\theta}}$. Therefore, Eqn. (5.6) became

$$
\begin{cases}
\dot{\Omega}_1 = i_{ds} - i_{ds}^* = \Omega_2 \\
\dot{\hat{\Omega}}_2 = \left[\; -\hat{\theta}_1 i_{ds} + \hat{\theta}_2 \omega_r i_{qs} + \hat{\theta}_3 u_{ds} \; \right] + \left[\; -\tilde{\theta}_1 i_{ds} + \tilde{\theta}_2 \omega_r i_{qs} + \tilde{\theta}_3 u_{ds} \; \right] \\
\dot{\Omega}_3 = \omega_r - \omega_r^* = \Omega_4 \\
\dot{\hat{\Omega}}_4 = \left[\; \hat{\theta}_8 \omega_r^2 - \hat{\theta}_9 i_{qs} \; \right] + \left[\; \tilde{\theta}_8 \omega_r^2 - \tilde{\theta}_9 i_{qs} \; \right] = \hat{\Omega}_5 + \left[\; \tilde{\theta}_8 \omega_r^2 - \tilde{\theta}_9 i_{qs} \; \right] \\
\dot{\hat{\Omega}}_5 = \left[\; 2\hat{\theta}_8 \omega_r (\hat{\theta}_8 \omega_r^2 - \hat{\theta}_9 i_{qs}) - \hat{\theta}_9 (-\hat{\theta}_4 \omega_r i_{ds} - \hat{\theta}_5 i_{qs} - \hat{\theta}_6 \omega_r + \hat{\theta}_7 u_{qs}) \; \right] \\
\qquad + \left[\; 2\hat{\theta}_8 \omega_r (\tilde{\theta}_8 \omega_r^2 - \tilde{\theta}_9 i_{qs}) - \hat{\theta}_9 (-\tilde{\theta}_4 \omega_r i_{ds} - \tilde{\theta}_5 i_{qs} - \tilde{\theta}_6 \omega_r + \tilde{\theta}_7 u_{qs}) \; \right] \\
\qquad + \left[\; \dot{\hat{\theta}}_8 \omega_r^2 - \dot{\hat{\theta}}_9 i_{qs} \; \right] \\
\dot{\hat{\Omega}}_6 = \left[\; \hat{\theta}_{10} i_{di} - \hat{\theta}_{11} i_{qi} + \hat{\theta}_{12} - u_{dl}^* \; \right] + \left[\; \tilde{\theta}_{10} i_{di} - \tilde{\theta}_{11} i_{qi} + \tilde{\theta}_{12} \; \right] \\
\quad = \hat{\Omega}_7 + \left[\; \tilde{\theta}_{10} i_{di} - \tilde{\theta}_{11} i_{qi} + \tilde{\theta}_{12} \; \right] \\
\dot{\hat{\Omega}}_7 = \left[\; \hat{\theta}_{10} (\omega_g i_{qi} - \hat{\theta}_{15} u_{dl}) - \hat{\theta}_{11} (-\omega_g i_{di} - \hat{\theta}_{15} u_{ql}) + \hat{\theta}_{15} (\hat{\theta}_{10} u_{di} - \hat{\theta}_{11} u_{qi}) \; \right] \\
\qquad + \left[\; \dot{\hat{\theta}}_{10} i_{di} - \dot{\hat{\theta}}_{11} i_{qi} + \dot{\hat{\theta}}_{12} \; \right] \\
\dot{\hat{\Omega}}_8 = \left[\; \hat{\theta}_{10} i_{qi} + \hat{\theta}_{11} i_{di} + \hat{\theta}_{13} - u_{ql}^* \; \right] + \left[\; \tilde{\theta}_{10} i_{qi} + \tilde{\theta}_{11} i_{di} + \tilde{\theta}_{13} \; \right] \\
\quad = \hat{\Omega}_9 + \left[\; \tilde{\theta}_{10} i_{qi} + \tilde{\theta}_{11} i_{di} + \tilde{\theta}_{13} \; \right] \\
\dot{\hat{\Omega}}_9 = \left[\; \hat{\theta}_{10} (-\omega_g i_{di} - \hat{\theta}_{15} u_{ql}) + \hat{\theta}_{11} (\omega_g i_{qi} - \hat{\theta}_{15} u_{dl}) + \hat{\theta}_{15} (\hat{\theta}_{11} u_{di} + \hat{\theta}_{10} u_{qi}) \; \right] \\
\qquad + \left[\; \dot{\hat{\theta}}_{10} i_{qi} + \dot{\hat{\theta}}_{11} i_{di} + \dot{\hat{\theta}}_{13} \; \right] \\
\dot{\Omega}_{10} = E_{dc} - E_{dc}^* = \Omega_{11} \\
\dot{\Omega}_{11} = u_{dc} i_{sdc} - \dfrac{3}{2} i_{di} u_{di} + P_{bat} \\
\dot{\Omega}_{12} = i_{lb} - i_{lb}^* = \Omega_{13} \\
\dot{\hat{\Omega}}_{13} = \hat{\theta}_{14} \left[\; u_{bat} - D u_{dc} \; \right] + \tilde{\theta}_{14} \left[\; u_{bat} - D u_{dc} \; \right]
\end{cases}
\tag{5.7}
$$

From Eqn. (5.7), the new output vector, $\overline{y}_d$, is obtained as

$$
\overline{y}_d = [\dot{\hat{\Omega}}_2, \dot{\hat{\Omega}}_5, \dot{\hat{\Omega}}_7, \dot{\hat{\Omega}}_9, \dot{\hat{\Omega}}_{11}, \dot{\hat{\Omega}}_{13}]^T \tag{5.8}
$$

To linearize the system in Eqn. (5.8), the following control input, $\overline{u} = [u_{ds}, u_{qs}, u_{di}, u_{qi}, P_{bat}, D]^T$, is selected.

$$\overline{u} = \left[B(\overline{x,\hat{\theta}})\right]^{-1}\left[-A(\overline{x,\hat{\theta}}) + \overline{v}\right] \tag{5.9}$$

$$\underbrace{\begin{bmatrix} u_{ds} \\ u_{ds} \\ u_{di} \\ u_{qi} \\ P_{bat} \\ D \end{bmatrix}}_{\overline{u}} = \underbrace{\begin{bmatrix} \hat{\theta}_3 & 0 & 0 & 0 & 0 & 0 \\ 0 & \hat{\theta}_9\hat{\theta}_7 & 0 & 0 & 0 & 0 \\ 0 & 0 & \hat{\theta}_{10}\hat{\theta}_{15} & -\hat{\theta}_{11}\hat{\theta}_{15} & 0 & 0 \\ 0 & 0 & \hat{\theta}_{11}\hat{\theta}_{15} & \hat{\theta}_{10}\hat{\theta}_{15} & 0 & 0 \\ 0 & 0 & 0 & 0 & 1 & 0 \\ 0 & 0 & 0 & 0 & 0 & -\hat{\theta}_{14}u_{dc} \end{bmatrix}^{-1}}_{[B(\overline{x})]^{-1}} \left[- \underbrace{\begin{bmatrix} A_1 \\ A_2 \\ A_3 \\ A_4 \\ A_5 \\ A_6 \end{bmatrix}}_{A(\overline{x})} + \underbrace{\begin{bmatrix} v_1 \\ v_2 \\ v_3 \\ v_4 \\ v_5 \\ v_6 \end{bmatrix}}_{\overline{v}} \right] \tag{5.10}$$

where

$$B = \begin{bmatrix} \hat{\theta}_3 & 0 & 0 & 0 & 0 & 0 \\ 0 & \hat{\theta}_9\hat{\theta}_7 & 0 & 0 & 0 & 0 \\ 0 & 0 & \hat{\theta}_{10}\hat{\theta}_{15} & -\hat{\theta}_{11}\hat{\theta}_{15} & 0 & 0 \\ 0 & 0 & \hat{\theta}_{11}\hat{\theta}_{15} & \hat{\theta}_{10}\hat{\theta}_{15} & 0 & 0 \\ 0 & 0 & 0 & 0 & 1 & 0 \\ 0 & 0 & 0 & 0 & 0 & -\hat{\theta}_{14}u_{dc} \end{bmatrix}$$

$A(\overline{x}) = [A_1, A_2, A_3, A_4, A_5, A_6]$ with
$A_1 = -\hat{\theta}_1 i_{ds} + \hat{\theta}_2\omega_r i_{qs}$
$A_2 = 2\hat{\theta}_8\omega_r(\hat{\theta}_8\omega_r^2 - \hat{\theta}_9 i_{qs}) - \hat{\theta}_9(-\hat{\theta}_4\omega_r i_{ds} - \hat{\theta}_5 i_{qs} - \hat{\theta}_6\omega_r)$
$A_3 = \hat{\theta}_{10}(\omega_g i_{qi} - \hat{\theta}_{15}u_{dl} - \hat{\theta}_{11}(-\omega_g i_{di} - \hat{\theta}_{15}u_{ql}) + \dot{\hat{\theta}}_{12}$
$A_4 = \hat{\theta}_{10}(-\omega_g i_{di} - \hat{\theta}_{15}u_{ql}) + \hat{\theta}_{11}(\omega_g i_{qi} - \hat{\theta}_{15}u_{dl}) + \dot{\hat{\theta}}_{13}$
$A_5 = u_{dc}i_{sdc} - \frac{3}{2}i_{di}u_{dl}$
$A_6 = \hat{\theta}_{14}u_{bat}$
and $\overline{v} = \left[\ v_1, v_2, v_3, v_4, v_5, v_6, \ \right]^T$

v_1, v_2, v_3, v_4, v_5 and v_6 are the auxiliary input yet to be determined.

The close loop model of the system in Eqn. (5.8) is obtained when Eqn. (5.9) is substituted into Eqn. (5.8). Therefore, Eqn. (5.7) becomes as

$$\begin{cases} \dot{\Omega}_1 = \Omega_2 \\ \dot{\hat{\Omega}}_2 = v_1 + \left[\; -\tilde{\theta}_1 i_{ds} + \tilde{\theta}_2 \omega_r i_{qs} + \tilde{\theta}_3 u_{ds} \; \right] \\ \dot{\Omega}_3 = \Omega_4 \\ \dot{\hat{\Omega}}_4 = \hat{\Omega}_5 + \left[\; \tilde{\theta}_8 \omega_r^2 - \tilde{\theta}_9 i_{qs} \; \right] \\ \dot{\hat{\Omega}}_5 = v_2 + \left[\; 2\hat{\theta}_8 \omega_r (\tilde{\theta}_8 \omega_r^2 - \tilde{\theta}_9 i_{qs}) - \hat{\theta}_9 (-\tilde{\theta}_4 \omega_r i_{ds} - \tilde{\theta}_5 i_{qs} - \tilde{\theta}_6 \omega_r + \tilde{\theta}_7 u_{qs}) \; \right] \\ \qquad + \left[\; \dot{\hat{\theta}}_8 \omega_r^2 - \dot{\hat{\theta}}_9 i_{qs} \; \right] \\ \dot{\hat{\Omega}}_6 = \hat{\Omega}_7 + \left[\; \tilde{\theta}_{10} i_{di} - \tilde{\theta}_{11} i_{qi} + \tilde{\theta}_{12} \; \right] \\ \dot{\hat{\Omega}}_7 = v_3 + \left[\; \dot{\hat{\theta}}_{10} i_{di} - \dot{\hat{\theta}}_{11} i_{qi} + \dot{\hat{\theta}}_{12} \; \right] \\ \dot{\hat{\Omega}}_8 = \hat{\Omega}_9 + \left[\; \tilde{\theta}_{10} i_{qi} + \tilde{\theta}_{11} i_{di} + \tilde{\theta}_{13} \; \right] \\ \dot{\hat{\Omega}}_9 = v_4 + \left[\; \dot{\hat{\theta}}_{10} i_{qi} + \dot{\hat{\theta}}_{11} i_{di} + \dot{\hat{\theta}}_{13} \; \right] \\ \dot{\Omega}_{10} = \Omega_{11} \\ \dot{\hat{\Omega}}_{11} = v_5 \\ \dot{\Omega}_{12} = \Omega_{13} \\ \dot{\hat{\Omega}}_{13} = v_6 + \left[\; \tilde{\theta}_{14} u_{bat} - \tilde{\theta}_{14} D u_{dc} \; \right] \end{cases} \tag{5.11}$$

One can notice that Eqn. (5.11) is in the form of

$$\dot{\hat{\Omega}} = A_{ad} \hat{\overline{\Omega}} + B_{ad} \overline{v} + \psi_{ad} \tilde{\overline{\theta}} + W_{ad} \dot{\hat{\overline{\theta}}} \tag{5.13}$$

The following state feedback stabilizing controller is proposed for the auxiliary input vector

$$\overline{v} = [v_1, v_2, v_3, v_4, v_5, v_6]^T = -k_{pq} \hat{\overline{\Omega}} \tag{5.14}$$

where k_{pq} is chosen such as the closed loop matrix
$A_{sad} = [A_{ad} - B_{ad} k_{pq}]$ is Hurwitz. Note that the system (A_{ad}, B_{ad}) is controllable.

By substituting Eqn. 5.14 into Eqn. (5.13), Eqn. (5.13) becomes

$$\dot{\hat{\Omega}} = A_{sad}\hat{\overline{\Omega}} + \psi_{ad}\tilde{\overline{\theta}} + W_{ad}\dot{\tilde{\overline{\theta}}} \tag{5.15}$$

The matrix A_{ad}, B_{ad}, W_{ad} and ψ_{ad} are given in the Appendix Section.

Let define $\overline{\varepsilon}$ and $\overline{e}$ such that respectively

$$\begin{cases} \dot{\overline{\varepsilon}} = A_{sad}\overline{\varepsilon} + W_{ad}\dot{\tilde{\overline{\theta}}}, \text{ where } \varepsilon(0) = 0 & \text{(5.16a)} \\ \overline{e} = \hat{\overline{\Omega}} - \overline{\varepsilon} & \text{(5.16b)} \end{cases}$$

$\overline{\varepsilon}$ and $\overline{e}$ are referred to as the *error augmentation* and the *augmented error*, respectively.

The dynamics of $\overline{e}$ is obtained as follows

$$\begin{aligned} \dot{\overline{e}} &= \dot{\hat{\overline{\Omega}}} - \dot{\overline{\varepsilon}} \\ &= (A_{sad}\hat{\overline{\Omega}} + \psi_{ad}\tilde{\overline{\theta}} + W_{ad}\dot{\tilde{\overline{\theta}}}) - (A_{sad}\overline{\varepsilon} + W_{ad}\dot{\tilde{\overline{\theta}}}) \\ &= A_{sad}\overline{e} + \psi_{ad}\tilde{\overline{\theta}} \end{aligned} \tag{5.17}$$

Next section discusses how the adaptive law used to update the estimated parameters that appear in the controller equations is derived.

5.3.3 Adaptive Control Law

This section presents how the adaptive law is obtained. It is obtained by showing that both $\dot{\tilde{\overline{\theta}}}$ is *bounded* and $\dot{\hat{e}}$ converges to zero using the *Lyapunov* stability criteria and *Barbalat Lemma* [152].

Let consider the following Lyapunov function candidate

$$V_{Lyap} = \overline{e}^T P \overline{e} + \tilde{\overline{\theta}}\Gamma^{-1}\tilde{\overline{\theta}} \tag{5.18}$$

where Γ is a positive definite matrix given in Table 5.3.

The main idea of Lyapunov's theory is that if the derivative of the Lyapunov function candidate ($\dot{V}_{Lyap}$) is negative along the trajectories of the system, then V_{Lyap} will decrease as time goes forward. Therefore, the adaptation law is selected in sush a way that $\dot{V}_{Lyap}$ is negative semi-definite. The derivative of V_{Lyap} has the following expression

$$\dot{V}_{Lyap} = \overline{e}^T ({A_{sad}}^T P + P A_{sad})\overline{e} + 2\tilde{\overline{\theta}}^T \Gamma^{-1} \dot{\tilde{\overline{\theta}}} + 2\tilde{\overline{\theta}} \psi_{ad}^T P \overline{e} \tag{5.19}$$

$$= -\overline{e}^T Q \overline{e} + 2\tilde{\overline{\theta}}(\Gamma^{-1} \dot{\tilde{\overline{\theta}}} + \psi_{ad}^T P \overline{e}) \tag{5.20}$$

if $\overline{\theta} = C^{ste} \implies \dot{\overline{\theta}} = 0$, then $\dot{\tilde{\overline{\theta}}} = -\dot{\hat{\overline{\theta}}}$

Considering that the following inegality is always true

$$-\overline{e}^T Q\ \overline{e} < 0 \tag{5.21}$$

$\dot{V}_{Lyap}$ will be negative ($\dot{V}_{Lyap} < 0$) if $\dot{\hat{\overline{\theta}}}$ is chosen as

$$\dot{\hat{\overline{\theta}}} = \Gamma \psi_{ad}^T P \overline{e} \tag{5.22}$$

The Eqn. (5.22) is the adaptive law for the unknown parameters. The matrix P is the solution of the following Lyapunov equation and I is the identity matrix. They are provided in the Appendix section.

$$A_{sad}^T P + P A_{sad} = -I \tag{5.23}$$

5.4 Results

To Demonstrate the effectiveness of the proposed stand-alone and grid-connected nonlinear nonlinear controller, simulation was carried out using the SimPowerSystems toolbox [13] in Matlab/Simulink software. The system is shown in Fig. 5.1. It composes of a 2.45 MW wind power generator supplying a 2 MW variable load. In this work, a different generator is used, variable speed salient-pole permanent magnet synchronous machine, that the one used in [28]. The generator parameters and the nonlinear controller feedback gains k_{pq}, are given in Table 5.1 [21] and 5.3, respectively. k_{pq}, was chosen so that the eigenvalues of the closed loop system are *Hurwitz*. They were calculated in such a way that the slowest dynamic, which was that of the mechanical speed, stabilized in 0.3 seconds with a damping coefficient of 0.9. The desired poles were determined accordingly and given in the Table 5.2 below. The closed loop system was asymptotically stable. Consequently, errors between outputs and references converged to zero.

Table 5.2: Performance Specifications

Dynamics	$\tilde{i}_{ds}$	$\tilde{\omega}_r$	$\tilde{u}_{dql}$	$\tilde{E}_{dc}$	$\tilde{i}_{lb}$
Desired Poles	$\begin{bmatrix} -50 \\ -10000 \end{bmatrix}$	$\begin{bmatrix} -15 \pm 6.5i \\ -1470 \end{bmatrix}$	$\begin{bmatrix} -2, -50 \\ -1, -10 \end{bmatrix}$	$\begin{bmatrix} -13 \\ -50 \end{bmatrix}$	$\begin{bmatrix} -6 \\ -700 \end{bmatrix}$

Table 5.3: Controller Gains k_{pq}

Controller Gains Description	Value
$\tilde{i}_{ds}$ and $\dot{\tilde{i}}_{ds}$ Gains	$[K_{11}K_{12}] = [500, 1].10^3$
$\tilde{\omega}_r$, $\dot{\tilde{\omega}}_r$ and $\ddot{\tilde{\omega}}_r$ Gains	$[K_{21}K_{22}K_{23}] = [400, 45, 1.5].10^3$
$\tilde{u}_{dl}$ and $\dot{\tilde{u}}_{dl}$ Gains	$[K_{31}K_{32}] = [800, 600]$
$\tilde{u}_{ql}$ and $\dot{\tilde{u}}_{ql}$ Gains	$[K_{41}K_{42}] = [30, 300]$
$\tilde{E}_{dc}$ and $\dot{\tilde{E}}_{dc}$ Gains	$[K_{51}K_{52}] = [300, 0.3]$
$\tilde{i}_{lb}$ and $\dot{\tilde{i}}_{lb}$ Gains	$[K_{61}K_{62}] = [4000, 700]$

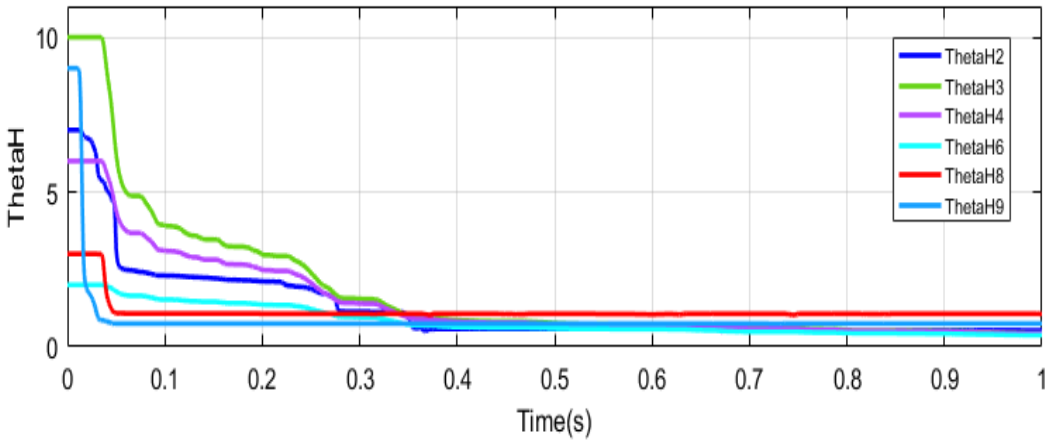

Figure 5.4: Estimated Parameters $\hat{\theta}$.

First, the effectiveness of the proposed nonlinear adaptive controller to estimate the parameters of system on-line was evaluated. Fig. 5.4 shows the estimated parameters within the same order of magnitude. Initially, random values were assigned to them at the beginning of the simulation. Noticed that they behave as expected, that is, they are bounded. In addition, they converge to stable values.

To investigate the dynamic and steady-state performance of the system, simulations have been carried out under different wind speeds. The test begins with a stand-alone mode and at the time $t = 0.4$ sec when the switch *Sw1*, in Fig. 5.1, closes, it switches in the grid-connected mode. The wind speed is 12 m/s, from 0 to 0.2 sec, 14 m/s, from 0.2 to 0.6 sec, 17 m/s, from 0.6 to 0.8 and 13 m/s from 0.8 to 1 sec, respectively.

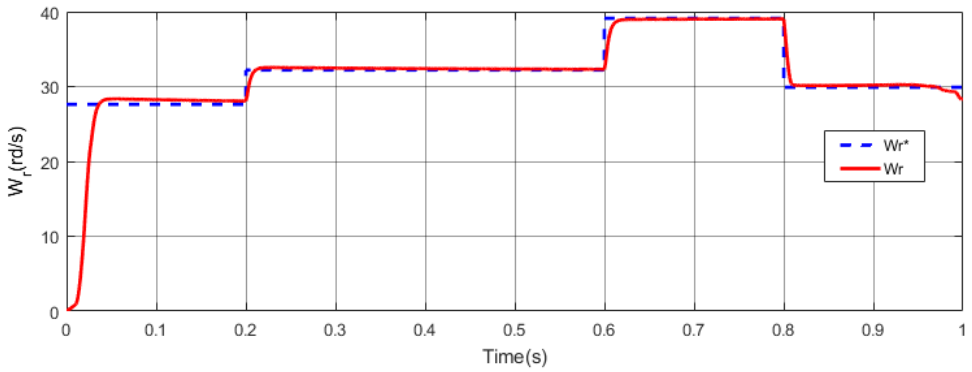

(a) Optimum Rotor Speed.

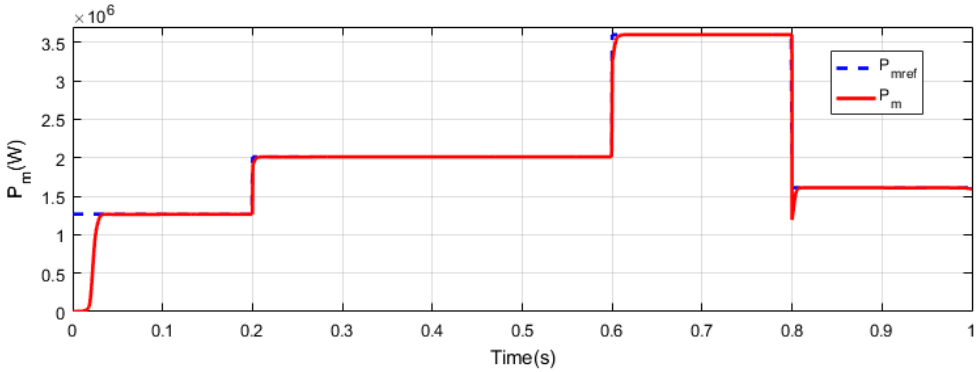

(b) Optimum Output Power.

Figure 5.5: (a) Optimum Rotor Speed and (b) Output Power.

The generator rotor reference speed (dashed line) and the actual speed (solid line) are shown in Fig. 5.5(a), while the output power is shown in Fig. 5.5(b). It can be observed that the waveforms reach their steady state fast and smoothly within approximately 0.05 sec. Whereas the nonadaptive controller, in the same operation conditions, takes 0.5 sec.

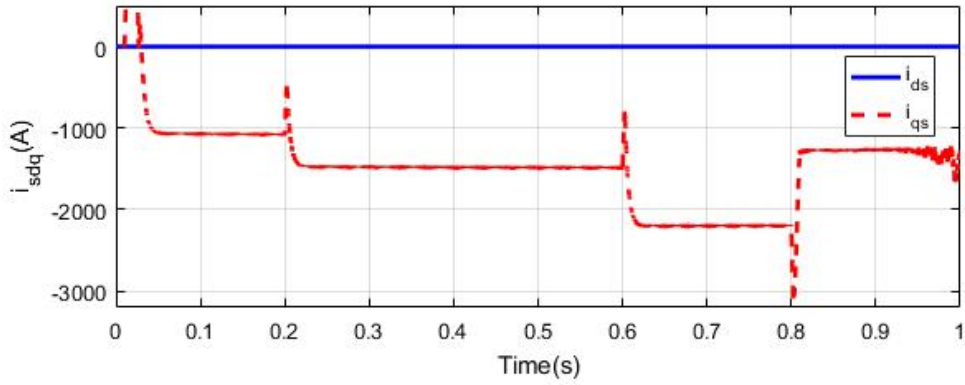

(a) dq-components of the Generator Current.

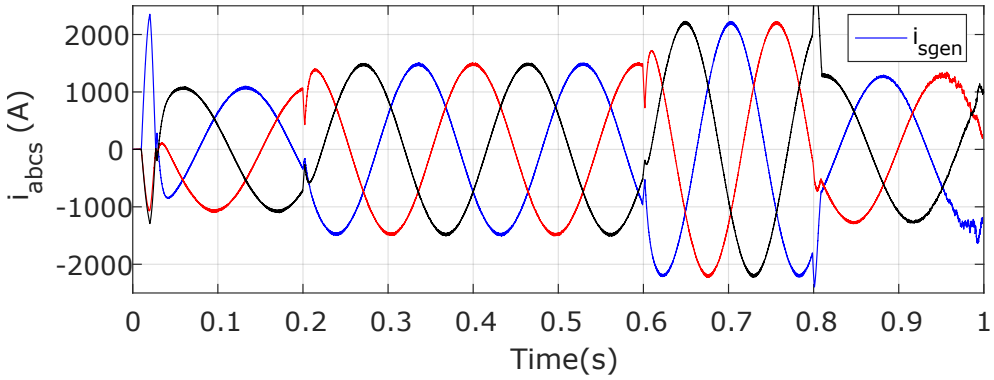

(b) 3-Phase Current of the Generator.

Figure 5.6: (a) dq-components and (b) 3-Phase of the Generator Current.

The d-axis current, i_{dl} (solid line), q-axis current, i_{ql} (dashed line) and the three-phase stator current, i_{abcs}, are shown in Fig. 5.6. The objective here is to maintain to zero the d-axis current, so that the stator current (i_{qs}) will have linear relationship with the torque. Hence i_{qs} and P_m have similar profiles.

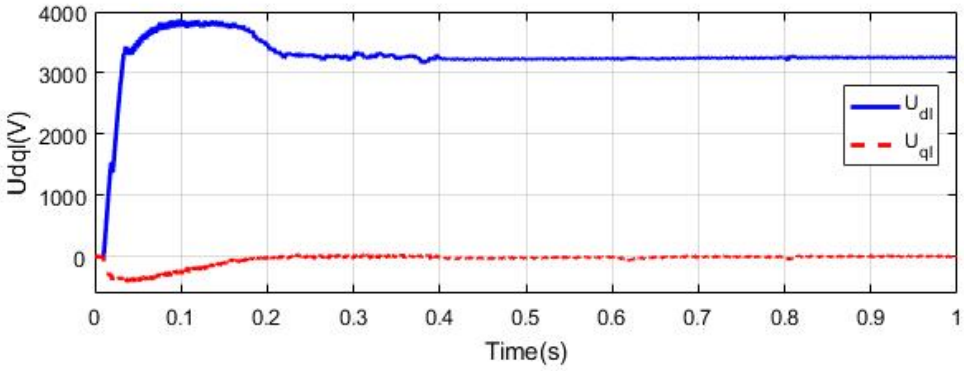

(a) dq-components of the Load Voltage.

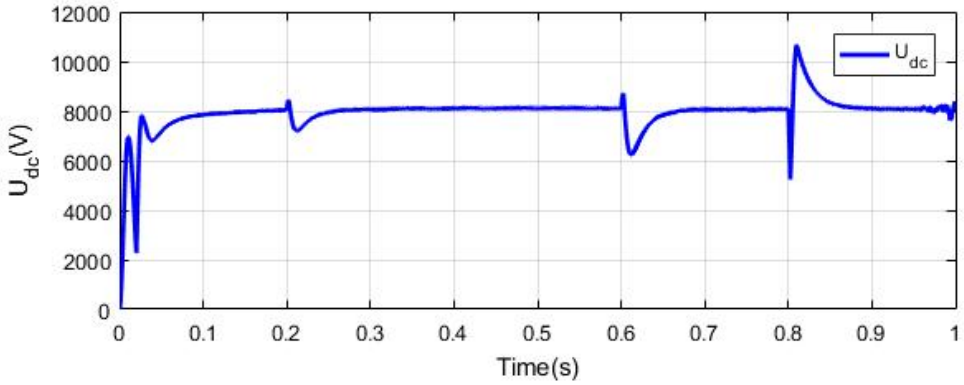

(b) dc-link Voltage.

Figure 5.7: (a) dq-components of the Load Voltage., (b) dc-link Voltage.

The dq-components of the load voltage are shown in Fig. 5.7(a). Despite the variation of the generated power on the wind turbine side, it can be observed that the d-axis load voltage, v_{dl} (solid line), and the q-axis load voltage, i_{ql} (dashed line) remain constants. To allow power transfer between the two converters, the dc-link voltage, u_{dc}, is controlled to a constant reference as shown in Fig. 5.7(b). One may notice in Fig. 5.5(a), 5.6 and 5.7, that the transition between the stand-alone mode and the grid-connected mode, at time $t = 0.4$ sec, is fast and smooth in spite of that no islanding detection mechanism was utilized.

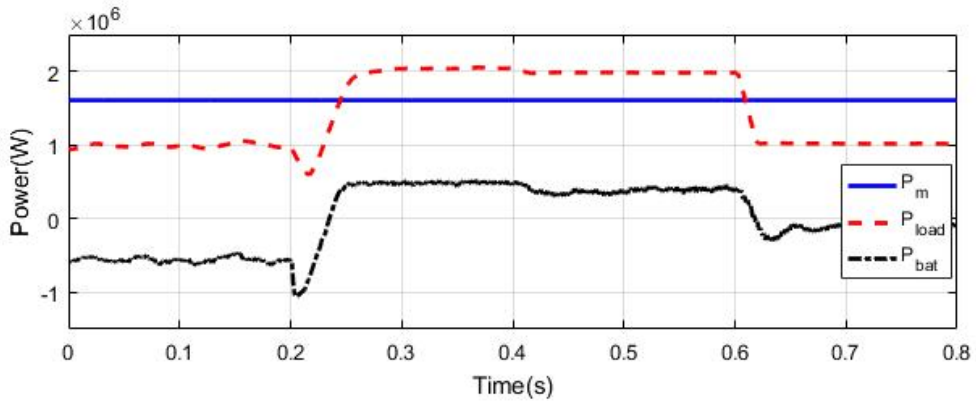

Figure 5.8: Powers of the Wind Turbine, the Load and the Battery with a Constant Wind Speed ($V_w = 13m/s$) with Nonadaptive Controller.

It took less than 0.25 sec to stabilize the load voltage and reach the steady state. In addition, the excess electricity generated by wind turbine is captured and stored in the battery whenever the generated power is higher than the required power of the load.

A test was conducted to evaluate the capability of the nonlinear controller to efficiently manage the power between the wind-turbine, the battery-storage, the load and grid based on the load power requirement. Two different wind speed profiles were used for the test. A constant wind speed was applied in the first test. The system starts in the stand-alone mode and the battery was initially charged at 70% while the load power is $2MW$. The wind-turbine output power (solid line), the load power (dashed line) and the battery power (dotted line) are shown in Fig. 5.8. At the beginning $t = 0$ sec, the produced power was greater than the load power. The extra energy was stored in the battery unit. This is shown in Fig. 5.8 (dotted line) by the negative power for the battery. At $t = 0.2$ sec, while the system was operating in stand-alone mode, the load power increases from 1 MW to 2 MW when the switch *Sw2* closes. The produced power was therefore insufficient to supply the load. Hence, the battery provided the deficit of the required power. This is shown by the positive power for the battery. At $t = 0.4$ sec the switch *Sw1* closes, the system switched back into grid-connected mode. The battery continued on providing almost the same amount of power to

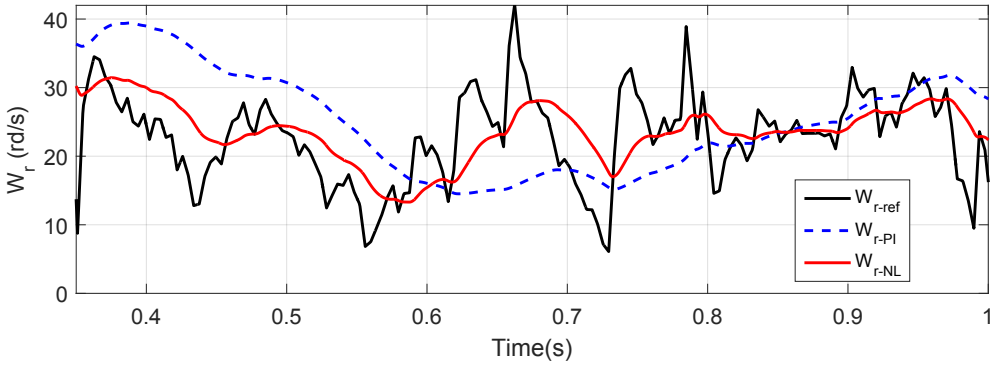

(a) Nonadaptive Rotor Speed.

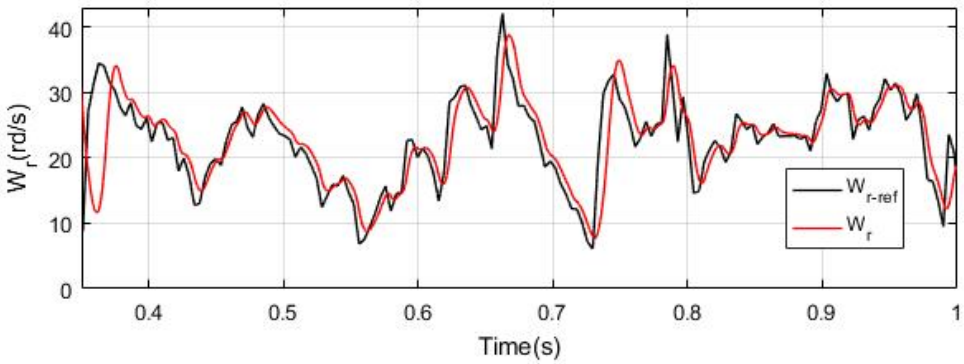

(b) Adaptive Rotor Speed.

Figure 5.9: (a) Nonadaptive Rotor Speed, (b) Adaptive Rotor Speed.

the load. This reduced significantly the grid contribution. At $t = 0.6$ sec, while the system was operating in grid-connected mode, the load power decreased from 2 MW to 1 MW at $t = 3$ sec. At this moment, the generated power higher than the load demand. The surplus of power was stored now in the battery as indicated in Fig. 5.8 (dotted line).

The battery charging and discharging performance of the proposed adaptive controller was compared to the nonadaptive and PI controllers using real wind speed data [120]. Fig. 5.9 and 5.10 show the generator rotor speed and output power, respectively. The black solid line, the dashed line and the red solid line

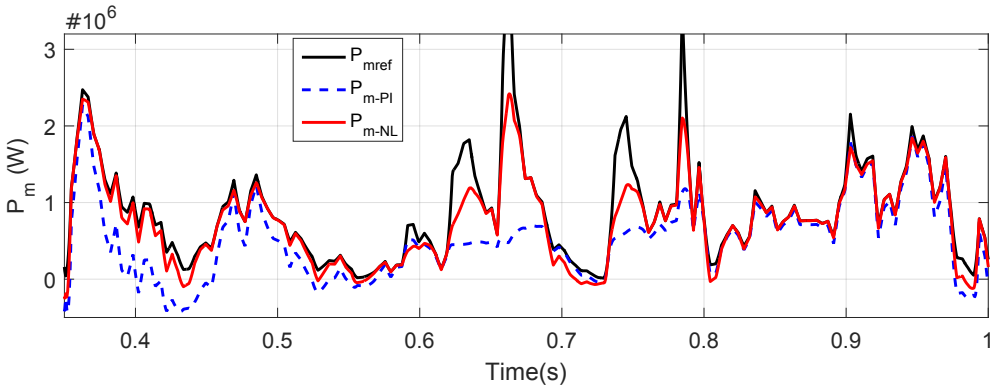

(a) Nonadaptive Output Power.

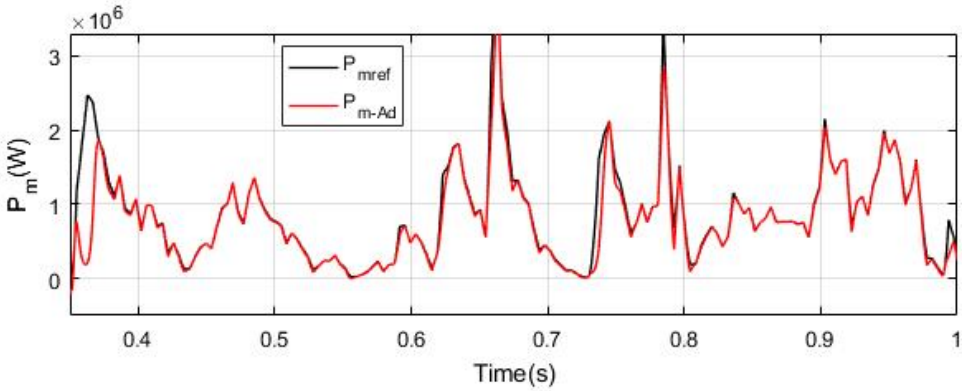

(b) Adaptive Output Power.

Figure 5.10: (a) Nonadaptive Output Power, (b) Adaptive Output Power.

stand for the reference signal, the signal for the PI controller and the signal for the nonlinear controller in Fig. 5.9(a) and Fig. 5.10(a), respectively. Whereas, the red solid line represents the adaptive controller signal in Fig. 5.9(b) and Fig 5.10(b). It can be observed that the adaptive controller has a fast and better dynamic behavior as well as a good tracking performance.

To demonstrate the robustness of the proposed nonlinear adaptive control system despite that the parameters of the system were unknown, simulation was run using three different loads as described in Table 5.4 below: balanced three-phase load, unbalanced three-phase series RL load and a nonlinear single-phase parallel RC load. The results of the currents when the load power levels change as well as when the system switches from one mode of operation to another are plotted in Fig. 5.11. The test starts with stand-alone mode and then switches into the grid-connected mode at $t = 0.6$ sec. On can observe that the Waveforms of the currents show good performance, despite, the variation of the load and the change of the mode of operation. Although, some amplitude mismatches were observed in Fig. 5.11(b) current waveform due to the unbalanced phases. Also, Small ripples, due to nonlinearities, can be observed in in Fig. 5.11(c). However, the waveforms were close to sinusoidal.

Table 5.4: Loads

Loads	H_1	H_2	H_3
Type of Load	Balanced Load	Unbalanced three-phase Load	Nonlinear Load
Value	R_1=16 Ω L_1=16 mH	R_{21}=10 Ω, L_{21}=11 mH R_{22}=20 Ω, L_{22}=11 mH R_{23}=30 Ω, L_{23}=11 mH	R_3=50 Ω C_3=20 nF

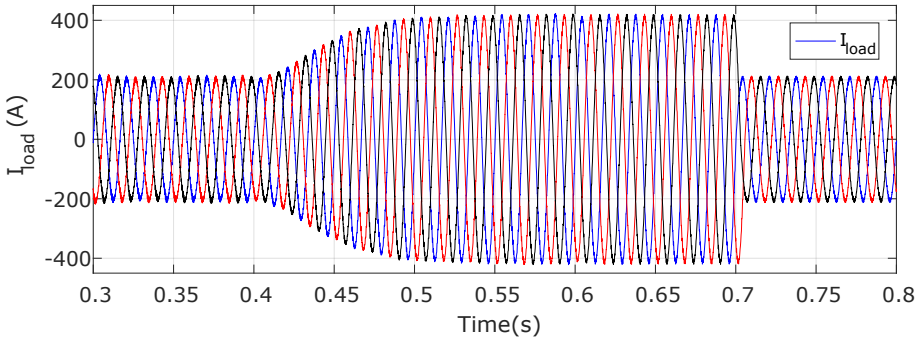

(a) Current of Balanced 3-Ph Load.

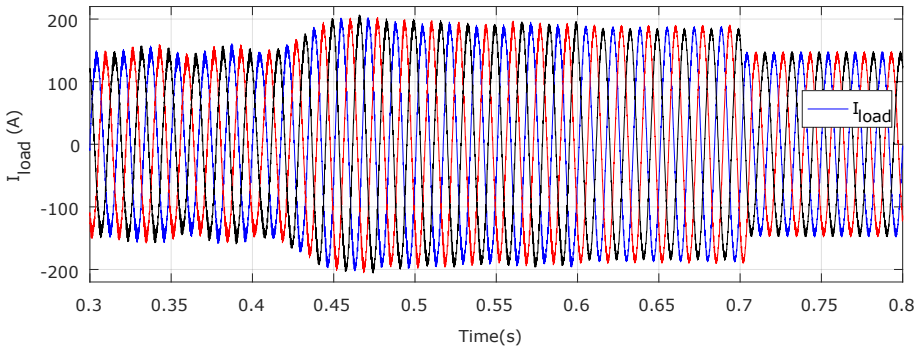

(b) Current of Unbalanced 3-Ph Load.

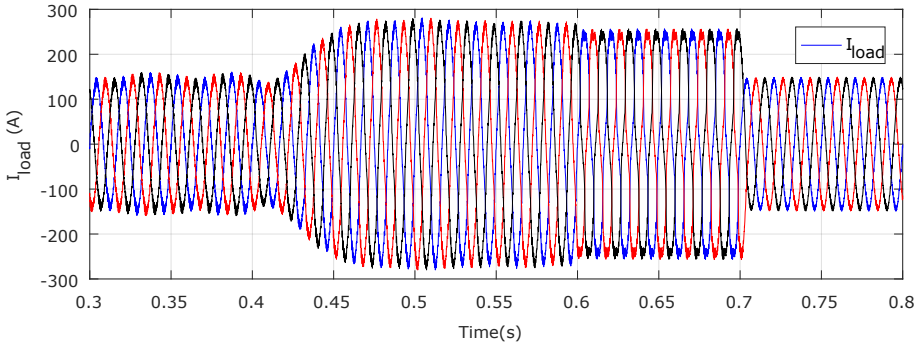

(c) Current of 1-Ph Nonlinear Load.

Figure 5.11: Current of (a) Balanced 3-Ph Load, (b) Unbalanced 3-Ph Load, (c) 1-Ph Nonlinear Load.

5.5 Conclusion

In this paper, online parameter estimation of a hybrid wind energy system has been studied. Although, all the parameters of the system were assumed unknown, the hybrid system is capable to flexibly operate in both grid-connected and stand-alone mode using a single controller. A Lyapunov-based adaptive control law that guarantees that the parameters are bounded was proposed. The adaptive controller allowed the system, through its backup battery source, to stay stable and continue to operate when the grid is connected or disconnected due to power outage. Hence, improving the resilience of the power grid and prevent energy delivery interruption. Moreover, a change from the generator, the grid or the load, due to environmental condition, does not affect the efficiency of the system. This was achieved by continuously updating the parameters of the system by means of the adaptive controller. Unlike conventional control design, the proposed control scheme uses a single controller for both grid-connected and stand-alone operation modes. And this without the need of an islanding detection module. Therefore, problems related to the grid detection and islanding during the transition of mode can be avoided. In addition, the controller was capable of accommodating wind turbine system nonlinearities and uncertainties. This has been illustrated in the results section where unbalanced and nonlinear loads were used. The MPPT and power management have been successfully evaluated for both grid-connected and stand-alone modes using real wind speed profile. The simulation results show that the proposed control scheme can effectively track its references achieving the desired control objectives.

Appendix Chapter 5

On-grid/Off-grid System model Dynamic

Regardless the mode of operation, the system to be controlled is represented by Eqs.(5.28), (5.29), (5.30) and (5.31). It is a seven-order nonlinear multivariable system that has six inputs and six outputs. The vector of state variables, $\overline{x} \in \mathbb{R}^n$, the vector of control inputs, $\overline{u} \in \mathbb{R}^m$, and the vector of controlled outputs, $\overline{y} \in \mathbb{R}^m$, are respectively

$$\begin{cases} \overline{x} = [i_{ds}, i_{qs}, \omega_r, i_{di}, i_{qi}, i_{bl}, E_{dc}]^T & \text{(5.24a)} \\ \overline{u} = [u_{ds}, u_{qs}, u_{di}, u_{qi}, P_{bat}, D]^T & \text{(5.24b)} \\ \overline{y} = [\tilde{i}_{ds}, \tilde{\omega}_r, \tilde{u}_{dl}, \tilde{u}_{ql}, \tilde{E}_{dc}, \tilde{i}_{lb}]^T & \text{(5.24c)} \end{cases}$$

where $\tilde{i}_{ds}, \tilde{\omega}_r, \tilde{u}_{dl}, \tilde{u}_{ql}, \tilde{E}_{dc}$ and $\tilde{i}_{lb}$ are defined as follows

$$\tilde{i}_{ds} = \int (i_{ds} - i^*_{ds}) d\delta, \qquad \tilde{\omega}_r = \int (\omega_r - \omega^*_r) d\delta \tag{5.25}$$

$$\tilde{u}_{dl} = \int (u_{dl} - u^*_{dl}) d\delta, \qquad \tilde{u}_{ql} = \int (u_{ql} - u^*_{ql}) d\delta \tag{5.26}$$

$$\tilde{E}_{dc} = \int (E_{dc} - E^*_{dc}) d\delta, \qquad \tilde{i}_{lb} = \int (i_{lb} - i^*_{lb}) d\delta \tag{5.27}$$

The output variables $\tilde{i}_{ds}, \tilde{\omega}_r, \tilde{u}_{dl}, \tilde{u}_{ql}, \tilde{E}_{dc}$ and $\tilde{i}_{lb}$ represent the integral of the errors between the variables $i_{ds}, \omega_r, u_{dl}, u_{ql}, E_{dc}$ and i_{lb} to be regulated, and their references $i^*_{ds}, \omega^*_r, u^*_{dl}, u^*_{ql}, E^*_{dc}$ and i^*_{bl}, respectively. Integral actions are added into the control-loop to ensure zero steady state errors and to increase the robustness of the controller when the system structure changes.

$$\frac{\mathrm{d}\omega_m}{\mathrm{d}t} = \frac{P}{J}(T_m - T_e) \tag{5.28}$$

$$\begin{cases} u_{ds} = R_s i_{ds} + L_d \dfrac{\mathrm{d}i_{ds}}{\mathrm{d}t} - \omega_r L_q i_{qs} & (5.29a) \\ u_{qs} = R_s i_{qs} + L_q \dfrac{\mathrm{d}i_{qs}}{\mathrm{d}t} + \omega_r L_d i_{ds} + \omega_r \lambda_r & (5.29b) \\ T_e = \dfrac{3P}{2} \left[\lambda_r i_{qs} - (L_d - L_q) i_{ds} i_{qs} \right] & (5.29c) \end{cases}$$

$$\begin{cases} u_{di} = L_f \dfrac{\mathrm{d}i_{di}}{\mathrm{d}t} - \omega_g L_f i_{qi} + u_{dl} & (5.30a) \\ u_{qi} = L_f \dfrac{\mathrm{d}i_{qi}}{\mathrm{d}t} + \omega_g L_f i_{di} + u_{ql} & (5.30b) \end{cases}$$

$$\begin{cases} \dfrac{\mathrm{d}i_{lb}}{\mathrm{d}t} = \dfrac{1}{L_b}(u_{bat} - D u_{dc}) & (5.31a) \\ \dfrac{\mathrm{d}E_{dc}}{\mathrm{d}t} = u_{dc} i_{sdc} - \dfrac{3}{2} u_{di} i_{di} + P_{bat} & (5.31b) \end{cases}$$

$$\begin{cases} u_{dl} = R_{th} i_{di} - \omega_g L_{th} i_{qi} + E_{thd} & (5.32a) \\ u_{ql} = R_{th} i_{qi} + \omega_g L_{th} i_{di} + E_{thq} & (5.32b) \end{cases}$$

Matrix

$$P = \begin{bmatrix} -39.999 & -0.5 & 0 & 0 & 0 & 0 & 0 & 0 & 0 & 0 & 0 & 0 & 0 \\ -0.5 & 200 & 0 & 0 & 0 & 0 & 0 & 0 & 0 & 0 & 0 & 0 & 0 \\ 0 & 0 & 0.5670 & -0.5 & -0.2673 & 0 & 0 & 0 & 0 & 0 & 0 & 0 & 0 \\ 0 & 0 & -0.5 & 0.2673 & -0.5 & 0 & 0 & 0 & 0 & 0 & 0 & 0 & 0 \\ 0 & 0 & -0.2673 & -0.5 & 0.5045 & 0 & 0 & 0 & 0 & 0 & 0 & 0 & 0 \\ 0 & 0 & 0 & 0 & 0 & 0.0163 & -0.5 & 0 & 0 & 0 & 0 & 0 & 0 \\ 0 & 0 & 0 & 0 & 0 & -0.5 & 25 & 0 & 0 & 0 & 0 & 0 & 0 \\ 0 & 0 & 0 & 0 & 0 & 0 & 0 & 0.0163 & -0.5 & 0 & 0 & 0 & 0 \\ 0 & 0 & 0 & 0 & 0 & 0 & 0 & -0.5 & 25 & 0 & 0 & 0 & 0 \\ 0 & 0 & 0 & 0 & 0 & 0 & 0 & 0 & 0 & -0.5 & 4.4 & 0 & 0 \\ 0 & 0 & 0 & 0 & 0 & 0 & 0 & 0 & 0 & -4.4 & -0.5 & 0 & 0 \\ 0 & 0 & 0 & 0 & 0 & 0 & 0 & 0 & 0 & 0 & 0 & 0.1 & -0.5 \\ 0 & 0 & 0 & 0 & 0 & 0 & 0 & 0 & 0 & 0 & 0 & -0.5 & 0.1 \end{bmatrix} \tag{5.33}$$

$$\Gamma = 10^{-8} I, \text{ where } I \text{ is matrix identity 15x15.} \tag{5.34}$$

$$A_{ad} = \begin{bmatrix} 0 & 1 & 0 & 0 & 0 & 0 & 0 & 0 & 0 & 0 & 0 & 0 & 0 \\ 0 & 0 & 0 & 0 & 0 & 0 & 0 & 0 & 0 & 0 & 0 & 0 & 0 \\ 0 & 0 & 0 & 1 & 0 & 0 & 0 & 0 & 0 & 0 & 0 & 0 & 0 \\ 0 & 0 & 0 & 0 & 1 & 0 & 0 & 0 & 0 & 0 & 0 & 0 & 0 \\ 0 & 0 & 0 & 0 & 0 & 0 & 0 & 0 & 0 & 0 & 0 & 0 & 0 \\ 0 & 0 & 0 & 0 & 0 & 0 & 1 & 0 & 0 & 0 & 0 & 0 & 0 \\ 0 & 0 & 0 & 0 & 0 & 0 & 0 & 0 & 0 & 0 & 0 & 0 & 0 \\ 0 & 0 & 0 & 0 & 0 & 0 & 0 & 0 & 1 & 0 & 0 & 0 & 0 \\ 0 & 0 & 0 & 0 & 0 & 0 & 0 & 0 & 0 & 0 & 0 & 0 & 0 \\ 0 & 0 & 0 & 0 & 0 & 0 & 0 & 0 & 0 & 0 & 1 & 0 & 0 \\ 0 & 0 & 0 & 0 & 0 & 0 & 0 & 0 & 0 & 0 & 0 & 0 & 0 \\ 0 & 0 & 0 & 0 & 0 & 0 & 0 & 0 & 0 & 0 & 0 & 0 & 1 \\ 0 & 0 & 0 & 0 & 0 & 0 & 0 & 0 & 0 & 0 & 0 & 0 & 0 \end{bmatrix} \tag{5.35}$$

$$B_{ad} = \begin{bmatrix} 0 & 0 & 0 & 0 & 0 & 0 \\ 1 & 0 & 0 & 0 & 0 & 0 \\ 0 & 0 & 0 & 0 & 0 & 0 \\ 0 & 0 & 0 & 0 & 0 & 0 \\ 0 & 1 & 0 & 0 & 0 & 0 \\ 0 & 0 & 0 & 0 & 0 & 0 \\ 0 & 0 & 1 & 0 & 0 & 0 \\ 0 & 0 & 0 & 0 & 0 & 0 \\ 0 & 0 & 0 & 1 & 0 & 0 \\ 0 & 0 & 0 & 0 & 0 & 0 \\ 0 & 0 & 0 & 0 & 1 & 0 \\ 0 & 0 & 0 & 0 & 0 & 0 \\ 0 & 0 & 0 & 0 & 0 & 1 \end{bmatrix} \tag{5.36}$$

$$W_{ad} = \begin{bmatrix} 0 & 0 & 0 & 0 & 0 & 0 & 0 & 0 & 0 & 0 & 0 & 0 & 0 & 0 & 0 \\ 0 & 0 & 0 & 0 & 0 & 0 & 0 & 0 & 0 & 0 & 0 & 0 & 0 & 0 & 0 \\ 0 & 0 & 0 & 0 & 0 & 0 & 0 & 0 & 0 & 0 & 0 & 0 & 0 & 0 & 0 \\ 0 & 0 & 0 & 0 & 0 & 0 & 0 & 0 & 0 & 0 & 0 & 0 & 0 & 0 & 0 \\ 0 & 0 & 0 & 0 & 0 & 0 & 0 & \omega_r^2 & -i_{qs} & 0 & 0 & 0 & 0 & 0 & 0 \\ 0 & 0 & 0 & 0 & 0 & 0 & 0 & 0 & 0 & 0 & 0 & 0 & 0 & 0 & 0 \\ 0 & 0 & 0 & 0 & 0 & 0 & 0 & 0 & 0 & i_{di} & -i_{qi} & 1 & 0 & 0 & 0 \\ 0 & 0 & 0 & 0 & 0 & 0 & 0 & 0 & 0 & 0 & 0 & 0 & 0 & 0 & 0 \\ 0 & 0 & 0 & 0 & 0 & 0 & 0 & 0 & 0 & i_{qi} & i_{di} & 0 & 1 & 0 & 0 \\ 0 & 0 & 0 & 0 & 0 & 0 & 0 & 0 & 0 & 0 & 0 & 0 & 0 & 0 & 0 \\ 0 & 0 & 0 & 0 & 0 & 0 & 0 & 0 & 0 & 0 & 0 & 0 & 0 & 0 & 0 \\ 0 & 0 & 0 & 0 & 0 & 0 & 0 & 0 & 0 & 0 & 0 & 0 & 0 & 0 & 0 \\ 0 & 0 & 0 & 0 & 0 & 0 & 0 & 0 & 0 & 0 & 0 & 0 & 0 & 0 & 0 \end{bmatrix} \tag{5.37}$$

$$\psi_{ad} = \begin{bmatrix} 0 & 0 & 0 & 0 & 0 & 0 & 0 & 0 & 0 & 0 & 0 & 0 & 0 & 0 & 0 \\ -i_{ds} & \omega_r i_{qs} & u_{ds} & 0 & 0 & 0 & 0 & 0 & 0 & 0 & 0 & 0 & 0 & 0 & 0 \\ 0 & 0 & 0 & 0 & 0 & 0 & 0 & 0 & 0 & 0 & 0 & 0 & 0 & 0 & 0 \\ 0 & 0 & 0 & 0 & 0 & 0 & 0 & \omega_r^2 & -i_{qs} & 0 & 0 & 0 & 0 & 0 & 0 \\ 0 & 0 & 0 & \hat{\theta}_9\omega_r i_{ds} & \hat{\theta}_9 i_{qs} & \hat{\theta}_9\omega_r & -\hat{\theta}_9 u_{qs} & 2\hat{\theta}_8\omega_r^3 & -2\hat{\theta}_8\omega_r i_{qs} & 0 & 0 & 0 & 0 & 0 & 0 \\ 0 & 0 & 0 & 0 & 0 & 0 & 0 & 0 & 0 & i_{ds} & -i_{qs} & 1 & 0 & 0 & 0 \\ 0 & 0 & 0 & 0 & 0 & 0 & 0 & 0 & 0 & 0 & 0 & 0 & 0 & 0 & 0 \\ 0 & 0 & 0 & 0 & 0 & 0 & 0 & 0 & 0 & i_{qi} & i_{di} & 0 & 1 & 0 & 0 \\ 0 & 0 & 0 & 0 & 0 & 0 & 0 & 0 & 0 & 0 & 0 & 0 & 0 & 0 & 0 \\ 0 & 0 & 0 & 0 & 0 & 0 & 0 & 0 & 0 & 0 & 0 & 0 & 0 & 0 & 0 \\ 0 & 0 & 0 & 0 & 0 & 0 & 0 & 0 & 0 & 0 & 0 & 0 & 0 & 0 & 0 \\ 0 & 0 & 0 & 0 & 0 & 0 & 0 & 0 & 0 & 0 & 0 & 0 & 0 & 0 & 0 \end{bmatrix} \tag{5.38}$$

Chapter 6

Single-Phase Stand-Alone and Grid-Connected DQ Nonlinear Controller Design for Enhancing the Resilience of Hybrid Wind-Battery Microgrid

Abstract

This paper presents a novel DQ synchronous frame nonlinear controller design for a single-phase residential wind-battery system. The main contribution of the proposed controller is its ability to improve the resilience of the power grid and prevent energy delivery interruption. It allows the microgrid to either operate in grid-connected mode or stand-alone mode with no requirement for switching between two different controllers, as opposed to traditional techniques. In addition, the hybrid system provides backup capability to preserve system reliability. It can also support the grid by selling power back to the grid during high wind condition. A single-phase DQ transformation module is used to convert the grid-side converter signals in DQ synchronous frame. The proposed nonlinear controller has been successfully tested using a variable speed nonsalient-pole PMSG driven by a wind turbine under real wind speed profile as well. The simulation results shows that the system can capture the maximum power available from the wind, control

load voltage, as well as perform power management control, regardless of the mode of operation.

Index terms— Battery storage, energy management, feedback linearization, grid-connected, nonlinear control, reliability, resilience, single-phase, stand-alone, wind turbine.

6.1 Introduction

Electricity plays a key role in economic and social development, yet more than 1.3 billion people in remote areas still don't have access to it. More than 99% of them live in developing regions, and 4/5 of them are in rural South Asia and sub-Saharan Africa [29]. In 2012, about 70 developing countries now have renewable energy targets in place [127]. Developing countries have the particularity of having a growing population coupled with underinvestment in the electricity sector. This situation has led to the increase in energy demand without any significant investment in capacity or grid infrastructure. Diesel generators are commonly used as alternative backup during power outages and the majority of people use traditional wood and charcoal for their regular needs, such as cooking and heating. As a result, rolling blackouts have become more frequent or even a normal daily event in many developing countries [153, 154].

In most of developing countries, wind power is one of the most abundant and increasingly cost-competitive energy resources. Which makes it a viable solution to the growing power outage problem in these countries. More and more grid-connected wind farms and small wind turbines are being installed in these regions. Over the past decade, their use has increased more than 25% per year [155]. However, the current installed wind turbines are mainly either stand-alone (or off-grid) or grid-connected (or on-grid) systems. They are not designed to operate in both modes. Consequently, when a power outage happens, the grid-connected WECS are automatically disengaged from the utility grid. This causes important monetary losses to electrical energy suppliers [14, 15]. Nowadays, the trend is that they should be maintained under operation in both situations to continue supply

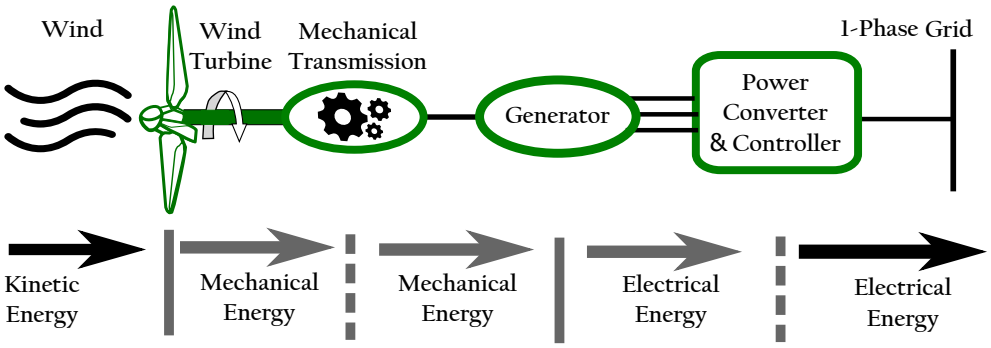

Figure 6.1: Wind Energy Conversion System.

power to critical loads [156]. In addition, transition between the two modes ought to be quick and consistent to limit any sudden voltage or current changes [119].

Improving the reliability of the power grid now became a crucial factor. To meet this goal, the power grid needs to be resilient [157, 158]. This depends upon the ability of the system controller to react, absorb and rapidly recover from an outage [159, 160]. On-grid/off-grid wind turbine systems can play a key role in this regard. Particular attention has been paid to the on-grid/off-grid wind turbine systems in recent years. Authors in [135] and [32] suggest a control technique for a PMSG (Permanent Magnet Synchronous Generator) driven by a small wind turbine capable to operate in both grid-connected and stand-alone modes. In the grid-connected mode, a PI current controller is used for the grid-side converter. The active and reactive power are controlled independently. The authors in [16] utilize a asynchronous generator and PI current controllers. A modified space-vector pulse width modulation based (SVPWM) for stand-alone and grid-connected three-phase converter has been proposed in [34]. In the aforementioned works, two different controllers are utilized. One controller for each mode of operation. An islanding detection module is required in this case to take the decision to switch between the two controllers.

A main feature of the proposed stand-Alone and grid-connected nonlinear control method is that it doesn't require any additional dynamics to apply it to a single phase residential systems or a three-phase systems. A dq synchronous frame transformation module for single-phase full-bridge inverter is added into the

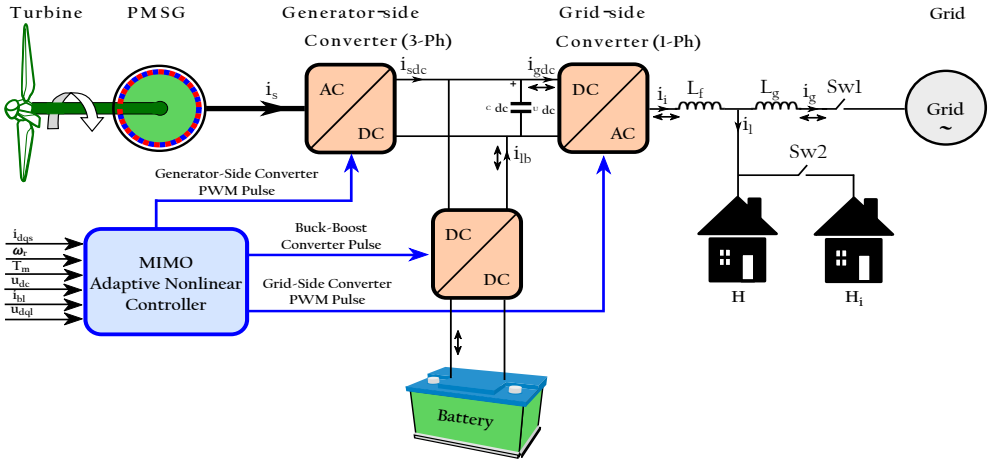

Figure 6.2: On-grid/Off-grid WECS based permanent magnet synchronous generator.

controller.

Several researchers have explored the possibility of transforming a single-phase inverter control signals into a DQ synchronous frame signals and vise versa. In [161] a current control method has been proposed using the dq synchronous frame for single-phase converters. The method consists of transforming the actual single-phase input current and a fictitious current, from a stationary to a rotating frame. Similar methods have been suggested in [162, 163, 164, 165]. A modified method that improves the inverter output power quality and dynamic performance has been presented in [166]. Other DQ controllers for Single-Phase vehicle-grid system in railway and grid-connected PV inverters have been reported in [167] and [168, 169], respectively. Most of these proposed control methods are PI-based. In spite of the fact that PI controllers have the benefit of being simple and convenient, they have some disadvantages. They are sensitive to highly nonlinear systems such as wind energy battery-storage systems [11]. They have a poor transient response and a weak disturbance rejection for non constant perturbations. They have difficulty to limit the converter current rise below the allowable limit during the stand-alone and the grid detection transition time [16].

This paper presents a single nonlinear DQ controller design for a hybrid wind-battery system used in single-phase domestic dwelling applications. The control

system has the ability to enhance the resilience and reliability by allowing micro-grids to either operate in grid-connected mode or stand-alone mode. Contrary to conventional methods found in the literature, in the proposed approach, a single controller is used for both operation modes. And there is no need for an islanding detection system [121, 122].

Regardless of the mode of operation, the single controller performs the power point tracking, load voltage regulation and power management between the battery the load and the grid. Therefore, issues related to the islanding detection, such as poor dynamic performance [123, 38], low quality load current waveform [124, 125] and inrush grid current [126] throughout the transition of operation mode, can be avoided. The design approach is based on the MIMO feedback linearization control method. A three-phase rectifier and a full-bridge single-phase power converter are utilized to connect the wind turbine to the load and the grid. Additionally, the dc-link voltage and the power of the load are directly controlled through a bi-directional buck-boost DC/DC converter based on the power balance and also the system stability. To the best of our knowledge, this is the first study investigating a stand-alone and grid-connected WECS for single-phase domestic dwelling applications.

In the following pages, first, an overview of the problem study and the dynamic equations of the hybrid wind/battery system are given in Section 6.2. In Section 6.3, the design of the proposed DQ synchronous reference frame nonlinear controller is presented. The validity and the performance of the proposed method is evaluated in Section 6.4. The conclusion is presented in Section 6.5.

6.2 Hybrid Wind/Battery System Dynamic Modeling

6.2.1 Wind Turbine

Fig. 6.1 describes the principal of operation of wind turbines. Wind turbine converts part of the kinetic energy of the wind into useful mechanical energy.

By means of the generator, this energy is converted into electrical energy. Since the generator output frequency depends on the wind conditions, a back-to-back converter is used to synchronized its output with the grid frequency. Depending on the position of the rotor axis, wind turbines are classified into vertical-axis and horizontal-axis ones [21].

The power produced by the wind turbine is given by [21]

$$P_m = 0.5\pi\rho C_p(\lambda, \beta)R^2 v_w^3 \tag{6.1}$$

where R is the radius of the turbine, v_w is the wind speed, ρ is the air density, C_p is the power coefficient, λ is the tip speed ratio and β is the pitch angle.

The tip speed ratio is given by [21]

$$\lambda = \frac{\omega_m R}{v_w} \tag{6.2}$$

where ω_m is the turbine angular speed. Neglecting the friction forces, the dynamic equation of the wind turbine is given by [21]

$$\frac{\mathrm{d}\omega_m}{\mathrm{d}t} = \frac{P}{J}(T_m - T_e) \tag{6.3}$$

where J is the system inertia, T_m is the torque developed by the turbine, T_e is the torque due to load which in this case is the generator torque. The target optimum power from a wind turbine can be written as [21]

$$P_{max} = k_{opt}\omega_{mopt}^3 \tag{6.4}$$

where [21]

$$k_{opt} = \frac{0.5\pi\rho C_{pmax}R^5}{\lambda_{opt}^3} \text{ and } \omega_{mopt} = \frac{\lambda_{opt}v_w}{R} \tag{6.5}$$

In order to have maximum possible power, the turbine should always operate at λ_{opt}. This is possible by controlling the rotational speed of the turbine so that it always rotates at the optimum speed of rotation. C_p is optimum when $\lambda = \lambda_{opt}$.

6.2.2 PMSG Model

The dq reference frame model for the PMSG is given by [21]

$$\begin{cases} u_{ds} = R_s i_{ds} + L_d \dfrac{\mathrm{d}i_{ds}}{\mathrm{d}t} - \omega_r L_q i_{qs} & \text{(6.6a)} \\ u_{qs} = R_s i_{qs} + L_q \dfrac{\mathrm{d}i_{qs}}{\mathrm{d}t} + \omega_r L_d i_{ds} + \omega_r \lambda_r & \text{(6.6b)} \end{cases}$$

where, i_{ds} and i_{qs} are the stator dq-axis currents (V); R_s is the stator winding resistance (Ω); L_d and L_q are the stator dq-axis self-inductances (H); ω_r is the rotor electrical angular speed (rad/s); and λ_r is the rotor flux generated by the permanent magnets.

A round rotor PMSG is considered in this study. The d- and q-axis magnetizing inductions are therefore equal ($L_d = L_q = L_s$). However, we keep L_d, L_q notations so that the derived equations can be applied to both salient and nonsalient (round) PMSG. The electromagnetic torque is given by [21]

$$T_e = \frac{3P}{2} \left[\lambda_r i_{qs} - (L_d - L_q) i_{ds} i_{qs} \right] \tag{6.7}$$

6.2.3 Battery Storage Unit Model

A bi-directional buck-boost converter is used to connect the battery-storage to the back-to-back converter dc-link. A *Nickel-Metal-Hydride* Model is used for the battery [136]. During the discharging mode of the battery, the bi-directional converter operates as a boost converter and during the charging mode as a buck. The dynamic equations of the current through the inductor, L_b, is given by

$$\begin{cases} \dfrac{\mathrm{d}i_{lb}}{\mathrm{d}t} = \dfrac{1}{L_b}(u_{bat} - D u_{dc}) & \text{(6.8a)} \\ \dfrac{\mathrm{d}E_{dc}}{\mathrm{d}t} = u_{dc} i_{sdc} - \dfrac{3}{2} u_{di} i_{di} + P_{bat} & \text{(6.8b)} \end{cases}$$

where u_{bat}, i_{lb}, i_{sdc}, P_{bat} and D are the battery voltage, the current through the inductor L_b, the generator-side converter dc current, the battery power and the

duty cycle respectively. Note that D and $\bar{D}$ are logical complement of each other. Instead of the grid-side converter, the bi-directional buck-boost converter is utilized to control the back-to-back converter dc-link capacitor voltage, u_{dc}, through E_{dc} where $E_{dc} = \frac{1}{2}C_{dc}u_{dc}^2$. From the energy storage variation of the dc-link capacitor, Eqn. (6.8b) can be obtained [119].

6.2.4 PWM Voltage Source Converter Model

If the inverter, the load and the grid were three-phase, it has been shown in [28] that the mathematical model in the dq frame of the wind energy battery-storage system, can be represented by Eqn.(6.14), regardless the mode of operation. The description of the different variables is given in Table 6.1.

One may observe that the system is a seven-order nonlinear multi-input-multi-output (MIMO) system. It has six inputs and six outputs. The vector of state variables, $\overline{x} \in \mathbb{R}^n$, the vector of control inputs, $\overline{u} \in \mathbb{R}^m$, and the vector of controlled outputs, $\overline{y} \in \mathbb{R}^m$, are respectively

$$\begin{cases} \overline{x} = [i_{ds}, i_{qs}, \omega_r, i_{di}, i_{qi}, i_{bl}, E_{dc}]^T & \text{(6.9a)} \\ \overline{u} = [u_{ds}, u_{qs}, u_{di}, u_{qi}, P_{bat}, D]^T & \text{(6.9b)} \\ \overline{y} = [i_{ds}, \omega_r, u_{dl}, u_{ql}, E_{dc}, i_{lb}]^T & \text{(6.9c)} \end{cases}$$

For the design of a unique controller for the wind energy battery storage system that can operate in both grid-connected and stand-alone modes, the grid-side circuit is represented by a model which is valid in both modes of operation. When the system operates in the grid-connected mode, the grid-side circuit is composed of a RL load, a filter, L_f, the line inductance, L_g, and the grid. The transformer leakage inductance is included in L_g for the sake of simplicity. The principal concept behind this modeling approach is to represent the grid and the load by an equivalent Thevenin model. This model will be connected in series with L_f.

The Thevenin voltage and impedance in grid-connected mode are as follows respectively by Eqn. (6.10)

$$\begin{cases} E_{th} = \dfrac{(R_l + j\omega_g L_l)(u_{dg} + ju_{qg})}{R_l + j\omega_g(L_l + L_g)} & \text{(6.10a)} \\ Z_{th} = \dfrac{j\omega_g L_g(R_l + j\omega_g L_l)}{R_l + j\omega_g(L_l + L_g)} & \text{(6.10b)} \end{cases}$$

where $Z_l = R_l + j\omega_g L_l$ and and $u_g = u_{dg} + ju_{qg}$ are the load impedance and the grid voltage, respectively. R_l and L_l can be obtained from the load active and reactive power as given

$$R_l = \frac{\sqrt{3}u_{ll}^2 P_l}{P_l^2 + Q_l^2} \text{ and } L_l = \frac{\sqrt{3}u_{ll}^2 Q_l}{P_l^2 + Q_l^2} \tag{6.11}$$

where u_{ll} is the load line-to-line RMS voltage. The load active and reactive power of the system are respectively P_l and Q_l. They can be calculated from the load voltage and current.

$$P_l = \frac{1}{2}(u_{dl}i_{dl} + u_{ql}i_{ql}) \text{ and } Q_l = \frac{1}{2}(u_{ql}i_{dl} - u_{dl}i_{ql}) \tag{6.12}$$

In off-grid mode, $E_{th} = 0$ and $Z_{th} = Z_l$.

The grid-side circuit is assumed in a quasi-static mode, hence, the dq components of the load voltage can be written as

$$\begin{cases} u_{dl} = R_{th}i_{di} - \omega_g L_{th}i_{qi} + E_{thd} & \text{(6.13a)} \\ u_{ql} = R_{th}i_{qi} + \omega_g L_{th}i_{di} + E_{thq} & \text{(6.13b)} \end{cases}$$

where R_{th} and $\omega_g L_{th}$ are real and imaginary parts of the Thevenin impedance, respectively ($Z_{th} = R_{th} + j\omega_g L_{th}$).

$$\frac{\mathrm{d}}{\mathrm{d}t}\begin{bmatrix} i_{ds} \\ i_{qs} \\ \omega_r \\ i_{di} \\ i_{qi} \\ i_{bl} \\ E_{dc} \end{bmatrix} = \begin{bmatrix} -\frac{R_s}{L_d} & \frac{L_q}{L_d}\omega_r & 0 & 0 & 0 & 0 & 0 \\ -\frac{L_d}{L_q}\omega_r & -\frac{R_s}{L_q} & -\frac{\lambda_r}{L_q} & 0 & 0 & 0 & 0 \\ 0 & -\frac{3P^2\lambda_r}{2J} & \frac{k_{opt}}{JP}\omega_r & 0 & 0 & 0 & 0 \\ 0 & 0 & 0 & 0 & \omega_g & 0 & 0 \\ 0 & 0 & 0 & -\omega_g & 0 & 0 & 0 \\ 0 & 0 & 0 & 0 & 0 & 0 & 0 \\ 0 & 0 & 0 & -\frac{3}{2}u_{di} & 0 & 0 & 0 \end{bmatrix} \begin{bmatrix} i_{ds} \\ i_{qs} \\ \omega_r \\ i_{di} \\ i_{qi} \\ i_{bl} \\ E_{dc} \end{bmatrix}$$
$$+ \begin{bmatrix} \frac{1}{L_d} & 0 & 0 & 0 \\ 0 & \frac{1}{L_q} & 0 & 0 \\ 0 & 0 & 0 & 0 \\ 0 & 0 & -\frac{1}{L_f} & 0 \\ 0 & 0 & 0 & -\frac{1}{L_f} \\ 0 & 0 & -\frac{u_{dc}}{L_b} & 0 \\ 0 & 0 & 0 & 1 \end{bmatrix} \begin{bmatrix} u_{ds} \\ u_{qs} \\ u_{di} \\ u_{qi} \\ D \\ P_{pat} \end{bmatrix} + \begin{bmatrix} 0 \\ 0 \\ 0 \\ \frac{1}{L_f}u_{dl} \\ \frac{1}{L_f}u_{ql} \\ \frac{1}{L_b}u_{bat} \\ i_{sdc}u_{dc} \end{bmatrix} \tag{6.14}$$

6.3 Proposed Control Strategy and Design

6.3.1 Robust Nonlinear Feedback Linearization Controller Design

This section presents the design of the proposed control scheme developed to stabilize the wind energy battery storage system and to meet the control objective, which are as follows: 1) keep the wind turbine operating at its maximum power by controlling ω_r; 2) achieve a linear relationship between the stator current and the electromagnetic torque by controlling the stator d-axis current, i_{ds}; 3) meet the load voltage requirement by controlling both load d-axis and q-axis voltages, u_{dl} and u_{ql} respectively; 4) ensure the regulation of the dc-link voltage by controlling, u_{dc}; 5) perform power management between the battery, load and grid subsystems by controlling the battery current, i_{lb}.

Table 6.1: System Variables

Parameter	Description
i_{ds}, i_{qs}	Generator stator d- and q-axis currents (A)
u_{ds}, u_{qs}	Generator stator d- and q-axis voltages (V)
ω_r	Rotor electrical angular speed (rd/s)
i_{di}, i_{qi}	Grid-side converter output d- and q-axis currents (A)
u_{di}, u_{qi}	Grid-side converter output d- and q-axis voltage (V)
i_{lb}	Current through the dc/dc converter inductor (A)
E_{dc}	Electric energy of the dc-link capacitor (A)
P_m	Rated Mechanical Power (MW)
λ_r	Rated Rotor Flux Linkage (Wb)
P	Number of Pole Pairs
J	Moment Inertia of the Generator $(kg.m^2)$
R_s	Stator Winding Resistance (Ohm)
L_{ds}	d-axis Synchronous Inductance (H)
L_{qs}	q-axis Synchronous Inductance (H)
V_w	Rated Wind speed (m/s)
R	Blade Radius (m)
β	Pitch Angle $(degree)$
Rho	Air Density
λ_{opt}	Optimal Tip Speed Ratio
u_g	Grid Voltage Line-to-Line Module (V)
u_{dc}	dc-link Voltage (V)
C_{dc}	dc-link Capacitor (F)
L_f	Grid-side Filter (H)
L_g	Grid Inductance (H)
u_{bat}	Battery Rated Voltage (V)
P_{bat}	Battery Power (MW)

6.3.2 Feedback Linearization based Three-Phase

To find the controller equation and its structure, the input-output feedback linearization control is considered as design method. The controller structure is illustrated in Fig. 6.3. It includes a change of variables $T(x)$, a nonlinear control, $\overline{u}(\overline{x})$, and the stabilizing linear control $\overline{v}$.

Integral actions are added into the control-loop to ensure zero steady state errors when the system structure changes, namely when the system switches from the grid-connected mode to the stand-alone mode. Therefore the output vector, $\overline{y}$, becomes $\overline{y}_i = [\tilde{i}_{ds}, \tilde{\omega}_r, \tilde{u}_{dl}, \tilde{u}_{ql}, \tilde{E}_{dc}, \tilde{i}_{lb}]^T$

where the output variables $\tilde{i}_{ds}, \tilde{\omega}_r, \tilde{u}_{dl}, \tilde{u}_{ql}, \tilde{E}_{dc}$ and $\tilde{i}_{lb}$ represent the integral of the errors between the variables $i_{ds}, \omega_r, u_{dl}, u_{ql}$ and E_{dc}, to be controlled, and their references $i^*_{ds}, \omega^*_r, u^*_{dl}, u^*_{ql}, E^*_{dc}$ and i^*_{bl}, respectively.

$$\tilde{i}_{ds} = \int (i_{ds} - i^*_{ds}) d\delta, \qquad \tilde{\omega}_r = \int (\omega_r - \omega^*_r) d\delta \tag{6.15}$$

$$\tilde{u}_{dl} = \int (u_{dl} - u^*_{dl}) d\delta, \qquad \tilde{u}_{ql} = \int (u_{ql} - u^*_{ql}) d\delta \tag{6.16}$$

$$\tilde{E}_{dc} = \int (E_{dc} - E^*_{dc}) d\delta, \qquad \tilde{i}_{lb} = \int (i_{lb} - i^*_{lb}) d\delta \tag{6.17}$$

Eqs. (6.18) represents the new system to be controlled. It is now a 13-order nonlinear model as the added integrators have increased the order of the system.

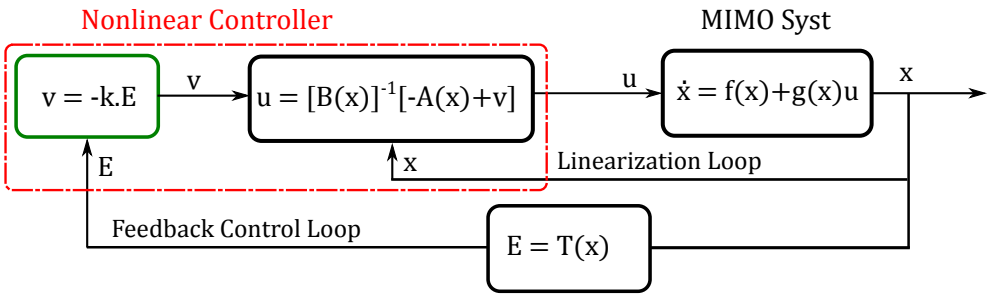

Figure 6.3: Proposed MIMO Nonlinear controller structure.

$$\begin{cases} \overline{x} = [i_{ds}, i_{qs}, \omega_r, i_{di}, i_{qi}, i_{bl}, E_{dc}]^T & \text{(6.18a)} \\ \overline{u} = [u_{ds}, u_{qs}, u_{di}, u_{qi}, P_{bat}, D]^T & \text{(6.18b)} \\ \overline{y}_i = [\tilde{i}_{ds}, \tilde{\omega}_r, \tilde{u}_{dl}, \tilde{u}_{ql}, \tilde{E}_{dc}, \tilde{i}_{lb}]^T & \text{(6.18c)} \end{cases}$$

It has been shown in [119] that input-output feedback linearization design method could be used to obtain the change of variables required for the linearization. Therefore, we got

$$\underbrace{\begin{bmatrix} \ddot{\tilde{i}}_{ds} \\ \dddot{\tilde{\omega}}_r \\ \ddot{\tilde{u}}_{dl} \\ \ddot{\tilde{u}}_{ql} \\ \ddot{\tilde{E}}_{dc} \\ \ddot{\tilde{i}}_{lb} \end{bmatrix}}_{y_d(\overline{x})} = \underbrace{\begin{bmatrix} A_1 \\ A_2 \\ A_3 \\ A_4 \\ A_5 \\ A_6 \end{bmatrix}}_{A(\overline{x})} + \underbrace{\begin{bmatrix} \frac{1}{L_d} & 0 & 0 & 0 & 0 & 0 \\ 0 & \frac{3P^2\lambda_r}{2JL_q} & 0 & 0 & 0 & 0 \\ 0 & 0 & \frac{R_{th}}{L_f} & -\frac{\omega_g L_{th}}{L_f} & 0 & 0 \\ 0 & 0 & \frac{\omega_g L_{th}}{L_f} & \frac{R_{th}}{L_f} & 0 & 0 \\ 0 & 0 & 0 & 0 & 1 & 0 \\ 0 & 0 & 0 & 0 & 0 & -\frac{u_{dc}}{L_b} \end{bmatrix}}_{B(\overline{x})} \underbrace{\begin{bmatrix} u_{ds} \\ u_{qs} \\ u_{di} \\ u_{qi} \\ P_{bat} \\ D \end{bmatrix}}_{\overline{u}} \tag{6.19}$$

where $A(\overline{x}) = [A_1, A_2, A_3, A_4, A_5, A_6]$
with $A_1 = -\frac{R_s}{L_d} i_{ds} + \frac{L_q}{L_d} \omega_r i_{qs}$
$A_2 = -\frac{3P^2}{2JL_q} \lambda_r (-L_d \omega_r i_{ds} - R_s i_{qs} - \lambda_r \omega_r)$
$-\frac{2K_{opt}\omega_r}{PJ^2} (\frac{3P^2\lambda_r}{2} i_{qs} - \frac{K_{opt}\omega_r^2}{P})$
$A_3 = R_{th}(\omega_g i_{qi} - \frac{u_{dl}}{L_f}) - \omega_g L_{th}(-\omega_g i_{di} - \frac{u_{ql}}{L_f}) + \dot{Eth}_d$
$A_4 = R_{th}(-\omega_g i_{di} - \frac{u_{ql}}{L_f}) + \omega_g L_{th}(\omega_g i_{qi} - \frac{u_{dl}}{L_f}) + \dot{Eth}_q$
$A_5 = u_{dc} i_{sdc} - \frac{3}{2} i_{di} u_{di}$ and $A_6 = \dfrac{u_{bat}}{L_b}$,

To linearize and decouple the nonlinear model in Eqs. (6.19), the following control input can be used

$$\overline{u} = [B(\overline{x})]^{-1} [-A(\overline{x}) + \overline{v}] \tag{6.20}$$

where

$$B(\overline{x}) = \begin{bmatrix} \frac{1}{L_d} & 0 & 0 & 0 & 0 & 0 \\ 0 & \frac{3P^2\lambda_r}{2JL_q} & 0 & 0 & 0 & 0 \\ 0 & 0 & \frac{R_{th}}{L_f} & -\frac{\omega_g L_{th}}{L_f} & 0 & 0 \\ 0 & 0 & \frac{\omega_g L_{th}}{L_f} & \frac{R_{th}}{L_f} & 0 & 0 \\ 0 & 0 & 0 & 0 & 1 & 0 \\ 0 & 0 & 0 & 0 & 0 & -\frac{u_{dc}}{L_b} \end{bmatrix} \tag{6.21}$$

and $\overline{v}$ is the new control inputs vector.

The nonlinearities in Eqn. (6.19) are eliminated by choosing u as in Eqn. (6.20). Therefore, a linear relationship between the new outputs $y_d(\overline{x})$ and the new inputs, $\overline{v}$, is found as follows

$$y_d(\overline{x}) = \overline{v} \tag{6.22}$$

where $y_d(x) = \left[\ddot{\tilde{i}}_{ds}, \dddot{\tilde{\omega}}_r, \ddot{\tilde{u}}_{dl}, \ddot{\tilde{u}}_{ql}, \ddot{\tilde{E}}_{dc}, \ddot{\tilde{i}}_{lb}\right]^T$
and $\overline{v} = [v_1, v_2, v_3, v_4, v_5, v_6]^T$.

A state feedback controller is used. It has the following equation:

$$v_p = -k_{pq} e_p \tag{6.23}$$

where e_p is defined as the errors between the outputs variables ($\tilde{i}_{ds}, \tilde{\omega}_r, \tilde{u}_{dl}, \tilde{u}_{ql}, \tilde{E}_{dc}$ and $\tilde{i}_{lb}$) and their references. k_{pq} ($p \in \{1,2,3,4,5,6\}$ and $q \in \{1,2,3\}$) is the feedback gain matrix. These references are equal to zero. Hence, the vector v_p ($p \in \{1,2,3,4,5,6\}$) will be

$$\begin{aligned} v_1 &= -k_{11}\tilde{i}_{ds} - k_{12}\dot{\tilde{i}}_{ds}, & v_2 &= -k_{21}\tilde{\omega}_r - k_{22}\dot{\tilde{\omega}}_r - k_{23}\ddot{\tilde{\omega}}_r, \\ v_3 &= -k_{31}\tilde{u}_{dl} - k_{32}\dot{\tilde{u}}_{dl}, & v_4 &= -k_{41}\tilde{u}_{ql} - k_{42}\dot{\tilde{u}}_{ql}, \\ v_5 &= -k_{51}\tilde{E}_{dc} - k_{52}\dot{\tilde{E}}_{dc}, & v_6 &= -k_{61}\tilde{i}_{lb} - k_{62}\dot{\tilde{i}}_{lb} \end{aligned} \tag{6.24}$$

k_{ij}, the feedback gain matrix, is selected so that the eigenvalues of the closed loop system are *Hurwitz*.

6.3.3 Single-Phase DQ Rotating Frame Transformation

In the previous section, the nonlinear controller equations were presented. In this section, we discuss how to apply the DQ-Transformation in the single-phase control systems. The main idea is to utilize the DQ-based on-grid/off-grid nonlinear controller, initially designed for three-phase system, for a single-phase system while keeping all its benefits without adding any additional dynamics to the controller equations.

The rotating frame (or dq-model) is commonly used as approach to analyze three-phase systems. First, the Clarke transformation abc to $\alpha\beta$ in a fixed reference frame is performed using Eqn. (6.25). Then, the Park transformation $\alpha\beta$ to dq in a rotating reference frame is done by using Eqn. (6.26). The dq frame is synchornized with the angular speed ω, where $\omega = 2\pi f_g$ and f_g is the fundamental frequency of the system.

$$\begin{bmatrix} x_\alpha \\ x_\beta \end{bmatrix} = \frac{2}{3}\begin{bmatrix} 1 & -1/2 & -1/2 \\ 0 & -\sqrt{3/2} & \sqrt{3/2} \end{bmatrix}\begin{bmatrix} x_a \\ x_b \\ x_c \end{bmatrix} \tag{6.25}$$

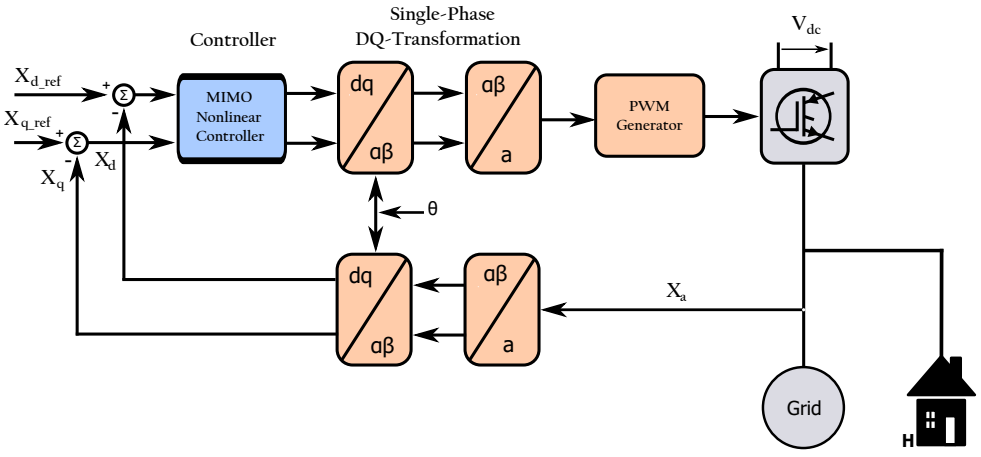

Figure 6.4: On-grid/Off-grid WECS based permanent magnet synchronous generator.

and

$$\begin{bmatrix} x_d \\ x_q \end{bmatrix} = \begin{bmatrix} \cos(\omega t) & \sin(\omega t) \\ -\sin(\omega t) & \cos(\omega t) \end{bmatrix} \begin{bmatrix} x_\alpha \\ x_\beta \end{bmatrix} \tag{6.26}$$

u_{al}, u_{bl} and u_{cl} are the three-phase time-domain signals of the system from a stationary phase coordinate system (abc).

For the dq-Transformation in single-phase systems, the orthogonal imaginary circuit concept is proposed. The basic idea of this method is illustrated in Fig. 6.4. It consists of having two variables, one real (voltage or current) and another fictitious with identical characteristics, but multiply by $\cos(\omega t)$. Here ω is the load voltage angular speed. Therefore, the single-phase a to $\alpha\beta$ transformation can be given as

$$\begin{bmatrix} x_\alpha \\ x_\beta \end{bmatrix} = \begin{bmatrix} \cos(\omega t) \\ 1 \end{bmatrix} \begin{bmatrix} |x_a| \\ x_a \end{bmatrix} \tag{6.27}$$

where $|x_a|$ is the magnitude of x_a.
In other words, the a to dq transformation can be done by using the equation below

$$\begin{bmatrix} x_d \\ x_q \end{bmatrix} = \begin{bmatrix} \cos^2(\omega t) + \sin(\omega t) \\ -\sin(\omega t)\cos(\omega t) + \cos(\omega t) \end{bmatrix} \begin{bmatrix} |x_a| \\ x_a \end{bmatrix} \tag{6.28}$$

To obtain back the single-phase variable x_a, Eqs. (6.29) is used, which was derived from (6.26).

$$x_a = \begin{bmatrix} \sin(\omega t) & \cos(\omega t) \end{bmatrix} \begin{bmatrix} x_d \\ x_q \end{bmatrix} \tag{6.29}$$

In the above equations the variable x can be replaced by any variable from the grid-side single-phase subsystem. Therefore, the controller dq state variables, i_{di}, i_{qi}, i_{dl} and i_{ql}, and input variables, u_{di}, u_{qi}, u_{dl} and u_{ql}, are obtained using Eqn. (6.29)

6.4 Results

To Demonstrate the effectiveness of the single-phase stand-alone and grid-connected nonlinear DQ controller, simulation is carried out using the SimPowerSystems toolbox [13] in Matlab/Simulink software. The system is shown in Fig. 6.2. It composes of a 2.45 MW wind power generator supplying a 2 MW variable load. The generator used here is a variable speed nonsalient-pole permanent magnet synchronous machine. A three-phase rectifier (AC/DC), single-phase inverter (DC/AC) and a bi-directional buck-boost (DC/DC) are utilized to connect the generator to the grid and the load, and the battery-storage-unit to the dc-link voltage, respectively. The generator parameters and the nonlinear contoller feedback gains k_{pq}, are given in Table 6.2 [21] and 6.3, respectively.

The proposed nonlinear controller has been tested in three different case studies. First, the dynamic and steady-state performances of the system when it switches from one mode of operation to another has been analyzed in *Case 1*. Also, the maximum power point tracking capability of the controller under variable wind speed has been verified. In *Case 2*, the power management ability of

Table 6.2: System Parameters

Parameter	Rated Value	Parameter	Rated Value
P_m	2.45 MW	u_g	4000 V
ω_m	4.3 rd/s	u_{dc}	8000 V
λ_r	28 Wb	C_{dc}	1667 μF
P	8	L_f	16.884 mH
J	4000 $kg.m^2$	L_g	1.6884 mH
R_s	24.21 $m\Omega$	F_{gen}	740 Hz
L_{ds}, L_{ds}	9.81 mH	F_{grid}	2040 Hz
V_w	15 m/s	u_{ll}	4000 V
R	28.16 m	P_l	2 MW
ρ	1.25	u_{bat}	4000 V
λ_{opt}	8.1	P_{bat}	1.5 MW

Table 6.3: Controller Gains k_{pq}

Controller Gains Description	Value
$\tilde{i}_{ds}$ and $\dot{\tilde{i}}_{ds}$ Gains	$[K_{11}K_{12}] = [500, 1].10^3$
$\tilde{\omega}_r$, $\dot{\tilde{\omega}}_r$ and $\ddot{\tilde{\omega}}_r$ Gains	$[K_{21}K_{22}K_{23}] = [400, 45, 1.5].10^3$
$\tilde{u}_{dl}$ and $\dot{\tilde{u}}_{dl}$ Gains	$[K_{31}K_{32}] = [5, 2]$
$\tilde{u}_{ql}$ and $\dot{\tilde{u}}_{ql}$ Gains	$[K_{41}K_{42}] = [10, 5]$
$\tilde{E}_{dc}$ and $\dot{\tilde{E}}_{dc}$ Gains	$[K_{51}K_{52}] = [600, 60]$
$\tilde{i}_{lb}$ and $\dot{\tilde{i}}_{lb}$ Gains	$[K_{61}K_{62}] = [4000, 700]$

the controller has been tested . Finally, the effectiveness of the proposed controller has been evaluated under real wind speed profile in both grid-connected and stand-alone modes in *Case 3*.

6.4.1 *Case 1: Dynamic Performance and Steady-State Analysis in On-grid/Off-grid Modes*

Simulations have been carried out under different wind speeds to investigate the dynamic and steady-state performance of the system. The test begins with a stand-alone mode and at the time $t = 1.2$ sec when the switch *Sw1*, in Fig. 6.2, closes, it switches in the grid-connected mode . The wind speed is 14 m/s, from 0 to 0.4 sec, 12 m/s, from 0.4 to 0.8 sec, 15 m/s, from 0.8 to 1.6 sec, 13 m/s from 1.6 to 2.2 sec and 17 m/s from 2.2 to 2.5 sec, respectively. Fig. 6.5(a) shows the generator rotor reference speed (dashed line) and the actual speed (solid line), while Fig. 6.5(b) shows the generator output power. One can notice that the generator speed and output power attain their steady state quick and smoothly within about 0.5 sec.

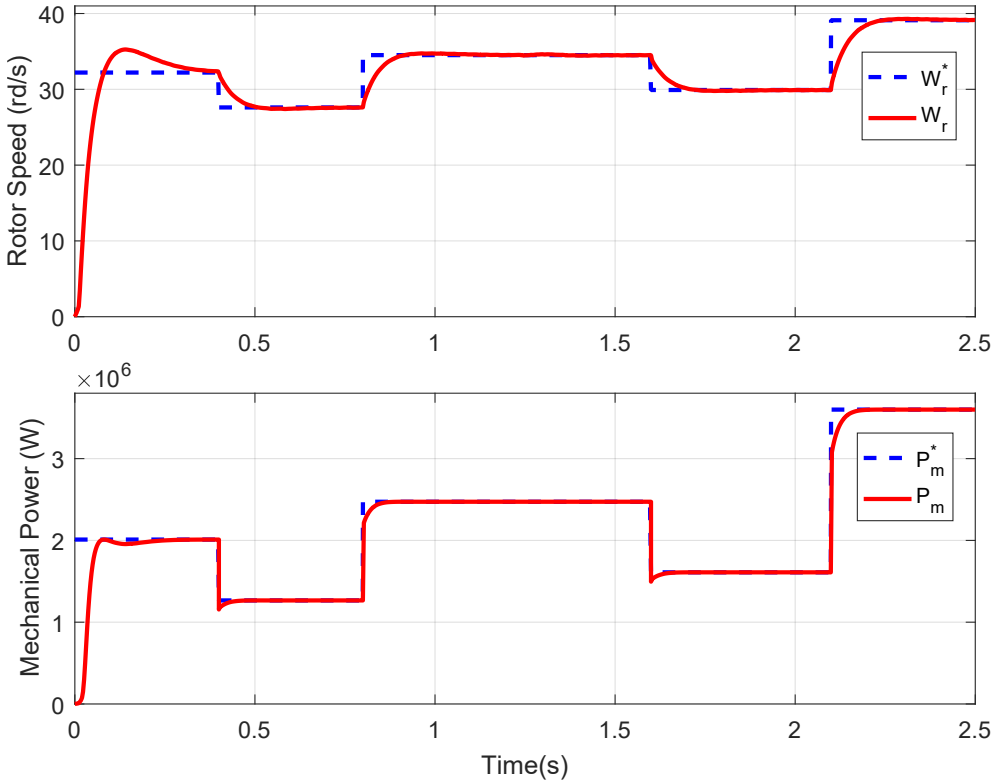

Figure 6.5: (a) Optimum Rotor Speed and (b) Output Power of the Generator.

The three-phase generator current and its corresponding dq-axis current are shown in Fig. 6.6. It can be observed that the d-axis current (solid line) is maintained to zero, while the q-axis (dashed line) and generated power profiles are similar. Hence, performing Zero d-axis current (ZDC) control.

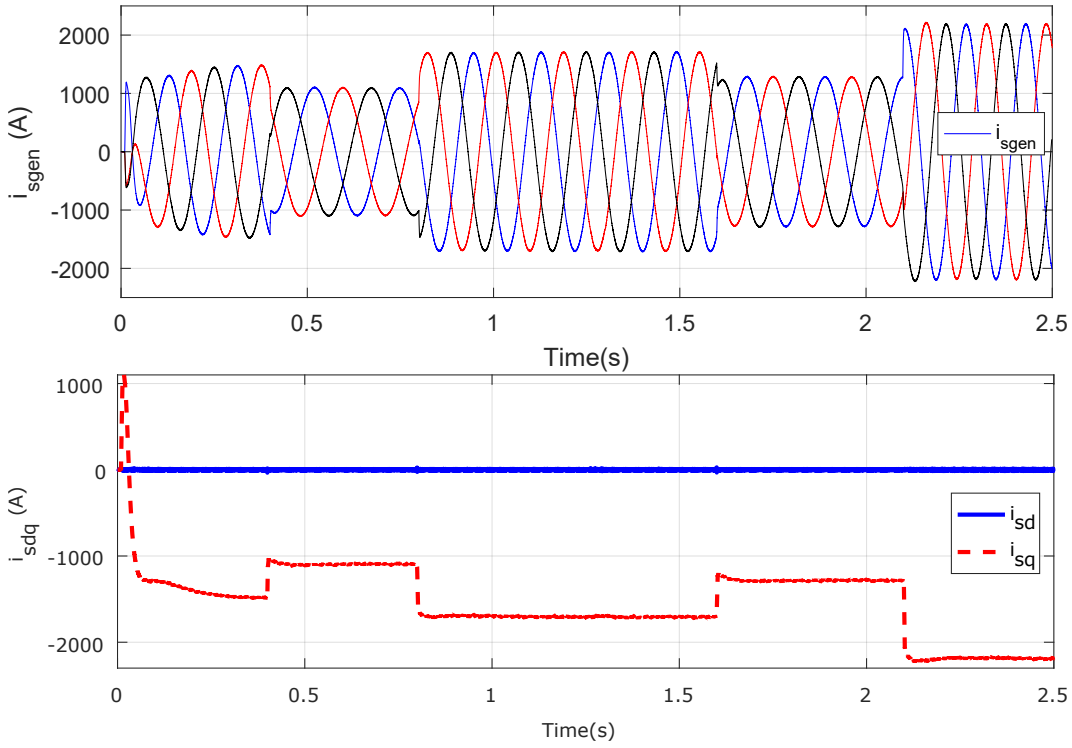

Figure 6.6: Tree-Phase and *dq*-Components of the Generator Stator Current.

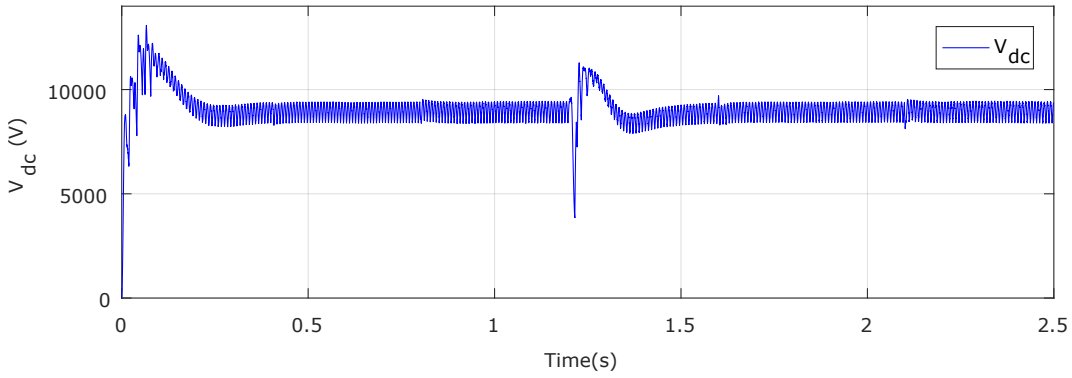

Figure 6.7: Back-to-Back Converter dc-Link Voltage.

Fig. 6.8 and 6.9 show the single-phase load voltage and current with their respective *dq*-components. The load voltage is controlled to its reference voltage. The *dq*-axis load current remain constants, despite the variation of the generated power on the wind turbine side. The excess electricity generated is captured and stored in the battery whenever the produced power of the wind turbine is higher than the required power of the load.

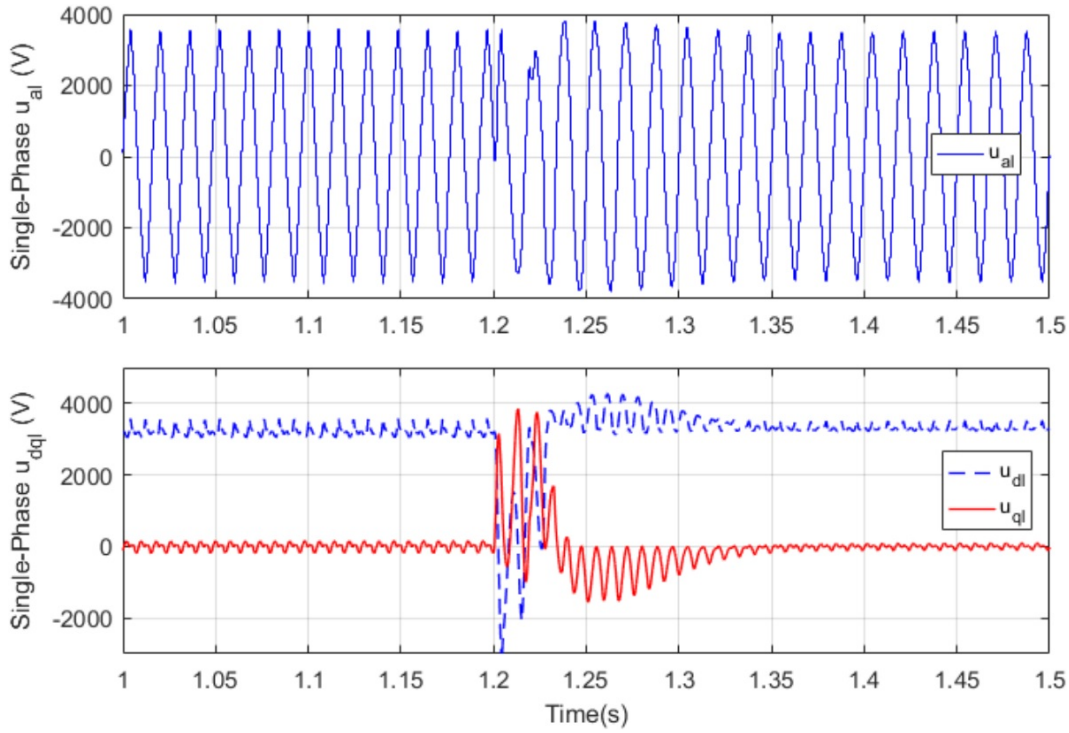

Figure 6.8: Single-phase and *dq*-components of the Load voltage.

One may notice in Fig. 6.8 and 6.9, that the transition between the stand-alone mode and the grid-connected mode, at time $t = 1.2$ sec, is fast and smooth in spite of that no islanding detection mechanism was utilized. It took less than 0.15 sec to stabilize the load voltage and reach the steady state. Also, it can be observed that the dc-link voltage (Fig. 6.7), the generator (Fig. 6.5 and 6.6) and the load controlled variables ($u_{dc}, \omega_r, i_{ds}, u_{dl}$ and u_{ql}) are stables before and after the switching time ($t = 1.2$ sec.).

In this case study, the controller capability to continually operating the wind

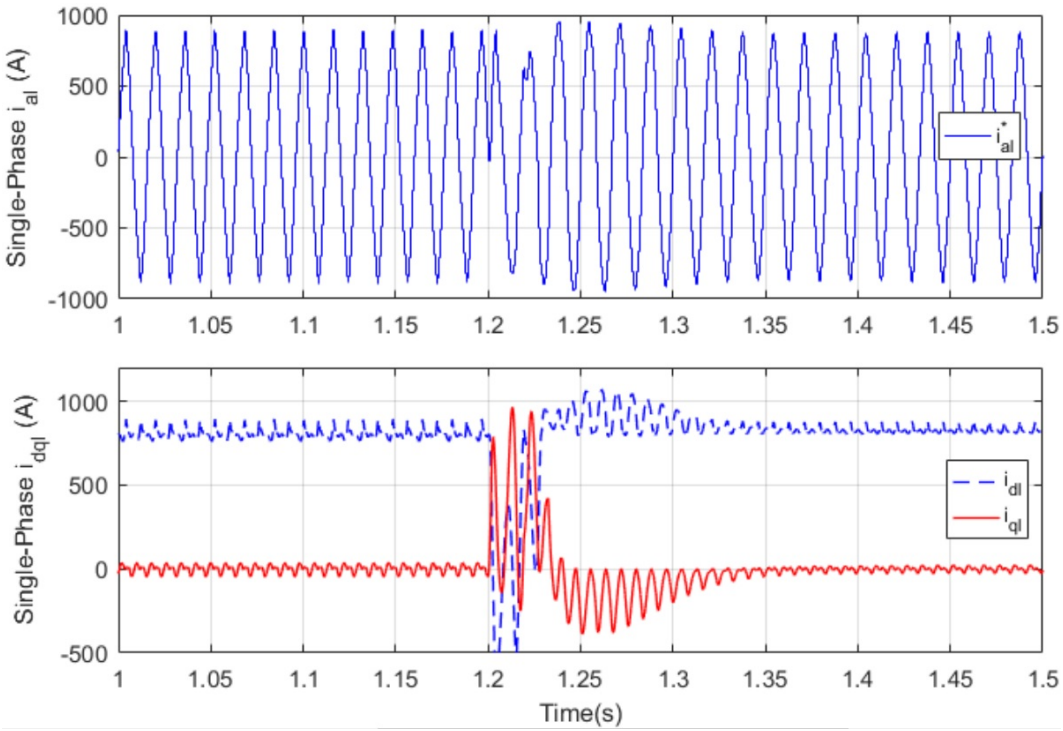

Figure 6.9: Single-phase and *dq*-components of the Load Current.

energy conversion system at its maximum power (*MPPT*) has been examined. The generator rotor speed reference is generated by the MPPT control module for the *MIMO* controller. The speed reference corresponds to the speed at which the wind-turbine can provide its maximum energy to the generator. The maximum power operating points (MPP) for various wind speeds are shown in Fig. 6.10. The wind was changed from 10 m/s to 11 m/s, 12 m/s, 13 m/s, 14 m/s, and 15 m/s for the tests. The corresponding generated active power were 0.5341 MW, 0.7327 MW, 0.9752 MW, 1.2660 MW, 2.0104 MW and 2.4727 MW respectively. It can be seen that these maximum power correspond to the operating points *B*, *C*, *D*, *E*, *F* and *G*, respectively. The MIMO controller is therefore able to operate the system at maximum power operating points. As outlined in Fig. 6.10, the transitions between operating points are fast and smooth.

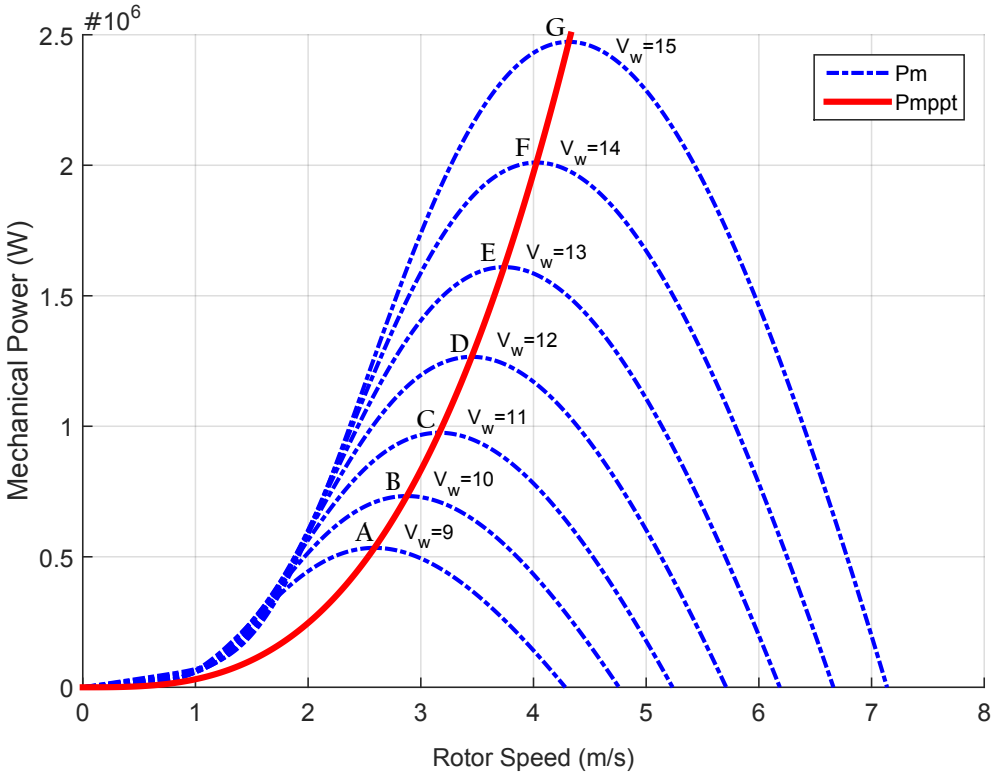

Figure 6.10: MPPT control: Wind Turbine Output Power.

6.4.2 *Case 2: Power management between the wind-turbine, the load, the battery-storage and the grid*

In this case study, a test has been conducted to evaluate the capability of the nonlinear controller to efficiently manage the power between the wind-turbine, the battery-storage, the single-phase load and grid based on the load power requirement. Two different wind speed profiles have been used for the test. A wind speed profile, same as in *case*1, is used in the first test. The system starts in the stand-alone mode and the battery is initially charged at 70% while the load power is $2MW$. The wind-turbine output power (solid line), the load power (dashed line) and the battery power (dotted line) are shown in Fig. 6.11. In time interval $[0.4, 0.8]$ sec and $[1.6, 2.2]$ sec, the produced power is insufficient to supply the

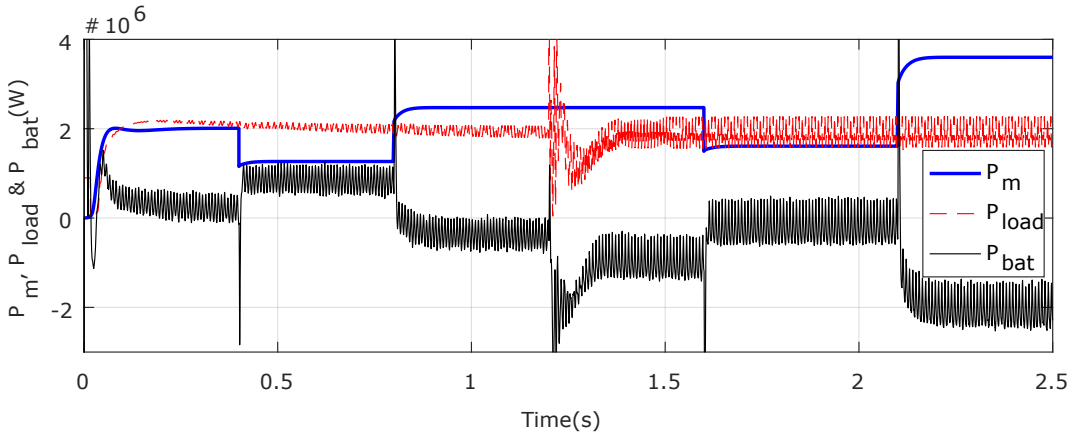

Figure 6.11: Power Management: Wind Turbine, Load and Battery Powers under Different Wind Speed.

load as it is lower than the load power. The battery provides the deficit of the required power. This is shown in Fig. 6.11 (dotted line) by the positive power for the battery. In time interval $[0.8, 1.6]$ sec and $[2.2, 2.5]$ sec, the produced power is greater than the load power. The extra energy is stored in the battery unit. This is shown in Fig. 6.11 (dotted line) by the negative power for the battery. The system switches in the grid-connected mode when the switch *Sw1* closes at $t = 1.2$ sec, while it was operating in stand-alone mode. As shown in Fig. 6.11 (dotted line), the battery continues on delivering nearly the same quantity of power to the load. Consequently, the grid contribution is significantly reduced.

6.4.3 *Case 3: Test Under Real Wind Speed Profile*

In this test, a real wind speed profile is used [120]. Fig. 6.12(a) shows the generator rotor reference speed (dashed line) and the actual speed (solid line), while Fig. 6.12(b) shows the generator output power. It can be observed that the nonlinear controller has a fast and a good dynamic behavior as well as a good tracking overall performance under real wind speed. Fig. 6.13 shows the DQ synchronous frame nonlinear controller power management capability under real wind speed profile. One can observe the battery-storage charging and discharging capability of the stand-Alone and grid-connected hybrid wind/battery system. The battery stores

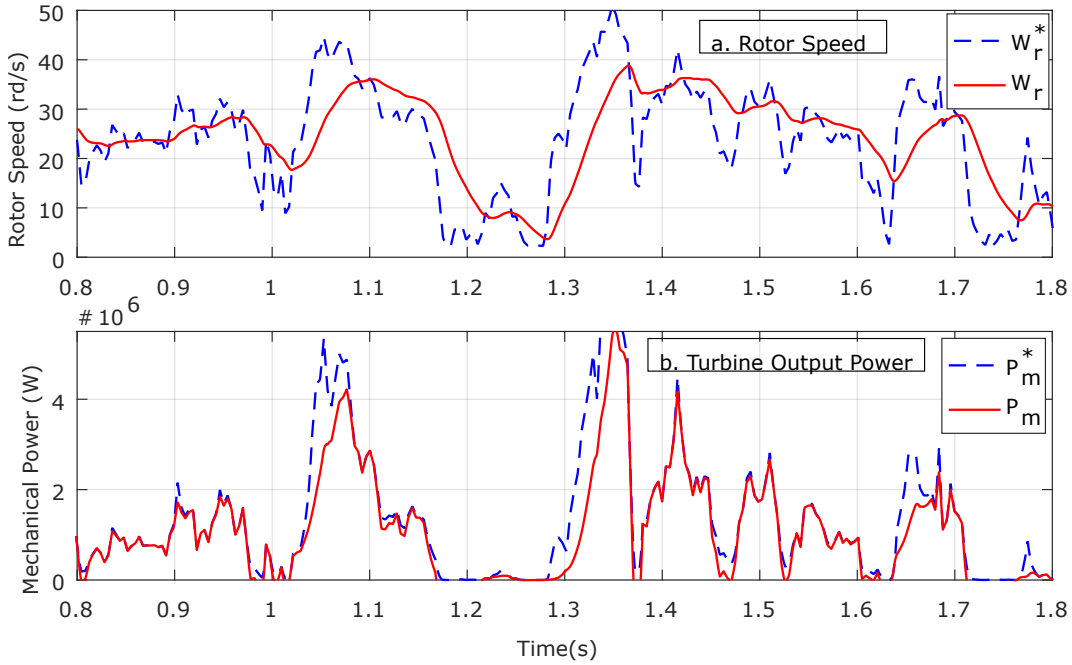

Figure 6.12: (a) Optimum Rotor Speed and (b) Output Power of the Generator under Real Wind Speed.

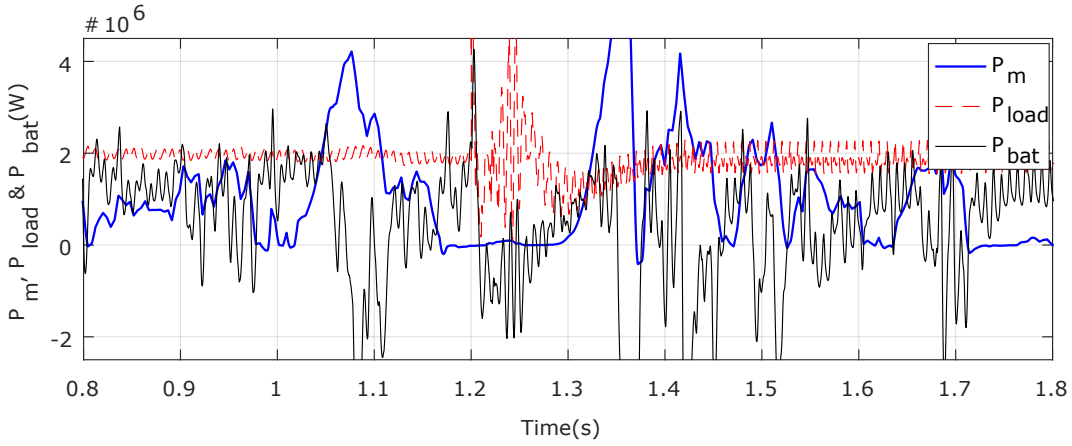

Figure 6.13: Power Management: Wind Turbine, Load and Battery Powers under Real Wind Speed.

more energy when the produced power is high and it compensates to furnish the load requirements when the produced power is low.

6.5 Conclusion

In this paper, a single-phase stand-alone and grid-connected DQ nonlinear controller design for domestic dwelling WECS systems has been presented. The goal is to strengthen the resilience of the power grid and provide power to the load in a consistent manner with as less disruptions as possible. Hence, improving the reliability of the power grid. The design method is based on the MIMO feedback linearization control technique. A DQ transformation module is utilized to convert the grid-side single-phase converter signals in DQ synchronous reference frame. The system has the capability to either operate in grid-connected and stand-alone mode using a single controller, contrary to conventional methods. Moreover a seamless transition between the two modes of operation was achieved with no need for an islanding detection system. In addition, the system provide backup capability to preserve system reliability. As seen in Section 6.4, the MPPT, power management and load voltage control performance of the proposed controller has been successfully tested using a variable speed nonsalient-pole PMSG driven by a wind turbine under real wind speed. The simulation results show fast and smooth transient and steady state responses. To the best of our knowledge, this is the first study investigating a stand-alone and grid-connected WECS for single-phase domestic dwelling applications.

Chapter 7

Conclusion and Future Work

7.1 Conclusion

This research project occurred in a context where the nature of grid users is drastically changing due to the fact that electricity generation is becoming less controllable. The electricity consumption is becoming more and more diversified. As a consequence, the frameworks and technology used for energy production, transmission and distribution and their system interaction will need to change. Traditional control systems must be adapted to the new environment of the electricity system and grids. Future wind turbines should have the ability to continue to operate supplying emergency loads when the grid is not available.

In this thesis, the analysis, the development and the design of a grid-connected/stand-alone controller for WECS were presented. The main challenge of using a single controller to flexibly operate a WECS in both grid-connected and stand-alone mode has been addressed. A new control approach has been proposed to overcome the challenge of a seamless transition between the two modes of operation.

The key contributions and conclusions of this thesis are summarized as follows:

1. The feedback linearization based nonlinear control design is an effective technique for controlling high order nonlinear dynamic system such as WECS. The results of Chapter 3 demonstrate its good control performance compared to the conventional PI-based and Taylor series expansion linear approxima-

tion based control method. This is characterized by a negligible overshoot during the transient periods and fast response time. The input-output linearization method was used to linearize the nonlinear system model. This lead to a decoupled overall system and hence provide good steady-state stability and reference tracking quality, which is necessary for variable-speed WECS.

2. The thesis introduced a novel MIMO nonlinear control approach for WECS with the ability to operate in both grid-connected and stand-alone modes. The proposed approach, described in Chapter 4, uses a single controller to perform the following tasks: the wind turbine generator zero d-axis current control scheme, MPPT control, the dual-inverter dc-linc voltage control, load voltage, and frequency control, power management based on the load power demand, and smooth transition between the two modes of operation. The integral actions added to the control-loop strongly reinforce the robustness of the controller when the system structure changes. This robustness has been successfully evaluated in both grid-connected and stand-alone modes using real wind speed profile. Despite that the controller was initially designed for a balanced three-phase load, it was able to perform successfully for an unbalanced three-phase load, a nonlinear load, and a dynamic load. In addition, the controller is able to stabilize the system when its structure changes from the standalone mode to the grid-connected mode. Therefore, an explicitly robust nonlinear control method is not necessary for the design.

3. The system studied in this work was equipped with back-up storage capability. Hence, the energy management strategy has been proposed to deal with high and low energy generation situations. The main purpose was to ensure a continuous supply of the load and to provide reliable, affordable power to the grid, enhancing grid resilience and performance. Therefore, a power estimation module has been developed for the grid-connected/stand-alone WECS. The results demonstrate that the control system dynamically adjusts the phase shift between the inverter voltage and its current to accommodate the active and reactive power exchange that is required by the

load while keeping the load voltage and frequency constant.

4. The primary purpose of Chapter 5 was to provide extra flexibility to the closed-loop system against uncertainties and parameter change in the system that could destabilize it. The risk of parameter change is high especially in a harsh environment such as extreme temperature and high wind velocity. Therefore, nonlinear adaptive control and online parameter estimation algorithm have been proposed. By applying Lyapunov stability theory, an adaptive law, that guarantee parameters are bounded, has been derived. The results demonstrate that the proposed adaptive nonlinear controller is effective in tracking the time-varying and constant desired output signals in the case of full unknown parameters of the power generation system.

5. We also evaluate the performance of the proposed approach from a different perspective, applying the control concept to single-phase residential hybrid system. For this purpose, a novel DQ-synchronous frame nonlinear controller design has been proposed. The DQ-transformation module converts the grid-side converter single-phase signals into DQ synchronous frame. The effectiveness of the proposed controller in this regard has also been presented in Chapter 6 using real wind speed profile.

7.2 Future Work

As seen in the previous sections, the proposed unified grid-connected/stand-alone nonlinear control method provides faster and better control performance than conventional PI-based controllers. However, more research and study are suggested in the following points:

1. Variable frequency drives such as converters and high power generators are known to be a source of electromagnetic interference (EMI). Therefore, the challenge regarding noise amplification and control saturation should be further investigated experimentally. Additional filter or more accurate sensors may need to be used to filter out signal instability that could be caused by

EMI. However, the fact that the proposed designed controller doesn't require accurate knowledge of system parameters, should help in this regard.

2. Double feed induction generator (DFIG) is the second most commonly used electrical machine for wind turbine applications. The proposed control approach could be explored using different generator such as DFIG for a grid-connected/stand-alone control system.

3. The adaptive control technique developed for parameter estimation employed a constant gain matrix, Γ, for the parameter update law. Future work could focus on using dynamic matrix Γ instead of a constant one. The accuracy of the parameter estimation is usually best observed when dynamic matrix Γ is used, in particular, in the presence of disturbance in the system.

4. As the thesis involves battery storage unit, future development should focus on control techniques to extend better the life of the battery and boost its range. In hybrid electric systems, variable switching frequency control methods are often utilized for the bi-directional buck-boost converter instead of fixed frequency. For instance, the converter switching frequency is reduced under light load conditions and increased in otherwise.

5. Finally, This work focused on the control and operation of a single wind-turbine. Future work should be extended to incorporate multiple wind-turbines in the context of distributed energy systems. This would require the development of a higher layer of control at the system level to describe the interactions between the wind-turbines.

Bibliography

[1] U. E. I. A. (EIA), "Annual energy outlook 2018 with projections to 2050 - eia," *EIA Report*, 2018.

[2] J. L. Sawin, J. Rutovitz, and F. Sverrisson, "Renewables 2018, global status report," *Paris: REN21 (Renewable Energy Policy Network for the 21st Century) Secretariat, REN21*, 2018.

[3] N. R. C. (NRCan), "Energy fact book 2016–2017," *NRCan Report*, 2018.

[4] ——, "Renewable energy facts 2018," *NRCan Report*, 2018.

[5] ——, "Electricity facts 2018," *NRCan Report*, 2018.

[6] C. W. E. A. (CANWEA), "News release archive 2018," *CANWEA Report*, 2018.

[7] T. M. Weis and A. Ilinca, "The utility of energy storage to improve the economics of wind–diesel power plants in canada," *Renewable energy*, vol. 33, no. 7, pp. 1544–1557, 2008.

[8] H. Ibrahim, R. Younes, T. Basbous, A. Ilinca, and M. Dimitrova, "Optimization of diesel engine performances for a hybrid wind–diesel system with compressed air energy storage," *Energy*, vol. 36, no. 5, pp. 3079–3091, 2011.

[9] J. L. Sawin, J. Rutovitz, and F. Sverrisson, "Renewables 2013, global status report," *Paris: REN21 (Renewable Energy Policy Network for the 21st Century) Secretariat, REN21*, 2013.

[10] P. McMullen, "The true cost of outages in canada: $12 billion," *SC Electric Company*, 2018.

[11] T. Chaiyatham and I. Ngamroo, "Optimal fuzzy gain scheduling of pid controller of superconducting magnetic energy storage for power system stabilization," *International Journal of Innovative Computing, Information and Control*, vol. 9, no. 2, pp. 651–666, 2013.

[12] N. Instruments, "Improving pid controller performance," 2009.

[13] The-MathWorks-Inc., "Simscape power systems user's guide (specialized technology)," 2016. [Online]. Available: www.mathworks.com

[14] S. Padrón, M. Hernández, and A. Falcón, "Reducing under-frequency load shedding in isolated power systems using neural networks. gran canaria: A case study," *IEEE Trans. on Power Systems*, vol. 31, 2016.

[15] A. Gholami, F. Aminifar, and M. Shahidehpour, "Front lines against the darkness: enhancing the resilience of the electricity grid through microgrid facilities," *IEEE Electrification Magazine*, vol. 4, 2016.

[16] R. Teodorescu and F. Blaabjerg, "Flexible control of small wind turbines with grid failure detection operating in stand-alone and grid-connected mode," *IEEE Transactions on Power Electronics*, vol. 19, no. 5, pp. 1323–1332, Sept. 2004.

[17] M. N. Arafat, S. Palle, Y. Sozer, and I. Husain, "Transition control strategy between standalone and grid-connected operations of voltage-source inverters," *Industry Applications, IEEE Transactions on*, vol. 48, no. 5, pp. 1516–1525, 2012.

[18] T. E. T. S. I. (ETSI), "Smart grids," 2019. [Online]. Available: www.etsi.org

[19] T. E. T. P. S. G. (ETPSG), "Smartgrids sra 2035 strategic research agenda update of the smartgrids sra 2007 for the needs by the year 2035," March 2012. [Online]. Available: www.smartgrids.eu

[20] F. D. Bianchi, H. De Battista, and R. J. Mantz, *Wind turbine control systems: principles, modelling and gain scheduling design.* Springer, 2006.

[21] B. Wu, Y. Lang, N. Zargari, and S. Kouro, *Power conversion and control of wind energy systems.* John Wiley & Sons, 2011, vol. 77.

[22] A. Dixit, P. Singh, N. Mishra, and D. Singh, "Maximum power tracking with voltage stability studies in wind energy conversion system: A review," in *Sustainable Energy and Intelligent Systems (SEISCON 2012), IET Chennai 3rd International on*. IET, 2012, pp. 1–9.

[23] B. Subudhi and R. Pradhan, "A comparative study on maximum power point tracking techniques for photovoltaic power systems," *Sustainable Energy, IEEE Transactions on*, vol. 4, no. 1, pp. 89–98, 2013.

[24] M. Abdullah, A. Yatim, and C. W. Tan, "A study of maximum power point tracking algorithms for wind energy system," in *Clean Energy and Technology (CET), 2011 IEEE First Conference on*. IEEE, 2011, pp. 321–326.

[25] F. Blaabjerg, M. Liserre, and K. Ma, "Power electronics converters for wind turbine systems," *Industry Applications, IEEE Transactions on*, vol. 48, no. 2, pp. 708–719, 2012.

[26] Z. Chen, J. M. Guerrero, and F. Blaabjerg, "A review of the state of the art of power electronics for wind turbines," *Power Electronics, IEEE Transactions on*, vol. 24, no. 8, pp. 1859–1875, 2009.

[27] U. S. D. of Energy Renewable, "United states department of energy renewable portfolio standards in the united states," 2007.

[28] B. Housseini, F. Okou, and R. Beguenane, "Robust nonlinear controller design for on-grid/off-grid wind energy battery-storage system," *IEEE Transactions on Smart Grid*, 2017.

[29] R. energy policy network for the 21st century (REN21), "Renewable global status report 2013," 2013. [Online]. Available: www.ren21.net

[30] A. Milczarek and M. Malinowski, "Monitoring and control algorithms applied to small wind turbine with grid-connected/stand-alone mode of operation," *Przeglad Elektrotechniczny*, no. 12a, pp. 18–23, 2012.

[31] M. Fatu, F. Blaabjerg, and I. Boldea, "Grid to standalone transition motion-sensorless dual-inverter control of pmsg with asymmetrical grid voltage sags and harmonics filtering," *IEEE Transactions on Power Electronics*, vol. 29, no. 7, pp. 3463–3472, Jul. 2014.

[32] M. Fatu, L. Tutelea, R. Teodorescu, F. Blaabjerg, and I. Boldea, "Motion sensorless bidirectional pwm converter control with seamless switching from power grid to stand alone and back," in *Power Electronics Specialists Conference, 2007. PESC 2007. IEEE.* IEEE, 2007, pp. 1239–1244.

[33] M. Ranjbar, H. Ebrahimirad, S. Mohaghegh, and A. Ghaleh, "Seamless transfer of three-phase grid-interactive microturbine inverter between grid-connected and stand-alone modes," in *Electrical Engineering (ICEE), 2011 19th Iranian Conference on.* IEEE, 2011, pp. 1–6.

[34] B. Mirafzal, M. Saghaleini, and A. K. Kaviani, "An svpwm-based switching pattern for stand-alone and grid-connected three-phase single-stage boost inverters," *Power Electronics, IEEE Transactions on*, vol. 26, no. 4, pp. 1102–1111, 2011.

[35] Z. Yao, L. Xiao, and Y. Yan, "Seamless transfer of single-phase grid-interactive inverters between grid-connected and stand-alone modes," *Power Electronics, IEEE Transactions on*, vol. 25, no. 6, pp. 1597–1603, 2010.

[36] Y. Sozer and D. A. Torrey, "Modeling and control of utility interactive inverters," *Power Electronics, IEEE Transactions on*, vol. 24, no. 11, pp. 2475–2483, 2009.

[37] H. Tao, J. L. Duarte, and M. A. Hendrix, "Control of grid-interactive inverters as used in small distributed generators," in *Industry Applications Conference, 2007. 42nd IAS Annual Meeting. Conference Record of the 2007 IEEE.* IEEE, 2007, pp. 1574–1581.

[38] F. Gao and M. R. Iravani, "A control strategy for a distributed generation unit in grid-connected and autonomous modes of operation," *Power Delivery, IEEE Transactions on*, vol. 23, no. 2, pp. 850–859, 2008.

[39] J. C. Vasquez, J. M. Guerrero, A. Luna, P. Rodríguez, and R. Teodorescu, "Adaptive droop control applied to voltage-source inverters operating in grid-connected and islanded modes," *Industrial Electronics, IEEE Transactions on*, vol. 56, no. 10, pp. 4088–4096, 2009.

[40] M. Rizo, E. Bueno, A. Dell'Aquila, M. Liserre, and R. Mastromauro, "Generalized controller for small wind turbines working grid-connected and standalone," in *Clean Electrical Power (ICCEP), 2011 International Conference on*. IEEE, 2011, pp. 51–55.

[41] L. Arnedo, S. Dwari, S. Motapon, and V. Blasko, "System level wind turbine controls with seamless transitions between standalone and grid connected mode," in *Power Electronics and Machines in Wind Applications (PEMWA), 2012 IEEE*. IEEE, 2012, pp. 1–5.

[42] L. Asiminoaei, R. Teodorescu, F. Blaabjerg, and U. Borup, "Implementation and test of an online embedded grid impedance estimation technique for pv inverters," *Industrial Electronics, IEEE Transactions on*, vol. 52, no. 4, pp. 1136–1144, 2005.

[43] . F. Bertling and S. Soter, "A novel converter integrable impedance measuring method for islanding detection in grids with widespread use of decentral generation," *in Proc. Power Electron., Elect. Drives, Autom. Motion*, pp. 503–507, 2006.

[44] M. Sumner, B. Palethorpe, and D. W. Thomas, "Impedance measurement for improved power quality-part 2: a new technique for stand-alone active shunt filter control," *Power Delivery, IEEE Transactions on*, vol. 19, no. 3, pp. 1457–1463, 2004.

[45] J. Huang and K. Corzine, "Ac impedance measurement by line-to-line injected current," in *Industry Applications Conference, 2006. 41st IAS Annual Meeting. Conference Record of the 2006 IEEE*, vol. 1. IEEE, 2006, pp. 300–306.

[46] J. P. Rhode, A. W. Kelley, and M. E. Baran, "Complete characterization of utilization-voltage power system impedance using wideband measurement," *Industry Applications, IEEE Transactions on*, vol. 33, no. 6, pp. 1472–1479, 1997.

[47] J. M. Guerrero, J. C. Vasquez, J. Matas, L. G. de Vicuña, and M. Castilla, "Hierarchical control of droop-controlled ac and dc microgrids—a general ap-

proach toward standardization," *Industrial Electronics, IEEE Transactions on*, vol. 58, no. 1, pp. 158–172, 2011.

[48] Y. A.-R. I. Mohamed, E. F. El-Saadany, and M. M. Salama, "Adaptive grid-voltage sensorless control scheme for inverter-based distributed generation," *IEEE Trans. on Energy Conversion*, vol. 24, no. 3, 2009.

[49] F. Katiraei and M. Iravani, "Power management strategies for a microgrid with multiple distributed generation units," *Power Systems, IEEE Transactions on*, vol. 21, no. 4, pp. 1821–1831, 2006.

[50] A. Timbus, M. Liserre, R. Teodorescu, P. Rodriguez, and F. Blaabjerg, "Evaluation of current controllers for distributed power generation systems," *Power Electronics, IEEE Transactions on*, vol. 24, no. 3, pp. 654–664, 2009.

[51] M. Liserre, R. Teodorescu, and F. Blaabjerg, "Stability of photovoltaic and wind turbine grid-connected inverters for a large set of grid impedance values," *Power Electronics, IEEE Transactions on*, vol. 21, no. 1, pp. 263–272, 2006.

[52] E. Twining and D. G. Holmes, "Grid current regulation of a three-phase voltage source inverter with an lcl input filter," *Power Electronics, IEEE Transactions on*, vol. 18, no. 3, pp. 888–895, 2003.

[53] M. Dai, M. N. Marwali, J.-W. Jung, and A. Keyhani, "Power flow control of a single distributed generation unit," *Power Electronics, IEEE Transactions on*, vol. 23, no. 1, pp. 343–352, 2008.

[54] R. Zaimeddine and T. Undeland, "Direct power control strategies of a grid-connected three-level voltage source converter vsi-npc," in *Power Electronics and Applications (EPE 2011), Proceedings of the 2011-14th European Conference on.* IEEE, 2011, pp. 1–7.

[55] Y.-R. Mohamed and A. A. Radwan, "Hierarchical control system for robust microgrid operation and seamless mode transfer in active distribution systems," *Smart Grid, IEEE Transactions on*, vol. 2, no. 2, pp. 352–362, 2011.

[56] H. Gu, Z. Yang, D. Wang, and W. Wu, "Research on control method of double-mode inverter with grid-connection and stand-alone," in *Power Electronics and Motion Control Conference, 2006. IPEMC 2006. CES/IEEE 5th International*, vol. 1. IEEE, 2006, pp. 1–5.

[57] Y. Zhang, Z. Li, W. Xu, J. Hu, and J. G. Zhu, "Grid synchronization of dfig using model predictive direct power control," in *Electrical Machines and Systems (ICEMS), 2011 International Conference on*. IEEE, 2011, pp. 1–6.

[58] G. Bode and D. Holmes, "Implementation of three level hysteresis current control for a single phase voltage source inverter," in *Power Electronics Specialists Conference, 2000. PESC 00. 2000 IEEE 31st Annual*, vol. 1. IEEE, 2000, pp. 33–38.

[59] P. Dahono, "New current controllers for single-phase full-bridge inverters," in *Power System Technology, 2004. PowerCon 2004. 2004 International Conference on*, vol. 2. IEEE, 2004, pp. 1757–1762.

[60] C.-M. Ho, V. S. Cheung, and H.-H. Chung, "Constant-frequency hysteresis current control of grid-connected vsi without bandwidth control," *Power Electronics, IEEE Transactions on*, vol. 24, no. 11, pp. 2484–2495, 2009.

[61] Z. Yao, Z. Wang, L. Xiao, and Y. Yan, "A novel control strategy for grid-interactive inverter in grid-connected and stand-alone modes," in *Applied Power Electronics Conference and Exposition, 2006. APEC'06. Twenty-First Annual IEEE*. IEEE, 2006, pp. 5–pp.

[62] F. Blaabjerg, Z. Chen, and S. B. Kjaer, "Power electronics as efficient interface in dispersed power generation systems," *Power Electronics, IEEE Transactions on*, vol. 19, no. 5, pp. 1184–1194, 2004.

[63] J.-J. E. Slotine, W. Li *et al.*, *Applied nonlinear control*. Prentice-Hall Englewood Cliffs, NJ, 1991, vol. 199, no. 1.

[64] K.-H. Kim, Y.-C. Jeung, D.-C. Lee, and H.-G. Kim, "Lvrt scheme of pmsg wind power systems based on feedback linearization," *Power Electronics, IEEE Transactions on*, vol. 27, no. 5, pp. 2376–2384, 2012.

[65] S. Zhou, J. Liu, L. Zhou, and Y. Zhu, "Improved dc-link voltage control of pmsg wecs based on feedback linearization under grid faults," in *Applied Power Electronics Conference and Exposition (APEC), 2013 Twenty-Eighth Annual IEEE*. IEEE, 2013, pp. 2895–2899.

[66] T.-S. Lee, "Input-output linearization and zero-dynamics control of three-phase ac/dc voltage-source converters," *Power Electronics, IEEE Transactions on*, vol. 18, no. 1, pp. 11–22, 2003.

[67] D.-C. Lee, G.-M. Lee, and K.-D. Lee, "Dc-bus voltage control of three-phase ac/dc pwm converters using feedback linearization," *Industry Applications, IEEE Transactions on*, vol. 36, no. 3, pp. 826–833, 2000.

[68] D.-E. Kim and D.-C. Lee, "Feedback linearization control of three-phase ups inverter systems," *Industrial Electronics, IEEE Transactions on*, vol. 57, no. 3, pp. 963–968, 2010.

[69] O. Akhrif, F.-A. Okou, L.-A. Dessaint, and R. Champagne, "Application of a multivariable feedback linearization scheme for rotor angle stability and voltage regulation of power systems," *Power Systems, IEEE Transactions on*, vol. 14, no. 2, pp. 620–628, 1999.

[70] C. Evangelista, F. Valenciaga, and P. Puleston, "Active and reactive power control for wind turbine based on a mimo 2-sliding mode algorithm with variable gains," *Energy Conversion, IEEE Transactions on*, vol. 28, no. 3, pp. 682–689, 2013.

[71] J. Matas, M. Castilla, J. M. Guerrero, L. Garcia De Vicuna, and J. Miret, "Feedback linearization of direct-drive synchronous wind-turbines via a sliding mode approach," *Power Electronics, IEEE Transactions on*, vol. 23, no. 3, pp. 1093–1103, 2008.

[72] M. I. Martinez, A. Susperregui, G. Tapia, and L. Xu, "Sliding-mode control of a wind turbine-driven double-fed induction generator under non-ideal grid voltages," *IET Renewable Power Generation*, vol. 7, no. 4, pp. 370–379, 2013.

[73] B.-H. Kwon, J.-H. Choi, and T.-W. Kim, "Improved single-phase line-interactive ups," *IEEE Transactions on Industrial Electronics*, vol. 48, no. 4, pp. 804–811, 2001.

[74] F. A. Okou, D. Nganga-Kouya, and M. Tarbouchi, "A backstepping approach for the design of a nonlinear controller for a two-wheeled autonomous vehicle," in *Electrical and Computer Engineering, 2009. CCECE'09. Canadian Conference on.* IEEE, 2009, pp. 641–645.

[75] G.-D. Wang, R.-J. Wai, and Y. Liao, "Design of backstepping power control for grid-side converter of voltage source converter-based high-voltage dc wind power generation system," *IET Renewable Power Generation*, vol. 7, no. 2, pp. 118–133, 2013.

[76] M. Morawiec, "The adaptive backstepping control of permanent magnet synchronous motor supplied by current source inverter," *Industrial Informatics, IEEE Transactions on*, vol. 9, no. 2, pp. 1047–1055, 2013.

[77] L. Zhang and Y. Li, "Optimal energy management of wind-battery hybrid power system with two-scale dynamic programming," *Sustainable Energy, IEEE Trans. on*, vol. 4, no. 3, pp. 765–773, 2013.

[78] M. A. Tankari, M. B. Camara, B. Dakyo, and G. Lefebvre, "Use of ultracapacitors and batteries for efficient energy management in wind–diesel hybrid system," *IEEE Trans. on Sustainable Energy*, vol. 4, 2013.

[79] M. P. Kazmierkowski and L. Malesani, "Current control techniques for three-phase voltage-source pwm converters: A survey," *IEEE Transactions on industrial electronics*, vol. 45, no. 5, pp. 691–703, 1998.

[80] D. Gaonkar, R. Patel, and G. Pillai, "Dynamic model of microturbine generation system for grid connected/islanding operation," in *Industrial Technology, 2006. ICIT 2006. IEEE International Conference on.* IEEE, 2006, pp. 305–310.

[81] Y. Sozer and D. A. Torrey, "Control of utility interactive inverters," *Advanced Energy Conversion*, 2009.

[82] E.-H. Kim, J.-M. Kwon, J.-K. Park, and B.-H. Kwon, "Practical control implementation of a three-to single-phase online ups," *IEEE Transactions on Industrial Electronics*, vol. 55, no. 8, 2008.

[83] J. M. Guerrero, L. G. de Vicuna, J. Miret, J. Matas, and M. Castilla, "A nonlinear feed-forward control technique for single-phase ups inverters," in *IECON 02 [Industrial Electronics Society, IEEE 2002 28th Annual Conference of the]*, vol. 1. IEEE, 2002, pp. 257–261.

[84] K. Inagaki and S. Okuma, "High frequency link dc/ac converters using three phase output pwm cycloconverters for uninterruptible power supplies," in *Telecommunications Energy Conference, 1991. INTELEC'91., 13th International*. IEEE, 1991, pp. 580–586.

[85] Q. Lei, F. Z. Peng, and S. Yang, "Multiloop control method for high-performance microgrid inverter through load voltage and current decoupling with only output voltage feedback," *IEEE Transactions on Power Electronics*, vol. 26, no. 3, pp. 953–960, 2011.

[86] Q. Lei, S. Yang, and F. Z. Peng, "Multi-loop control algorithms for seamless transition of grid-connected inverter," in *Applied Power Electronics Conf. and Exposition (APEC)*. IEEE, 2010, pp. 844–848.

[87] N. M. Abdel-Rahim and J. E. Quaicoe, "Analysis and design of a multiple feedback loop control strategy for single-phase voltage-source ups inverters," *IEEE Trans. on power electronics*, vol. 11, 1996.

[88] J. G. Kassakian, M. F. Schlecht, and G. C. Verghese, *Principles of power electronics*. Graphis, 2000.

[89] S. Kouro, P. Cortés, R. Vargas, U. Ammann, and J. Rodríguez, "Model predictive control—a simple and powerful method to control power converters," *Industrial Electronics, IEEE Transactions on*, vol. 56, no. 6, pp. 1826–1838, 2009.

[90] J. Rodriguez, J. Pontt, P. Correa, P. Lezana, and P. Cortes, "Predictive power control of an ac/dc/ac converter," in *Industry Applications Confer-*

ence, 2005. Fourtieth IAS Annual Meeting. Conference Record of the 2005, vol. 2. IEEE, 2005, pp. 934–939.

[91] R. Vargas, P. Cortés, U. Ammann, J. Rodríguez, and J. Pontt, "Predictive control of a three-phase neutral-point-clamped inverter," *IEEE Trans. on Industrial Electronics*, vol. 54, no. 5, pp. 2697–2705, 2007.

[92] P. Cortés, A. Wilson, S. Kouro, J. Rodriguez, and H. Abu-Rub, "Model predictive control of multilevel cascaded h-bridge inverters," *IEEE Trans. on Industrial Electronics*, vol. 57, no. 8, pp. 2691–2699, 2010.

[93] P. Lezana, R. Aguilera, and D. E. Quevedo, "Model predictive control of an asymmetric flying capacitor converter," *IEEE Transactions on Industrial Electronics*, vol. 56, no. 6, pp. 1839–1846, 2009.

[94] S. Alepuz, S. Busquets-Monge, J. Bordonau, P. Cortes, J. Rodriguez, and R. Vargas, "Predictive current control of grid-connected neutral-point-clamped converters to meet low voltage ride-through requirements," in *PESC Conference*. IEEE, 2008, pp. 2423–2428.

[95] P. Cortes, J. Rodriguez, S. Vazquez, and L. G. Franquelo, "Predictive control of a three-phase ups inverter using two steps prediction horizon," in *Industrial Technology (ICIT), 2010 IEEE International Conference on*. IEEE, 2010, pp. 1283–1288.

[96] V. Yaramasu, B. Wu, M. Rivera, J. Rodriguez, and A. Wilson, "Cost-function based predictive voltage control of two-level four-leg inverters using two step prediction horizon for standalone power systems," in *Applied Power Electronics Conference and Exposition (APEC), 2012 Twenty-Seventh Annual IEEE*. IEEE, 2012, pp. 128–135.

[97] V. Yaramasu, J. Rodriguez, B. Wu, M. Rivera, A. Wilson, and C. Rojas, "A simple and effective solution for superior performance in two-level four-leg voltage source inverters: Predictive voltage control," in *Industrial Electronics (ISIE)*. IEEE, 2010, pp. 3127–3132.

[98] Y. Hu, L. Chang, and B. Cao, "Novel predictive voltage controlled ups inverter for an improved stand-alone wind turbine system," in *CCECE'09*. IEEE, 2009, pp. 398–402.

[99] A. R. Munoz and T. A. Lipo, "On-line dead-time compensation technique for open-loop pwm-vsi drives," *IEEE Transactions on power electronics*, vol. 14, no. 4, pp. 683–689, 1999.

[100] R. Tirumala, N. Mohan, and C. Henze, "Seamless transfer of grid-connected pwm inverters between utility-interactive and stand-alone modes," in *Applied Power Electronics Conference and Exposition Conference*, vol. 2. IEEE, 2002, pp. 1081–1086.

[101] S. Muyulema, E. J. Bueno, F. J. Rodríguez, S. Cóbreces, and D. Díaz, "Response of the grid converters synchronization using pu magnitude in the control loop," in *Industrial Electronics, 2007. ISIE 2007. IEEE International Symposium on*. IEEE, 2007, pp. 186–191.

[102] F. D. Freijedo, J. Doval-Gandoy, O. Lopez, and J. Cabaleiro, "Robust phase locked loops optimized for dsp implementation in power quality applications," in *Industrial Electronics, 2008. IECON 2008. 34th Annual Conference of IEEE*. IEEE, 2008, pp. 3052–3057.

[103] R. De Camargo and H. Pinheiro, "Synchronisation method for three-phase pwm converters under unbalanced and distorted grid," *IEE Proceedings-Electric Power Applications*, vol. 153, no. 5, pp. 763–772, 2006.

[104] G.-C. Hsieh and J. C. Hung, "Phase-locked loop techniques. a survey," *IEEE Transactions on Industrial Electronics*, vol. 43, no. 6, pp. 609–615, 1996.

[105] Y. Yu, "Research on single-phase grid-connected solar inverter," *Hang Zhou, Zhejiang University*, 2008.

[106] J. Rodriguez, J. Pontt, C. A. Silva, P. Correa, P. Lezana, P. Cortés, and U. Ammann, "Predictive current control of a voltage source inverter," *IEEE transactions on industrial electronics*, vol. 54, no. 1, 2007.

[107] C. Ramos, A. Martins, and A. Carvalho, "Complex state-space current controller for grid-connected converters with an lcl filter," in *Industrial Electronics, 2009. IECON Conference.* IEEE, 2009, pp. 296–301.

[108] M. Ciobotaru, V. G. Agelidis, R. Teodorescu, and F. Blaabjerg, "Accurate and less-disturbing active antiislanding method based on pll for grid-connected converters," *Power Electronics, IEEE Transactions on*, vol. 25, no. 6, pp. 1576–1584, 2010.

[109] C. Wang, X. Li, L. Guo, and Y. Li, "A seamless operation mode transition control strategy for a microgrid based on master-slave control," *Science China Technological Sciences*, vol. 55, no. 6, pp. 1644–1654, 2012.

[110] T.-T. Ma, "Notice of violation of ieee publication principles quantitative design of active anti-islanding controllers for power-converter-based distributed generators," *IEEE Transactions on Industrial Electronics*, vol. 57, no. 10, pp. 3448–3455, 2010.

[111] M. Brenna, G. C. Lazaroiu, G. Superti-Furga, and E. Tironi, "Bidirectional front end converter for dg with disturbance insensitivity and islanding-detection capability," *IEEE Transactions on Power Delivery*, vol. 23, no. 2, pp. 907–914, 2008.

[112] M. Liserre, A. Pigazo, A. Dell'Aquila, and V. M. Moreno, "An anti-islanding method for single-phase inverters based on a grid voltage sensorless control," *IEEE Transactions on Industrial Electronics*, vol. 53, no. 5, pp. 1418–1426, 2006.

[113] H. Karimi, A. Yazdani, and R. Iravani, "Negative-sequence current injection for fast islanding detection of a distributed resource unit," *IEEE Transactions on power electronics*, vol. 23, no. 1, 2008.

[114] G. Hernandez-Gonzalez and R. Iravani, "Current injection for active islanding detection of electronically-interfaced distributed resources," *IEEE Transactions on power delivery*, vol. 21, no. 3, 2006.

[115] H. Koizumi, T. Mizuno, T. Kaito, Y. Noda, N. Goshima, M. Kawasaki, K. Nagasaka, and K. Kurokawa, "A novel microcontroller for grid-connected

photovoltaic systems," *IEEE Transactions on Industrial Electronics*, vol. 53, no. 6, pp. 1889–1897, 2006.

[116] Z. Liu, J. Liu, and Y. Zhao, "A unified control strategy for three-phase inverter in distributed generation," *IEEE Trans. on Power Electronics*, vol. 29, no. 3, pp. 1176–1191, 2014.

[117] B. Housseini, A. F. Okou, and R. Beguenane, "Energy management strategy of on-grid/off-grid wind energy battery-storage system," in *CCECE Conference*. IEEE, 2016, pp. 1–6.

[118] ——, "Nonlinear adaptive control of on-grid/off-grid wind energy battery-storage system," in *EVER Conf.* IEEE, 2017, pp. 1–8.

[119] B. Housseini, F. A. Okou, and R. Beguenane, "A unified nonlinear controller design for on-grid/off-grid wind energy battery-storage system," in *Industrial Electronics Society, IECON 2015-41st Annual Conference of the IEEE*. IEEE, 2015, pp. 005 273–005 278.

[120] A. A. A. Zidan, *Reconfiguration and Self-healing Mechanisms in Distribution Systems with High Distributed Generation (DG) Penetration*. PhD Thesis, University of Waterloo, 2013. [Online]. Available: http://hdl.handle.net/10012/8091

[121] P. Gupta, R. Bhatia, and D. Jain, "Average absolute frequency deviation value based active islanding detection technique," *IEEE Trans. on Smart Grid*, vol. 6, no. 1, pp. 26–35, 2015.

[122] S. M. Ashabani and Y. A.-R. I. Mohamed, "A flexible control strategy for grid-connected and islanded microgrids with enhanced stability using nonlinear microgrid stabilizer," *IEEE Trans. on Smart Grid*, vol. 3, no. 3, pp. 1291–1301, 2012.

[123] Y. A.-R. I. Mohamed, H. H. Zeineldin, M. Salama, and R. Seethapathy, "Seamless formation and robust control of distributed generation microgrids via direct voltage control and optimized dynamic power sharing," *IEEE Trans. on Power Electronics*, vol. 27, no. 3, 2012.

[124] P. K. Ray, N. Kishor, and S. R. Mohanty, "Islanding and power quality disturbance detection in grid-connected hybrid power system using wavelet and-transform," *IEEE Trans. on Smart Grid*, vol. 3, 2012.

[125] A. Yafaoui, B. Wu, and S. Kouro, "Improved active frequency drift anti-islanding detection method for grid connected photovoltaic systems," *IEEE trans. on power electronics*, vol. 27, no. 5, pp. 2367–2375, 2012.

[126] S.-H. Hu, C.-Y. Kuo, T.-L. Lee, and J. M. Guerrero, "Droop-controlled inverters with seamless transition between islanding and grid-connected operations," in *ECCE Conference*. IEEE, 2011, pp. 2196–2201.

[127] G. W. E. G. Council, "Global wind report 2015," 2016. [Online]. Available: www.gwec.net

[128] J. Thongam, R. Beguenane, A. Okou, M. Tarbouchi, A. Merabet, and P. Bouchard, "A method of tracking maximum power points in variable speed wind energy conversion systems," in *Power Electronics, Electrical Drives, Automation and Motion (SPEEDAM), 2012 International Symposium on*. IEEE, 2012, pp. 1095–1100.

[129] S. Li, T. A. Haskew, R. P. Swatloski, and W. Gathings, "Optimal and direct-current vector control of direct-driven pmsg wind turbines," *IEEE Transactions on power electronics*, vol. 27, no. 5, pp. 2325–2337, 2012.

[130] C. Lumbreras, J. M. Guerrero, P. García, F. Briz, and D. D. Reigosa, "Control of a small wind turbine in the high wind speed region," *IEEE Transactions on Power Electronics*, vol. 31, no. 10, pp. 6980–6991, 2016.

[131] N. Orlando, M. Liserre, R. Mastromauro, and A. Dell Aquila, "A survey of control issues in pmsg-based small wind-turbine systems," 2013.

[132] B. K. Bose, "Power electronics and ac drives," *Englewood Cliffs, NJ, Prentice-Hall, 1986, 416 p.*, vol. 1, 1986.

[133] T. Ashish, "Modern control design-with matlab and simulink," *Indian Institute of Technology, Kanpur, India, John Wiley & Sons*, 2002.

[134] R. Walling, R. Saint, R. C. Dugan, J. Burke, and L. A. Kojovic, "Summary of distributed resources impact on power delivery systems," *IEEE Trans. on Power Delivery*, vol. 23, no. 3, pp. 1636–1644, 2008.

[135] M. Fatu, F. Blaabjerg, and I. Boldea, "Grid to standalone transition motion-sensorless dual-inverter control of pmsg with asymmetrical grid voltage sags and harmonics filtering," *IEEE Transactions on Power Electronics*, vol. 29, no. 7, pp. 3463–3472, Jul. 2014.

[136] O. Tremblay and L.-A. Dessaint, "Experimental validation of a battery dynamic model for ev applications," *World Electric Vehicle Journal*, vol. 3, no. 1, pp. 1–10, 2009.

[137] R. N. Beres, X. Wang, M. Liserre, F. Blaabjerg, and C. L. Bak, "A review of passive power filters for three-phase grid-connected voltage-source converters," *IEEE Journal of Emerging and Selected Topics in Power Electronics*, vol. 4, no. 1, pp. 54–69, 2016.

[138] NRCAN, "Effect of cold climate on wind energy production in canada (2010 – 2016)," 2017. [Online]. Available: www.nrcan.gc.ca

[139] S. Nalakath, M. Preindl, and A. Emadi, "Online multi-parameter estimation of interior permanent magnet motor drives with finite control set model predictive control," *IET Electric Power Applications*, vol. 11, no. 5, pp. 944–951, 2017.

[140] M. T. Angulo and R. V. Carrillo-Serrano, "Estimating rotor parameters in induction motors using high-order sliding mode algorithms," *IET Control Theory & Applications*, vol. 9, no. 4, pp. 573–578, 2014.

[141] R. De Doncker, "Parameter sensitivity of indirect universal field-oriented controllers," *IEEE transactions on power electronics*, vol. 9, no. 4, 1994.

[142] Y.-L. Hu and Y.-K. Wu, "Review on model validation and parameter estimation approaches of wind power generators," *The Journal of Engineering*, vol. 2017, no. 13, pp. 2407–2411, 2017.

[143] A. Susperregui, J. Jugo, I. Lizarraga, and G. Tapia, "Automated control of doubly fed induction generator integrating sensorless parameter estimation

and grid synchronisation," *IET Renewable Power Generation*, vol. 8, no. 1, pp. 76–89, 2014.

[144] M. Benadja and A. Chandra, "Adaptive sensorless control of pmsgs-based offshore wind farm and vsc-hvdc stations," *IEEE Journal of Emerging and Selected Topics in Power Electronics*, vol. 3, no. 4, 2015.

[145] A. Kusiak and Z. Zhang, "Adaptive control of a wind turbine with data mining and swarm intelligence," *IEEE Transactions on Sustainable Energy*, vol. 2, no. 1, pp. 28–36, 2011.

[146] J. Bocker and S. Mathapati, "State of the art of induction motor control," in *Electric Machines & Drives Conference, 2007. IEMDC'07. IEEE International*, vol. 2. IEEE, 2007, pp. 1459–1464.

[147] X.-P. Pan, P. Ju, F. Wu, and Y.-Q. Jin, "Parameter estimation of drive system in a fixed-speed wind turbine by utilising turbulence excitations," *IET Generation, Transmission & Distribution*, vol. 7, no. 7, 2013.

[148] Y. Ma, W. Cao, L. Yang, F. F. Wang, and L. M. Tolbert, "Virtual synchronous generator control of full converter wind turbines with short-term energy storage," *IEEE Transactions on Industrial Electronics*, vol. 64, no. 11, pp. 8821–8831, 2017.

[149] J. Liu, Y. Miura, T. Ise *et al.*, "Comparison of dynamic characteristics between virtual synchronous generator and droop control in inverter-based distributed generators," *IEEE Trans. Power Electron*, vol. 31, no. 5, pp. 3600–3611, 2016.

[150] B. Housseini, A. F. Okou, and R. Beguenane, "Robust nonlinear controller design for on-grid/off-grid wind energy battery-storage system," *IEEE Transactions on Smart Grid*, vol. 9, no. 6, pp. 5588–5598, 2018.

[151] O. Akhrif, *Nonlinear Adaptive Control with Application to Flexible Structures*. PhD Thesis, University of Maryland, 1989.

[152] R. Marino and P. Tomei, *Nonlinear control design: geometric, adaptive and robust*. Prentice Hall International (UK) Ltd., 1996.

[153] G. Timilsina, "Electricity reliability, economic output and welfare," in *Energy Security, Technology and Sustainability Challenges Across the Globe, 38th IAEE International Conference, May 25-27, 2015*. International Association for Energy Economics, 2015.

[154] B. H. Krogh and H. R. Schmidtke, "Electrical power in africa: Challenges and opportunities," *IEEE Smartgrid Newsletter*, 2012.

[155] W. Europe, "Wind in power 2017: Annual combined onshore and offshore wind energy statistics," 2018. [Online]. Available: windeurope.org

[156] Y. Xu, C.-C. Liu, K. P. Schneider, F. K. Tuffner, and D. T. Ton, "Microgrids for service restoration to critical load in a resilient distribution system," *IEEE Transactions on Smart Grid*, vol. 9, no. 1, pp. 426–437, 2018.

[157] Z. Li, M. Shahidehpour, F. Aminifar, A. Alabdulwahab, and Y. Al-Turki, "Networked microgrids for enhancing the power system resilience," *Proceedings of the IEEE*, vol. 105, no. 7, pp. 1289–1310, 2017.

[158] H. Farzin, M. Fotuhi-Firuzabad, and M. Moeini-Aghtaie, "Enhancing power system resilience through hierarchical outage management in multi-microgrids," *IEEE Transactions on Smart Grid*, vol. 7, no. 6, pp. 2869–2879, 2016.

[159] M. Rayati and A. M. Ranjbar, "Resilient transactive control for systems with high wind penetration based on cloud computing," *IEEE Transactions on Industrial Informatics*, vol. 14, no. 3, pp. 1286–1296, 2018.

[160] Y. Liu, Q. Wu, and X. Zhou, "Co-ordinated multiloop switching control of dfig for resilience enhancement of wind power penetrated power systems," *IEEE Transactions on Sustainable Energy*, vol. 7, no. 3, pp. 1089–1099, 2016.

[161] U. d. A. Miranda, L. Rolim, and M. Aredes, "A dq synchronous reference frame current control for single-phase converters," in *Power Electronics Specialists Conference, 2005. PESC'05. IEEE 36th.* IEEE, 2005, pp. 1377–1381.

[162] B. Li, S. Huang, X. Chen, and Y. Xiang, "A simplified dq-frame current controller for single-phase grid-connected inverters with lcl filters," in *Elec-*

trical Machines and Systems (ICEMS), 2017 20th International Conference on. IEEE, 2017, pp. 1–5.

[163] C. R. Baier, M. Torres, J. A. Muñoz, J. M. Mauricio, J. Rohten, and M. Rivera, "Nonlinear control strategy for current source cascaded h-bridge inverters—an approach considering single-phase dq components," in *Industrial Technology (ICIT), 2015 IEEE International Conference on*. IEEE, 2015, pp. 3079–3084.

[164] Y. Tang, Z. Qin, F. Blaabjerg, and P. C. Loh, "Dq reference frame modeling and control of single-phase active power decoupling circuits," in *Applied Power Electronics Conference and Exposition (APEC), 2015 IEEE*. IEEE, 2015, pp. 2725–2732.

[165] N. Weise *et al.*, "Implementation and validation of dq current control of a bidirectional sic single-phase ac-dc converter," in *Applied Power Electronics Conference and Exposition (APEC), 2015 IEEE*. IEEE, 2015, pp. 3143–3149.

[166] M. Ebrahimi, S. A. Khajehoddin, and M. Karimi-Ghartemani, "Fast and robust single-phase *dq* current controller for smart inverter applications," *IEEE transactions on power electronics*, vol. 31, no. 5, pp. 3968–3976, 2016.

[167] Y. Liao, Z. Liu, X. Hu, and B. Wen, "A dq-fvame impedance measurement method based on hilbert transform for single-phase vehicle-grid system," in *Transportation Electrification Asia-Pacific (ITEC Asia-Pacific), 2017 IEEE Conference and Exp*. IEEE, 2017, pp. 1–6.

[168] A. M. Mnider, D. J. Atkinson, M. Dahidah, and M. Armstrong, "A simplified dq controller for single-phase grid-connected pv inverters," in *Renewable Energy Congress (IREC), 2016 7th International*. IEEE, 2016, pp. 1–6.

[169] J. F. Sultani, "Modelling, design and implementation of dq control in single-phase grid-connected inverters for photovoltaic systems used in domestic dwellings." 2013.

Appendices

Feedback Linearization of MIMO Systems

Let consider the following MIMO system [63]

$$\begin{cases} \dot{\overline{x}} = f(\overline{x}) + g(\overline{x})\overline{u} & \text{(1a)} \\ \overline{y} = h(\overline{x}) & \text{(1b)} \end{cases}$$

where $\overline{x} \in \mathbb{R}^n$ is the state vector. $\overline{u} \in \mathbb{R}^m$ is the vector of m inputs u_i $(i = 1, ..., m)$. $\overline{y} \in \mathbb{R}^m$ is the vector of m outputs y_j $(j = 1, ..., m)$. f and g are smooth vector and matrix fields, respectively. h is the smooth vector function.

The input-output linearization method for MIMO systems consists of differentiating the outputs y_j until at least one input appears.

Consider $\mathcal{L}_f h$ and $\mathcal{L}_g h$ the Lie derivatives of h with respect to f and g, $\dot{y}_j$ can be written as

$$\dot{y}_j = \mathcal{L}_f h_j + \sum_{i=1}^{m} (\mathcal{L}_{g_i} h_j) u_i \tag{2}$$

If $\mathcal{L}_{g_i} h_j(x) = 0$ for all i, then no inputs appears and one has to differentiate again. Assumed that y_j needs to be differentiated r_j times before at least one input appears, then

$$y_j^{(r_j)} = \mathcal{L}_f^{r_j} h_j + \sum_{i=1}^{m} \mathcal{L}_{g_i} \mathcal{L}_f^{r_j - 1} h_j u_i, \ (j = 1, ..., m) \tag{3}$$

Eqn. (3) can be written into a matrix form as follows

$$\begin{bmatrix} y_1^{(r_1)} \\ \vdots \\ y_m^{(r_m)} \end{bmatrix} = \begin{bmatrix} \mathcal{L}_f^{r_1} h_1(x) \\ \vdots \\ \mathcal{L}_f^{r_m} h_m(x) \end{bmatrix} + B(x) \underbrace{\begin{bmatrix} u_1 \\ \vdots \\ u_m \end{bmatrix}}_{\overline{u}} \tag{4}$$

where the $m \times m$ matrix $B(x)$ is referred to as the decoupling matrix for the MIMO system. It has the following expression.

$$B(x) = \begin{bmatrix} \mathcal{L}_{g_1}\mathcal{L}_f^{r_1-1}h_1 & \cdots & \mathcal{L}_{g_m}\mathcal{L}_f^{r_1-1}h_1 \\ \vdots & \ddots & \vdots \\ \mathcal{L}_{g_1}\mathcal{L}_f^{r_m-1}h_m & \cdots & \mathcal{L}_{g_m}\mathcal{L}_f^{r_m-1}h_m \end{bmatrix} \tag{5}$$

Eqn. (4) is linearized by choosing the control input vector u as follows.

$$\overline{u} = -B^{-1}\begin{bmatrix} \mathcal{L}_f^{r_1}h_1(x) \\ \vdots \\ \mathcal{L}_f^{r_m}h_m(x) \end{bmatrix} + B^{-1}\underbrace{\begin{bmatrix} v_1 \\ \vdots \\ v_m \end{bmatrix}}_{\overline{v}} \tag{6}$$

where v is the new input yet to be determined.

The closed loop equation of the system is obtained by substituting Eqn. (6) into Eqn. (4) to get

$$\begin{bmatrix} y_1^{(r_1)} \\ \vdots \\ y_m^{(r_m)} \end{bmatrix} = \begin{bmatrix} v_1 \\ \vdots \\ v_m \end{bmatrix} \tag{7}$$

The input-output relationship given by Eqn. (7) is not only linear but also decoupled.